FINAL REPORT

Integrating Remote Sensing and Field Measurements to Identify Environmental Nonstationarity on Interior Alaska DoD Training Lands

SERDP Project RC18-1486

SEPTEMBER 2019

Jennifer Watts
The Woods Hole Research Center

Distribution Statement A
This document has been cleared for public release

SERDP
DOD ▪ EPA ▪ DOE

Page Intentionally Left Blank

This report was prepared under contract to the Department of Defense Strategic Environmental Research and Development Program (SERDP). The publication of this report does not indicate endorsement by the Department of Defense, nor should the contents be construed as reflecting the official policy or position of the Department of Defense. Reference herein to any specific commercial product, process, or service by trade name, trademark, manufacturer, or otherwise, does not necessarily constitute or imply its endorsement, recommendation, or favoring by the Department of Defense.

Page Intentionally Left Blank

REPORT DOCUMENTATION PAGE

Form Approved
OMB No. 0704-0188

The public reporting burden for this collection of information is estimated to average 1 hour per response, including the time for reviewing instructions, searching existing data sources, gathering and maintaining the data needed, and completing and reviewing the collection of information. Send comments regarding this burden estimate or any other aspect of this collection of information, including suggestions for reducing the burden, to Department of Defense, Washington Headquarters Services, Directorate for Information Operations and Reports (0704-0188), 1215 Jefferson Davis Highway, Suite 1204, Arlington, VA 22202-4302. Respondents should be aware that notwithstanding any other provision of law, no person shall be subject to any penalty for failing to comply with a collection of information if it does not display a currently valid OMB control number.
PLEASE DO NOT RETURN YOUR FORM TO THE ABOVE ADDRESS.

1. REPORT DATE *(DD-MM-YYYY)*	2. REPORT TYPE	3. DATES COVERED *(From - To)*
09/29/2019	SERDP Final Report	6/29/2018 - 6/29/2019

4. TITLE AND SUBTITLE
Integrating Remote Sensing and Field Measurements to Identify Environmental Nonstationarity on Interior Alaska DoD Training Lands

5a. CONTRACT NUMBER
18-P-0052

5b. GRANT NUMBER

5c. PROGRAM ELEMENT NUMBER

6. AUTHOR(S)
Jennifer Watts

5d. PROJECT NUMBER
RC18-1486

5e. TASK NUMBER

5f. WORK UNIT NUMBER

7. PERFORMING ORGANIZATION NAME(S) AND ADDRESS(ES)
The Woods Hole Research Center
149 WOODS HOLE ROAD
FALMOUTH, MA 02540

8. PERFORMING ORGANIZATION REPORT NUMBER
RC18-1486

9. SPONSORING/MONITORING AGENCY NAME(S) AND ADDRESS(ES)
Strategic Environmental Research and Development Program
4800 Mark Center Drive, Suite 17D03
Alexandria, VA 22350-3605

10. SPONSOR/MONITOR'S ACRONYM(S)
SERDP

11. SPONSOR/MONITOR'S REPORT NUMBER(S)
RC18-1486

12. DISTRIBUTION/AVAILABILITY STATEMENT
DISTRIBUTION STATEMENT A. Approved for public release: distribution unlimited.

13. SUPPLEMENTARY NOTES

14. ABSTRACT
This one-year SEED project was conducted to characterize contemporary heterogeneity in landscape change occurring across Alaska with a focus on DoD training lands in Interior Alaska. This study was designed to integrate observations from visible, near-infrared, thermal (VIS-NIRTIR) and microwave satellite remote sensing to detect shifts in three Earth System Indicators: 1) Terrain Thermal State; 2) Ecosystem Water Stress; 3) Vegetation State.

15. SUBJECT TERMS
Satellite remote sensing, Machine learning, Google Earth Engine, Microwave remote sensing, Permafrost, Disturbance, Wildfire, Ecosystem transitions, Arctic and subarctic, Boreal systems, Hydrology, Climate warming, Ecosystem wetting, Vegetation greening, Habitat, Alaska, Terrain monitoring system

16. SECURITY CLASSIFICATION OF:			17. LIMITATION OF ABSTRACT	18. NUMBER OF PAGES	19a. NAME OF RESPONSIBLE PERSON
a. REPORT	b. ABSTRACT	c. THIS PAGE			Jennifer Watts
					19b. TELEPHONE NUMBER *(Include area code)*
UNCLASS	UNCLASS	UNCLASS	UNCLASS	179	406-581-8449

Page Intentionally Left Blank

TABLE OF CONTENTS

TABLE OF CONTENTS I
LIST OF TABLES II
LIST OF FIGURES III
LIST OF ACRONYMS IV
KEYWORDS VI
ACKNOWLEDGEMENTS VII
1. ABSTRACT 1
OBJECTIVES 1
TECHNICAL APPROACH 2
SUMMARY OF RESULTS 2
BENEFITS 5
2. OBJECTIVE 5
2.1 INDICATOR 1: TERRAIN THERMAL STATE 16
2.2 INDICATOR 2: ECOSYSTEM WATER STRESS 17
2.3 INDICATOR 3: VEGETATION STATE 18
2.4 SATELLITE DATA FUSION FOR EARTH SYSTEM INDICATORS 19
3. BACKGROUND 20
3.1 TERRAIN NONSTATIONARITY IN ALASKA 20
3.2 NONSTATIONARITY IN INTERIOR ALASKA 21
3.3 REMOTE SENSING DETECTION OF TERRAIN STATE 22
4. MATERIALS AND METHODS 25
INTRODUCTION AND SCOPE 25
4.1 SATELLITE RETRIEVALS 26
4.1.1. TERRAIN THERMAL STATE 26
4.1.2. LANDSCAPE WATER STRESS 28
4.1.3. VEGETATION 29
4.1.4. ANCILLARY DATA 29
4.2 TIME SERIES ANALYSIS 32
4.2.1. MANN-KENDALL TREND TEST 32
4.2.2. BREAK POINT ANALYSIS 33
4.3 SATELLITE DATA FUSION (DOWNSCALING) 33
5. RESULTS AND DISCUSSION 39
5.1 INDICATOR STATE CHANGES 39
5.1.1 TERRAIN THERMAL STATE 39
5.1.1.1 RESULTS FOR ALASKA 39
5.1.1.2 RESULTS FOR THE INTERIOR ALASKA AOI 42
5.1.1.3 DISCUSSION AND SUMMARY OF TERRAIN THERMAL STATE 59
5.1.2 ECOSYSTEM WATER STRESS 61
5.1.2.1 ALASKA 61
5.1.2.2 INTERIOR ALASKA 63
5.1.2.3 DISCUSSION AND SUMMARY OF ECOSYSTEM WATER STRESS 72
5.1.3 VEGETATION STATE 74

5.1.3.1 Alaska 74
5.1.3.2 Interior Alaska 76
5.1.3.3 Discussion and summary of Vegetation State 88
5.2 Data fusion (downscaling) 91
5.2.1 Terrain Thermal State 92
5.2.2 Water stress 98
5.2.3 vegetation state 107
5.2.4 Discussion and summary of data fusion (downscaling) 111

6. CONCLUSIONS AND IMPLICATIONS FOR TRAINING RANGE MANAGEMENT AND FUTURE RESEARCH/IMPLEMENTATION 112

6.1 Introduction 112
6.1.1 Terrain Thermal State 114
6.1.2 Ecosystem Water Stress 114
6.1.3 Vegetation State 115
6.1.4 Indicator downscaling for localized change analysis 116
6.2 Ramifications for DoD in Alaska 117
6.3 Towards an automated remote sensing change platform 117

APPENDIX A. DELIVERABLES, OUTREACH, AND LEVERAGING EFFORTS 131

A.1 Conference Presentations 131
A.2 Outreach 131
A.3 Leveraging/collaborative activities with related ongoing efforts 131
A.4 Interactions with Department of Defense and Other Governmental Endusers 132
A.6 Data Transfer 132

APPENDIX B. SUPPLEMENTARY FIGURES AND TABLES 133

LIST OF TABLES

Table 1. Configurations of Sentinel SAR images used in this study……...29
Table 2. Ancillary datasets used in this analysis……..31
Table 3. Reclassification of land cover types from the Rogers et al. Alaska land cover map… 31
Table 4. All predictor variables used for downscaling the Freeze/Thaw cycle……...35
Table 5. All predictor variables used for downscaling vegetation optical depth (VOD)……35
Table 6. All predictor variables used for downscaling surface soil moisture……..36
Table 7. All predictor variables used for surface water inundation…….37
Table 8. Summary of regional terrains in the Interior Alaska AOI having significant ($p < 0.1$) change in Indicator metrics of Thermal State……..58
Table 9. Summary of terrains in the Interior Alaska AOI having significant ($p < 0.1$) change in Indicator metrics of Ecosystem Water Stress……..72
Table 10. Summary of terrains in the Interior Alaska AOI having significant ($p < 0.1$) change in Indicator metrics of Vegetation State……..86
Table 11. Summary of the performance of Random Forest models used for data fusion (downscaling) and open water classification of Sentinel-1 SAR imagery……..92
Table 12. Sentinel-1 SAR water and land classification accuracy…….107

LIST OF ACRONYMS

ABoVE	NASA's Arctic Boreal Vulnerability Experiment
ALFD	Alaska Large Fire Database
ALOS	Advanced Land Observing Satellite DAICHI
AWS	Amazon Wet Services
AMSR-E	Advanced Microwave Scanning Radiometer for EOS
AMSR-2	Advanced Microwave Scanning Radiometer 2
AOI	Area of interest
ARCUS	Arctic Research Consortium of the United States
ASAR	Advanced Synthetic Aperture Radar
AVHRR	Advanced Very High Resolution Radiometer
CRREL	Cold Regions Research and Engineering Laboratory
DEM	Digital elevation model
DoD	Department of Defense
DOY	Day of year
DMSP	U.S. Air Force Defense Meteorological Satellite Program
EE	Google Earth Engine
EOS	Earth Observing System
ERDC	Engineer Research and Development Center
ETM+	Enhanced Thematic Mapper Plus
Fw	Fractional surface water inundation
GHz	Gigahertz (wave frequency)
GNSS	Global Navigation Satellite System
GMAO	Global Modeling and Assimilation Office
GMTED2010	Global multi-resolution terrain elevation data 2010 (USGS)
GPS	Global Positioning System
H	Horizontal (polarization)
IW	Interferometric Wide Swath (for SAR)
JAXA	Japanese Space Agency
LANDSAT	Land Remote Sensing Satellite (System)
LPDR	UMT Land Parameter Data Record
LST	Land surface temperature
MERRA2	Modern-Era Retrospective analysis for Research and Applications, Version 2
MODIS	Moderate Resolution Imaging Spectroradiometer
MetOp	Meteorological Operational Satellite Program (MetOp)
MSS	Landsat Multispectral Scanner
NASA	National Aeronautics and Space Administration
NIR	Near infrared
NASA	National Aeronautics and Space Administration
NOAA	National Oceanographic and Atmospheric Administration
NTSG	Numerical Terradynamic Simulation Group
OLI	Operational Land Imager
SAR	Synthetic Aperture Radar
SERDP	Strategic Environmental Research and Development Program
SM	Stripmap mode (for SAR)

SNOTEL	SNOpack TELemetry
SPOT5	Satellite Pour observation de la Terre
SRTM	Shuttle Radar Topography Mission
SMD	Snow melt duration
SMM/I	Special Sensor Microwave/Imager
SSMIS	Special Sensor Microwave Imager/Sounder
SSMR	Scanning Multichannel Microwave Radiometer (SMMR)
Tb	(Microwave) brightness temperature
TIR	Thermal infrared
TIRS	Thermal infrared sensor
TIROS-N	Television and Infrared Observation Satellite
TM	Thematic Mapper
TPI	Topographic position index
UMT	University of Montana
USARAK	U.S. Army Alaska
USGS	United States Geological Survey
V	Vertical (polarization)
VOD	Vegetation optical depth
VSM	Volumetric surface moisture
WOD	Water occurance dataset

KEYWORDS

Satellite remote sensing
Machine learning
Google Earth Engine
Microwave remote sensing
Permafrost
Disturbance
Wildfire
Ecosystem transitions
Arctic and subarctic
Boreal systems
Hydrology
Climate warming
Ecosystem wetting
Vegetation greening
Habitat
Alaska
Terrain monitoring system

ACKNOWLEDGEMENTS

This research reflects a one-year intensive SEED project sponsored by the SERDP program (RC18-LC-1486). We wish to acknowledge the efforts of our Co-Investigators for this work: Drs. Sue Natali and Brendan Rogers at the Woods Hole Research Center; Dr. Jinyang Du at the Numerical Terradynamic Simulation Group, University of Montana; Dr. Thomas Douglas at the U.S. Army Cold Regions Research and Engineering Laboratory in Fairbanks; and Stefano Potter at Woods Hole Research Center. A special thanks to Mr. Potter for the dedicated effort spent on data processing and trend analysis. Drs. Du, Douglas, Rogers, and Natali contributed to the writing of this report, as did Mr. Potter. We also thank collaborators Dr. Eugenie Euskirchen (University of Alaska Fairbanks), Dr. Alexander Kholodov (University of Alaska Fairbanks), Dr. Ted Schuur (Northern Arizona University), Drs. Ueyama Masahito and Hiroli Iwata (International Arctic Research Center at the University of Alaska Fairbanks) for field observations provided as a reference to our remote sensing retrievals. Special thanks to Dr. John Kimball and Caleb Pan (Numerical Terradynamic Simulation Group) for access to passive microwave datasets and assistance with snow cover analysis over Alaska.

We would like to acknowledge the NASA Arctic Boreal Vulnerability Experiment (ABoVE) for project access to NASA computing facilities and remote sensing datasets. The project also benefitted from data and research time leveraged from companion projects funded by the NASA New (Early Career) Investigator Program and NASA ABoVE.

1. ABSTRACT

Objectives

Over 60% of lands in Alaska (out of 1.72 M km^2) are administered by the U.S. Government, with approximately 1,115,948 acres (4,516 km^2) managed by the U.S. Department of Defense (DoD). The majority of these DoD lands are managed by the Army and are located near Fairbanks. These lands are remote, with many terrains inaccessible by roads. Off-road access is limited during the summer by extremely wet soils over permafrost (ground that has remained frozen for at least two years) and an abundance of surface water distributed across lakes, rivers and wetlands. The frozen winter period allows for better access to the landscape, but safety and ease of travel greatly depend on ice and snow conditions which are difficult to quantify remotely. The DoD has already invested heavily in infrastructure across Alaska, including Air Force radar and launch sites, Air Force and Army bases, and Army Arctic training ranges and test sites. Recent emphasis on future DoD development and Arctic operations in Alaska, identified in the 2016 DoD Report to Congress on National Security Interests in the Arctic and echoed in the FY2019 DoD Budget Request, includes new investments in Alaska's missile defense systems and on-the-ground training exercises in addition to long-term plans for road building to access remote training areas (e.g., Tanana Flats and Yukon Training Areas in Interior Alaska) and ongoing support and maintenance for existing infrastructure.

Alaska is warming at twice the rate of the global average, and climate models now predict that temperatures across the state will increase by up to 6 ºC (10.8°F) before 2099. This warming will yield potentially severe consequences for frozen ground conditions, vegetation, hydrology, habitat characteristics, transportation and infrastructure across the state. A changing climate places Alaska ecosystems at greater risk for disturbance and, as a consequence, will increasingly affect major military installations and their terrains through nonstationarity in environmental conditions.

This one-year SEED project was conducted to characterize contemporary heterogeneity in landscape change occurring across Alaska with a focus on DoD training lands in Interior Alaska. This study was designed to integrate observations from visible, near-infrared, thermal (VIS-NIR-TIR) and microwave satellite remote sensing to detect shifts in three Earth System Indicators: 1) Terrain Thermal State; 2) Ecosystem Water Stress; 3) Vegetation State. Through statistical trend analysis, Alaska regions experiencing nonstationarity in these focus areas from $\leq$2002 to 2017 were identified and mapped to provide the DoD with geospatial information indicating the locations of terrains experiencing longer-term ecosystem shifts. This study also explored and tested new methods for satellite data fusion (downscaling), using machine learning, to produce new Earth System Indicator records having greatly improved (30 m; 500 m) spatial resolutions to better support localized change detection and decision-making for DoD land managers. The ultimate goal of this work was to identify, test, and validate potential remotely sensed observational tools that can be used to identify areas where landscape change is occurring or may occur in the future. Due to the remote nature of many of the training ranges, remotely sensed tools and applications have the potential to save time and money and reduce environmental and safety risks for land management and training activities.

Technical Approach

This project included multiple remote sensing measurements obtained from a suite of U.S. supported satellite platforms available for both regional (e.g., Alaska) and global analysis. Specifically, this study used multi-spectral observations from Landsat, MODIS, SSM/I, SMMR, SMMIS, AMSR-E and AMSR2 to investigate nonstationarity in landscape frozen state, surface hydrology and vegetation over a period spanning 1979 (for Freeze/Thaw state; $\geq$ 2002 for other indicators) to 2017. Image collection was daily for all sensors, except Landsat which had a 16 day repeat interval. When possible, the satellite observations were supported by in situ data provided through existing field monitoring efforts including work funded by NASA, the U.S. Army Basic Research Program, U.S. Army Alaska, and SERDP. In addition, we used observations from NASA's MERRA2 reanalysis data assimilation system, from 1980 to 2017, to detect changes in air temperature and precipitation over Alaska.

A Mann-Kendall statistical time series analysis was applied to each long-term satellite and reanalysis data record on a per grid cell basis. The time series change detection analysis provided information on longer-term monotonic trends and rates of change across Alaska. In addition, we evaluated the use of Breaks for Additive Season and Trend (BFAST) detection in Interior Alaska to identify the occurrence of abrupt landscape change.

The project employed machine learning to integrate high temporal frequency, yet coarser spatial resolution, passive microwave remote sensing retrievals with higher spatial resolution VIS-NIR-TIR observations to examine the feasibility of providing new, spatially-improved Earth System Indicator time series records for DoD terrains in Interior Alaska. Although the change detection and data fusion methodology developed for this project were demonstrated for Alaska, they were designed to be globally applicable and readily transferable to other regions.

Summary of Results

Terrain Thermal State

Our change detection analysis for Alaska, using a multi-sensor suite of data from VIS-NIR-TR and microwave satellite remote sensing, showed that the length of the spring (April 15th to May 31st) transitional period decreased at an average rate of 6 days per decade over the 16 year (2002 to 2017) observation period. For our purposes, the transitional state is defined as where a terrain surface had changed from thawed to frozen state, or vice versa, within a 24-hour period. In addition, we found that the spring thaw period had increased at an average rate of 8 days per decade. These detected rates of change are higher than the ~ 3.5 days per decade increase in annual non-frozen period reported in past studies for years prior to 2006 (Smith et al. 2004; Zhang et al. 2011).

This study also observed a significant increase in the length of the autumn (September 1 to October 15) transitional period, at an average rate of 2 days per decade. In addition, the satellite records showed a significant increase in transitional state for Alaska during the winter period (October 16 to April 14) at a rate of 1.5 days per decade. For Interior Alaska, we found that the number of thawed days in autumn and early winter increased over the major DoD terrains of Donnelly Training Area and the Tanana Flats Training Area at a rate of 7 days per decade, based on the AMSR-E/AMSR2 satellite record.

Ecosystem Water Stress

This study detected a significant increase in summer precipitation over 11% of Alaska's terrains (at a rate of up to 3 mm per year) from 1980 to 2017 within the MERRA2 reanalysis record. This increase occurred along the Alaska Range, the southern coastal region, and Yukon-Kuskokwim Delta. This finding is in agreement with estimates from Atmosphere-Ocean General Circulation Models which indicate that precipitation amounts are increasing within Alaska (Larsen et al. 2008). Our analysis also detected a significant and multi-year decrease in summer precipitation over Interior Alaska, including on DoD terrains (at a rate of 1.5 mm per year).

Our trend analysis using the 16 year (2002 to 2017) AMSR-E/AMSR2 satellite record revealed a significant increase in summer surface soil moisture over much of Alaska, including the Interior. The DoD Yukon Training Area and the Tanana Flats Training Area were observed to have significant positive trends in summer and autumn soil moisture, at a rate of 0.2 cm^3/cm^3 per decade. However, we also detected a significant decrease in summer surface soil moisture (0.2 cm^3/cm^3 per decade) occurring over the Donnelly Training Area.

We observed a significant increase in summer surface water inundation across coastal zones and within localized (lowland) terrains in Interior Alaska, as detected in the AMSR-E/AMSR2 25 km (2002 to 2017) and 5 km (2002 to 2015) records. This increase in standing water occurred over 21% of the state (368,000 km^2). Within our Interior Alaska Area of Interest (AOI; centered on Fairbanks and encompassing nearby DoD lands), we found that 9.7% of terrains (out of 453,248 km^2) had experienced a significant increase in surface inundation during this period. Conversely, only 5.8% of Interior AOI terrains showed a significant decrease in summer inundation, including in the western portion of Fort Wainwright, over Fort Greely and Donnelly Training Area. In autumn, substantial increases in inundation were observed over ~ 18% of the Interior AOI, primarily in lowland regions including Fort Greely.

Vegetation State

Our study showed multi-year increases in biomass water content (indicated by AMSR vegetation optical depth; VOD) and vegetation greenness (indicated by MODIS vegetation indices) over Alaska's coastal regions, occurring within the 16 year (2002 to 2017) satellite observation period. This coastal greening and increase in VOD coincide with regional increases in precipitation and summer soil moisture, in addition to a lengthening of the annual non-frozen period, which are also reported in this study.

In the Alaska Interior AOI we instead observed a significant decrease in biomass water content (i.e., VOD), mostly within boreal forests. These trends in VOD primarily reflect a decrease in standing live forest biomass following major fire events that have occurred over 7.6 million acres (31,000 km^2) in this region since 2002. We also observed a significant decrease in VOD in spring and summer for wetlands and grass/shrub habitat within this region, coinciding with areas of terrain wetting (which could indicate the encroachment of vegetation by open water), but the terrain area affected was minimal compared to the forested terrains.

Although a significant decline in VOD was observed across much of Interior Alaska when considering the 2003 to 2017 AMSR remote sensing record, we also observed a strong increase in VOD from 2014 through 2017 on DoD and surrounding terrains that coincided with biomass recovery. In contrast to VOD, the MODIS vegetation indices showed significant greening

occurring within the Interior region. The most substantial greening was observed within fire scars, indicating the recovery of leaf canopy and understory foliage.

The results from our case study using BFAST time series decomposition to detect severe vegetation disturbance events (e.g., fire) confirms that this approach can detect breaks in remote sensing records, but also shows that the detected break point is highly dependent on what occurred in the landscape before and after a disturbance event. This portion of the investigation also highlighted the need for an on-the-ground terrain monitoring system on Interior Alaska DoD lands, coinciding with an ongoing remote sensing based terrain disturbance detection, to provide in situ observations needed to better understand what is driving the responses observed in satellite remote sensing records.

Downscaling (Data Fusion) of Remote Sensing Records

The data fusion component in this study focused on developing and testing methodologies for downscaling Earth System Indicator metrics based on spatially coarse 25 km passive microwave retrievals (e.g. AMSR; SSMI). The methods developed here can be readily applied in Google Earth Engine over the microwave data record ($\leq$ 2002 to 2017) to produce daily $\leq$ 500 m estimators of terrain state over Alaska and elsewhere on Earth. These long-term, downscaled records can be used to assist in identifying more localized and spatially precise patterns of nonstationarity through the application of Mann-Kendall and BFAST change detection to detect respective monotonic trends and abrupt disturbances in the time series.

For this study, we developed and evaluated machine learning algorithms for the downscaling of Freeze/Thaw, surface soil moisture, open water and vegetation. We also developed and improved machine learning methods to classify open water time series within Sentinel-1 Synthetic Aperture Radar (SAR) retrievals. The resulting downscaled products, provided for Interior Alaska in this one year SEED study, have greatly improved spatial resolutions of 500 m (Freeze/Thaw, soil moisture and vegetation) and 30 m (open water). Each downscaled product produced and evaluated in this study was able to capture spatial and temporal patterns of terrain change with a documented improvement over the original, coarse resolution microwave retrievals.

The relatively high accuracies ($R^2 > 0.80$, compared to the original microwave data) achieved in Freeze/Thaw and vegetation products indicates that this project component is ready for the next phase, which is applying the developed downscaling algorithms to the full satellite time series (2002 to present) for the Interior Alaska domain to support a finer scale change detection analysis. The SAR results also showed favorable spatial accuracy for delineating water/land patterns at 30 m resolution and the potential of near-real time flood monitoring and risk mitigation.

The slightly reduced accuracy ($R^2 = 0.49$) for surface soil moisture is still promising, especially given the ability of the product to represent finer spatial variability in surface wetness, but indicates a need for further algorithm refinement and reference with soil moisture data from multiple in situ monitoring stations before moving forward to regional applications. Next steps here should include additional efforts to identify which terrain characteristics correspond with better or worse performance in the downscaling approach, to allow for model improvements.

Benefits

Identifying contemporary environmental change is a critical first step in mitigating terrain risk under a warming climate. Knowledge of the location and characteristics of change occurring in Earth System Indicators of Terrain Thermal State, Ecosystem Water Stress, and Vegetation State on and surrounding DoD lands is fundamental to inform the extent and magnitude of nonstationarity that is affecting U.S. ecosystems and to provide DoD managers with the information necessary to identify and mitigate for risk to existing and future infrastructure. The remote sensing-based geospatial change detection framework developed through this SEED project provides new tools and methodologies to better support decision making for conservation and training lands management, infrastructure development, and risk assessment across the Alaska DoD domain.

This study benefits the DoD through the design and testing of a remote sensing informed geospatial change analysis platform to identify the location, trajectory, and characteristics (e.g., change distribution shape) of ecosystem shifts occurring on DoD lands. The resulting Earth System Indicator change maps and terrain delineations can be readily incorporated into DoD supported geographic systems, including the Geographic Information Supporting Military Operations (GISMO) platform and, more broadly, to the Army Geospatial Center's various platforms, the Army Installation Management Command's cloud based tools, and the Army Installation Atlas. Though this study focuses on Alaska, this detection framework can be readily applied to other geographic locations including Russia, Canada and the conterminous United States (with appropriate modifications).

This study also identifies the need for a coordinated network of on-the-ground observations for soil temperature, soil moisture and above-ground vegetation water content to strategically verify patterns observed in the remote sensing retrievals and as a reference for new products being produced through VIS-NIR-TIR and microwave data fusion. Though this study provides proof-of-concept for the downscaling of microwave remote sensing data, and the detection of surface water change using Sentinel-1 radar, these methods can be strengthened for Interior Alaska by linking satellite data with on-the-ground references of terrain condition (e.g. time lapse camera retrievals, thermal and moisture sensor data, and microwave derived vegetation water content) strategically positioned on DoD and neighboring terrains.

2. OBJECTIVE

The U.S. Department of Defense (DoD) manages approximately 1,115,948 acres (4,516 km^2) of land in Alaska and includes multiple Air Force and Army installations across the state (Figure 1). A majority of the DoD training lands for U.S. Army Alaska (USARAK), and other key infrastructure, are located in Interior Alaska. These sites include Fort Wainwright, the U.S. Ground Based Missile Defense infrastructure at U.S. Army Fort Greely, Eielson Air Force Base and Clear Air Force Station. Terrains across Alaska (Figure 2) are characterized by severely cold climates, seasonally thawed wet surface soils, and underlying permafrost (ground remaining frozen for at least two consecutive years). Vegetation across this vast landscape (~ 424 million acres, or 17,180 km^2) varies from treeless tundra in temperature limited, water saturated, and permafrost affected terrains to mixed species forest and wetlands in the Interior and eastern coastal communities (Figure 3).

Alaska is warming at a rate that is more than twice the global average, and climate models estimate that temperatures across the state will increase by more than 5.6ºC (10°F) by 2099 (Sun et al. 2015). With climate change, seasonal snow cover and the length of the frozen season are decreasing leading to permafrost that is increasingly susceptible to thaw. Regional precipitation may be either increasing or decreasing (Dai et al. 2004; Larsen et al. 2008) depending on the study. The northern latitudes, including Alaska, have already experienced an average advance and lengthening of the non-frozen season by > 3 days/decade (Zhang et al. 2011). Changes in the frequency and timing of winter thaw-refreeze events in Alaska can also influence the susceptibility of permafrost to heightened thaw and vegetation to thermal stress, but these freeze-thaw events are spatially and temporally variable, and therefore difficult to quantify in absence of a detailed spatial analysis. However, as temperatures warm, Interior Alaska may start to experience a higher frequency of thaw events, indicating a transition to climate conditions more like those further south in western Canada and the U.S. Northwest (Wilson et al. 2013).

These thaw events pose heightened risk to transportation networks by increasing the extent of large floods made worse by snow melt over frozen surfaces (Watts et al. 2012; Toniolo et al. 2017). An increase in transitional freeze/thaw cycles may also result in greater stress and damage to road and building infrastructure (Melvin et al. 2017). To address this risk, the Alaska Department of Transportation and Public Facilities is limiting road access on low-volume roadways through spring load restrictions to minimize damage (Kraatz et al. 2019). The risk of freeze/thaw to roadways is especially important in Alaska given the relatively limited road network within the state. Ground instability in permafrost affected landscapes, and soil collapse in severe cases, also threatens Alaska's airfields, railways and pipeline, bridges and other infrastructure (Edlund et al. 2018) – leaving many agencies struggling to collect systematic data on temperature and freeze/thaw change, which are needed for risk mitigation and utility planning (McBeath 2003).

Increases in the seasonal duration of thawed surface soils is also problematic for off-road travel in Alaska. Terrain disturbance from off-road vehicles, including those used for military training and site access, have been documented following military operations in Alaska including Donnelly Training Area (Affleck et al. 2005). These disturbances can be severe when occurring on extremely wet to saturated soils that are common across the landscape and can result in ruts, loss of vegetation, increased erosion for years after the event, and can further permafrost thaw. The capability of Alaska terrains to support DoD on-the-ground training exercises without substantial harm to the environment will likely become more restricted in future years, especially during transitional spring and autumn periods, as non-frozen conditions become more prevalent (Shoop et al. 2005).

The impacts of a lengthening non-frozen season on regional surface hydrology are more difficult to gauge, especially since precipitation, seasonal snow characteristics, vegetation and organic litter cover, underlying soil and permafrost properties, sub-surface water flow paths, and land-atmosphere evaporative demand influence changes in terrain wetness (Ling & Zhang 2003; Kim et al. 2018; Schuur & Mack 2018). Initial melt and release of water stored in permafrost affected terrain, or an increase in precipitation events over frozen ground, can increase terrain wetting in permafrost landscapes at earlier to mid stages of thaw, having limited drainage networks within frozen sub-subsurface soils (Bring et al. 2016). Sub-surface drainage often increases with active layer deepening and more advanced stages of permafrost thaw, which, over time, can lead to the drainage and disappearance of surface water bodies (Jepsen et al. 2012;

Watts et al. 2014). The loss of permafrost and increase in soil drainage, combined with warmer summers and evapotranspiration, have also contributed to the drying and disappearance of small ponds and wetlands across Alaska (Riordan et al. 2006).

Drier soil conditions and increasing temperatures across Alaska are expected to heighten vegetation vulnerability to drought stress, tree mortality, and wildfire (Chapin et al. 2010; Turetsky et al. 2011; Rogers et al. 2018; Loranty et al. 2016; Park et al. 2016; Sniderhan & Baltzer 2016). Localized tree mortality can also occur with the expansion of wetlands in landscapes experiencing earlier to mid stages of permafrost thaw (Roach et al. 2011; Lara et al. 2016). A lengthening non-frozen season, combined with more occurrences of summer temperature extremes and drought, is already contributing to widespread browning of forest vegetation in northern boreal zones (Park et al. 2017). Higher summer temperatures and drought stress, increase the susceptibility of boreal forests to insect outbreaks, including the widespread spruce beetle infestation observed across Alaska in recent years (Berg et al. 2006). Drought impacted forests are also much more prone to widespread fire following ignition from lightning strikes (Veraverbeke et al. 2017).

The DoD and surrounding lands in Interior Alaska (Figure 4) include complex gradients of vegetation cover, underlying permafrost, and hydrology. Forested landscapes in this region are dominated by black (*Picea mariana*) and white (*Picea glauca*) spruce and mixed deciduous communities of birch (*Betula papyrifera*), aspen (*Populus tremuloides*) and alder (*Alnus* spp.) (Figure 5). Wetland habitat in Interior Alaska is diverse and abundant, found in both lowland terrain and in foothill microtopography. Wetland types include forested peatland (sphagnum moss communities), open (non-treed) peat bogs and poor to moderate fens (brown moss, *Sphagnum* spp., graminoids and herbaceous species). Some wetlands may be hydrologically isolated, while others are hydrologically connected to surface waters of nearby lakes, streams and rivers. In some cases, the wetlands may have hydric soils year-round but only seasonal (e.g., spring) flooding. These wetlands provide a wealth of ecosystem services and are important for animal habitat, waterfowl migration, nutrient uptake, flood water and carbon storage (Racine 1994). Despite the wet terrain conditions, these lands in Interior Alaska, including DoD terrains, have been characterized by large amounts of live, above-ground forest biomass (Blackard et al. 2008) on the order of 20 – 50 Mg/ha (8.9 – 22.3 U.S ton/acre). A large portion of this landscape remains affected by near-surface (within 1 m depth) permafrost (Figure 6) and the entire domain experiences seasonal freezing of surface soils and water bodies that can often persist from November through mid-April.

The effects of climate change on terrain thermal state, moisture, and vegetation are often non-linear with a myriad of feedbacks to the environment (Beck et al. 2011). Many of these changes are apparent on the landscape, but many major changes have emergent properties that can only be fully detected when assessing landscapes across multiple spatial and temporal scales (Soranno & Schimel 2014). Understanding the indicators of ecosystem change is necessary for recognizing ecological warning signals prior to high impact disturbance events. These feedbacks are likely to have widespread consequences for habitat, human communities, transportation, and infrastructure (Ford et al. 2015; Melvin et al. 2017). Identifying changes in key Earth System Indicator metrics, including vegetation, terrain temperature, frozen or thawed state, and landscape water availability and distribution is necessary for recognizing ecosystem warning signals. This knowledge can better mitigate risk (DoD 2019) by informing the DoD when and where a change in ecosystem condition has occurred. This information is also necessary for U.S.

strategic planning, security, and policy to ensure installation adaptation and resilience (Wuebbles et al. 2017; CRS 2018; DoD 2019). Identifying DoD landscapes undergoing both rapid and abrupt change, or longer, sustained transitions from one state to another is necessary for human adaptation to changing landscape conditions and will provide more informed planning of future development.

Because of the extreme size of Alaska, and the great expanse of DoD lands within the state, remotely sensed measurements from satellites are well suited to provide the most up to date information on terrain properties, and to identify changes in ecosystem state. Although permafrost, vegetation, and hydrology monitoring sites have been established within Alaska, the geographic sparsity of these locations makes it difficult to detect abrupt and subtler long-term shifts in ecosystem state occurring across the domain (Biskaborn et al. 2015). Lack of coverage and inconsistencies in on-the-ground environmental monitoring networks for Alaska, including on DoD lands, have long been recognized and are likely to remain given shortages in state and federal funding (Clark et al. 2010).

Regional Earth System and local ecosystem models can provide projections of landscape vulnerability to change. However, Earth System models can be inconsistent in their projections of future surface and soil moisture conditions (Berg et al. 2017), and changes in ecosystem freeze/thaw and permafrost degradation within Alaska (Mishra & Riley 2014). For example, a recent inter-comparison project for Alaska using 40 ecosystem models reported a lack of agreement in vegetation state, with some models indicating a multi-year loss of vegetation productivity and others showing vegetation greening trends (Fisher et al. 2014). It is also very difficult to verify the output of model simulations over remote landscapes, including Earth System Coupled Model Intercomparison Project (CMIP) simulations over Alaska, given a lack of ground observations (Sun et al. 2015). In addition, Earth System models are not capturing all of the physical changes that are occurring across the landscape, including the persistence of unfrozen soils into the autumn and the effect of this prolonged thawed period on vegetation and greenhouse gas emissions from soil (Commane et al. 2017).

An ideal detection system will identify contemporary state change and trajectories using a suite of spatially continuous observations from satellite remote sensing, combined with on-the-ground measurements whenever possible. Satellite remote sensing will not only provide much needed information on landscape change in Alaska to inform the DoD, it can also help to diagnose uncertainties in Earth System and ecosystem models to make better predictions of current and future ecosystem states (Jorgenson & Grosse 2016; Fisher et al. 2018).

Recent assessments by the DoD indicate that U.S. military lands in Alaska are at risk under a warming climate, and that DoD infrastructure is increasingly under threat from land thaw, floods, droughts and fire (DoD 2019). In order to identify and mitigate risk across the large Alaska domain, this project developed a science-based geospatial framework using satellite remote sensing to identify landscape changes occurring on and surrounding DoD training lands and cantonments.

The framework investigated through this project utilizes a suite of multi-scale satellite remote sensing monitoring platforms to quantify key Earth System Indicators of landscape freeze/thaw state, ecosystem water stress, and vegetation state. This was made possible using multiple data streams VIS-NIR-TIR and microwave remote sensing. For this study we applied statistical time series analysis methodology to identify terrains having significant, longer-term changes in Earth System State Indicators and the general location and timing of abrupt ecosystem disturbances.

We also investigated the use of machine learning for the data fusion of multi-scale and multi-spectral information from satellites to produce new, higher resolution gridded Indicator metric datasets to more precisely detect the locations of changes occurring within the landscape. This geospatial monitoring and detection framework will better support decision making for conservation and training lands management, infrastructure development, and risk assessment across the Interior Alaska DoD domain and elsewhere on Earth. These pilot study protocols were designed to be easily applied to other geographic regions to identify and address ecosystem change.



Figure 1. Locations of U.S. DoD infrastructure across Alaska, including multiple long-range radar and air stations, Air Force ranges and bases (blue circles), Arctic test sites and USARAK Cantonments and cold regions training ranges (black triangles) [*map provided by REPI 2015*].

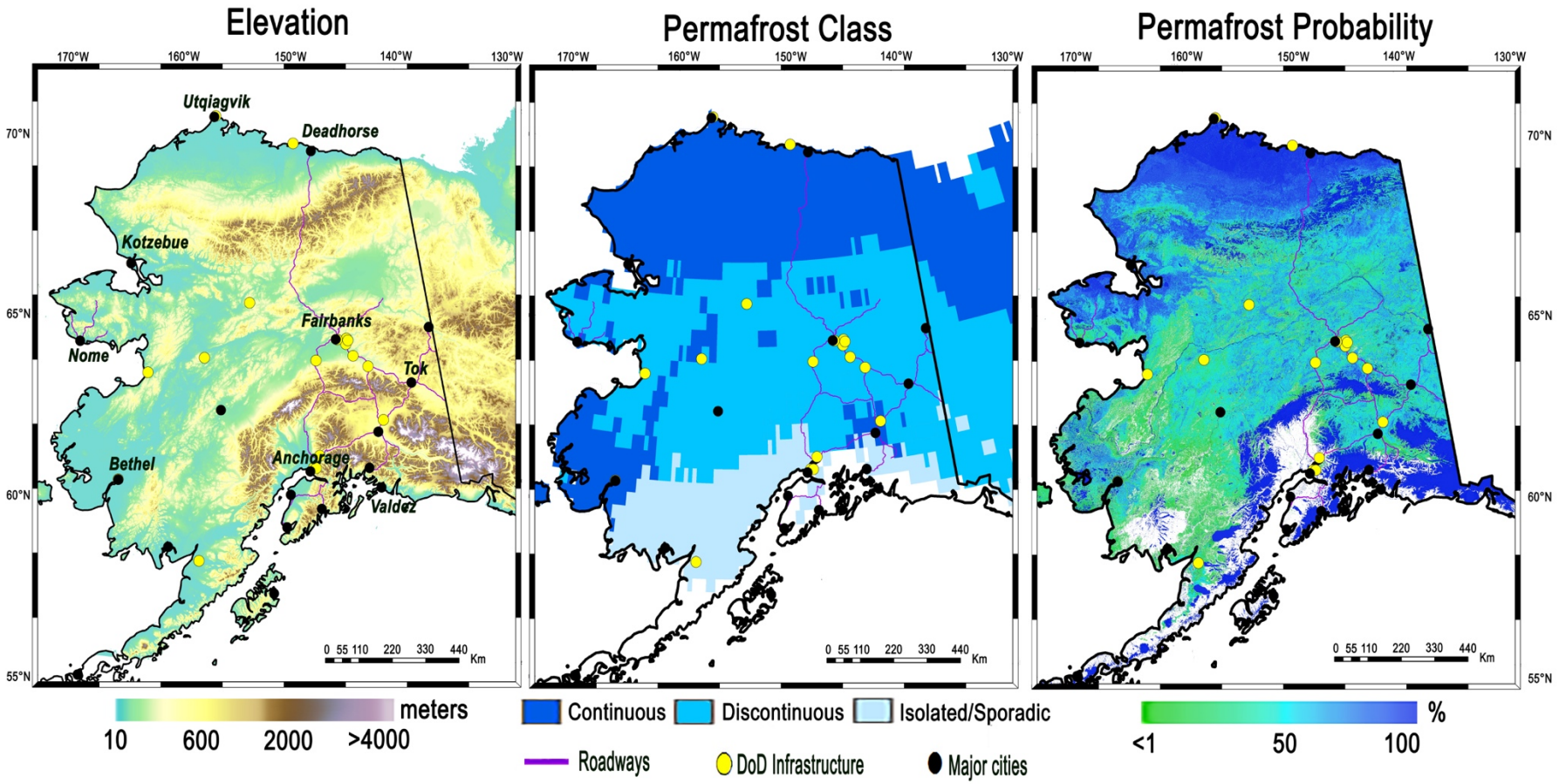


Figure 2. Elevation and permafrost coverage across Alaska, and locations of primary roadways, cities, and DoD managed sites (the yellow circles represent the locations of major infrastructure, which are a subset of those presented in Figure 1). Terrain across the state ranges from the highest point at Denali (6,190 m) to barely above sea level along coastal plains (left panel). The state is largely characterized by the presence of year-round, sub-surface frozen ground (permafrost). Major permafrost classes (middle panel) for the state include continuous, discontinuous and isolated/sporadic. Terrains at higher elevations, and within the colder northern landscapes, have up to a 100% probability of near-surface (< 1 m depth) permafrost coverage (right panel). Near-surface permafrost is minimal to nonexistent in warmer, lower elevation and more southernly regions of Alaska. [*Elevation from USGS SRTM DEM; Permafrost classes from Brown et al. 1997; Permafrost probability is from the USGS Pastick et al. 2015 map*]

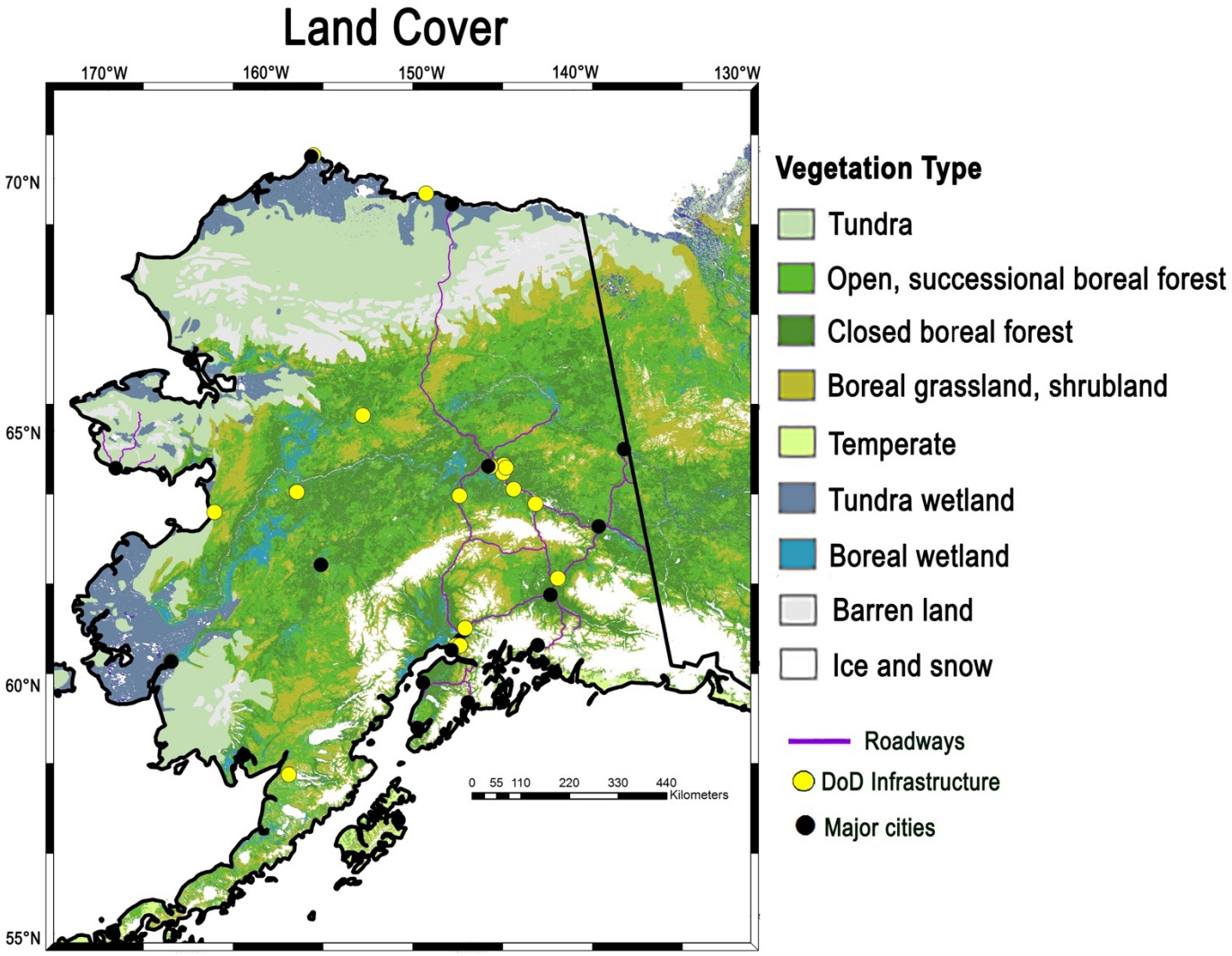


Figure 3. Landcover in Alaska is characterized by predominately black (*Picea mariana*) and white (*Picea glauca*) spruce evergreen and birch (*Betula papyrifera*), aspen (*Populus tremuloides*) and alder (*Alnus* spp.) deciduous forest mixed with fen and bog wetlands in the Interior and southern region. Tundra (vegetation absent of trees) is dominant along western and northern coastal regions. Temperate forest is defined as vegetation where average annual temperature exceeds 3 °C. [*Alaska land cover provided by B. Rogers, WHRC*]

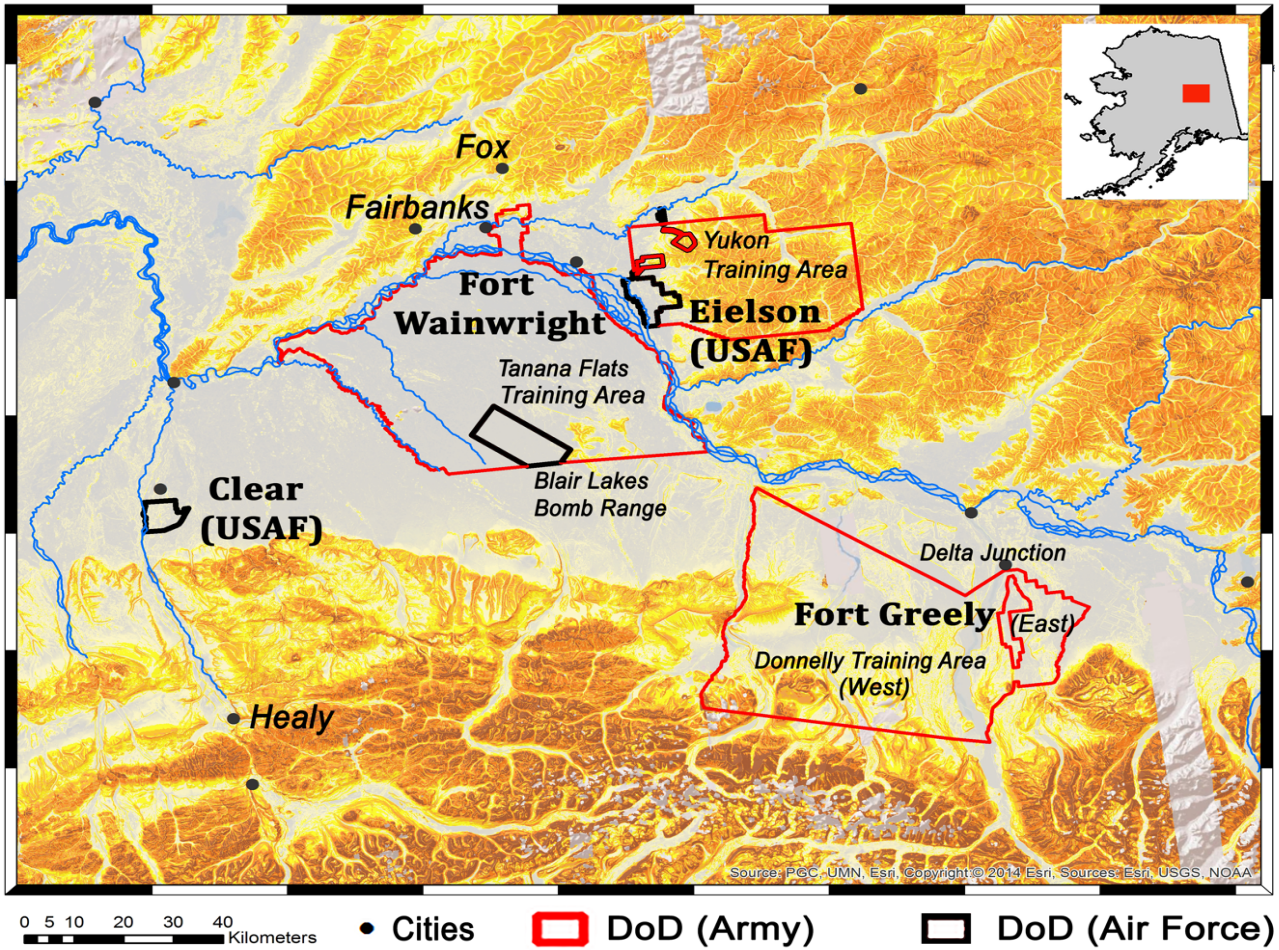


Figure 4. The locations of DoD installations, cantonments and training lands within Interior Alaska. The U.S. Army facilities (red outline) include Fort Wainwright and Fort Greely. U.S. Air Force facilities (black outline) include Clear Air Base and Eielson Air Force Base. Training lands managed by Fort Wainwright include Yukon, Tanana Flats, and Donnelly East and West. Also shown here is the diverse topography across these terrains, ranging from flat lowlands (in gray) to higher elevation foothills (dark orange).

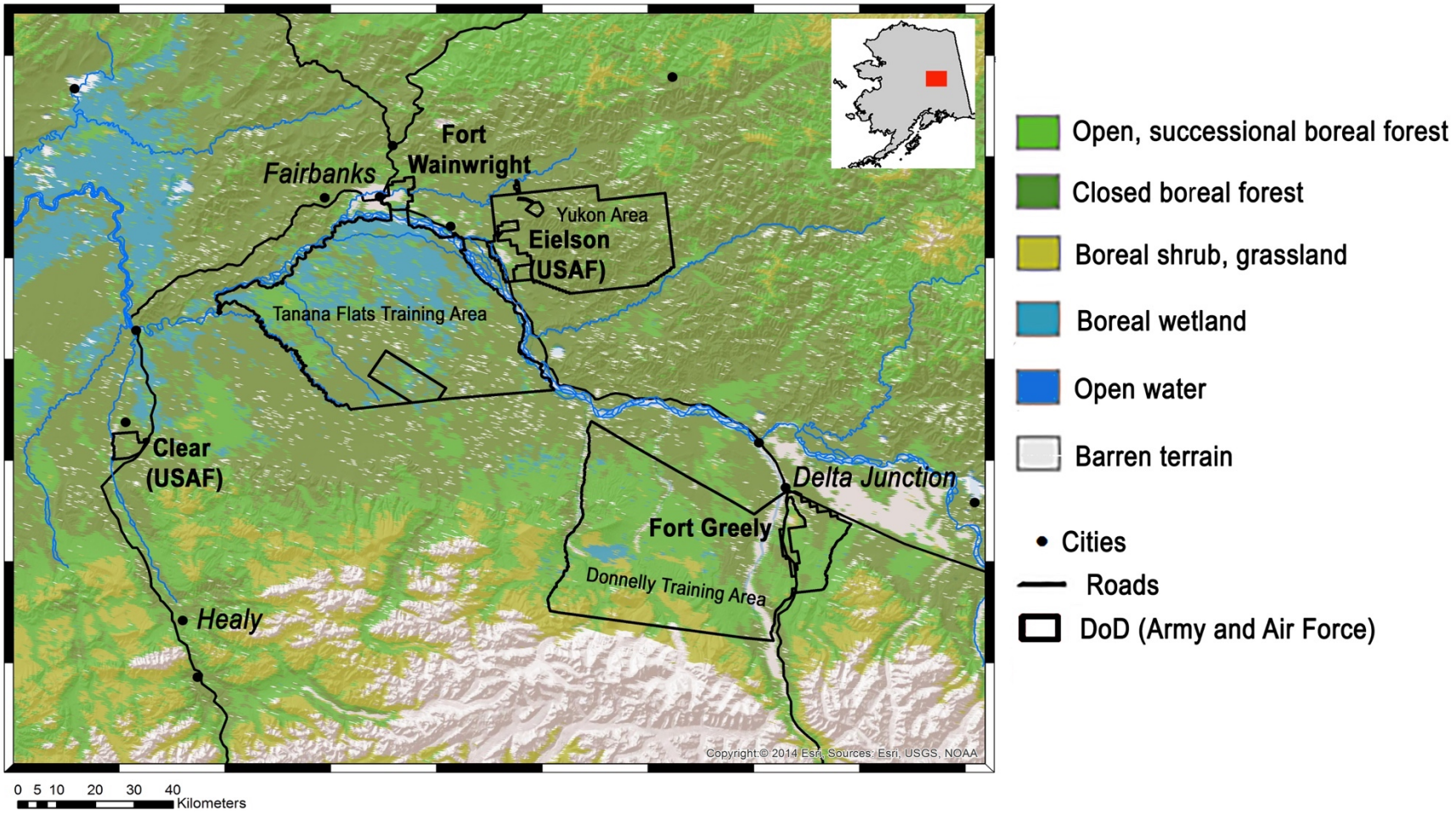


Figure 5. Vegetation types within and surrounding DoD lands in Interior Alaska. Forests are dominated by black and white spruce, birch, aspen and alder. Wetland habitat is also common throughout the landscape. Small ponds, lakes, streams and rivers are abundant. Various wetland types found here include forested peatland and open bog (non-treed peat with sphagnum moss), fen (brown moss and herbaceous) and sedge (*Cyperaceae*) lands. [*Alaska land cover provided by B. Rogers, WHRC*]

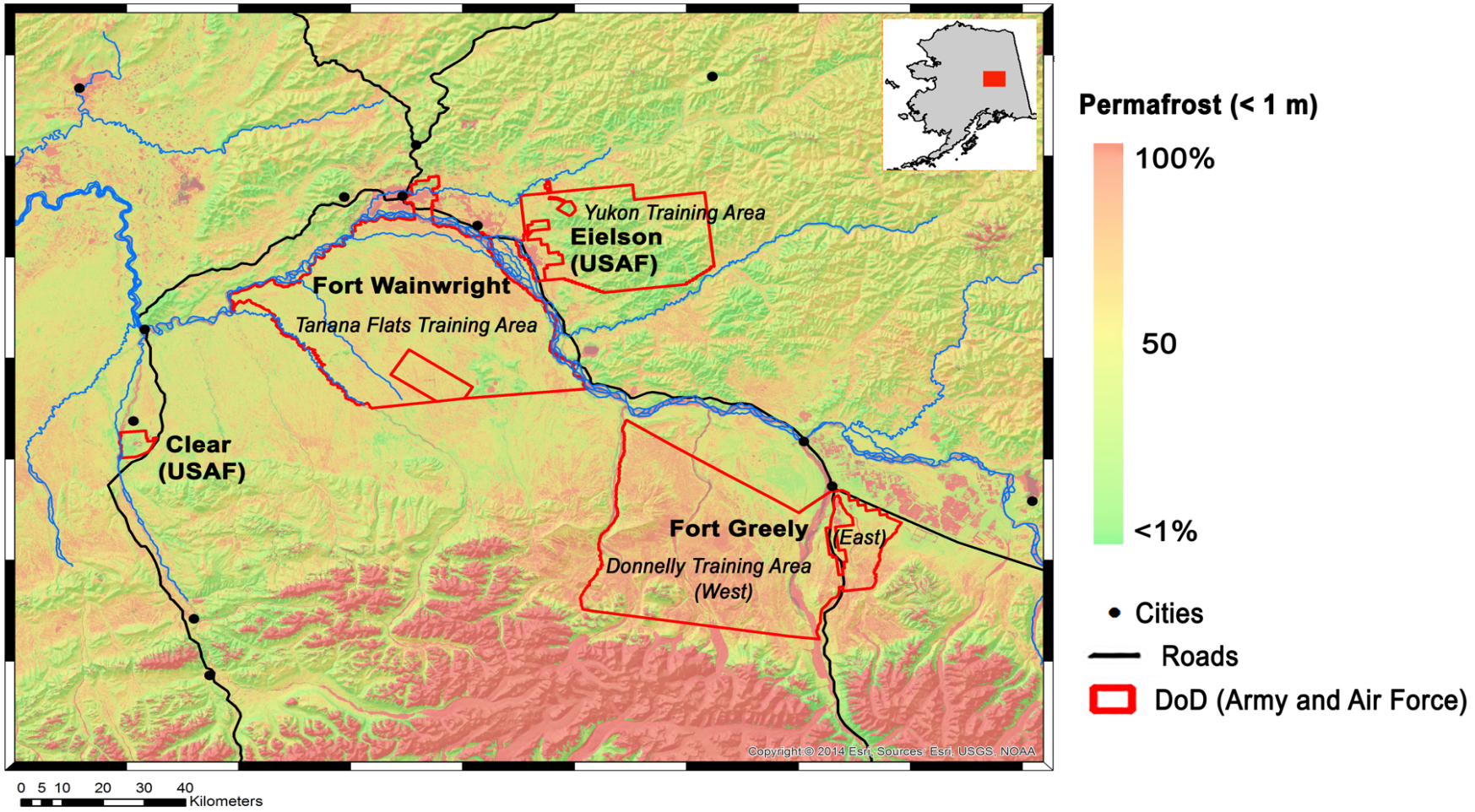


Figure 6. Distribution of near-surface (> 1 m depth) permafrost on and surrounding DoD terrains in Interior Alaska. The probability of near-surface permafrost being present varies from almost 100% in the higher elevations of the Alaska Range, to less than 1% in lower elevation, south facing hillslopes, and very wet lowlands (e.g., portions of Tanana Flats). Note that permafrost deeper than 1 m may still be present where near-surface permafrost is absent. [*Permafrost extent from Pastick et al. 2015*]

Focus of this SEED Project

Our research was designed to address key research needs outlined in the SERDP Statement of Need RCSON-18-L2 to improve understanding of nonstationarity as it relates to environmental shifts at temporal and spatial scales. Our objectives and approaches for the project were as follows:

1) We compiled a multi-year time series database of satellite remote sensing information for Alaska that included imagery from VIS-NIR-TIR and microwave (radiometer and radar) sensors. In addition, we also compiled precipitation and air temperature information from NASA MERRA2 reanalysis.

2) We applied statistical time series trend and monotonic (Mann-Kendall) change detection analyses to the suite of remote sensing and reanalysis data to identify regions in Alaska having experienced significant environmental non-stationarity over the last 16+ years (≤ 2002 through 2017). Our focus was on three Earth System Indicators targeting Terrain Thermal State, Ecosystem Water Stress, and Vegetation State. We applied the Mann-Kendall change detection to all of Alaska, including an Interior Alaska Area of Interest (AOI; Figure S2) encompassing U.S. Army terrains of Fort Wainwright, Fort Greely, Donnelly and Tanana Flats training areas and the Air Force terrains of Clear Station, Eielson Base, and Blair Lakes bombing range (used by Eielson and Elmendorf bases).

3) We applied additional change detection methods to a test region in the Interior AOI to assess the ability of this method to identify the occurrence of abrupt environmental nonstationarity (e.g., fire events) within the 16-year remote sensing observation record.

4) We developed and tested data fusion (downscaling) techniques to integrate multi-scale information from VIS-NIR-TIR and microwave remote sensing to produce improved resolution (30 m; 500 m) gridded maps of landscape freeze/thaw status, surface soil moisture, surface water (incl. land flooding), and vegetation water content. Evaluations of the data fusion test results were conducted for DoD terrains in Interior Alaska.

This integrated geospatial analysis framework, developed and tested during our one-year SEED project, provides a new multi-spectral remote sensing approach to detect changes in terrain states over complex landscapes and at local to regional scales. Identifying regions of terrain nonstationarity using this approach better supports decision making for conservation and training lands management, infrastructure development, and risk assessment across the Interior Alaska DoD domain. This approach is also readily transferable for application over other cold and temperate regions.

Our project was comprised of four primary research focus areas. The first three center around detection and understanding of terrain nonstationarity for Earth System Indicators: 1) Terrain Thermal State; 2) Ecosystem Water Stress; 3) Vegetation State. The fourth focuses on the technical development of data fusion methods for satellite data VIS-NIR-TIR and microwave retrievals to obtain improved resolution Indicators. The research objectives are introduced below. Throughout this report these four technical areas are presented as separate topics and outcomes.

2.1 Indicator 1: Terrain Thermal State

Annual seasonal cycles of transition between frozen and non-frozen (thawed) state are prevalent across northern high latitude terrains. In Alaska, the duration of the winter frozen period varies depending on location. From the North Slope down to the Interior the frozen period can persist from November through April. In autumn and spring, the landscape undergoes a series of relatively abrupt transitions between frozen and unfrozen states prior to full surface freeze (in winter) or thaw (summer). This freeze/thaw period can influence the deterioration of infrastructure, especially those having concrete materials (Vinson et al. 1996; Green et al. 2000; Kraatz et al. 2019). An increase in the number of days that a landscape undergoes transitional freeze/thaw, instead of remaining in a frozen state, also contributes to a thickening of the active layer and furthers warming of the soil. This can lead to warming of deeper soils, permafrost thaw, and ultimately ground surface subsidence (Brown et al. 2000; Qi et al. 2006; Schuur et al. 2008).

A lack of frozen surface is also disadvantageous for winter road travel. Across high northern latitudes, frozen winter conditions allow for easier access to remote terrains that cannot be reached by permanent roadways. Frozen and ice-covered surfaces can support the weight of motor vehicles including snowmobiles and trucks for travel across remote landscapes for recreation and for delivery of supplies and equipment. In Alaska, the DoD relies on frozen winter surfaces for travel by fuel tankers and tactical vehicles to reach difficult-to-access DoD facilities and training lands (USAGA 2018).

Changes in the timing and duration of freeze/thaw and frozen ground conditions can also affect ecological processes including microbial activity and greenhouse gas release from the soil (Natali et al. 2014; Watts et al. 2014; Schuur et al. 2018). Altered periods of freeze/thaw have the potential to trigger an earlier onset of vegetation growing season (Kobayashi et al. 2016) but can also increase vegetation water stress, decrease vegetation carbon assimilation and growth (Cahoon et al. 2018), and increase tree mortality (van Mantgem et al. 2009; Peng et al. 2011).

A study using satellite data from the Scanning Multichannel Microwave Radiometer (SMMR) and Special Sensor Microwave/Imager (SSM/I) indicated that from 1988-2002 there was a trend towards later freeze in evergreen forests in boreal North America by 3.1 days per decade (Smith et al. 2004). Another study using SMMR and SSM/I reported a lengthening non-frozen season of 3.5 days per decade in the northern hemisphere, coinciding with advance in the timing of spring thaw (Zhang et al. 2011). Changes in freeze/thaw state have also corresponded with a significant increase in the above-permafrost active layer at long-term ground monitoring sites in Interior Alaska (Shiklomanov et al. 2012), including at U.S. Army Cold Regions Research and Engineering Laboratory (CRREL) monitoring sites near Fairbanks. Regional advances in the timing of spring snow melt have also been reported across Alaska (Cox 2018) as has an increase in winter thaw and rain-on-snow events (Bartsch 2010; Pan et al. 2018).

Accordingly, two hypotheses framed the Terrain Thermal State research in this study.

Hypothesis 1: The length of the non-frozen season in Alaska, including the Interior, has increased over the past 16+ year (<2002 to 2017) period at a rate exceeding 3 days per decade due to amplified warming, and a shift towards earlier spring melt and delayed autumn freeze.

Hypothesis 2: The frequency of annual winter thaw events has increased in Interior Alaska over the 2002 through 2017 period.

2.2 Indicator 2: Ecosystem Water Stress

Warming at high latitudes and changes in Arctic sea ice cover could have profound implications for the hydrological cycle, including regional increases in precipitation (Kopec et al. 2015). Some regions in Alaska have experienced a lessening of annual precipitation, coinciding with land warming, starting as far back as the 1950s (Dai et al. 2004). Reduced amounts of precipitation, especially in summer, can greatly increase periods of ecosystem drought stress. This increase in drought stress can affect vegetation communities, enhance fuel flammability and increase fire activity within Alaska's forests (Xiao & Zhuang 2007). Fuel flammability is a major concern on DoD terrains because of its impact on training, which is not allowed to occur on DoD lands if terrain conditions are too dry because of the increased risk of fire.

Changes in ecosystem water availability are also influenced by local permafrost conditions and permafrost degradation. Permafrost-affected boreal and tundra communities are characterized by an abundance of wet to saturated soils and small ponds that persist, despite the relatively low levels of precipitation, across terrains where sub-surface drainage is minimized by the presence of frozen ground (Smith et al. 2007). Water loss to the atmosphere in these systems is limited by low rates of evaporation that are restricted by cold temperatures and low energy states (Woo & Young 2012). Thick layers of organic soils and peat cover are also important for maintaining wetlands. The organic materials increase moisture storage capacity, but also provide an insulating blanket shielding frozen soils from surface warming (Woo & Young 2006).

Water is released from ground ice under initial stages of permafrost thaw. This can be followed by thermokarst (hollows produced by melting permafrost) evident by ground subsidence and formation of water-filled pits, troughs, and eventually larger ponds and small lakes (Jorgenson et al. 2006; Jones et al. 2011). As permafrost degradation progresses, and the seasonal active layer deepens, water flow pathways can deepen, increasing the depth and volume of lateral transport of water across the landscape. Eventually, enhanced sub-surface flow associated with permafrost degradation can cause lake drainage, as has been observed in the discontinuous and sporadic permafrost zones in Alaska (Muskett & Romanovsky 2011; Jones et al. 2011) and elsewhere (Watts et al. 2014b). Wetlands are estimated to cover over 40% of Alaska (Hall et al. 1994). In some places within Interior Alaska, a warming, drying climate has already contributed to a loss of boreal wetland extent (Corcoran et al. 2008).

Land surface flooding is a common occurrence across Alaska and other high latitude regions. Snowmelt or rainfall over frozen surfaces can lead to widespread, and sometimes severe, flood events so large they can be observed from space (Watts et al. 2012). In spring, ice-jam floods can occur and increase high water levels along streams and rivers (Turcotte et al. 2017). Extreme flow floods related to snowmelt and summer storms have occurred in recent years in arctic Alaska (Kane et al. 2008). Although flooding can be devastating to infrastructure (Curran et al. 2016), it also provides a water recharge mechanism for thermokarst lakes (McKnight et al. 2008, Jepsen et al. 2015).

Changes in soil moisture and surface water affect local wildlife habitat (Marcot et al. 2015) and vegetation community characteristics (Hollingsworth et al. 2010). Changes in moisture also directly impact ecosystem carbon cycling including vegetation uptake of carbon dioxide (CO_2) and the regulation of greenhouse gas emissions including CO_2 and methane (CH_4) (Douglas et al. 2014; Watts et al. 2014b; Schuur et al. 2018) at high latitudes and globally (Hursh et al. 2016).

Three hypotheses framed the Ecosystem Water Stress research in this study.

Hypothesis 1: Ecosystem water stress has increased across Alaska over the past 16+ years (≤ 2002 to 2017), observed in multi-year decreases in summer and autumn precipitation.

Hypothesis 2: The magnitude of ecosystem water stress has increased within the Alaska Interior, over the past 16+ years (≤ 2002 to 2017), as observed in multi-year drying trends in summer surface soil moisture.

Hypothesis 3: Significant reductions in surface open water (e.g., lakes and ponds) have occurred across Interior Alaska and DoD terrains during this period.

2.3 Indicator 3: Vegetation State

Vegetation in Alaska includes treeless tundra along the permafrost affected coastlines, across the North Slope, and in mountainous regions, to diverse communities of coniferous spruce, understory shrub, and deciduous alder, birch and aspen in the boreal region. Wetlands occur throughout tundra and boreal landscapes and provide valuable habitat for wildlife, flood mitigation and nutrient cycling (Hall et al. 1994). Layers of vegetation cover and thick mats of understory organic debris and moss are important for the development and protection of permafrost in these landscapes and serve to insulate the soil from radiation loading and warming temperatures (Shur & Jorgenson 2007). This protective cover is susceptible to disturbances such as infrastructure development, fire and changes in hydrology.

Changes in vegetation communities are controlled primarily by disturbance and succession. Disturbances occur naturally in the form of fire and changes in hydrology. Very wet environments are dominated by wetland communities and, under colder conditions, tundra. In tundra, a shift to a drier environment can lead to lichen species (e.g., *Cetraria cucullata, Cladina rangiferia*) whereas wetter tundra is dominated by sedges (*Carex* spp., *Eriophorum* spp.) and moss (e.g. *Spagnum* spp). Fire, though infrequent, does occur in the tundra, and the impact to vegetation communities varies depending on the timing, frequency, severity of fire and the loss of organic layer. Sedges may be more resilient to fire, and in some cases lichens and mosses may not reestablish for decades following fire (Racine et al. 1987).

In boreal terrains, vegetation succession is also driven by changes in hydrology and fire. The expansion of wet soil conditions, under earlier-to-mid stages of permafrost thaw, can lead to localized tree mortality and the expansion of wetlands (Roach et al. 2011; Lara et al. 2016). In contrast, continued thickening of the active layer, in more advanced stages of permafrost degradation, deepens the water table, which reduces the extent of soil saturation and wetland habitat (Corcoran et al. 2009) but allows for reestablishment by spruce. However, loss of permafrost can amplify drought stress in black spruce, which are susceptible to changes in soil moisture content given their shallow rooting structure, but provide more favorable habitat for alder, willows and other deciduous communities (Sniderhan & Baltzer 2016).

The earlier thaw period occurring in spring could increase vegetation productivity by expanding the length of annual growing season (Parazoo et al. 2018), especially in tundra (Verbyla 2008). However, a lengthening of the non-frozen season, combined with warmer summers and drier soil conditions, may heighten vegetation vulnerability to drought stress, tree mortality, and wildfire (Chapin et al. 2010; Turetsky et al. 2011; Rogers et al. 2018). Drought stress has also contributed to changes in vegetation productivity observed in forest surveys, with drier forests in Interior Alaska showing longer-term (since 1982) decreases in growth as opposed

to trees occurring along the wetter boreal-tundra ecotones which could indicate a widespread biome shift (Beck et al. 2011). Other records have confirmed vegetation browning across Interior Alaska, but with less extensive browning occurring in forests having experienced an absence of fire in recent years (Ju & Masek 2016).

Two hypotheses for Vegetation State were addressed by this research.

Hypothesis 1: Significant vegetation greening occurred across the Alaska tundra domain over the 16-year (2002 to 2017) study observation period resulting from seasonal warming, an expansion of the annual non-frozen season, and wetter surface conditions.

Hypothesis 2: Vegetation browning occurred throughout Interior Alaska over the 16-year observation period, resulting from a lengthening non-frozen season and a decrease in summer soil moisture.

2.4 Satellite Data Fusion for Earth System Indicators

Remote sensing observations from spaceborne platforms provide continuous, long-term records of Earth System properties and can be used to identify and document changes in land surface features including freeze/thaw state, ecosystem moisture status, and vegetation. Ecosystem monitoring using remote sensing is crucial for identifying and quantifying landscape change (Kaab 2008; Baldocchi 2014). Satellite remote sensing provides almost 50 years of Earth observations that can be used to track decadal changes in environmental conditions across high latitude and global regions (Jorgenson & Grosse 2016). Satellite data provide a foundation to maximize the impact of knowledge gained through field observations by better identifying landscape change across heterogeneous spatial surfaces (Turner 2005; Heffernan et al. 2014).

The suite of remote sensing observations available for Earth System monitoring include multi-resolution retrievals of surface reflectance in the VIS-NIR spectrum, emission in the TIR spectrum, and both active (radar) and passive retrievals in the microwave spectrum. A list and description of available passive and active satellite sensors can be found at NASA Earth Data (NASA 2019). Passive microwave observations, including those used in this study, provide up to twice daily retrievals of northern landscapes but have relatively low spatial resolutions (> 5 km) relative to VIS-NIR-IR retrievals ($\leq$ 1 km). However, microwave retrievals are advantageous especially at northern latitudes because they are insensitive to changing solar illumination (permitting observations during light-limited polar winters), clouds, and smoke contamination of the atmosphere. Radar – active radio detection and ranging sensors - provide profiling of backscattered microwave radiation at much higher spatial resolutions than passive microwave sensors (e.g., radiometers) but with a more limited spatial footprint and terrain coverage.

In this study, we quantified abrupt and longer-term changes in Terrain Thermal State, Ecosystem Water Stress, and Vegetation State using a suite of multi-scale satellite-based VIS-NIR-TIR and passive microwave-based sensors. Applying change detection diagnostics to each remote sensing record individually provides valuable information of shifts in terrain freeze/thaw status, surface water inundation and soil moisture, vegetation water content and greening or browning. However, change analysis results from spatially-coarse retrievals do not readily provide the fine-scale details needed to inform terrain managers. Integrating information from multiple remote sensing platforms through data fusion (downscaling) can provide new, higher spatial resolution Earth System Indicators at scales relevant to land managers and can allow for a more targeted detection of terrain features and changes (Zhang 2010).

Our objective here was to test data fusion strategies, merging VIS-NIR-TIR, passive microwave and radar retrievals to produce higher spatial resolution images of surface frozen or unfrozen conditions, surface soil moisture status, vegetation water content, and surface water inundation (flood detection).

Two hypotheses for Data Fusion were addressed by this research.

Hypothesis 1: The synergistic use of satellite microwave and VIS-NIR-TIR observations allows for enhanced measurements of land surface conditions, enabling high-resolution and near real-time mapping of the Earth System Indicators and supporting assessment of local terrain state, environmental changes, and monitoring of natural disasters.

Hypothesis 2: The heterogeneity of surface hydrologic and thermal conditions governs the spatial distributions of Earth System Indicators, which are likely to be quantified at local scales by exploring surface topography, vegetation information and multi-source remote sensing observations.

3. BACKGROUND

3.1 Terrain Nonstationarity in Alaska

Northern high latitude regions, including Alaska, continue to warm at an accelerated rate relative to elsewhere on Earth (Huang et al. 2017). Across Alaska, this warming is already leading to accelerated thaw and degradation of permafrost, changes in the timing and duration of seasonal frozen period, shifts in surface hydrology, and drought-related stressors on vegetation (Hinzman et al. 2005). Costs to Alaska's public infrastructure resulting from thawing permafrost, land erosion and flooding are estimated at $3.6 to $6.1 billion between now and 2030 (Larsen et al. 2008). In some places, coastal erosion is forcing villages to relocate to more stable land (Bronen & Chapin 2013). These coastal regions are also home to Air Force radar stations and Army National Guard sites (Figure 1). Inland, the risk of extreme fire seasons is increasing with warmer temperatures, drought-stressed vegetation and drier fuels (Trainor et al. 2009; Rogers et al. 2018). Damages to roadways and buildings from flooding, and permafrost-thaw related damages to airports, roadways and pipelines are also occurring, and are expected to worsen over the next century (Melvin et al. 2017). The threat of climate change to Alaska's infrastructure is so great that this was called out explicitly in the Fourth U.S. National Climate Assessment (Jay et al. 2018). Further, a recent DoD report on climate change has stressed that DoD infrastructure in Alaska is under active threat from flooding, permafrost thaw, drought and fire (DoD 2019).

Alaska's ecosystem structure and services are also under threat. It is projected that boreal forests in Alaska will undergo functional and structural changes in the next few decades that have not occurred in the past 6,000 years (Chapin et al. 2010). Ecosystem structure is related to pools and sinks of energy and matter, comprised of abiotic and biotic components, and their relationships to each other. Ecosystem services are the benefits that society receives from ecosystems (Fisher & Turner 2008; Chapin et al. 2015) – food and timber; diversity of wildlife and plant species; cycling of energy, carbon and nutrients; climate regulation through albedo and greenhouse gas exchange; flood regulation; and recreation and tourism, to name a few. Ecosystem resilience is the capacity of an ecosystem to absorb disturbance without shifting to an alternative state and losing function and services (Ives & Carpenter 2007). Climate change is now the dominant and far-reaching driver of ecological change. A changing climate, combined

with local stressors influenced by land use and management, will continue to lessen ecosystem resilience (Côté & Darling 2010). As a result, terrain nonstationarity is likely to increase. Yet, exactly when and where Alaska's biomes and permafrost systems have already undergone shifts, and where changes in ecosystem structure are most rapid, is not well understood (Beck et al. 2011).

3.2 Nonstationarity in Interior Alaska

Interior Alaska is a hot spot of change, most apparent in the more advanced stages of permafrost degradation (Jorgenson & Osterkamp 2005), landscape drying (Parida & Buermann 2014), browning of boreal forests (Parent & Verbyla 2010; Beck & Goetz 2011) and increasing susceptibility to fire (Johnstone et al. 2010). Understanding and quantifying the spatiotemporal nature of these changes is especially important given the location of major U.S. Army and Air Force infrastructure and high latitude training ranges within this region. Fairbanks, located near Fort Wainwright, is also an important transportation hub linking the northern, eastern and southern portions of the state through the Glenn, Richardson, and Dalton highways and regional air traffic.

In addition to the Interior being home to major DoD infrastructure at Clear Air Force Station, Eielson Air Force Base, Fort Wainwright, and Fort Greely, the U.S. Army conducts year-round training over 1.5 million acres (6,070 km^2) of terrain (Figure 4), with a substantial portion of the training lands located within the Tanana River Valley lowland region. These training areas include Tanana Flats (592,699 acres), Donnelly Training Area East and Donnelly Training Area West near Fort Greely (674,128 acres) and the Yukon Training Area (266,891 acres). Tanana Flats Training Area and Donnelly Training Area West are only accessible by air or winter ice roads.

Permafrost warming has been observed at undisturbed sites in the Tanana River region of Interior Alaska since the late 1970s, influenced by warming temperatures, deeper winter snow cover, and an increase in the annual non-frozen period (Osterkamp 2005; Biskaborn et al. 2019). The rate of permafrost thaw is also heavily influenced by local microtopography, vegetation and soil organic matter characteristics, hydrology and disturbance. Fire is a large contributor in the loss of soil organic layers that protect permafrost. The removal of vegetation and organic soil by fire can accelerate a deepening of the active layer and may lead to talik development, which is an unfrozen layer beneath the seasonally frozen soil (Yoshikawa et al. 2002). Local land disturbances, including the clearing of trees and brush near Fairbanks, have also led to permafrost thaw twice the natural thaw rate observed in neighboring forests (Osterkamp 2007).

Changes in surface water have also been reported across Alaska. Permafrost thaw has led to the development of thermokarst ponds and lakes within the Tanana Flats near Fairbanks (Osterkamp 2007). Attributed to increasing water connectivity within the landscape, groundwater flow along the Tanana River has increased by at least 20% from 1963 to 2005 (Walvoord & Striegl 2007). Changes in the distribution of permafrost has also influenced patterns of soil moisture, especially in spring. Interior Alaska terrains lacking permafrost tend to show greater inflow of water from melting snow and spring precipitation into soil layers, whereas water infiltration into the soil column is more limited where the active layer is shallower, increasing terrain vulnerability to surface runoff and flooding (Jones & Rinehart 2010). Generally, ecotone analyses for Alaska show that permanent surface water extent increases with near-surface permafrost coverage (Pastick et al. 2018). Surface water gains in boreal Interior Alaska are also

driven by ice-jam flooding events and recharge of adjacent lake bodies within floodplains (Pastick et al. 2018). Shifts in the timing of spring warmup, snowmelt and surface water flow can affect the timing of ice breakup on rivers, which are important for travel in winter (Bieniek & Bhatt 2011).

These changes in terrain thermal state, hydrologic dynamics and vegetation will have substantial ramifications for how, where, and when the DoD can operate in Interior Alaska. Identifying DoD landscapes undergoing rapid and abrupt change, or longer, sustained transitions from one state to another is necessary for human adaptation to changing terrain conditions and will provide more informed planning of future development (e.g., road-building for the Tanana Flats Training Area) and risk mitigation to existing infrastructure (Vincent et al. 2017; Kraatz et al. 2019). Identifying changes in thaw patterns will help inform the ongoing development of road access to the Tanana Flats Training Area from the recently constructed Tanana River Bridge to the Blair Lakes Range Complex (USAGA 2018). Detecting flooding, especially along the Tanana River (Yarie et al. 1998; DoD 2019), and changes in surface water will help land managers determine regions having greater risk to current and planned infrastructure and where terrains are becoming more problematic for vehicle and troop mobility.

Developing an integrated remote sensing-based monitoring and change detection platform for DoD terrains in the Interior and greater Alaska is critical. Information concerning the occurrence and nature of change is also necessary for U.S. strategic planning, security, and policy to ensure installation adaptation and resilience (Wuebbles et al. 2017; CRS 2018; DoD 2019).

3.3 Remote Sensing Detection of Terrain State

Detection of terrain nonstationarity, including ecosystem state changes and trajectories, across vast and remote landscapes, requires a multi-scale approach using long-term integrated remote sensing (Jorgenson & Grosse 2016). Because in situ observations in these regions are sparse, remote sensing observations from satellites provide the best option for the dense sampling in space and time that is required to characterize ecosystems and terrain disturbances (Schimel et al. 2014). Further, satellite remote sensing and geospatial applications are becoming increasingly important tools for monitoring environments for risk assessment and national security (Vedda 2009) given the wealth of data from multiple sensors now available for Earth System analysis.

Satellite remote sensing is advantageous for a variety of ecological applications that require data across spatial extents that cannot be adequately represented using field-based approaches (Kerr & Ostrovsky 2003). The suite of "big data" provided by satellite remote sensing is being used to track water cycles (Cui et al. 2018), vegetation condition and growth (Xie et al. 2008; Houborg et al. 2015; Jinru & Su 2017) and frozen ground and water characteristics (Westermann et al. 2015; Nolin 2017) at regional and global scales. Remote sensing has also been extremely important in studies of climate change, allowing the detection of phenomena not identified by climate models and on-the-ground observations (Yang et al. 2013).

Remote sensing provides detection of changes across a wide range of the electromagnetic spectrum. Satellite sensors can detect the reflectance of solar radiation from the Earth back into space (e.g., NIR and VIS) and the emission of radiation (TIR and microwave). Passive microwave sensors detect brightness temperatures (*Tb*), which is a measure of the radiance of the microwave radiation traveling upward from the emitting material to the satellite. Active microwave systems measure the signals transmitted by radar and scattered back to the receiver.

Microwave sensing, both passive and active, has the advantage of being insensitive to changes in solar radiation and atmospheric contaminants such as clouds, smoke, and aerosols that can attenuate VIS-NIR-TIR observations.

Earth surface materials have unique spectral reflectance, absorption or emission signatures which are used to characterize terrain states and changes in terrain properties. Resolution is extremely important in remote sensing and geospatial applications (Sabins 2007). With sensor design and satellite orbital positioning, tradeoffs are made between spatial, spectral and temporal coverage. Spatial coverage refers to the spatial area represented by each remote sensing retrieval. Spectral coverage relates to which wavelengths are detected by the sensor. Temporal repeat refers to the frequency, or revisit time, of the detector.

3.3.1. Frozen terrain

Detection of snow and ice cover and properties from satellites (Hall & Martinec 1985; Nolin 2017) has included multi-spectral sensing of VIS-NIR, TIR and microwave emissions or backscatter using satellite platforms. Sensing platforms used to characterize snow and ice using reflective portions of the spectrum (VIS-NIR) have included AVHRR (Advanced Very High-Resolution Radiometer), MODIS (Moderate Resolution Imaging Spectroradiometer) and Landsat (Land Remote-Sensing Satellite System) with multi-band imaging capabilities (Dietz et al. 2012).

The AVHRR sensors have been positioned on satellites TIROS-N (1978- 1980), NOAA-7 through NOAA-14 (1981 - 2013), NOAA-18 through NOAA-19 (2005 through present), MetOp-A and MetOp-B (2006 through present); providing observations with a 1.1 km spatial resolution and a daily revisit. The MODIS instrument is aboard the Terra (1999 to present) and Aqua (2002 to present) satellites, with a 1 to 2-day revisit and spatial resolutions of 250 m (red and NIR), 500 m VIS, 1 km TR). The Landsat series has included the Landsat Multispectral Scanner (MSS; Landsat 1-5; years 1973-2013), Thematic Mapper (TM: Landsat 4-5; 1982 - 2013), Enhanced Thematic Mapper Plus (ETM+; Landsat 7; 1999 – present), Operational Land Imager (OLI) and Thermal Infrared Sensor (TIRS; Landsat 8; 2013 to present) with 30 m shortwave infrared (SWIR) 30 m VIS-NIR, 120 m IR; satellite revisit is 16-day.

Snow and ice profiling and detection of surface frozen state have also been determined using passive microwave remote sensing (McDonald & Kimball 2006; Dietz et al. 2012; Nolin 2017). These include SSMIS (Special Sensor Microwave Imager/Sounder), SMMR (Scanning Multi-channel Microwave Radiometer), SSM/I (Special Sensor Microwave /Imager), AMSR-E (Advanced Microwave Scanning Radiometer – Earth Observing System) and AMSR2 (Advanced Microwave Scanning Radiometer 2). These instruments are radiometers having 1-3 day global revisits, bands of frequencies from 6.63 to 89 GHz and horizontal (H) and/or vertical (V) polarizations. Passive microwave sensing is advantageous for the detection of global freeze/thaw status because of the high temporal coverage and strong sensitivity to changes in dielectric properties at the surface that correspond to frozen and thawed states.

The SMMR was flown on the Seasat and NASA Nimbus 7 satellites (1978 – 1987) and measured dual-polarized microwave radiances at 6.63, 10.69, 18.0, 21.0 and 37 GHz with a posted spatial resolution of 25 km. The SSM/I (1988 to present) provides an update to SMMR and is on board the U.S. Air Force Defense Meteorological Satellite Program (DMSP) Block 5D-2 satellites (19.35, 22.24, 37, 85.5 GHz) with sampling resolutions of 12.5 to 25 km. The SSMIS, successor to SSM/I, is on the U.S. DMSP F-16 through F-19 satellites (2005 – present, except for

the F19 satellite which ended quality retrieval in 2016) and has 24-channels and 21-frequencies ranging from 19.35 to 183.31 GHz and spatial resolutions varying from ~13 to 45 km. The AMSR-E instrument was positioned on board Aqua and was operational from 2002 through 2011. This instrument measured V and H *Tb* at 6.93, 10.65, 18.7, 23.8, 36.6 and 89 GHz with twice daily revisit at high latitudes and at frequency dependent spatial resolutions of 6 km x 4 km to 75 km x 43 km. The AMSR2 sensor is onboard the GCOM-W satellite, also having a twice daily revisit and frequency channels identical to AMSR-E but with the addition of 7.3 GHz and higher spatial resolutions of 6 km x 3 km to 70 km x 40 km.

Radar remote sensing is also used to characterize frozen surface properties (McDonald & Kimball 2005). Radar systems have the advantage of higher spatial resolution detection than passive microwave but at the expense of spatial coverage and revisit time. Information from radar can also require more complex processing and development of dielectric mixing and multi-layer scattering models. An example of Synthetic Aperture Radar (SAR) instruments are the C-band sensors of Sentinel-1A and -1B (two polar orbiting satellites) that offer day and night imaging at 5.4 GHz, multi-polarizations, and resolutions from 40 to 5 m depending on the observation mode. Backscatter from Sentinel 1 C-band has been used to detect frozen soils, having better results in open terrains without vegetation canopy cover (Baghdadi et al. 2018). Lower-frequency microwave observations are suitable for studying vegetated land. For example, the Phased Array L-band Synthetic Aperture Radar (PALSAR) images have been used to generate 100 m freeze/thaw classifications over Alaska (Du et al. 2015).

3.3.2. Surface water

Observations from 30 m Landsat and 250 to 500 m MODIS have been most widely used to monitor regional and global changes in open water lake area (Carroll et al. 2009, 2011; Verpoorter et al. 2014; Fraser et al. 2014). The long-term record from Landsat (from 1984) has also been used to characterize the distribution of water presence and absence for individual 30 m terrain units over a 32-year period (Pekel et al. 2016), which is highly useful for understanding seasonal and interannual variability in flooding and other environmental and disturbance mechanisms that affect water body disappearance and recharge.

Other approaches used for regional surface water analysis include those from active microwave imaging (i.e., radar). For example, C-band data from ENVISAT ASAR (Advanced Synthetic Aperture Radar) has been used to detect changes in open water dynamics at high latitudes (Bartsch et al. 2011) and has the advantage of higher ($\leq$ 150 m) spatial resolution but can be limited by irregular data acquisition intervals, data processing requirements, and problems with backscatter over rough water. Very high resolution ($\leq$ 5 m) VIS imagery from CubeSat has been used to track detailed fluctuations in high latitude lake bodies (Cooley et al. 2019), but this approach is more suitable for shorter term monitoring over smaller spatial domains.

Passive microwave retrievals, though at a coarser ($\geq$ 5 km) spatial resolution, present a useful addition to VIS-NIR monitoring of surface water properties. The microwave retrievals have a strong sensitivity to surface water presence and are not affected by changes in solar illumination and atmospheric contamination. Satellite microwave radiometers such as AMSR-E and AMSR2 provide multi-frequency observations of surface wetness conditions for the past decades (Du et al. 2017) and are better suited to track changes in surface water that might be partially obscured by vegetation, atmospheric contamination and restricted solar illumination. Fractional water metrics obtained from 25 km AMSR-E 18.7 and 23.8 GHz retrievals have been used to detect patterns of surface water wetting and drying across high latitude regions (Watts et al. 2012;

2014b). Records using AMSR-E 89 GHz retrievals have also provided tracking of water body change with an improved 5 km resolution (Du et al. 2016).

Although the Normalized Difference Water Index (NDWI), using ratios of NIR and green reflectance, has been used to track changes in surface water content and drought detection (e.g., Pastick et al. 2018) the observations can be obscured by data dropout through atmospheric contamination and restricted solar illumination, which can be problematic during spring and autumn transitional periods. Satellite microwave observations from AMSR-E and AMSR2 provide daily observations of surface moisture (Du et al. 2017) that are unaffected by data dropout during the shoulder seasons.

3.3.3. Vegetation

For VIS-NIR retrievals, the normalized difference vegetation index (NDVI) has been widely used to detect the difference between NIR (around 0.86 μm), which healthy, "green" vegetation strongly reflects, and red light (around 0.66 μm) which the photosynthetic pigment chlorophyll strongly absorbs (Pettorelli et al. 2006). Records of NDVI from satellite sensors have been useful for detecting patterns of multi-year vegetation greening and browning for Alaska (Goetz et al. 2005; Verbyla 2008; Parent & Verbyla 2010) and globally (de Jong et al. 2011). Although moderate to high resolution (30 m to 1.1 km) observations from AVHRR, Landsat and MODIS are most commonly used to detect changes in vegetation at regional scales because of the longer term data record. Some studies are also using very high resolution (< 4 m) imagery (e.g., from WorldView2 and PlanetScope satellites) to track changes in boreal cover for more local study applications (Loranty et al. 2018).

While NDVI is optimal for tracking changes in vegetation greenness, it does not provide a measure of vegetation water content which is important for detecting changes in plant growth and potential plant water stress. Instead, the NDWI for vegetation uses combinations of SWIR and NIR spectral reflectance's to monitor leaf water content (Fuentes et al. 2001). A more direct method for monitoring change in canopy water content is provided by vegetation optical depth (VOD), derived from daily passive microwave remote sensing at 10.7 and 18.7 GHz but at a coarser 25 km resolution (Jones et al. 2011). Satellite VOD has shown greater sensitivity to changes in leaf water content, including those occurring during the seasonal changes in photosynthesis and following drought stress, relative to optical and infrared methods (Jones et al. 2011). The daily VOD indicator has also tracked well with vegetation growth and post-fire recovery in boreal forests and is advantageous at high latitudes where cloud and smoke contamination are common (Jones et al. 2013).

4. MATERIALS AND METHODS

Introduction and Scope

The objective of this one-year SERDP-funded SEED project was to detect—using a suite of multi-spectral and multi-resolution observations from satellite remote sensing—terrain nonstationarity occurring across Alaska, with a more focused look at terrains on and surrounding DoD lands in the Interior. This study was designed to integrate observations from VIS-NIR-TIR and microwave remote sensing to detect shifts in three key Earth System Indicators focused on Terrain Thermal State, Ecosystem Water Stress, and Vegetation State.

Statistical trend analyses were applied to the suite of remote sensing observations to identify terrains showing longer-term or abrupt shifts in ecosystem state. The project also employed machine learning to integrate high temporal frequency passive microwave retrievals with higher spatial resolution VIS-NIR-TIR observations to examine the feasibility of generating new, spatially-improved Earth System Indicator time series over DoD terrains. Although these change detection and data fusion (downscaling) methodologies are demonstrated for Interior Alaska, they are designed to be globally applicable, using methodology transferable to other regions.

4.1 Satellite Retrievals

4.1.1. Terrain thermal state

We used microwave information from SMMR, SSM/I, SSMIS, AMSR-E and AMSR2 to detect daily changes in terrain surface frozen or non-frozen state across Alaska. The integrated SMMR, SSMI/I and SSMIS database provided observations over a 39-year record from 1979 to 2017. The integrated AMSR-E and AMSR2 database provides a 15-year record from 2002 to 2016 for Freeze/Thaw and a 16-year record (2002 to 2017) for surface air temperature. In addition to the microwave data, we also examined the MODIS TIR land surface temperature record (2002 to 2017) and regional air temperatures from NASA's Modern-Era Retrospective analysis for Research and Applications, Version 2 (MERRA2) and AMSR-E/AMSR2. Snow cover phenology, including melt onset, snowoff and duration were obtained from SMMR, SSM/I and SMMIS multi-frequency observations from 1988 through 2017.

The microwave Freeze/Thaw record represents years of algorithm development and refinement provided by the Numerical Terradynamic Simulation Group (NTSG) at the University of Montana. Development of this record has been made possible through the NASA MEaSUREs (Making Earth System Data Records for Use in Research Environments) program with the recognition that ecosystem Freeze/Thaw is a critical regulator of permafrost state, and strongly influences hydrology, vegetation, and other biological processes.

The NTSG MEaSUREs Freeze/Thaw record was first developed using single channel classifications of 37 GHz, V-polarization *Tb* from SSM/I, linked to in situ air temperature measurements from a global weather station network (Kim et al. 2011). The Freeze/Thaw algorithm applies a threshold-based method that exploits the *Tb* responses to differences in landscape dielectric content. The database was then updated to include observations from SMMR to extend the dataset back to 1979, with Freeze/Thaw state provided twice daily using morning (AM) and evening (PM) overpass retrievals at a 25 km spatial resolution (Kim et al. 2012). Version 4 of the Freeze/Thaw record is now available (Kim et al. 2017a, 2017b). The Version 4 record completes the series by producing a consistent and continuous global daily record of landscape freeze/thaw from 1979 to the present and including observations from SSMIS (Kim et al. 2017a). A similar approach was applied to AMSR-E/AMSR2 observations to generate 25 km and 6 km Freeze/Thaw products for the Northern Hemisphere over years 2002 to 2017 (Kim et al. 2018).

The AMSR Freeze/Thaw record was developed for the northern hemisphere over years 2002 to 2017 using observations from AMSR-E and AMSR2 (Kim et al. 2018). The AMSR Freeze/Thaw record uses V-polarization *Tb* observations from 36 GHz to provide indication of terrain frozen or non-frozen status for individual AM and PM overpasses, or combined daily overpass at a 6 km spatial resolution.

Detection of snow and snow melt onset date (Pan et al. In Prep) was provided through 19 and 37 GHz evening *Tb* retrievals at H- and V polarizations from the NASA MEaSUREs Calibrated Enhanced-Resolution Passive Microwave Daily EASE-Grid 2.0 Brightness Temperature ESDR, available at the National Snow and Ice Data Center (NSIDC) (Brodzik et al. 2016). This data record is a temporally extensive consortium of images from multiple sensors including SSM/I and the SMMIS (Brodzik et al. 2018). The image reconstruction retrievals were used to produce an enhanced resolution of 6.25 km x 6.25 km (19 GHz) and 3.125 km x 3.125 km (37 GHz) *Tb* data (Long and Brodzik 2016). The resulting snow products have a spatial resolution of 6.25 km x 6.25 km. A gradient ratio polarization (Dolant et al. 2016, Pan et al. 2018) and *Tb* differencing approach (Wang *et al* 2013, 2016) were then used to detect the main melt onset date (MMOD) and snowmelt duration (SMD) from 1988 to 2016. A 19 GHz and 37 GHz V *Tb* differencing was also used to detect snowoff (Metsämäki et al. 2018), defined here as the last day of snow, prior to the landscape becoming completely snow free for the season (Pan et al. In Prep).

The MODIS Land Surface Temperature record provides daily, global observations of land surface temperature (in Kelvin) from 2002 to present. For this study, we used MY11A2.006 observations from Aqua (Wan 2008). Land surface temperature retrievals are derived from MODIS TIR under clear-sky conditions using a split window algorithm (Wan & Dozier 1996). The split window algorithm considers TIR emitted from the land surface, in addition to emissivities estimated from various land cover types and relates these to air surface temperature and column water vapor. Coefficients for the split window algorithm are obtained from a regression analysis of MODIS simulation data created from atmospheric radiative transfer (using MODTRAN4 from the Air Force Research Laboratory; Berk et al. 2000) under wide ranges of surface and atmospheric conditions (Wan 1999).

The MODIS Normalized Differenced Snow Index (NDSI) provides daily snow cover (0-100) from 2002 to present (Hall et al. 2016). We used the MYD10A1.006 observations, in addition to MODIS derived land temperature, as a predictor for machine learning algorithms used to downscale Freeze/Thaw since snow cover and land temperature should be tied to patterns of frozen-transition-thawed conditions on the ground.

The AMSR air temperature product was developed through the NTSG AMSR Land Parameter program. This record was first developed using AMSR-E K band 18.7 and 23.8 GHz H- and V-polarized *Tb* and provides retrievals of daily minimum (from 1:30 AM overpass) and maximum (from 1:30 PM overpass) surface air temperatures (in Kelvin) at 2 m height and 25 km resolution (Jones et al. 2007; Jones et al. 2010b). The NTSG UMT Land Parameter Data Record (LPDR) uses a satellite observed microwave land emission algorithm that is theoretically described by components representing the upward emission of the atmosphere, land surface upward emission attenuated by the atmosphere, and downward atmosphere emission reflected by the land surface and attenuated by the atmosphere (Du et al. 2017b). The initial AMSR-E record has been updated to include AMSR2, providing long-term daily observations from 2002 to present (Du et al. 2017b).

The MERRA2 temperature product represents air temperature over land and water at a 2 m height, provided by the NASA Global Modeling and Assimilation Office (GMAO) reanalysis at an approximate 0.5° x 0.625° (around 55.8 x 69.8 km) spatial resolution and covering a period 1980 to present (Gelaro et al. 2017). The GMAO data assimilation incorporates NASA Earth Observing Satellite observations within an Earth System model framework to provide a gridded climate record for atmosphere and land. For this analysis, 3-hourly observations of air

temperature from the MERRA time averaged two-dimensional collection statD_2d_slv_Nx (M2SDNXSLV) single-level diagnostics were averaged to daily (T2MMEAN) from 1989 to 2017.

4.1.2. Landscape water stress

We used passive microwave information from AMSR-E and AMSR2 to detect daily changes in terrain soil moisture and fractional surface water inundation over Alaska for a 16-year period (2002 to 2017). In addition, we looked at higher spatial resolution retrieval records over the same period from the MODIS Land Surface Water Index (LSWI). Daily precipitation records were obtained from NASA GMAO MERRA2 reanalysis. For the data fusion analysis, we used the Landsat Water Occurrence Dataset (WOD) record, which incorporates time series of sensor retrievals from 1984 through 2015 (Pekel et al. 2016). Finally, retrievals from Sentinel-1 SAR were used in the development of a high-resolution inundation (flooding) classification product.

Surface volumetric soil moisture daily profiling was obtained from the NTSG UMT LPDR and is derived from X-band (10.7 GHz) AMSR-E and AMSR2 *Tb* observations from 2002 through 2017 at a 25 km spatial resolution (Du et al. 2017b). The multi-frequency UMT microwave retrieval algorithm calculates surface soil moisture (cm^3 cm^{-3}) after correcting for X-band atmosphere, surface water inundation and vegetation effects. The LPDR record has been updated from previous records (Jones et al. 2010) to include an improved vegetation correction using a dynamic selection of vegetation scattering albedo (Du et al. 2017b).

Surface fractional water inundation (Fw) with a 25 km resolution was also obtained daily from the NTSG UMT LPDR record using AMSR-E and AMSR2 H-and V-polarized 18.7 and 23.8 GHz *Tb* retrievals (Du et al. 2017b, c). Fw (dimensionless; 0-1) is the proportional surface water cover within equal area grid cells and can include open water lakes, ponds, rivers and flooded wetlands having minimal vegetation canopy. To obtain Fw, the UMT retrieval algorithm applies a forward radiometric *Tb* model to interactively estimate inundation, air temperature, and vegetation optical depth (Jones et al. 2010b; Watts et al. 2012). In addition to the 25 km Fw record, this study also evaluated a 5 km Fw product using 89 GHz *Tb* from AMSR-E and ancillary inputs (i.e., land cover) from MODIS (Du et al. 2016). The 5 km record provides 10 day repeat monitoring and is available from 2002 to 2015. The 89 GHz (W band) record is more sensitive to open water with relatively minimal detection of surface water within vegetated surfaces.

MERRA2 precipitation was obtained through the NASA Global Modeling and Assimilation Office (GMAO) reanalysis at an approximate 0.5° x 0.625° spatial resolution and covering a period 1980 to present (Gelaro et al. 2017). Daily total precipitation observations (kg m^{-2} s^{-1}) were obtained from the MERRA time averaged two-dimensional collection (JRA-55.atmos) precipitation flux for the 1989 to 2017 period.

Information from the WOD (Pekel et al. 2016) was used in this study to provide downscaled high-resolution water maps from original 25 km AMSR-E and AMSR2 retrievals for select sites in Interior Alaska. The WOD takes into account 32 years of observations from TM, ETM+ and OLI sensors and describes the frequency of land surface water occurrence at a 30 m resolution. The Landsat occurrence intensity maps summarize the location and persistence of surface water and describes how frequently water returned to a location from one year to another.

To investigate using C-band retrievals from Sentinel-1 to classify and map surface water at high spatial resolutions, SAR images were obtained for two locations in Interior Alaska, centered on the Tanana River Bridge and Jarvis Creek areas for select dates of May 11, 2017; August 13, 2017; August 14, 2016; October 12, 2017. Mode options for the SAR retrievals included stripmap (SM) and interferometric wide (IW) with varying spatial resolutions and polarizations (Table 1) and a revisit period of 6 to 12 days.

Table 1. Configurations of Sentinel SAR images used in this study.

Sentinel-1A/B SAR (5.405 GHz; since 2014)			
Mode	**Resolution**	**Polarization**	**Revisit**
SM	9x9 m/23x23 m/84x84 m	HH+HV, VV+VH,HH, VV	Observation on request
IW	20x22 m/88x87 m	HH+HV, VV+VH,HH, VV	6-12 days

4.1.3. Vegetation

We used the NDVI from MODIS to detect changes in the state of vegetation greening, from 2002 to 2017. Over the same period, daily retrievals of VOD from the NTSG UMT LPDR record were used to determine vegetation water content.

The MODIS NDVI product (MYD13A1.006) provides 16-day retrievals at a 500 m resolution (Didan et al. 2015) and is available through the NASA Land Processes Distributed Active Archive Center. All MODIS NDVI data used a bit flag of 0 which represents good data with high confidence. The NDVI observations are obtained as a normalized ratio of the NIR and red reflectance bands (Eq. 1):

$$NDVI = (NIR - Red)/(NIR + Red) \quad \text{(Eq. 1)}$$

The daily VOD observations were derived from X-band (10.7 GHz) H- and V-polarized *Tb* observations from AMSR-E and AMSR2 from 2002 through 2017 at a 25 km spatial resolution (Due et al. 2017b) and were provided through the UMT LPDR record. The VOD represents the slant-path opacity of vegetation layers to land surface microwave emissions (Du et al. 2017b). The retrieval algorithm for VOD takes into account simultaneous information on surface temperature and atmospheric water vapor to determine canopy attenuation of the microwave signal, which is influenced by vegetation biomass and water content (Jones et al. 2009; Jones et al. 2011)

4.1.4. Ancillary data

Additional datasets were used in this analysis for the regional change assessments or for the investigation of data fusion methods (Table 2). These include digital elevation model (DEM) estimates of elevation, slope, aspect and topographic position index (TPI) from the USGS Global Multi-resolution Terrain Elevation Data 2010 (GMTED2010), which is primarily derived from retrievals from the NASA Shuttle Radar Topography Mission (SRTM) and Satellite Pour I'Observation de la Terre (SPOT 5) (Danielson & Gesch 2011), and the global Digital Surface

Model (DSM) dataset generated by JAXA ALOS imagery (Theobald et al. 2015; Tadono et al. 2016); the DEM resolution is 7.5 arc seconds, or approximately 250 meters. The 30 m DSM generated by JAXA ALOS was also used in the study (Tadono et al. 2016).

Spatial coverage of permafrost terrains was obtained from three databases. The first is the International Permafrost Association Circum-Arctic map of permafrost and ground-ice conditions (Brown et al. 1997) which provides the spatial extent of general permafrost classes: continuous, discontinuous, sporadic, and isolated and is a compilation of various permafrost maps. The second, which is provided by the USGS and indicates the probability of near-surface (> 1 m depth) permafrost at a 30 m resolution (Pastick et al. 2015), combines remote sensing and field observations through machine learning.

Regional vegetation characteristics were obtained from the 30 m U.S. National Land Cover Database 2011 for Alaska, based on TM and ETM+ retrievals from Landsat (Selkowitz & Stehman 2011; Jin et al. 2013), and 500 m MODIS land cover dataset (MCD12Q1). Landscape percent tree cover was obtained from the 30 m Global Land Cover Facility tree dataset, derived using 250 m MODIS and circa- 2000 and 2005 Landsat images (Sexton et al. 2013).

Regional vegetation characteristics over Alaska (provided by B. Rogers; WHRC), used for nonstationarity trend summary statistics, were derived a vegetation mask using the 2005 Land Cover of North America product (250 m; CCRS 2013; Pouliot & Latifovic 2013; Pouliot et al. 2014), MODIS land cover type with International Geosphere-Biosphere Programme classification (Collection 5; year 2005; 500 m; Friedl et al. 2010), long-term climate (1950 – 2000; ~1 km; Hijmans et al. 2005) and the Circumpolar Arctic Vegetation Map (CAVM 2003), all re-gridded to MODIS sinusoidal 500 m resolution. Boreal vegetation was distinguished from temperate using a mean annual temperature threshold of 3°C, as recommended in Wolfe (1979) and implemented in Rogers et al. (2015).

Fire history was provided by the Alaska Large Fire Database (ALFD; Kasischke et al. 2002; Jandt 2015) product. Fires recorded in the ALFD are derived from historical fire reports starting in 1950; the database is maintained through present by the Alaska Fire Service. The ALFD was used to determine years where a burn occurred and the areal extent of a specific burn event.

The United States Geological Survey (USGS) daily river discharge measurements (https://waterdata.usgs.gov/nwis/) for the Tanana river (Site No. USGS 15515500) were used for identifying dry and wet periods and analyzing the high-resolution inundation changes derived from Sentinel-1 SAR images. Daily soil moisture of the top 2-inch soil layer was measured from a SNOTEL site (Name: Granite Crk; Site number: 963; longitude -145.4^{o}, latitude 63.94^{o}) near Fort Greely for initial evaluations of satellite 25 km products and 500 m downscaled soil moisture. In addition, we also tested and evaluated our SAR inundation mapping approach over Addicks/Park Ten and George Bush Park of Houston, Texas for August 30, 2017 during the flood event caused by Hurricane Harvey (Du et al. 2019) as part of a collaborative effort with an ongoing NTSG project. For this evaluation, high quality and high resolution (< 1 m) NOAA aerial photos were used to assess the relative accuracy of the radar inundation mapping algorithm (https://storms.ngs.noaa.gov).

Table 2. Ancillary datasets used in this analysis. These include indicators of terrain topography, permafrost, vegetation and burn disturbance.

Variable	Resolution	Source
DEM		
Elevation	7 arc-seconds	Danielson & Gesch, 2011
Slope	7 arc-seconds	Danielson & Gesch, 2011 Tadono et al. 2016
Aspect	7 arc-seconds	Danielson & Gesch, 2011
Topographic Position Index	7 arc-seconds	Danielson & Gesch, 2011 Theobald et al. 2015
Slope	30 m	Tadono et al. 2016
Permafrost		
Permafrost Class	1:10,000,000	Brown et al. 1997
Permafrost Probability	30 m	Pastick et al. 2015
Vegetation		
Alaska Land Cover	500 m	Rogers et al. (WHRC)
Tree Cover	30 m	Sexton et al. 2013
Burn Area		
Alaska Large Fire Database	Polygon	Jandt, 2015

Table 3. Reclassification of land cover types from the Rogers et al. Alaska land cover map to provide a generalized land cover for this study. "*Removed*" designates a cover type that was not evaluated in the summary statistics.

Original Land Cover Type	New Class
Water	Water
Tundra	Tundra
Mountain/Barren	*Removed*
Wetland	Wetland
Open/Successional Boreal Forest	Boreal Forest
Closed Boreal Forest	Boreal Forest
Boreal Wetland	Wetland
Boreal Grasslands/Shrublands	Grass/Shrub
Ice/Barren	*Removed*
Cropland	*Removed*
Urban	*Removed*
Temperate Vegetation	Temperate Vegetation
Savannas	Shrub/Savanna
Permanent Wetlands	Wetland

4.2 Time Series Analysis

4.2.1. Mann-Kendall trend test

To identify and characterize heterogeneity in landscape change, a Mann-Kendall test was applied, on a per grid-cell basis, to each remote sensing or reanalysis dataset used to characterize Terrain Thermal state, Ecosystem Moisture Stress and Vegetation State. Mann-Kendall is a non-parametric and monotonic statistical time series trend detection method which accounts for and removes serial correlation prior to determining trend significance (Yue et al. 2002; Watts et al. 2014b). Non-parametric indicates that the estimator does not draw from any particular probability distribution and is ideal when detecting change over diverse and complex datasets that can be non-gaussian or otherwise exhibit atypical data distributions. A monotonic response describes a trend that is consistently increasing or decreasing over the time interval. The Mann-Kendall trend test provides information about whether significant change has occurred, and also the magnitude and direction of change, as characterized by the Theil-Sen slope. The Theil-Sen median approach to determining rates of change is robust to outliers and heteroscedastic error that can plague ordinately least squares parameter fitting (Ohlson & Kim 2014).

A Mann-Kendall trend test using prewhitening (removal of autocorrelation) was applied to the remote sensing products described in section 4.3 using the 'Zyp' package (Bronaugh et al. 2013) and the R statistical computing system (R Core Team 2018). This occurred for three distinct seasons: 1) Spring (Julian days 105 to 151; April 15 to May 31); 2) Summer (Julian days 152 to 243; June 1 to August 31); 3) Autumn (Julian days 244 to 288; September 1 to October 15). Mann-Kendall tests were evaluated across the annual means within each of these three seasons for all variables except for those related to Freeze/Thaw status, where trend tests were evaluated across annual sums. Additionally, Freeze/Thaw trends were also evaluated in the winter (Julian days 319 to 74).

Once the Mann-Kendall tests were applied, grid cell locations having significant trends detected at a $\alpha <= 0.10$ (90% probability) level were flagged. In addition to the gridded maps of change for terrain state that were produced through this analysis (geoTiff format), we also created geographic polygon boundaries (in shapefile format) outlining the locations of grid cells having significant positive or negative trend.

The Mann-Kendall tests, and the flagging of grid cells according to trend significance, were performed for the entire Alaska domain. Statistical summaries of the trends were then provided over three distinct areas of interest:

- All of Alaska.
- A 200 km buffer surrounding Interior Alaska DoD terrains, hereafter termed the Interior Alaska Area of Interest (AOI).
- All DoD lands in Interior Alaska including Fort Wainwright, Fort Greely and Eielson AFB, Yukon Training Area, Tanana Flats Training Area, Donnelly Training Area.

Segmenting these locations allowed us to determine and compare how much terrain area had undergone significant change within specific land regions, and to better characterize the direction of change. In our reporting of the Mann-Kendall results for Alaska, we reference specific ecoregions presented in Supplemental Figure 1 (Figure S1).

4.2.2. Break point analysis

In addition to the Mann-Kendall trend test, we also evaluated the use of a secondary screening for non-stationarity. This secondary screening, the Breaks for Additive Seasonal Trend (BFAST) time series (Verbesselt et al. 2010; Verbesselt 2014), decomposes the multi-year time series record into trend components, and then estimates the timing, magnitude, and direction of change events in a time series. BFAST works by applying an additive decomposition model to iteratively fit a piecewise linear trend and seasonal model to a time series. The model considers the determined trend component, the seasonal component, and a remainder component, which is the variation in the data beyond the trend and seasonal component (Verbesselt et al. 2010). The BFAST algorithm also applies an ordinary least squares residuals moving sum test to determine the occurrence and location of breakpoints in the time series.

After preliminary evaluation it was recognized that a full regional application of BFAST on a per-grid cell basis would be very computationally intensive. This application would require the development of semi-automation for the algorithm, which is outside the limited scope of this SEED study. For this study, we instead explored the application of BFAST for a known disturbance (burn) in Interior Alaska. This allowed us to compare non-monotonic break point disturbance characteristics that might be detected by BFAST, but not by the Mann-Kendall approach.

4.3 Satellite Data Fusion (downscaling)

4.3.1 Overview of approach

Passive microwave-based satellite sensors can provide daily retrievals that are advantageous over SWIR-VIS-NIR-IR images because of insensitivity to variability in solar illumination and atmospheric contaminants, and high sensitivity to changes in water and thermal states. However, these observations are limited in their ability to characterize smaller, and more localized, changes in terrain state given the coarse spatial resolutions of the retrievals. To overcome the limitations of coarse resolution data from passive microwave, downscaling techniques can be applied to provide finer resolution datasets (Atkinson 2013; Peng et al. 2017).

In this study we used data fusion, combined with machine learning, to produce four higher-resolution microwave-derived Earth System Indicator metrics: 1) Freeze/Thaw; 2) surface soil moisture; 3) VOD; 4) open water. The first three metrics were produced at a 500 m resolution, which is the native resolution of the MODIS predictors used in the downscaling. The final metric, open water, was derived using retrievals from Sentinel-1 SAR. All downscaling was implemented with a Random Forest algorithm (Brieman 2001; Breiman & Cutler 2018) in Google Earth Engine (Gorelick et al. 2017) using regression trees (metrics 2 and 3) and classification trees (metrics 1 and 4).

The use of Random Forest was motivated by the success of other studies using data fusion to downscale soil moisture data from coarser microwave retrievals (Im et al. 2016; Peng et al. 2017). Random Forest uses bagging (sampling with replacement) to form an ensemble of decision trees (classification or regression), thereby creating a forest (Watts & Lawrence 2008). Classification and Regression Trees (CART) form the basis of the Random Forest. The CART algorithms for machine learning split a dataset based on the homogeneity of the input data. CART operates by assessing all input explanatory variables and determining which binary divisions of data best reduce deviance in the response variable (Lawrence & Wright 2001). The

data are recursively split until end points (terminal nodes) are achieved; the end node criteria are usually based on having a set minimal number of observations remaining after the splits.

For regression trees (when the response variable is continuous), regression models are fit using subsets of explanatory variables, and the residual "error" between the predicted values and actual values is assessed. In the case of classification trees (when the response variable is categorical), measures of classification impurity are used to gauge the accuracy of the classifications after data splits, and the end (terminal) response is the assignment of an observation to a class. Random Forests apply this CART type of approach many (e.g., 100) times, using a separate subset (obtained by bagging) of the full dataset for each tree. The final classification or regression results obtained from a forest provide more accurate and stable predictions than is achieved using a single tree.

The stepwise process we used for downscaling was developed for this project, and is as follows:

1) Rescale all predictor variables to 500 m MODIS Sinusoidal if this was not the native resolution using bilinear interpolation.
2) Randomly sample and select 4,000 grid cells across Alaska to train the Random Forest algorithm.
3) Randomly sample 1,000 grid cells across Alaska as an independent model validation set.
4) Train the random forest model on the 4,000 grid cells using 100 trees in the 'forest'.
5) Predict on the 1,000 grid cell validation set and acquire coefficient of determination (R^2) and the root mean square error (RMSE) between the observed and predicted values.
6) Use the trained random forest model to predict values across all of Alaska.
7) Re-calibrate the predictions with equation 2 (not done for Freeze/Thaw and open water since they used classifications, not regression):

$$C = \hat{y} * (y \div \hat{y}_m) \quad \text{(Eq. 2)}$$

where C = calibrated values
$\hat{y}$ = predicted values
y = original values (within each 25 km grid cell)
$\hat{y}_m$ = mean of $\hat{y}$ in each 25 km y

For each of the metrics we then created a time series from April to August of downscaled maps in ~30 day intervals in the year 2014, except for Freeze/Thaw where we started the time series in March for full coverage of the transitional spring thaw period. When a specific date is presented with downscaled analysis (e.g. 07-01-2014) and MODIS vegetation indices were used as predictors, the predictors were filtered temporally by the 16-day window which the MYD13A1.006 downscale date fell within. When temperature was used as a predictor, the associated 8-day window was selected; a 16-day window was used for snow cover.

4.3.2 Input variables used for indicators

Each of the four target variables (i.e., Freeze/Thaw, surface soil moisture, VOD, open water) have a unique suite of predictor variables. The predictors used to downscale the AMSR-E/AMSR2 Freeze/Thaw record are provided in Table 4. These include elevation, slope and

aspect from the GMTED2010 DEM, MODIS Land Surface Temperature, MODIS snow cover, and the probability of permafrost existing at a 0-1 m depth.

Table 4. All predictor variables used for downscaling the Freeze/Thaw cycle.

Predictor	Spatial, Temporal Resolution	Band Math (nanometers)	Source
Elevation	7.5 arc-seconds	N/A	Danielson & Gesch, 2011
Slope	7.5 arc-seconds	N/A	Danielson & Gesch, 2011
Aspect	7.5 arc-seconds	N/A	Danielson & Gesch, 2011
MYD11A2.006 (Land Surface Temperature)	1 km, 8 day	N/A	NASA MODIS
MYD10A1.006 (Snow Cover)	500 m, daily	N/A	NASA MODIS
Permafrost Probability	30 m	N/A	Pastick et al. 2015

The predictors used to downscale VOD, along with the band math used to derive the specific VIS-NIR indices, are described in Table 5. These include the NDVI, the NDWI, a normalized differenced Infrared Index (NDII), a carotenoid reflectance index (CRI1), a cellulose absorption index (CAI), and an anthocyanin reflectance index (ARI1). Each index was derived from MODIS reflectance, and data was screened for good quality pixels. The NDVI is representative of sensitivity to photosynthetic vegetation while the NDII and NDWI are both sensitive to vegetation and landscape water content, both of which VOD is likely detecting. Additionally, the CRI1, CAI and ARI1 are sensitive to vegetation stress.

Table 5. All predictor variables used for downscaling vegetation optical depth (VOD).

Predictor	Spatial, Temporal Resolution	Band Math (nanometers)	Source
Normalized Differenced Vegetation Index (NDVI)	500 m, 16 day	$\frac{(R_{858} - R_{645})}{(R_{858} + R_{645})}$	Tucker 1979
Normalized Differenced Infrared Index (NDII)	500 m, 16 day	$\frac{(R_{858} - R_{1640})}{(R_{858} + R_{1640})}$	Hardisky et al. 1983
Normalized Differenced Water Index (NDWI)	500 m, 16 day	$\frac{(R_{858} - R_{555})}{(R_{858} + R_{555})}$	Gao, 1996
Carotenoid Reflectance Index I (CRI1)	500 m, 16 day	$(\frac{1}{R_{488}} - \frac{1}{R_{555}})$	Gitelson et al. 2002
Cellulose Absorption Index (CAI)	500 m, 16 day	$\frac{R_{2130}}{R_{1640}}$	Nagler et al. 2003
Anthocyanin Reflectance Index I (ARI1)	500 m, 16 day	$(\frac{1}{R_{555}} - \frac{1}{R_{678}})$	Gitelson et al. 2001

Table 6. All predictor variables used for downscaling surface soil moisture.

Predictor	Spatial, Temporal Resolution	Band Math (nanometers)	Source
MYD13Q1.006 Aqua (NDVI)	250 m, 16 day	N/A	NASA MODIS
MYD11A2.006 (Land Surface Temperature)	1 km, daily	N/A	NASA MODIS
TPI (Topographic Index)	30 m, static	See Theobald et al. 2015	Theobald et al. 2015; JAXA ALOS
Land Cover	500 m, yearly	N/A	Justice et al. 2002; NASA MODIS

The predictors used to downscale AMSR-E and AMSR2 soil moisture are described in Table 6. These include MODIS NDVI, MODIS land surface temperature and the TPI (Theobald et al. 2015). The TPI measures hillslope position and is a dominant control of soil moisture and temperature and was calculated using the 30 m ALOS DEM (Tadono et al. 2016). Finally, land cover from MODIS (Justice et al. 2002) was used to provide information for vegetation community type and relative biomass characteristics. To avoid inconsistency in land surface observations from different sensors, only MODIS products were selected.

4.3.3 High resolution inundation mapping

Our objective here was to test methodology to produce high resolution (30 m) surface water detection maps near the Tanana River Bridge and Jarvis Creek river crossing area in Interior Alaska. The Tanana River drains the central and eastern part of the Alaska Range and the Jarvis Creek drain into the Delta River before entering the Tanana River. Both glacier-melt water and precipitation affect the discharges of the two rivers (Liljedahl et al. 2017). The Tanana River Bridge section is used by the U.S. Army to access remote training grounds. U.S. Army access to training grounds across Jarvis Creek, southeast of Delta Junction, includes low water crossings. At both sites, understanding the temporal frequency and spatial distribution of surface water and flooding of river channels is important for the planning of DoD training activities to reduce risk to equipment and personnel.

To map high resolution surface water at 30 m resolution and obtain detailed changes of river channels and water bodies for major flood events over the past 17 years, two approaches were developed. The first method relies on coarse resolution (25 km) AMSR-E and AMSR2 (AMSR) Fw data sets and the ancillary Landsat WOD (Pekel et al. 2016). The WOD describes surface water inundation frequency at a 30 m resolution over the 32-year (1984-2015) Landsat image collection. For a given region, the area consisting of all the pixels with WOD > 0 represents the largest possible inundation observed over the Landsat record. For each 25 km AMSR grid cell, the inundated areas calculated by AMSR Fw are allocated sequentially to the 30 m pixels based on their WOD level or flood feasibility. This approach was first developed for downscaling NASA L-band Soil Moisture Active and Passive (SMAP) Fw retrievals (Du et al. 2018). This empirical downscaling method is most suitable for filling data gaps when no high-resolution optical images are available.

The first downscaling method, using AMSR Fw and information from WOD, may be problematic if a flooding event does not follow the same inundation pattern described by the WOD. The method also fails to identify newly emerged water bodies or inundations which are not recorded in the WOD. To address this, a second approach using spaceborne SAR was developed for this study for improved monitoring of flood events and recent changes in inundation. Different from passive microwave sensors, the SAR generally provides high-resolution imagery at 1-100 m, with an approximate weekly to monthly temporal sampling.

The radar signals are very sensitive to surface dielectric properties as well as vegetation structure and surface roughness (Du et al. 2010). Water bodies generally appear dark in mono-static SAR observations though similarly low-level signals can also be found for smooth soil/rock surface or road structures. Moreover, radar observations are incident-angle dependent and water signals may be weak in pixels having water mixing with vegetation or buildings. To partially overcome these difficulties, we developed an experimental SAR algorithm and applied it to Sentinel-1 SAR images. The algorithm detects water pixels in four steps: (1) image preprocessing (radiometric correction, terrain correction, incidence angle correction and de-speckling); (2) Random Forest based machine learning; (3) a change detection based water classification; and (4) finalized classifications of land or water.

The SAR-based approach was applied to the Tanana River Bridge region (centered on -147.07°, 64.56°) and Jarvis Creek region (centered on -145.72°, 64.02°) over selected dates of May 11, 2017; August 13, 2017; August 14, 2016; October 12, 2017. These dates correspond to major dry and wet periods within the regions identified from USGS Salcha river station near Fort Greely and Tanana river station near Fairbanks.

Table 7. All predictor variables used for surface water inundation.

Predictor	Spatial Resolution	Source
VV-polarized backscatter	30 m	ESA; https://scihub.copernicus.eu/
VH-polarized backscatter	30 m	ESA; https://scihub.copernicus.ed/
Slope	30 m	JAXA; Tadono et al. 2016

The Level-1 Ground Range Detected (GRD) Sentinel-1 SAR imagers were acquired from ESA Copernicus Open Access Hub (https://scihub.copernicus.eu/) and processed using ESA SNAP software (Figure 8, Step 1). The following preprocessing steps were made to derive the radar backscatter image: (a) Georeferencing by applying precise orbit data; (b) thermal noise removal; (c) radiometric calibration; and (d) terrain correction. To train the Random Forest model for image classification (Figure 8, Step 2), the 30 m grid cells with a WOD water occurrence > 0.8 and water occurrence = 0 were used to represent pure water and land. For this analysis, a binary classification of 0 (land) and 1 (water) was assigned to each grid cell. Up to 2,000 water and 2,000 land training samples were randomly selected within the focused region which is defined as a 0.25 by 0.25° area in our study. The input parameters used for the training (Table 7) were radar backscattering at VV and VH and slope, which was calculated from ALOS

30 m global elevation dataset. The random forest model was trained on 4,000 grid cells, with 25 generated trees. The number of trees used for this study is a compromise between slight performance improvement with tree numbers and the overall calculation time.

The change detection (Figure 8, Step 3) examines the backscattering changes between current observations and mean values of previous images (+/- one-month period). For newly flooded areas, a drop in significant backscattering is expected; grid cells were flagged as "potential water" if their backscattering decreased more than one standard deviation from the reference images. For the last step, a grid cell was determined as "water" if both step 2 and 3 classified it as "potential water" or if it had a WOD water occurrence > 0 and Step 2 classified it as water.



Figure 7. Locations of Tanana River Bridge and Jarvis Creek test sites used to refine downscaling methods for microwave SAR and passive microwave AMSR-E and AMSR2.

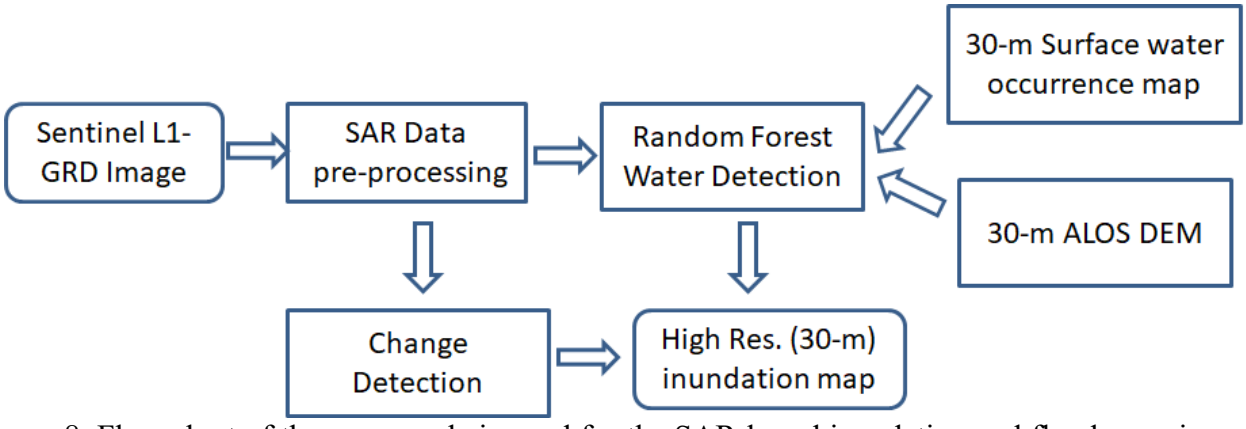


Figure 8. Flow chart of the process chain used for the SAR-based inundation and flood mapping for select locations in Interior Alaska.

5. RESULTS AND DISCUSSION

5.1 Indicator State Changes

In this section, we provide the results from our Mann-Kendall change analysis of satellite Earth System Indicators for: 1) Terrain Thermal State; 2) Ecosystem Water Stress; 3) Vegetation State. We first present these results for the full Alaska domain, followed by a more localized assessment for DoD terrains within Interior Alaska. The supplemental figures and tables for the full Alaska region can be found in Appendix B and are denoted by 'S' in the following sections. For vegetation, we also provide the results of BFAST break point analysis over select terrains within Interior Alaska as a case study showing the contrasting strengths of the Mann-Kendall and BFAST change detection algorithms.

5.1.1 Terrain Thermal State

5.1.1.1 Results for Alaska

(a) Snow cover

The timing of the spring main snow melt onset date (MMOD) in Alaska (Figure S2), examined over a 29-year record (1988 through 2016), occurred in early to mid-March (around day of year (DOY) 70) along the warmer and more southern coastal regions, including portions of the Yukon-Kuskokwim Delta and the Matanuska-Susitna Valley near Anchorage. In the more northern terrains, and along the higher elevation mountain ranges, the MMOD occurred in later May. Final snowoff was observed in late June for seasonal snow cover in northern Alaska and the higher elevation regions, and elsewhere in mid to late April, including the lowland regions within Interior Alaska. The snow melt duration (SMD) within Interior Alaska (Figure S3) typically occurred within an approximate 22 day period per year, with snow melting more rapidly in the Interior compared to the more cloudy (solar protected) western and coastal regions.

Over this period, the satellite microwave record indicated that the MMOD (Figure 9) had significant rates of decrease (i.e., snow melt occurring earlier) along the West Coast (western coastline) of Alaska, within the Interior, and across the North Slope (Arctic Coastal Plain; Figure S1) and that these negative trends were greater at higher elevations. This indicates that the higher elevation terrains experienced the largest rates of change, with the start of snowmelt occurring much earlier each spring at rate of up to 1 day per year. Most areas over the Alaska region did not show a significant changing trend in snow phenology. For the limited pixels showing significant changes, we identified that the higher elevation terrains experienced the largest rates of change, with the start of snowmelt occurring much earlier each spring at rate of up to 1 day per year. Along the Gulf (Pacific coastal mountains, the Cook Inlet, and the southern Alaska Range; Figure S1), and lower elevation terrains within the West Coast and the Interior, the MMOD showed positive trend, indicating that the annual start of snow melt had shifted towards later in the spring season. Most regions, with the exception of the North Slope, showed an annual increase in the timing of snowoff that coincided with an increase in the annual SMD.

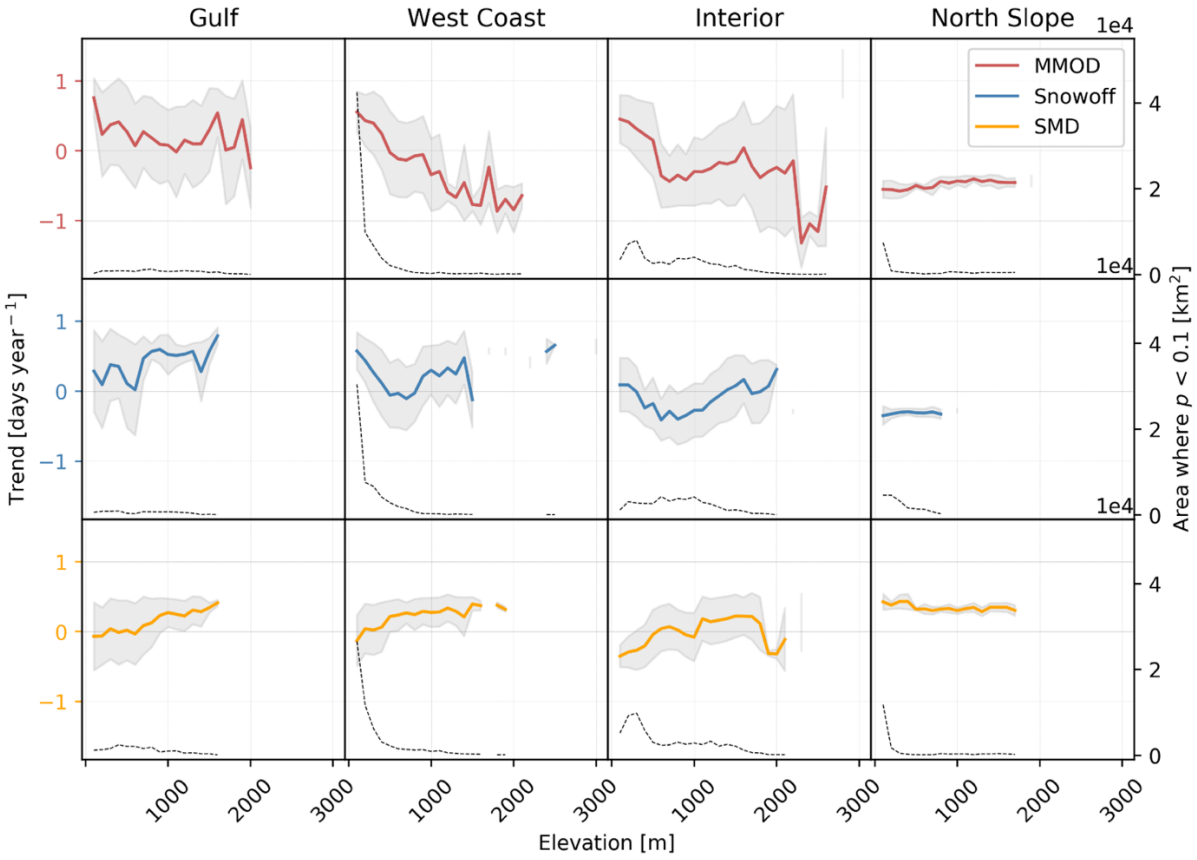


Figure 9. Trends (1988-2016) for Alaska main snow melt onset date (MMOD), the date of snowoff, and snow melt duration (SMD). Trends are shown by region, for the Alaska Gulf (southern coastline), West Coast, Interior and North Slope. Black dotted lines indicate the total area (km^2) of total grid cells having significant trend. [*Figure provided courtesy of Caleb Pan and NTSG*]

(b) Air and surface temperature

In this analysis we assessed MERRA2 daily mean air temperature (~2 m height), AMSR-E and AMSR2 LPDR (hereby referred to as AMSR LPDR) daily minimum air temperature (~2 m height) derived under non-frozen surface soil conditions, and MODIS land surface temperature for the Alaska domain. The spatial distributions of the air and land surface temperature records generally showed similar patterns across Alaska (Figure S4 a-c). Colder mean annual temperatures (MAT) of -3 to < -9°C were observed across the North Slope (Arctic Coastal Plain and Arctic Foothills) and Interior (including the Yukon Flats) in contrast to the warmer regions of the Subarctic Coastal Plains, the Yukon-Kuskokwim Delta, and the western coastal regions. Both air (MERRA2, AMSR LPDR) and land surface (MODIS) temperatures showed warmer MAT (~ -2°C) occurring within the lower elevation Yukon Flats region near Fairbanks and Delta Junction relative to the surrounding higher elevation terrains.

Strong regional differences in air temperature were observed in spring, summer and autumn (Figure S5), with local hotspots of warmer temperatures occurring in the AMSR 25 km microwave record over the Dalton highway on the North Slope in spring (Figure S5-d) and across the Yukon Basin in autumn (Figure S5-f). The Yukon Basin, including Fairbanks and

nearby DoD lands, was also observed to have less frozen days in spring (year 2016; < 10; Figure S6) compared to elsewhere in the Interior (~10-20 days).

The mean annual temperature records from MERRA2 (from 1980 to 2017), AMSR LPDR (2002 to 2016) and MODIS LST (2002 to 2017) did not show a significant trend when averaged across the full Alaska domain (Figure S7). However, the trend assessments for individual grid cells revealed a more complex landscape of change and highlighted the occurrence of nonstationarity across isolated regions within the state (Figure S8). These changes vary by the observed Earth System Indicator metric, and by season.

For this analysis, the seasons were separated into spring (April 15 to May 31), summer (June 1 to August 31), autumn (September 1 to October 15) and winter (October 16 to April 14) before applying the Mann-Kendall trend analysis and Theil-Sen estimate of median slope. Significant ($p < 0.1$) and positive changes in slope, indicating warming, were observed for spring in the AMSR LPDR record over the North Slope and in the southern region of the Seward Peninsula and western Yukon-Kuskokwim Delta. The MERRA2, AMSR LPDR air temperature and MODIS LST retrievals all showed warming patterns within Interior Alaska over the spring, summer and autumn periods. In general, a significant and multi-year increase air temperatures over Alaska was most prevalent in the summer and autumn (Figure S8), confirmed by all three records. The highest rates of change occurred in boreal forests, followed by tundra and boreal wetlands (Figure S9). When considered according to permafrost condition (Figure S10) the most change in temperature was observed in autumn and occurred over terrains where the probability of permafrost coverage (as of 2014) was over 60% (based on the Pastick et al. 2015 USGS map).

(c) Freeze/Thaw

The annual surface frozen period in Alaska in more recent years (2016 for AMSR; 2017 for SSMR/SSMI/SMMIS, hereafter referred to as SSMI) spanned up to 250 days per year in the North Slope Region, approximately 100 to 150 days in central Alaska including Fairbanks and was less than 100 days per year in the Alaska southwest and coastal region.

Within the long-term satellite records, we observed substantial variability in patterns of Freeze/Thaw change across the region. For spring, the 39-year (1979 to 2017) SSMI 25 km Freeze/Thaw record and 15-year (2002 to 2016) AMSR 6 km Freeze/Thaw record both indicated a negative slope (decrease in frozen status) over a large portion of northern Alaska and along the Alaska range (Figure S11). For the autumn period, these records indicated significant decreases (negative slope) in the number of days that ground was frozen along the Brooks Range and western North Slope Region and portions of Interior Alaska. This coincided with an increase in frozen days (positive slope) near Deadhorse (Prudhoe Bay), Utqiagvik (Barrow), and along the western coastline. In the finer resolution AMSR record, a decrease in autumn surface ground frozen condition (significant, positive slope in thawed state) was observed within Interior Alaska (Figure S11).

In addition to terrain frozen or thawed state, this study also examined changes in transitional terrain state, which provided an assessment of where a terrain area changed from frozen to thawed status or vice versa within a 24-hour period. We found significant and positive changes in Freeze/Thaw transition period in spring over the North Slope (Figure S12) within the longer term SSMI record (Figure S12-a). However, this was not observed in the shorter term AMSR record over the Brooks Range (Figure S12-d) which instead indicated a significant decline in the

transition period at a rate of >1 day per year. This directly highlights the need for continuous decadal remote sensing records to identify more subtle longer-term changes in terrain state.

In contrast to the SSMI records, the finer resolution AMSR observations indicated a strong accelerated increase in spring surface transitional state in central Alaska along the Yukon River Basin that spanned from near the Alaskan-Canadian border westward to the Yukon-Kuskokwim Delta (Figure S12-d). However, when the SSMI records are assessed over 2002-2016, instead of the extended 1979 to 2017 period, the results are more consistent with the AMSR observations (Figure S13). For autumn, an increase in transitional state was observed over the western portion of the North Slope and throughout Interior Alaska within the SSMI record (Figure S12-b). This was also observed in Interior Alaska in the AMSR record, however the locations showing significant change were more localized. In winter, Interior Alaska also showed a significant increase (0.1 days per year) in transitional Freeze/Thaw state (Figure S12-c and f).

Our satellite microwave assessment of seasonal thaw days further confirmed that Alaska ecosystems are indeed experiencing a regional increase in the number of days per year where the terrain surface is remaining in an unfrozen state (Figure S14). Across the North Slope, we observed a significant increase of up to 1.66 days per year in the spring unfrozen period which was especially evident in the AMSR record (Figure S14-d) and coincided with the decrease in spring transitional periods (Table S1). While the AMSR trend shows a larger increase in the number of thaw days in the spring (Figure S14-a) and a larger decrease in the autumn (Figure S14-b) over the North Slope, the MK trends again become more consistent between the SSMI and AMSR records when evaluated over the same time periods (Figure S15).

Besides the major changes in spring frozen period identified in both the long-term SSMI record and the shorter-term AMSR dataset, a significant decrease in the number of annual frozen days was also observed in winter at a rate 1.05 days per year; this occurred over 28.4% of terrain areas in Alaska land area (Table S1). The trend coincided with an increase in winter transitional state and thawed days which primarily occur in the southwest region of Alaska. In the AMSR record, we also observed a localized hotspot of increasing winter thaw (> 2 days per year) within the Interior Forested Lowlands of Alaska near Iditarod (Figure S14-f).

5.1.1.2 Results for the Interior Alaska AOI

(a) Snow cover

In the Interior Alaska AOI the MMOD for 2016, the most recent year available for the satellite SSMI record, occurred in late March near the DoD units of Fort Wainwright, Fort Greely, Eielson Air Base and Clear Air Station (Figure 10). The MMOD was similar on the Yukon and Tanana Flats training areas but extended to mid-April in the higher elevation Donnelly Training Area West. The final snowoff date ranged from mid-April along the Tanana river lowlands to later May in the foothills of the Alaska Range. The average duration of snow melt in this region spanned from approximately twenty days in the lowlands to well over sixty days in the Alaska Range towards Healy. A majority of the terrains in the region experienced an earlier start of the MMOD by up to 1.8 days per year over the 1988-2016 observation period (Figure 11) with significant negative trends in MMOD (i.e., earlier onset of snow melt) observed over Fort Wainwright and portions of the Tanana Flats Training Area and directly east of the Yukon Training Area. In contrast, the terrains surrounding Fort Greely showed a slight positive MMOD trend (i.e., later initiation of snow melt) of approximately 0.4 days per year even though this

coincided with a decrease in the annual duration of snow melt (i.e. the SMD; Figure 11). The environmental factors contributing to spatial differences observed between the MMOD, the date of snowoff, and the SMD within the AOI (Figure 10) are not readily apparent but may be influenced by differences in local topography and vegetation cover.

(b) Air and surface temperature

Annual temperature patterns over DoD terrains in Interior Alaska for the most recent observational year of 2017 (MERRA2) or 2016 (AMSR) indicated that warmer conditions generally occurred at lower elevations along the Tanana River (Figure 12). The coarser 0.5° MERRA2 record showed warmer regions (MAT ~ -1° C) occurring toward the southern portion of Tanana Flats Training Area and across Donnelly training area (Figure 12-a) relative to the surrounding terrains. The finer 25 km resolution satellite AMSR air temperature record, which only has retrievals obtained over non-frozen terrain surfaces, showed a slightly warmer MAT (2.8 °C) over the eastern half of Yukon Training Area and much cooler temperatures (MAT of -0.6 °C) over Donnelly, reflecting topographical gradients (Figure 4).

The annual average MODIS 1 km LST (Figure 11-c) was more locally variable compared to the coarser resolution air temperature products and had greater sensitivity to localized terrain warming which is greatly influenced by elevation, aspect, terrain wetness, and vegetation cover. The MERRA2 record showed warmer air temperatures (0.5 °C higher relative to surrounding terrains) in spring on Tanana Flats and Donnelly, and across all DoD terrains in summer (15 °C; Figure 12-a, b). In the MODIS record, hotspots of elevated LST were observed in autumn over localized terrains across the Tanana Flats Training Area and Yukon Training Area (Figure 12-f).

Although monotonic trends were not observed in the long-term (1980 to 2017) temperature records when averaged across the Interior AOI and DoD terrains (Figure 13), the per-grid cell trend detection showed a significant increase in MERRA2 summer temperature, at a rate of 0.03 °C per year, over 17.5% of the domain (Table 8). In addition, our Mann-Kendall grid cell analysis identified localized and significant changes in air temperature within and surrounding DoD terrain units (Figure 14). Significant ($p < 0.1$) long term warming in summer at a rate of 0.02 °C per year occurred over Fort Greely and Donnelly Training Area, indicated by the MERRA2 records. The AMSR LPDR record also showed significant warming in spring over a western section of Donnelly (Figure 14). The AMSR record showed a warming trend in autumn over the Tanana Flats Training Area, the Blair Lakes Bombing Range, and Yukon Training Area but the trend slope was not yet significant ($p = 0.6$ as of the last year on record, 2016).

These changes in temperature, grouped by dominant vegetation class (Figure 15), indicated that in summer the largest area with significant warming trends was boreal forests (over 1980 to 2017 the MERRA2 record) followed by shrub and grasslands, and wetlands. However, when accounting for landcover area, grassland/shrub had the largest percentage of area with significant warming trends, followed by wetlands, and forests. In autumn, this warming was most prevalent over boreal forests and boreal wetlands. When considering permafrost, long-term warming was observed in summer for DoD terrains having 40 to 80% near surface permafrost coverage (Figure 16). Whereas in autumn, significant warming was observed for terrains having 40 to 60% permafrost coverage.

(c) Freeze/Thaw

The number of frozen days in 2017 for DoD terrains in the Interior spanned from 100 to 150 days with the exception of Fort Greely Cantonment and portions of the nearby Donnelly Training Areas which had an extended frozen period of over 150 days in 2017. The number of frozen days in spring was under 10 over most terrains (Figure 17-a, c), with the exception of Yukon Training Area and western Donnelly Training Area (in the SSMI record). For autumn, the most terrains had < 10 days where the surface was fully frozen. During the spring period, the number of surface frozen days showed a significant decrease (by a rate of up to 0.14 days year^{-1}) over the western region of Donnelly Training Area West (Figure 18). In winter, the satellite microwave records also showed a decrease in the number of frozen days per year (~0.05 days year^{-1}) for most Interior AOI terrains.

Interior Alaska experienced a major decrease in the number of spring frozen days at a rate of 0.14 days per year (detected over 28% of the Interior AOI domain) and an increase in the number of spring thawed days at a rate of 0.19 days per year (detected over 45.6% of the Interior AOI domain) from 1979- 2017, as indicated by the SSMI record (Table 9). For winter, the AMSR record indicated that the number of frozen days significantly decreased at a rate of 0.32 days per year (detected over 14.3% of the Interior AOI). The SSMI record showed a decrease in the number of frozen days in winter, at a rate of 0.05 days per year for 8,750 km^2 of terrain (2,162,172 acres). The AMSR sensors detected an increase in the number of thawed days in spring at an average rate of 0.15 days per year, over 6,875 km^2 of terrain (1,698,849 acres).

The longer-term SMMI record detected a significant decrease in the spring number of transitional days (around 0.1 days per year; Figure 19) over the Tanana River Training Area. For autumn, the SMMI record showed a significant increase (~ 0.2 days per year) in transitional days over the southern Tanana Training Area region (including Blair Lakes) and Donnelly Training Area. The AMSR record indicated the opposite, and instead showed a significant decrease in transitional days (at a rate of up to 0.5 day per year) over Donnelly.

The SSMI microwave long-term records (1979-2017) showed a significant increase in annual thaw conditions for spring over the northern Tanana Flats Training area (~ 0.16 days per year; Figure 20) while in the autumn there was a decrease in the number of thaw days over the southern Tanana Flats Training area (~ 0.13 days per year) (Figure 20). In contrast, the AMSR record indicated an increase in the number of autumn thawed days over Donnelly Training Area (~0.70 days per year; Figure 20-e) and over Donnelly and Tanana River Training Area in winter (~0.1 days per year; Figure 20-f).

The Freeze/Thaw trends for DoD terrains in the Interior AOI, as summarized by dominant vegetation class (Figure 21), indicated that the most substantial changes in surface frozen state occurred over boreal forests in winter. Frozen conditions primarily decreased (less frozen days per winter) within forested terrains. The majority of terrains experiencing a change in surface frozen state were characterized by a near-surface (< 1 m) permafrost state occurrence probability of 40 to 60% (Figure 22). A less substantial but significant decrease in terrain surface frozen state was also observed for spring. For transitional state the most substantial change was observed for both autumn and winter and primarily over boreal forest terrain. As with frozen conditions, most of the observed changes in transitional state occurred over terrains having a permafrost probability of 40-60% (Figure 21). Considering thawed state, the largest increase was observed for spring, followed by winter and summer (Figure 22) and a small negative trend was observed in autumn, indicating a decrease in thawed state (and shift toward transitional state).

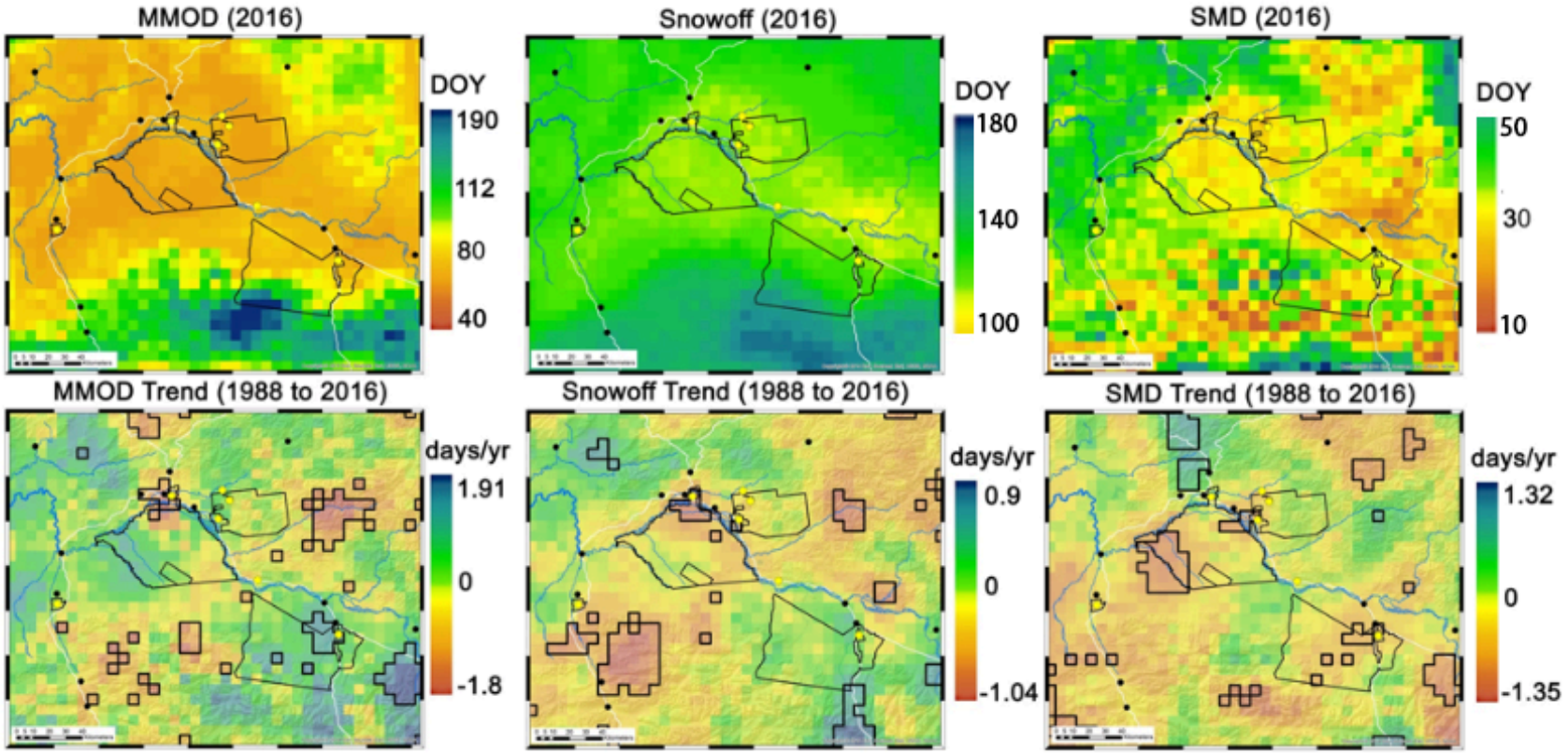


Figure 10. The main snow melt onset date (MMOD), the date of snowoff, and the snow melt duration (SMD) derived from the satellite SSMI record for 2016. Also shown are the corresponding trends for each snow melt metric over the 1988 to 2016 period. The black lines (upper and lower panel) show the locations of DoD terrains within the Interior Alaska AOI. The thicker black lines in the bottom panel show regions where the long term monotonic trend is significant at $p < 0.1$. [*The microwave based snow dataset was produced by NTSG (UMT) and was provided courtesy of Caleb Pan*]

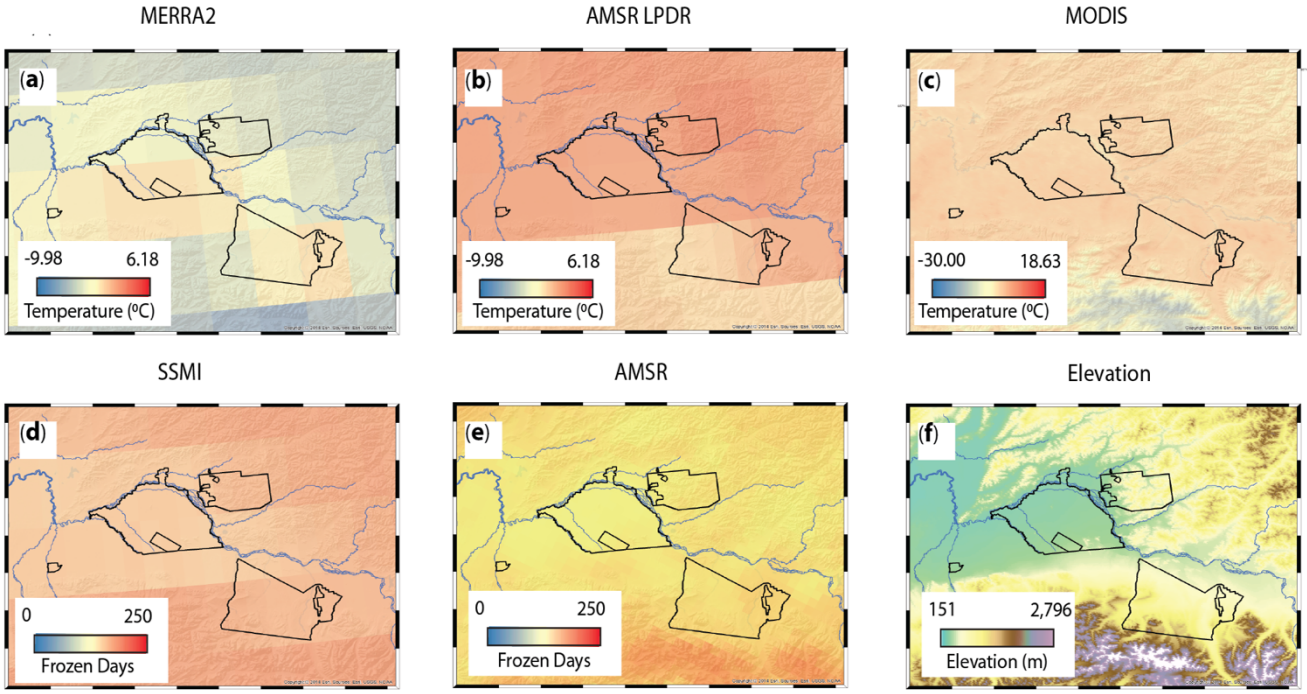


Figure 11. Maps showing average annual MERRA2 air temperature (2017; a), AMSR LPDR air temperature (2017; b) and MODIS land surface temperature (2017; c) over the Interior Alaska AOI and DoD terrains (outlined in black). Also shown is the annual number of Freeze/Thaw frozen terrain days observed in the SSMI (2017; d) and AMSR (2016; e) record. Elevation of terrains are shown in (f).

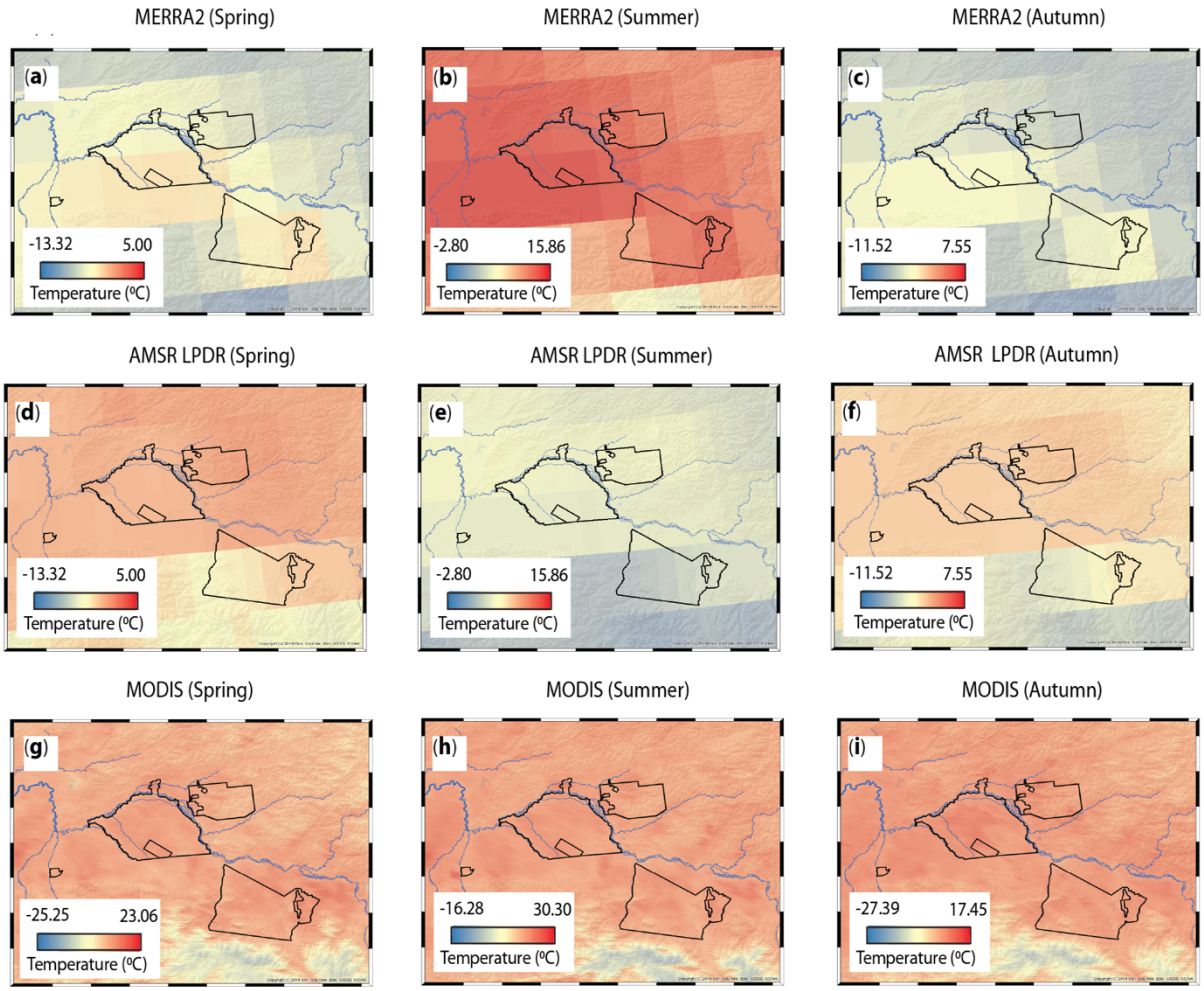


Figure 12. Maps showing seasonal patterns in average annual 0.5° MERRA2 air temperature (a-c; for 2017), 25 km AMSR LPDR (d – f; for 2017) air temperature, and 1 km MODIS land surface temperature (g – i; for 2017) over the Interior Alaska AOI and DoD terrains (outlined in black).

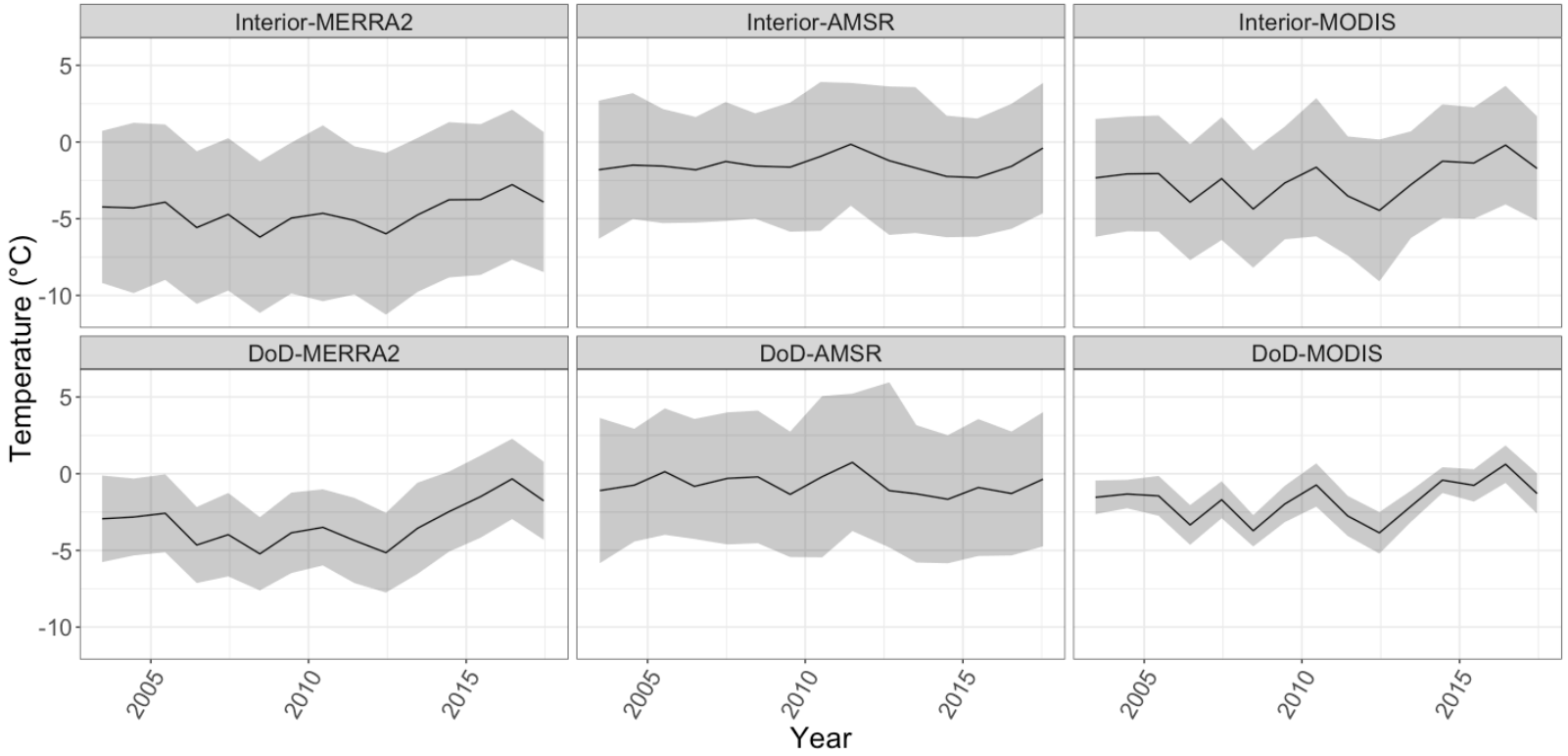


Figure 13. Time series of MERRA2 air temperature, AMSR LPDR air temperature, and MODIS land surface temperature for the Interior Alaska AOI and DoD terrains (2003 - 2017). The black line represents annual averages for the domain; the gray shading around the line represents two standard deviations around the regional averages.

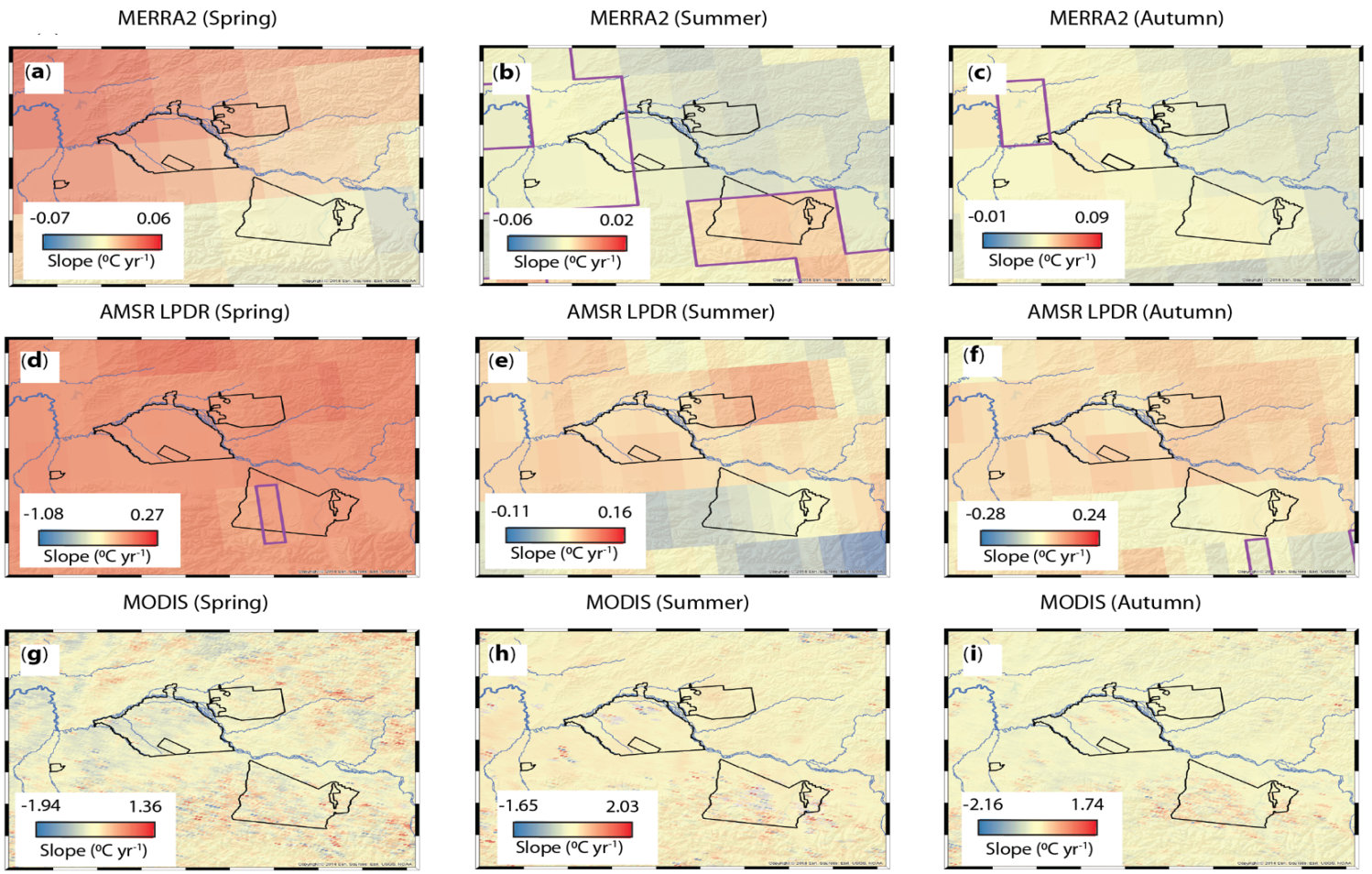


Figure 14. Sen slope results for 0.5° MERRA2 air temperature (1980 through 2017; a-c), 25 km AMSR LPDR air temperature (2002 to 2017; d-f) and 1 km MODIS land surface temperature (2002 to 2017; g-i) for the Interior Alaska AOI and DoD terrains (outlined in black). Regions where the slope trend is significant ($p < 0.1$) are outlined in purple.

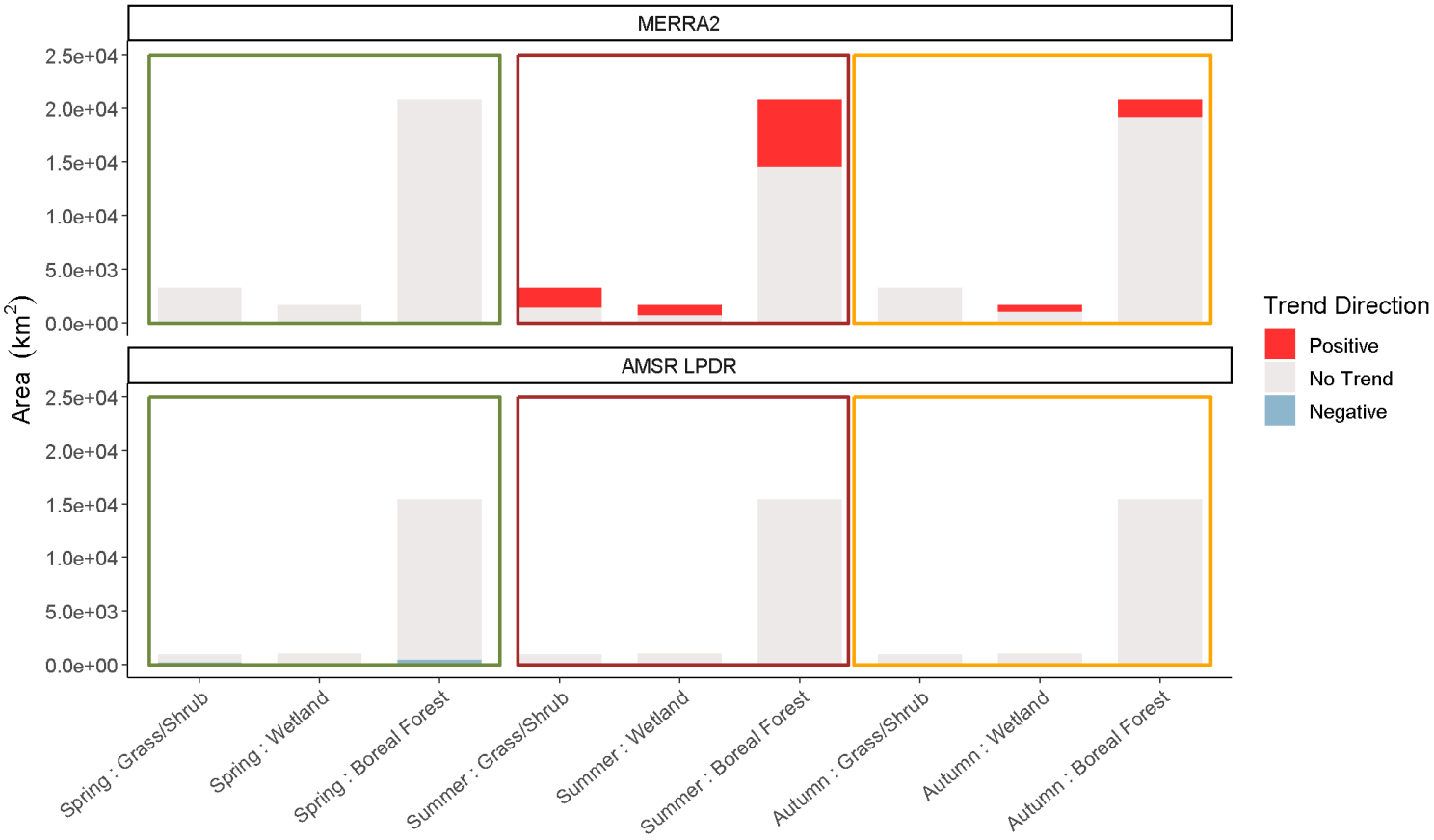


Figure 15. Patterns of change in Terrain Thermal State Indicator metrics (i.e., 2 m MERRA2 and AMSR LPDR air temperature) across DoD terrains in the Interior Alaska AOI as aggregated by generalized land cover classes (grass/shrub; wetland; boreal forest).

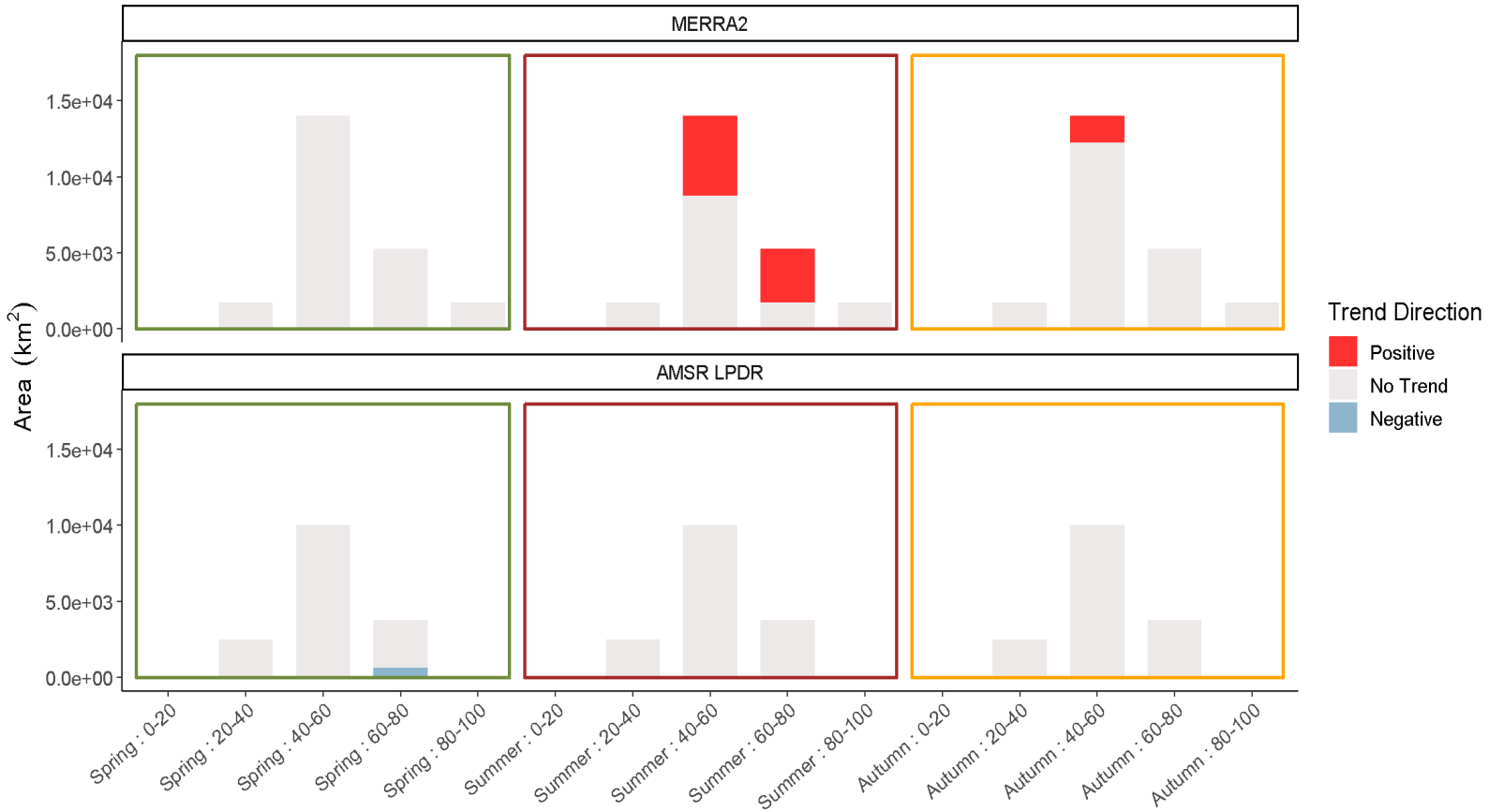


Figure 16. Patterns of change in Terrain Thermal State Indicator metrics (i.e., 2 m MERRA2 and AMSR LPDR air temperature) across DoD terrains in the Interior Alaska AOI aggregated by permafrost classes (0-20; 20-40; 40-60; 60-80; 80-100) which indicate the probability of a terrain unit having near surface (< 1 m) permafrost (from Pastick et al. 2015).

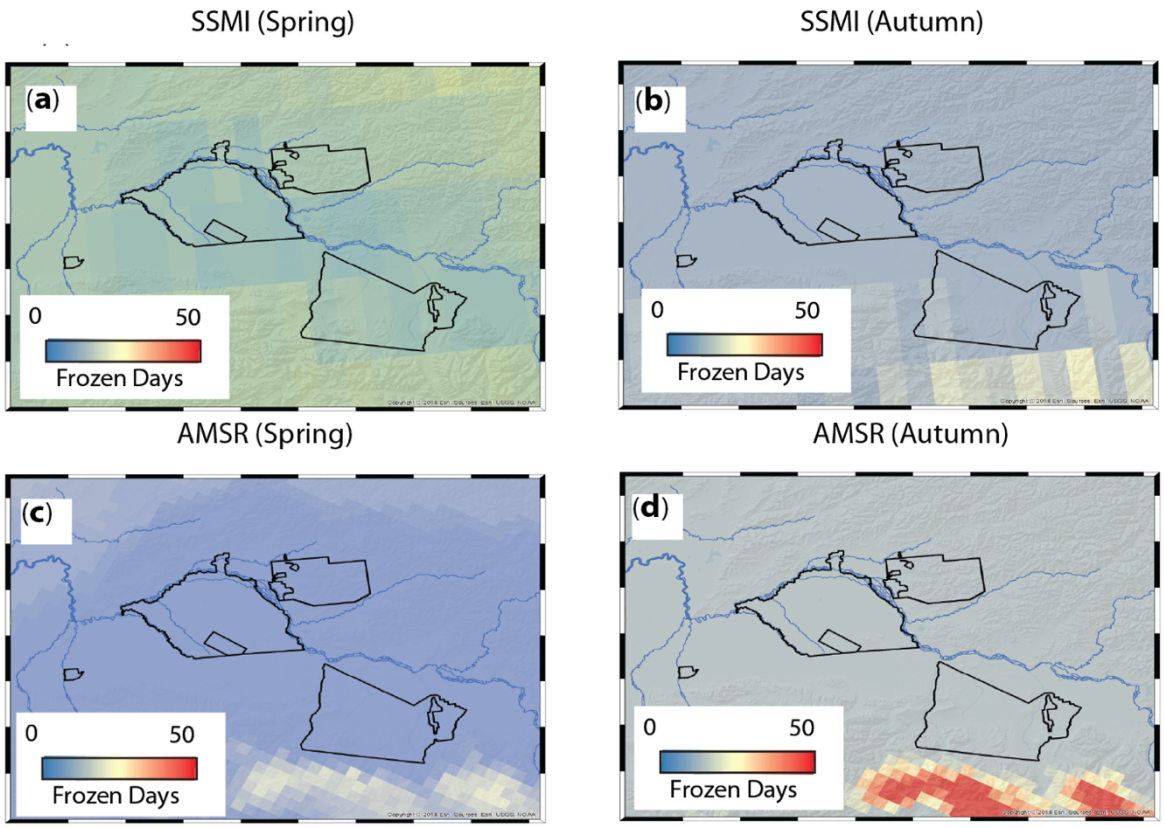


Figure 17. Number of Freeze/Thaw frozen days in the Interior Alaska AOI and DoD terrains (outlined in black) in 2017 derived from SSMI in the spring (a) and autumn (b) and number of frozen days in 2016 based on AMSR LPDR in the spring (c) and autumn (d).

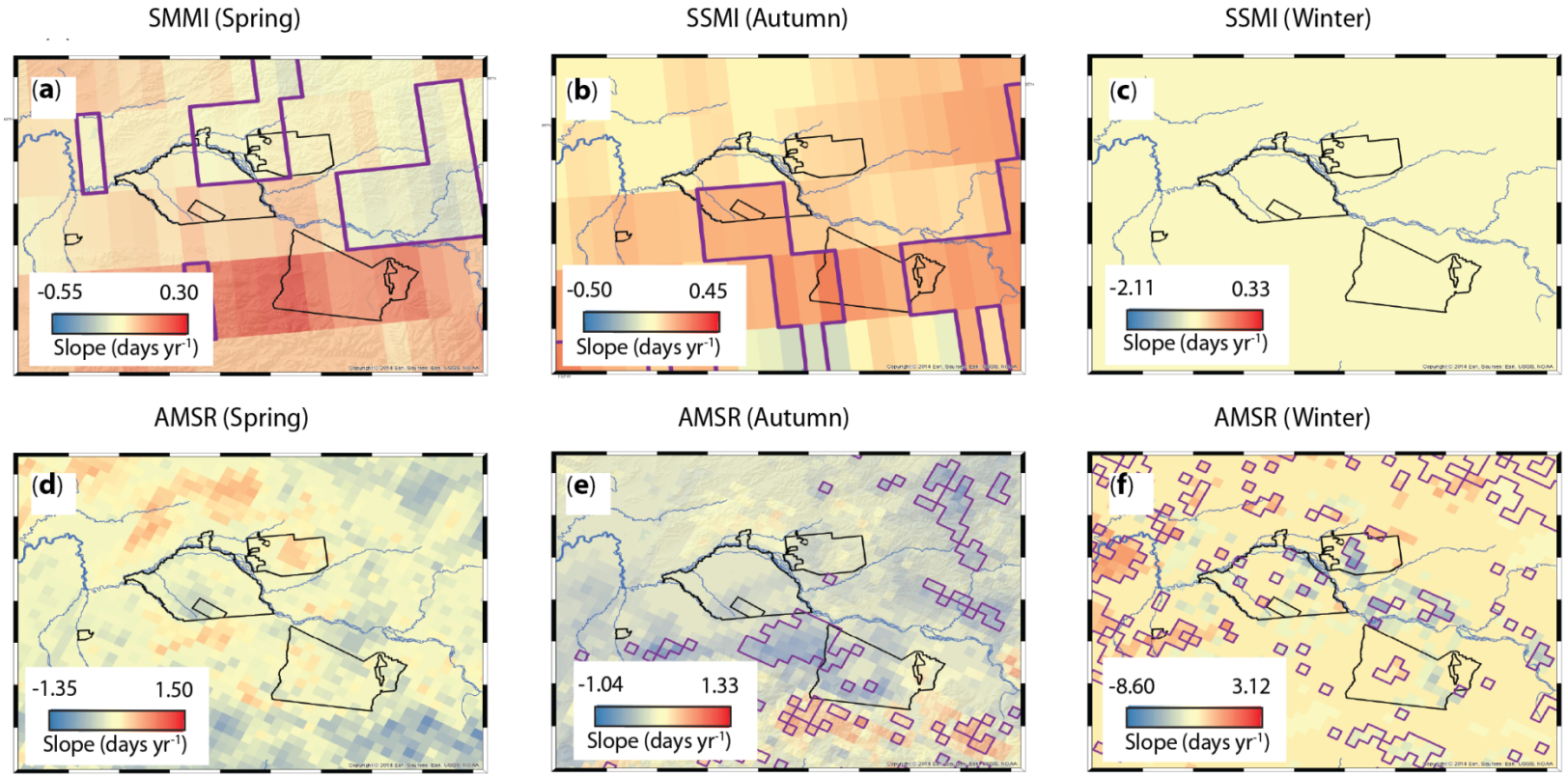


Figure 18. Sen slope results from 25 km SSMI (1979 to 2017) and 6 km AMSR (2002 to 2016) Freeze/Thaw frozen state records for the Interior Alaska AOI and DoD terrains (outlined in black) in spring, autumn and winter. Regions where the slope trend is significant ($p < 0.1$) are outlined in purple.

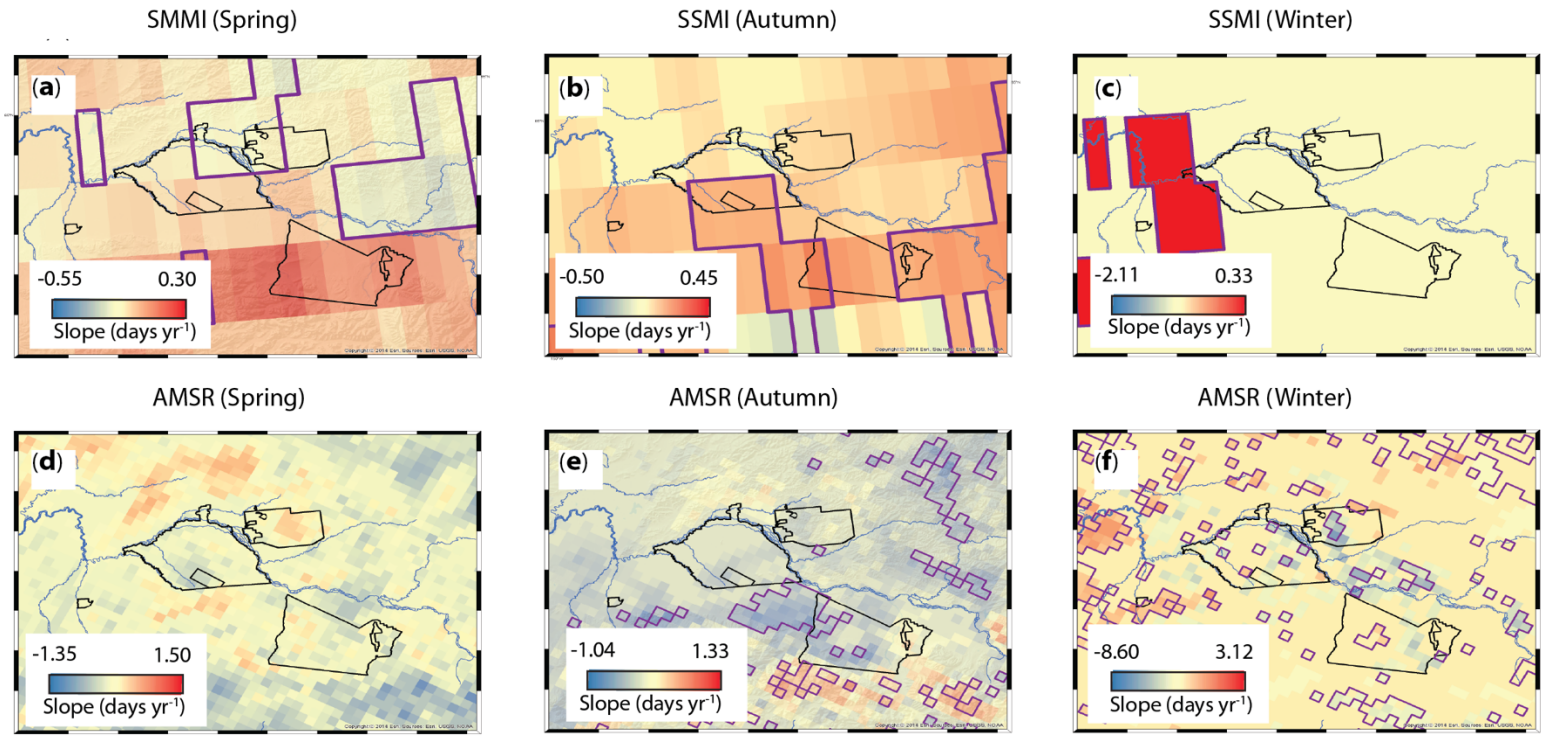


Figure 19. Sen slope results from 25 km SSMI (1979 to 2017) and 6 km AMSR (2002 to 2016) Freeze/Thaw transition records for the Interior Alaska AOI and DoD terrains (outlined in black) in spring, autumn and winter. Regions where the slope trend is significant ($p < 0.1$) are outlined in purple.

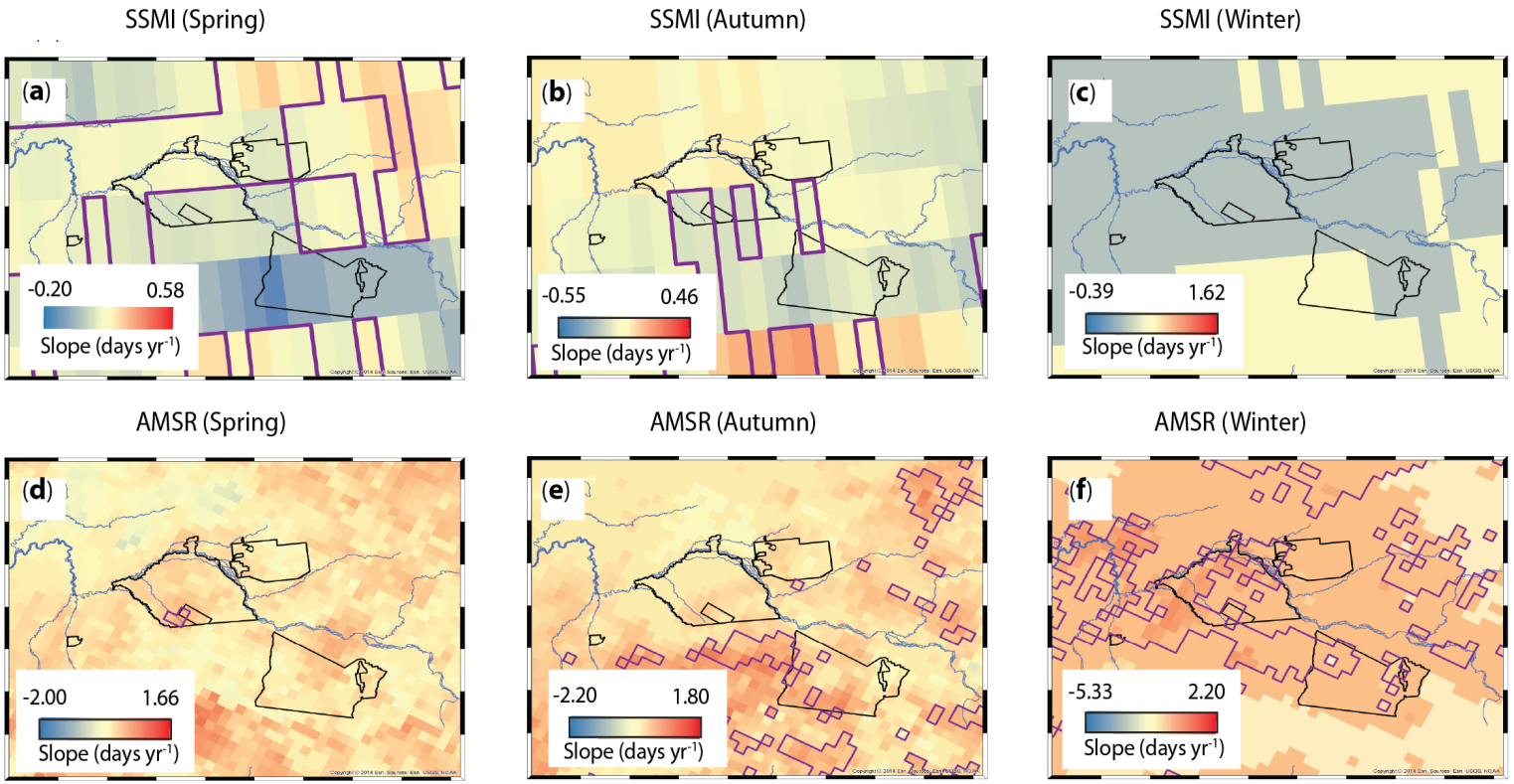


Figure 20. Sen slope results from 25 km SSMI (1979 to 2017) and 6 km AMSR (2002 to 2016) Freeze/Thaw thawed records for the Interior Alaska AOI and DoD terrains (outlined in black) in spring, autumn and winter. Regions where the slope trend is significant ($p < 0.1$) are outlined in purple.

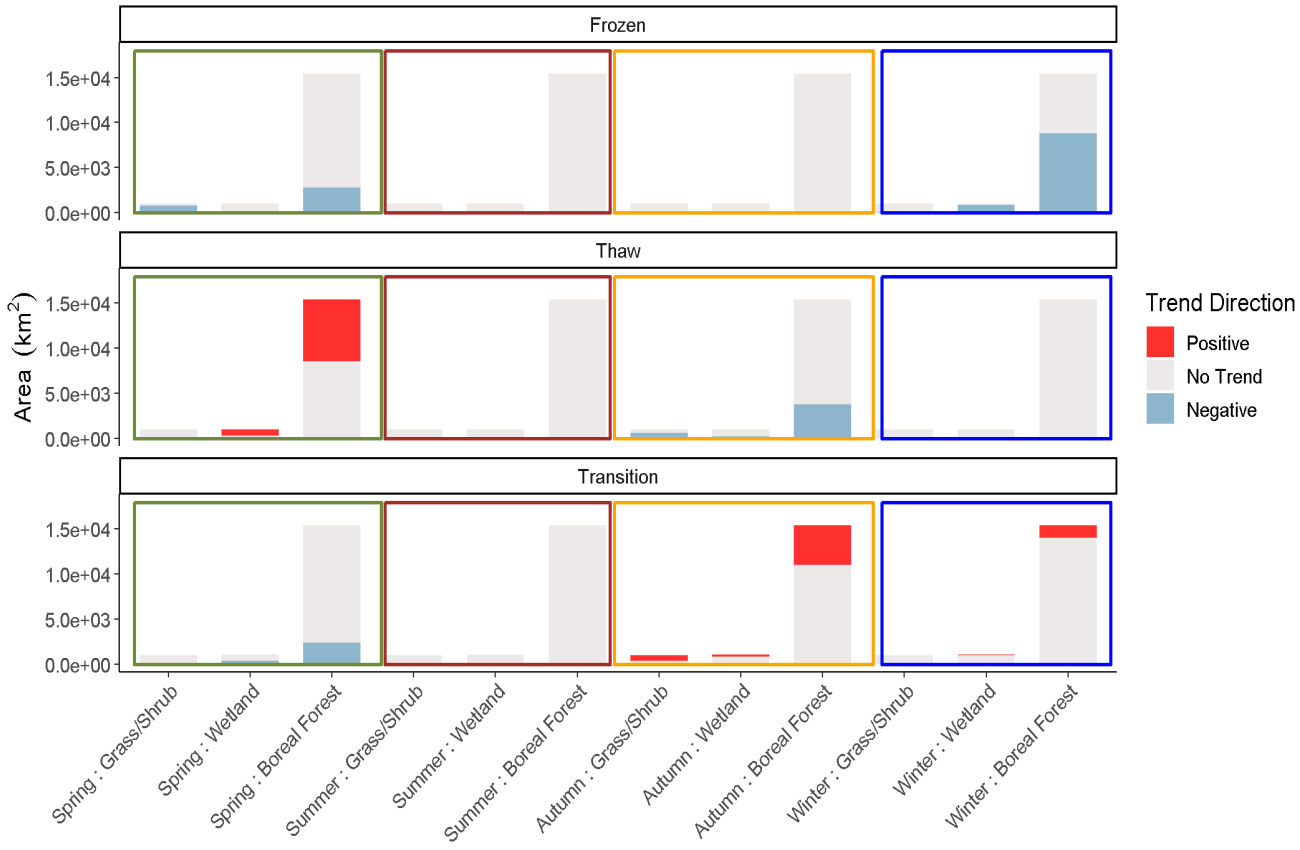


Figure 21. Patterns of change in terrain Freeze/Thaw state (shown here using the SSMI record) across DoD terrains in Interior Alaska as aggregated by generalized land cover class (grass/shrub; wetland; boreal forest).

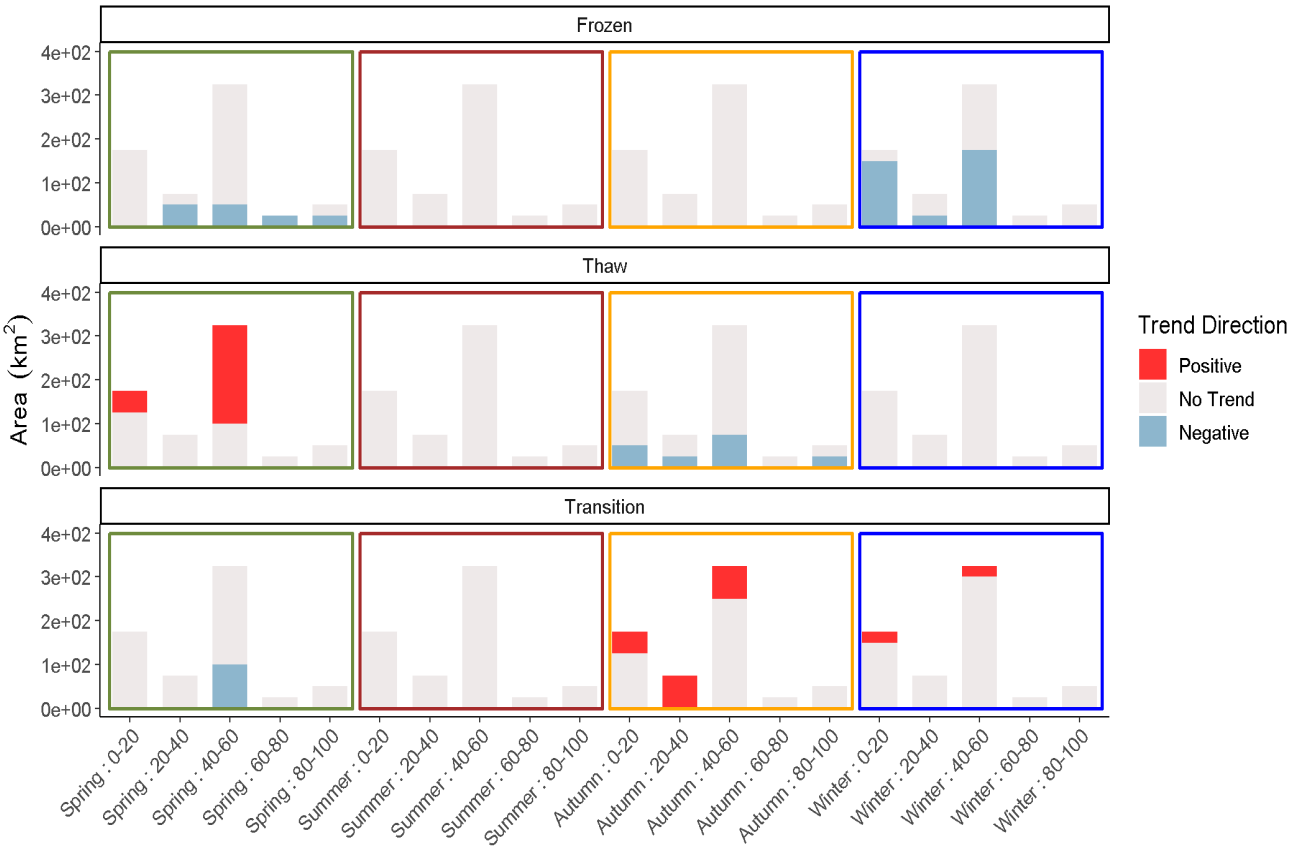


Figure 22. Patterns of change in terrain Freeze/Thaw state (shown here using the SSMI record) across DoD terrains in the Interior Alaska AOI, aggregated by permafrost classes (0-20; 20-40; 40-60; 60-80; 80-100) which indicate the probability of a terrain having near surface (< 1 m) permafrost (from Pastick et al. 2015).

Table 8. Summary of regional terrains in the Interior Alaska AOI having significant ($p < 0.1$) change in Indicator metrics of Thermal State, as observed in reanalysis and remote sensing records. These include air temperature (°C), land surface temperature (°C), and annual duration of frozen, transitional and thawed state (days year^{-1}). Here we provide terrain area (km^2) and the corresponding percentage of change relative to the Interior Alaska domain (453,248 km^2). Also provided is the average rate of change for the region. Major changes in terms of area and rate are highlighted in bold.

Metric	**Season**	**Increase** Area (10^3 km^2) (Percent)	**Rate**	**Decrease** Area (10^3 km^2) (Percent)	**Rate**
Air Temperature			(°C/yr)		(°C/yr)
MERRA2	Spring	2.06 (0.46%)	0.04	N/A	N/A
	Summer	**82.99 (18.31%)**	**0.03**	N/A	N/A
	Autumn	22.15 (4.89%)	0.04	N/A	N/A
AMSR	Spring	0.62 (0.14)	0.11	1.25 (0.28%)	-0.15
	Summer	N/A	N/A	1.88 (0.41%)	-0.10
	Autumn	18.75 (4.14%)	0.07	1.88 (0.41%)	-0.06
Freeze/Thaw			(days/year)		(days/year)
SMMR, SSMI(S) Frozen	Spring	1.25 (0.28%)	0	**130(28.68%)**	**-0.14**
	Summer	N/A	N/A	N/A	N/A
	Autumn	10.62 (2.34%)	0	6.88 (1.52%)	-0.21
	Winter	65.62 (14.48%)	0	39.38 (6.69%)	-0.06
SMMR, SSMI(S) Transition	Spring	2.50 (0.55%)	0.17	11.25 (2.48%)	-0.15
	Summer	13.75 (3.03%)	0	0.63 (0.14%)	-0.03
	Autumn	30.00 (6.62%)	0.17	0.63 (0.14%)	-0.13
	Winter	61.88 (13.65%)	0	N/A	N/A
SMMR, SSMI(S) Thawed	Spring	**45.63 (10.07%)**	**0.19**	N/A	N/A
	Summer	24.38 (5.38%)	0	N/A	N/A
	Autumn	6.88 (1.52%)	0.16	17.50 (3.86%)	-0.16
	Winter	28.75 (6.3%)	0.0	N/A	N/A
AMSR Frozen	Spring	0.04 (0.01%)	0.40	0.32 (0.07%)	-0.42
	Summer	N/A	N/A	N/A	N/A
	Autumn	8.03 (1.77%)	0	3.20 (0.71%)	-0.45
	Winter	40.14 (8.86%)	0	**64.87 (14.3%)**	**-0.32**
AMSR Transition	Spring	2.45 (0.54%)	0.34	N/A	N/A
	Summer	4.90 (1.08%)	0	1.30 (0.29%)	-0.32
	Autumn	3.42 (0.75%)	0.38	13.90 (3.07%)	-0.35
	Winter	**31.93 (7.05%)**	**0.04**	4.93 (1.09%)	-0.25
AMSR Thawed	Spring	0.11 (0.02%)	0.44	N/A	N/A
	Summer	23.87 (5.27%)	0.02	0.04 (0.01%)	-0.14
	Autumn	15.91 (3.51%)	0.38	0.83 (0.18%)	-0.28
	Winter	**37.26 (8.22%)**	**0.02**	0.29 (0.06%)	-0.18

5.1.1.3 Discussion and summary of Terrain Thermal State

Our analysis showed that, over the 15 year (2002 to 2016) AMSR Freeze/Thaw record, Alaska terrains on average experienced an increase in spring transitional and thawed period at respective rates of 5 and 8 days per decade. This rate of change is much higher than the ~ 3.5 days per decade reported in past studies (Smith et al. 2004; Zhang et al. 2011) which focused on years prior to 2006, suggesting that the rate of change in ground thaw has accelerated in recent years. We also observed a 4 days per decade increase in autumn transitional period. The occurrence of annual winter thaw events has also increased within Interior Alaska; we observed an increase of 0.4 days per decade in transitional state and 0.2 days per decade in thawed state during the winter. Increased winter thaw may negatively affect DoD winter trail networks planned for the region, including from the Tanana River Bridge to Blair Lakes Range (USAGA 2018).

Our analysis showed a significant long term change in the timing of snowmelt across Alaska. The timing of spring snowmelt occurred earlier each year, and the duration of snow melt also increased because of the earlier onset of melt. This change was most severe at higher elevation terrains across Alaska and within the Interior Alaska AOI, including the DoD terrains of Yukon Training Area, Tanana Flats Training Area, Donnelly Training Area. Here, the timing of snowmelt onset and snowoff shifted earlier in spring at rates of ~1 day per year. We also found that summer and autumn air temperatures on and surrounding the DoD terrains in the Interior Alaska AOI increased at a rate of 0.03 °C per year (1980 to 2017) as observed in NASA MERRA2 reanalysis record. This increase is similar to significant air temperature trends observed across the greater Alaska domain, at average rates of 0.03°C per year (in summer) and 0.06 °C (in autumn). It should be noted that because our analysis is limited to the years covered by the satellite and reanalysis products, we are missing the large increases in surface air temperature observed in Interior Alaska during the late 1970s. This sudden warming was a byproduct of a major phase shift in the Pacific Decadal Oscillation, and generated trends in station-observed surface air temperature of roughly 0.07 °C per year when considering the 1976-2018 time period (Alaska Climate Research Center, 2019).

The satellite records indicated that the number of frozen days in spring decreased significantly (1.4 days per decade) over much of Alaska. At the same time, the number of spring thaw days increased by ~ 2 days per decade. In the Interior, we found that the number of thawed days in autumn and early winter increased the most over Donnelly Training Area and Tanana River Training Area (by 1.5 days per decade) relative to the extended AOI. This is important because military training exercises are often scheduled to occur during this period, and the presence of unfrozen ground, which in some cases underlies recent snow cover (for example, Figure 23), can result in conditions that greatly restrict access to and travel across these remote and rugged terrains. Perhaps most alarming was our finding that the number of days in that the terrain surface remained frozen in spring decreased by 2 to 1.5 days per decade. The greatest decline in spring frozen days occurred in Alaska regions where the probability of permafrost occurring within 1 m of the surface (based on Pastick et al. 2015) was between 40 and 100%, primarily coinciding with zones of continuous and discontinuous permafrost. Terrains in Alaska that are characterized by the presence of less degraded continuous or discontinuous permafrost are likely the most vulnerable to more severe changes in ecosystem characteristics under a warming climate, given their susceptibility to heightened greenhouse gas emissions (Schuur et al. 2018), changes in soil wetness (Bring et al. 2016; Loranty et al. 2016) and terrain collapse (Edlund et al. 2018) as frozen subsurface soils continue to thaw.



Figure 23. New snow cover observed on wet, unfrozen ground in late October 2016 (left) at the Bonanza Creek research site near Fairbanks. This is in contrast to the frozen and snow covered surface soils observed a month later in November (right). Similar temporal patterns were detected in the satellite Freeze/Thaw records used in this study. [*Time lapse trail camera pictures provided by Dr. Sue Natali, NASA ABoVE project*]

5.1.2 Ecosystem Water Stress

5.1.2.1 Alaska

(a) Precipitation

The 0.5° resolution MERRA2 reanalysis records for 2017 showed that annual precipitation in Alaska ranged from under 20 cm per year in the semi-arid tundra regions of the North Slope and the northern Interior, to over 500 cm per year in the southern coastal regions (Figure S16). Seasonally, in the colder northern Alaska region the heavier precipitation patterns tended to occur in late summer and early autumn (Figure S17). The same precipitation patterns were observed over the Interior but with more precipitation occurring in autumn relative to more northern terrains. Conditions in southern Alaska remained rainy throughout the summer months and into autumn and winter. These patterns in the MERRA2 records agree with those reported elsewhere (see Shulski & Wendler 2007 for a general overview of Alaska climate).

The multi-year (1980 to 2017) time series of monthly grid cell precipitation for Alaska did not show a significant linear trend over the 38 year period (Figure S18). Instead, the records indicated substantial year-to-year variability and shorter term (2 to 3 year) wetting or drying patterns. However, our Mann-Kendall trend analysis for Alaska, applied on a per-grid cell basis, revealed regional hotspots of change in precipitation (Figure S19). In total, spring precipitation increased over 2.4% of terrains in Alaska (42,490 km^2) during this period and decreased over 5.7% of terrains (98,470 km^2; Table S2). Much of the significant multi-year increase in spring precipitation (> 20 mm per decade) occurred over the central North Slope, whereas a significant decrease in precipitation was observed further south towards Anchorage (~ 30 mm per decade).

In summer, precipitation significantly increased over 11% of Alaska terrains (194,010 km^2) and decreased over 2.4% (41,300 km^2; Table S2). Areas of significant increase occurred along the coastal regions, and the significant decrease primarily occurred in Interior Alaska within the upper Yukon basin (~ 10 mm per decade). Significant decreases in precipitation were also observed in autumn (1.96% of Alaska; Table S2), but this occurred primarily within northwest Alaska from the Brooks Range towards the Seward Peninsula. Whereas a significant increase in autumn precipitation was observed over 5.94% of Alaska's terrains (Table S2) but was primarily along the southern coastline.

Across Alaska over the 38 year MERRA2 record, spring precipitation significantly declined in boreal forests (primarily in the Interior) and increased in northern tundra communities. Summer precipitation also declined in the Interior boreal forests but increased in the southern coastal forests (Figure S19). Aggregating these changes according to permafrost zones (Figure S21) showed larger increases in summer precipitation over more coastal or southern terrains having little (0-20%) probability of near-surface (< 1 m) permafrost.

(b) Surface soil moisture

Regional patterns of surface soil moisture, observed in the most recent (2017) 25 km AMSR LPDR record year, showed generally drier surface conditions across mountainous terrains, and wetter soil conditions along lowland regions (Figure S16). In spring, the AMSR soil moisture showed wetter surface conditions across the Interior and down through the Yukon-Kuskokwim Delta relative to surrounding regions (Figure S17). The northern and mountainous regions had

drier conditions in spring because the presence of frozen or transitional surface states greatly reduced the amount of liquid water available for detection by the microwave sensor. In summer, soil surfaces generally remained very moist across Alaska (especially the coastal lowlands). In autumn, the Interior showed regionally drier surface conditions following warmer temperatures in late summer and absence of large rainfall events and deeper soil thaw.

Similar to precipitation, multi-year trends (2002 through 2017) were not detected in the time series of monthly average Alaska surface soil moisture (Figure S18). Instead, the time series revealed periods of wetting (including in the winter and spring) and drying. For example, large spikes in surface soil wetting were observed in January 2004 during a warming event, and March of 2007, 2010 and 2017 during snowmelt.

Our Mann-Kendall trend analysis, applied on a per-grid cell basis, showed substantial regional change in surface soil moisture occurring across Alaska (Figure S19). The 16-year 25 km AMSR record indicated significant patterns of drying in spring (up to 0.4 cm^3/cm^3 per decade) over 11% of the state (Table S2) and significant wetting in summer. The significant summer wetting trends occurred at a rate of 0.02 cm^3/cm^3 per decade over 34% of Alaska (Table S2), and up to 0.5 cm^3/cm^3 per decade within Interior Alaska. In autumn, moderate wetting trends were observed over 36% of Alaska (Table 10; 0.02 cm^3/cm^3 per decade) with more substantial changes occurring within the North Slope and the western Interior region (Figure S19). These trends generally agree with the observed regional increases in precipitation but may also reflect localized terrain wetting resulting from ground thaw and subsidence (Jorgenson et al. 2006).

Increased surface soil moisture was most substantial for boreal forests relative to the other vegetation categories, regardless of season (Figure S29), and occurred over greater land extent during summer and autumn. The increase in surface soil moisture was largest for permafrost terrains having a 40-60% probability of near-surface (< 1 m) permafrost (Figure S21).

(c) Water inundation

We evaluated changes in surface inundation using two passive microwave products, the 25 km AMSR LPDR Fw record (2002 to 2017) and the 5 km AMSR Fw record (2002 to 2015). The 25 km Fw is derived from *Tb* retrievals at 18.7 and 23.8 GHz and is sensitive to changes in standing water coverage (e.g., lakes, rivers, ponds) and flooding in vegetation (Watts et al. 2012). Whereas the 5 km Fw product uses *Tb* retrievals from 89 GHz that allows detection of surface open water (e.g., lakes, rivers, ponds), but not areas where there is an overlying vegetation canopy cover (Du et al. 2016).

Regional patterns of surface inundation, observed in the most recently available 25 km AMSR LPDR Fw (2017) and 5 km AMSR Fw (2015) record years, revealed strong spatial gradients in surface inundation (Figure S16). Surface inundation was more prevalent across Alaska's lowland coastal regions, within the Yukon-Kuskokwim Delta and the North Slope. These regions are characterized by an abundance of lakes, ponds and streams. The spatial patterns of inundation were similar between the two products, but the 5 km Fw was better able to capture local gradients and variability, as was expected. Seasonally, inundation was more widespread in spring (Figure S17) following snowmelt and rainfall occurring over frozen ground. Drying of lakes and the subsidence of river volume in summer resulted in lower Fw in summer and autumn, especially within the Interior (Figure S17).

As with precipitation and surface soil moisture, multi-year linear trends were not observed for the AMSR Fw records when considering the time series of monthly inundation averages for

Alaska (Figure S18). However, the per-grid cell Mann-Kendall trend analysis showed an increase in inundation in summer over 21% of Alaska (Table S2) at a rate of 0.12 grid cell fraction per year. This was observed primarily along coastal regions, but also in more localized areas within the Interior (Figure S19). In contrast, 15% of the state experienced a multi-year decrease in summer surface inundation, at a rate of 0.07 grid cell fraction per year (Table S2). This decrease occurred within the Interior, and within the Seward Peninsula (Figure S19). In autumn, an increase in surface inundation occurred over 36% of Alaska (at a rate of 0.14 grid cell fraction per year; Table S2) with the most substantial changes occurring within the North Slope, along state coastlines, and in the Interior (Figure S19).

Terrain flooding (i.e., water fraction) was most prevalent in boreal forest ecosystems, particularly in autumn (Figure S20). Significant increases in summer and autumn inundation also occurred within other land cover types, including tundra, wetlands and grass/shrub lands. Of interest is that the AMSR Fw also showed significant drying within boreal forest terrains (Figure S20); that this occurred in both the 5 and 25 km records indicates that this change likely reflects a decrease in open water (lakes, ponds, rivers), which is detected by both records. Considering the occurrence of these trends in regard to permafrost coverage, the 25 km Fw showed the largest increases (summer and autumn) in inundation within terrains having a 40-60% probability of near-surface permafrost (Figure S21), spatially coinciding with forest terrain in the Interior.

5.1.2.2 Interior Alaska

(a) Precipitation

The MERRA2 reanalysis record for 2017 showed spatial gradients of total annual precipitation within the Interior AOI (Figure 24) with generally wetter conditions (100 cm per year) occurring over higher elevation terrains towards the Alaska Range and northeast of Donnelly Training Area. This is in contrast to the slightly lower annual precipitation received over Yukon Training Area and Tanana Flats Training Area (45 to 55 cm per year). Seasonally, precipitation for these DoD terrains was approximately 20 cm in spring, 150 cm in summer and 55 cm in autumn (Figure 25).

For the Interior AOI, multi-year (1980 to 2017) linear trends were not observed in the regional Alaska MERRA2 precipitation totals (Figure 26-a). A slight decrease in regional precipitation was observed over Interior DoD terrains but the slope was not significant. The per-grid cell Mann-Kendall trend analysis detected a slight multi-year increase in spring precipitation amounts (~ 10 mm per decade) both east and west of the DoD terrains (Figure 27), whereas a decrease of 10.1 mm per decade was observed for 11% of the region (52,360 km^2; Table 9). Approximately 7.9% of the terrain area (35,590 km^2) showed a significant decrease in summer precipitation, at a rate of 15 mm per decade (Figure 27). In autumn, a very strong and significant increase in precipitation occurred over 2.9% of the domain at a rate of 26 mm per decade (Table 9). The significant decrease in spring precipitation on DoD land occurred primarily within forested terrains was also characterized by a 40 to 60% probability of near-surface permafrost (Figure 28, 29).

(b) Surface soil moisture

Surface soil moisture in the 2017 ASMR record showed wetter terrains (~0.2 cm^3/cm^3) within the Tanana River lowlands and including Donnelly and Tanana Flats (Figure 24), compared to the surrounding region. In the spring, soil moisture was relatively consistent across DoD terrains (~ 0.24 cm^3/cm^3). In the summer, soil moisture was spatially variable with higher surface soil moisture (~ 0.02 cm^3/cm^3) within the northern Tanana Flats and Fort Greely and lower soil moisture in the southern Tanana Flats (0.005 cm^3/cm^3; Figure S15). The generally drier surface soil moisture in autumn reflects an increase in transitional or frozen surface terrain state.

A slight but significant summer increase in surface soil moisture from 2003 to 2017 occurred over 27.5% of the region (125,000; Table 9) at an average rate of 0.02 cm^3/cm^3 per decade, and over 25.9% of the region in autumn (0.02 cm^3/cm^3 per decade). Spatial patterns in the Mann-Kendall trend results (Figure 27) revealed contrasting regions of change in summer and autumn surface soil moisture. In summer, a positive trend (indicating terrain wetting) occurred over Yukon Training Area and the more southern terrains in the Tanana Flats Training Area (an average rate of 0.02 cm^3/cm^3 per decade). Whereas terrain drying (at rates ranging from -0.004 to -0.01 cm^3/cm^3 per decade) was observed over Fort Wainwright (and northern Tanana Flats), Fort Greely, and a majority of the Donnelly Training Area. In autumn, significant terrain wetting occurred over the Northern Tanana Flats (rate of 0.03 cm^3/cm^3 per decade), while drying occurred over the Southern Tanana Flats (-0.05 cm^3/cm^3 per decade). The majority of the positive trend in spring, summer and autumn soil moisture occurred over DoD terrains classified as boreal forest (Figure 28). In spring and summer, there were significant increases in soil moisture during the past 15 years in terrains having a 20 to 60% probability of having near-surface permafrost (Figure 29). However, there were significant declines in soil moisture in summer during this time interval for terrains having a 60-80% probability of permafrost.

(c) Water inundation

The AMSR 5 km Fw observations (for 2015, the latest year on record) were able to capture the spatial patterns of surface open water within and near DoD terrains in the Interior AOI (Figure 24). A greater occurrence (up to 83% coverage within a grid cell) of open water was observed along the Tanana River. Substantial open water also occurred over western portions of the Tanana Flats Training Area, within Fort Wainwright and Eielson Air Base, Fort Greely and portions of the Donnelly Training Area. The 25 km Fw retrievals (for 2017) showed more general spatial gradients of surface open water (Figure 25), but without the detail offered by the 5 km Fw retrievals. The Tanana Flats Training Area had more open water in spring and autumn than in summer, whereas higher open water within Donnelly was observed in summer compared to other seasons.

There was no detected linear trend in annual surface water inundation (25 km or 5 km Fw) during the past 16 years within interior AOI and DoD terrain. (Figure 26). However, the Mann-Kendall per-grid cell trend analysis showed contrasting seasonal patterns of terrains having significant increase (wetting) or decrease (drying) in Fw inundation (Figure 27).

Overall, the 25 km AMSR Fw record showed that in 3.9% of terrains in the Interior AOI there were significant increases in surface water (Fw) in the spring (at a rate of 10% change in area per year) and in 9.7% of terrains there were significant increase in surface water in the summer (0.06% change in area per year). Both 25 km and 5 km records showed significant linear wetting trends in autumn over respective 25.9% and 7.8% of terrains (rates of 6 to 15% per year; Table

9). The relatively smaller extent of terrain wetting in autumn in the 5 km records reflects both the smaller retrieval footprint and the inability of 89 GHz *Tb* retrievals to detect surface water under vegetation canopies. In summer both the 25 km and 5 km Fw records showed significant multi-year drying of surface water over ~ 6% of the terrain (Table 9).

The 5 km Fw record showed the largest magnitudes of change across all seasons, although spatial heterogeneity was high even within the DoD terrains. In the spring and summer there were regions of both wetting and drying. In the spring wetting was most prevalent across the western section of Fort Wainwright (~ 0.10 Fw per year) while drying was most prevalent on the Northern Tanana Flats (-0.09 Fw per year). In the summer, most of Fort Wainwright experienced a wetting trend (~0.02 Fw per year) while the Donnelly Training Site experienced a strong drying trend (0.25 Fw per year). In the Autumn, drying trends in the 5 km Fw grid cells were observed over Fort Greely at rates up to 0.5 Fw per year, which could indicate the loss of open water lake bodies.

The significant trends in surface inundation observed for the Interior AOI and DoD units, aggregated by land cover, indicated that the most substantial decrease in AMSR Fw occurred in the summer and autumn within boreal forests (Figure 28). This decrease was observed primarily within the 25 km Fw record and likely reflects a reduction in surface flooding within forested terrains. However, boreal forests also experienced a relatively large increase in Fw in autumn, observed in both the 25 km and 5 km records. That this increase in Fw was also observed in the 5 m AMSR Fw records could indicate an expansion of open water lake, pond and river bodies during this period.

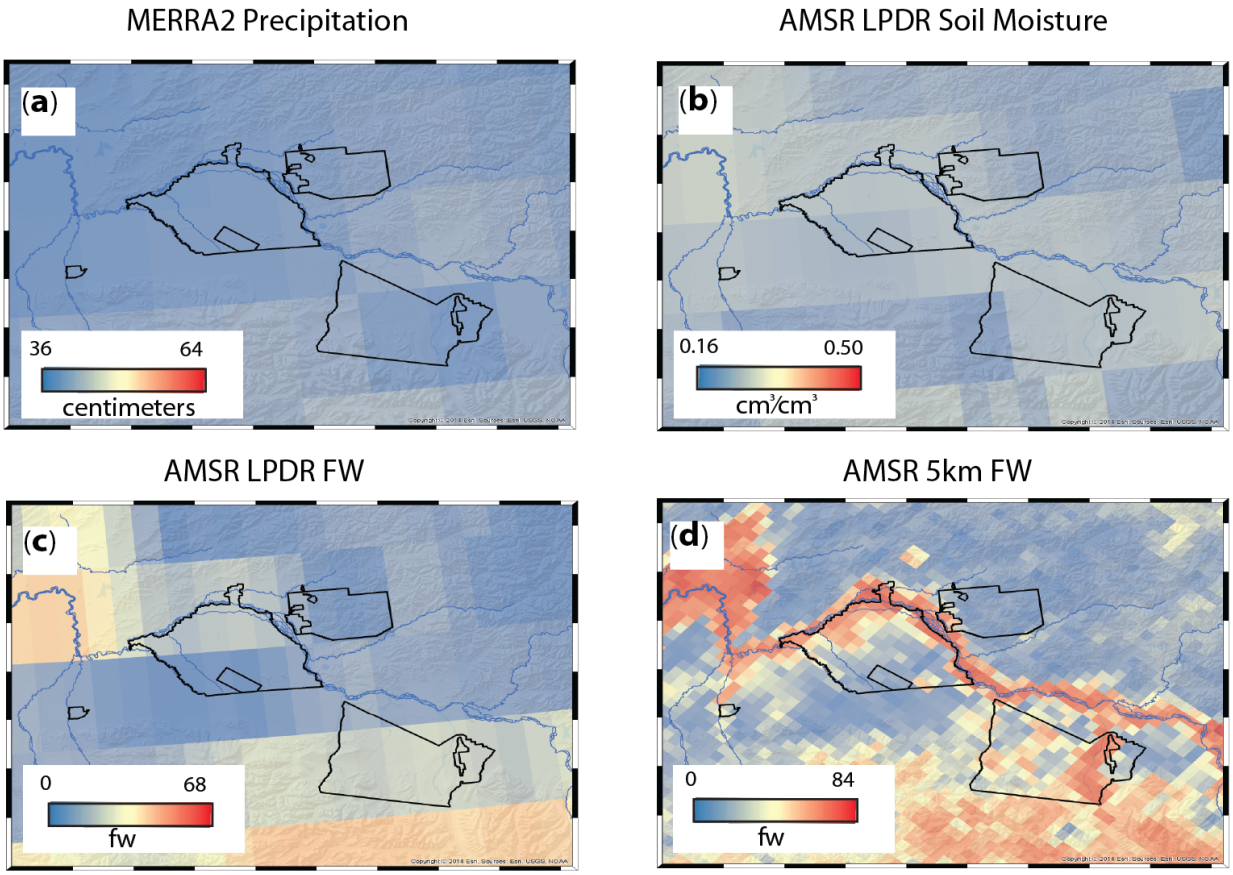


Figure 24. Water Stress Indicator metrics over the Alaska AOI and DoD terrains (outlined in black) for the 2017 (expect for 5 km Fw, which is for 2015) observation year. These include 0.5° MERRA2 total annual precipitation in cm per year (a) and annual averages for 25 km AMSR LPDR surface volumetric soil moisture in cm^3 cm^{-3} (b); 25 km AMSR LPDR Fw from 18.7 and 23.8 GHz *Tb* retrievals (c); 5 km AMSR Fw from 89 GHz *Tb* retrievals (d). Fw values represent percent surface water coverage within an equal area grid cell.

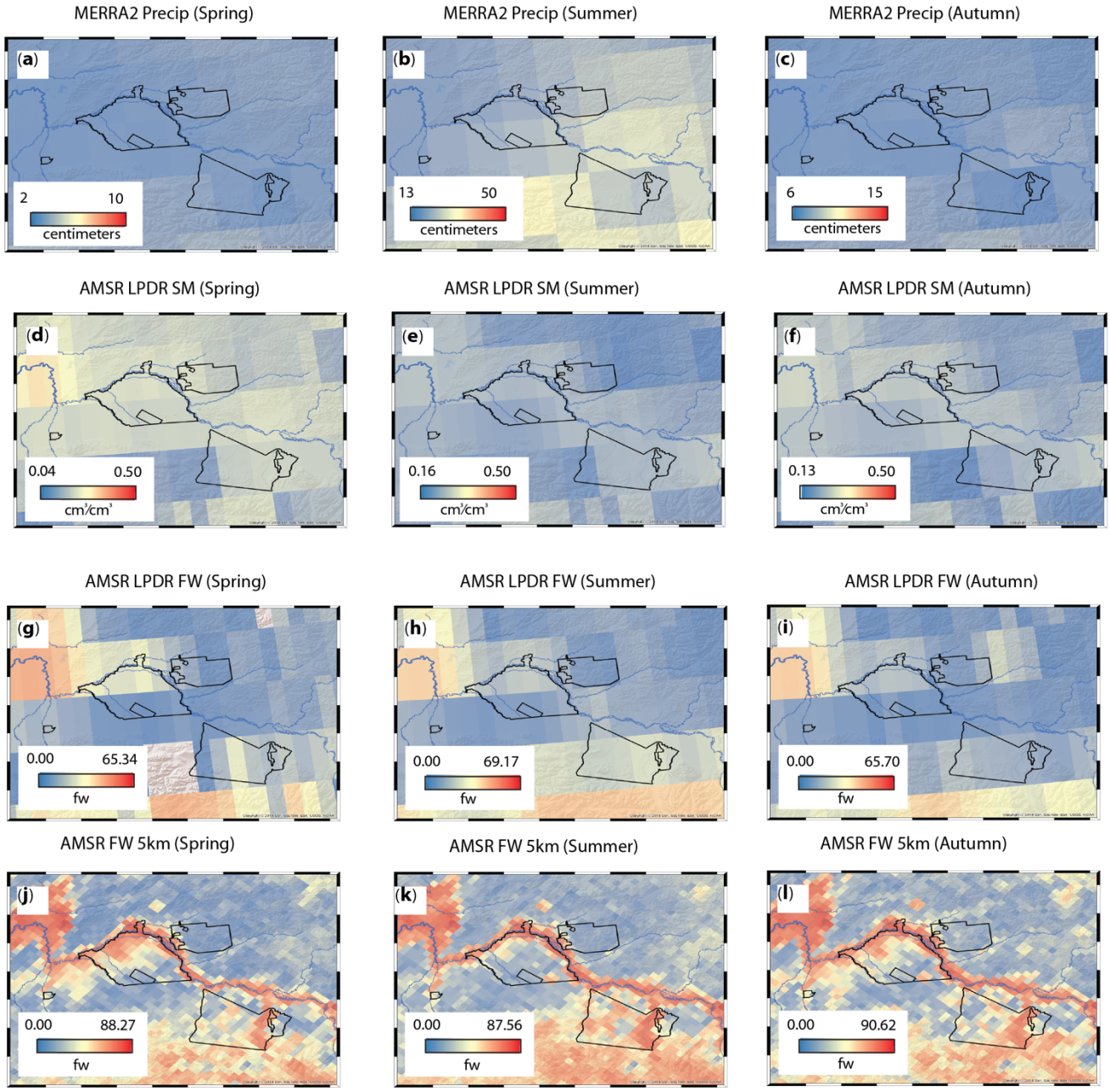


Figure 25. Seasonal Water Stress Indicators for the Alaska AOI and DoD terrains (outlined in black) for the 2017 (expect for 5 km Fw, which is for 2015) observation year. These include 0.5° MERRA2 total seasonal precipitation in cm. Also shown are the seasonal averages for 25 km AMSR LPDR surface volumetric soil moisture in $cm^3\ cm^{-3}$; 25 km AMSR Fw from 18.7 and 23.8 GHz *Tb* retrievals; 5 km AMSR Fw from 89 GHz *Tb* retrievals. Fw values represent percent surface water coverage within an equal area grid cell.

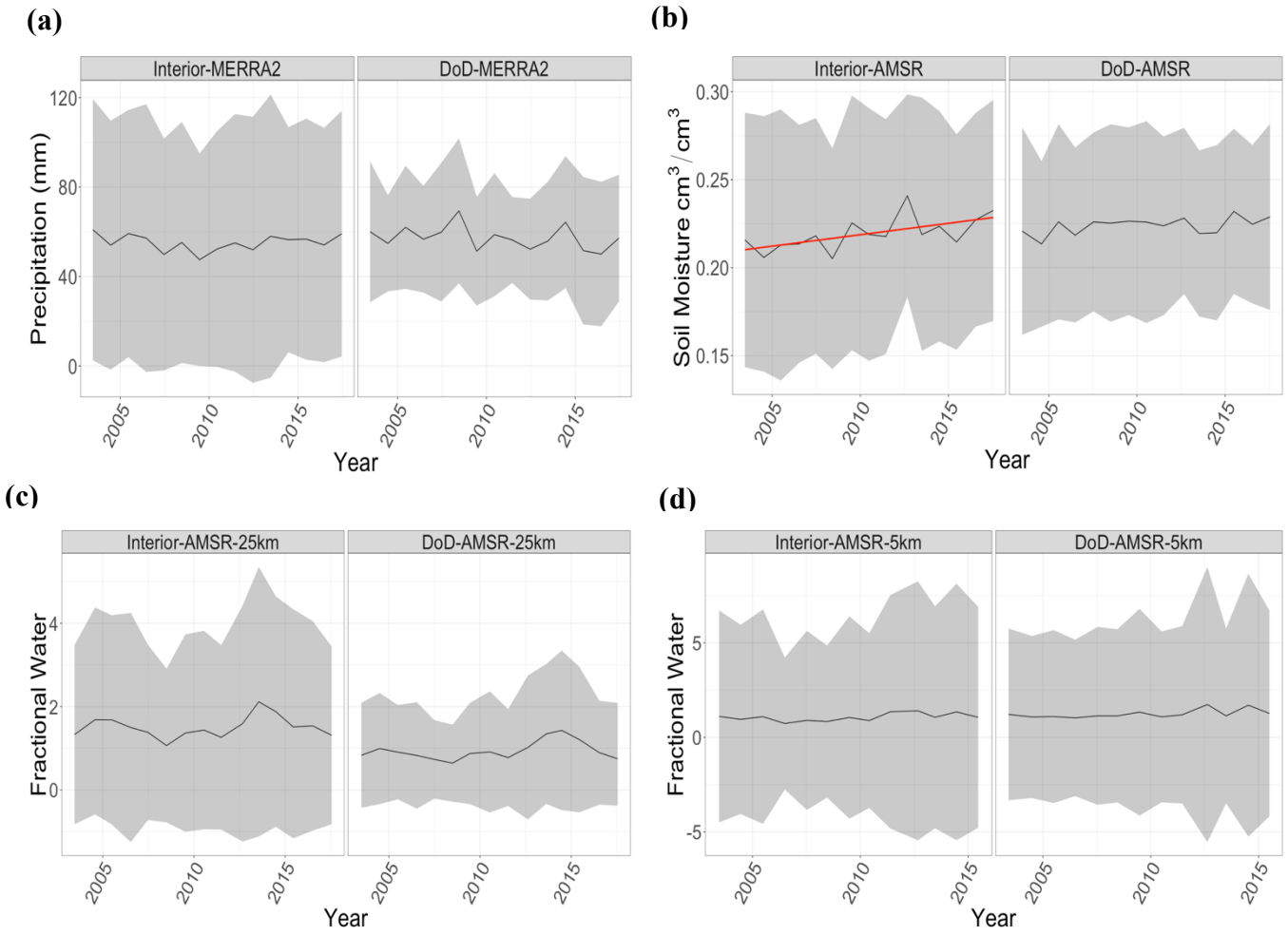


Figure 26. Time series of MERRA2 precipitation from 2003 to 2017 (a); AMSR LPDR surface soil moisture from 2003 to 2017 (b); AMSR fractional water (Fw) derived from 18.7 and 23 GHz *Tb* for 2003 to 2017 (c); AMSR Fw derived from 89 GHz *Tb* for 2003 to 2015 (d). The black line represents annual averages for the Interior Alaska AOI and DoD terrains. The gray shading around the line represents two standard deviations around the average. For the Interior AOI, soil moisture is significant ($p <= 0.05$, slope = 3.557e-06)

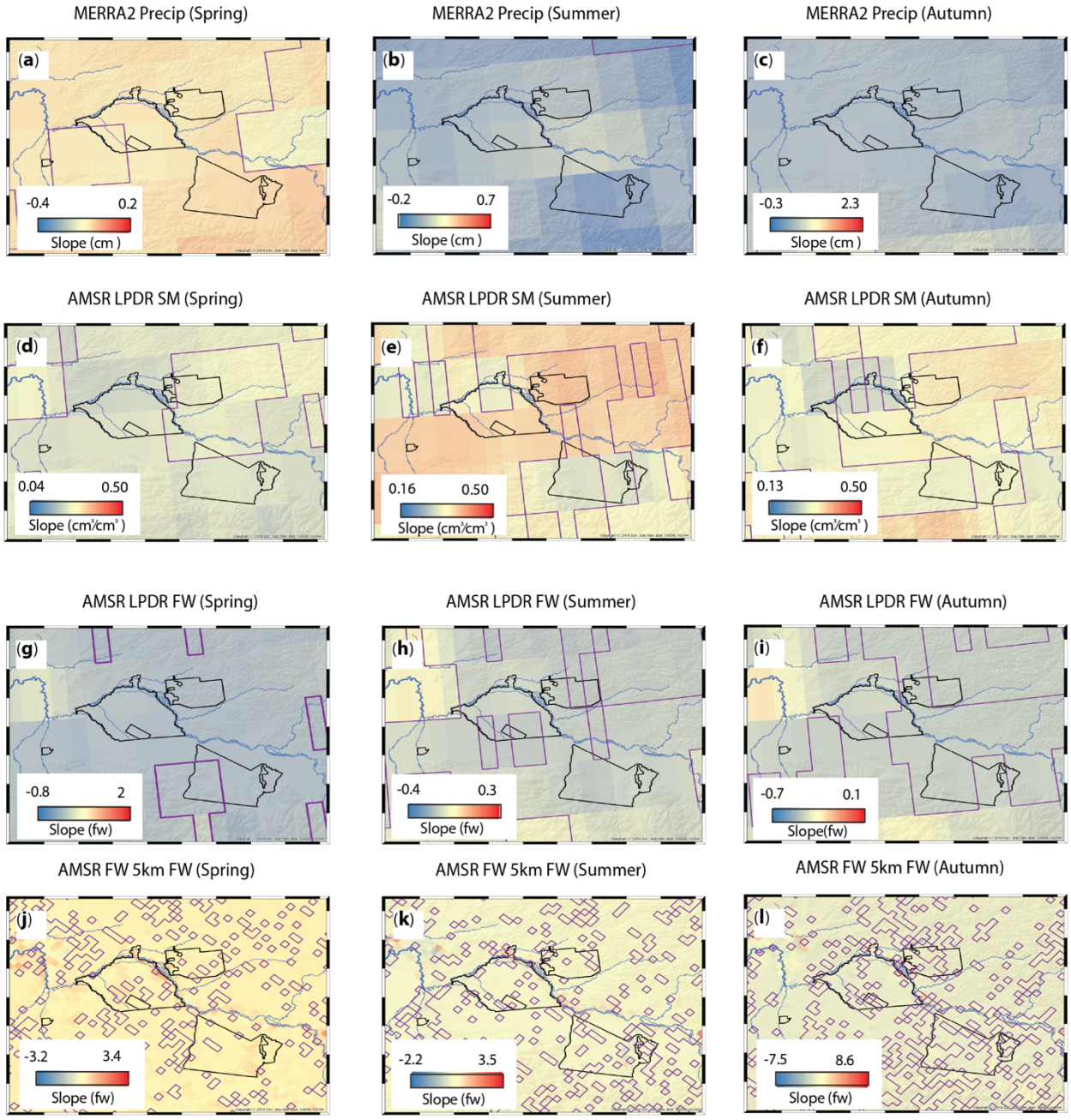


Figure 27. Sen slope results from MERRA2 precipitation (1980 to 2017) (a); AMSR (2002 to 2017) surface soil moisture (b); AMSR fractional water (Fw) derived from 18.7 and 23 GHz *Tb* for 2002 to 2017 (c); AMSR Fw derived from 89 GHz *Tb* for 2002 to 2015 (d) for Alaska in spring, summer and autumn. Regions where the slope trend (rates of unit per year) is significant ($p < 0.1$) are outlined in purple.

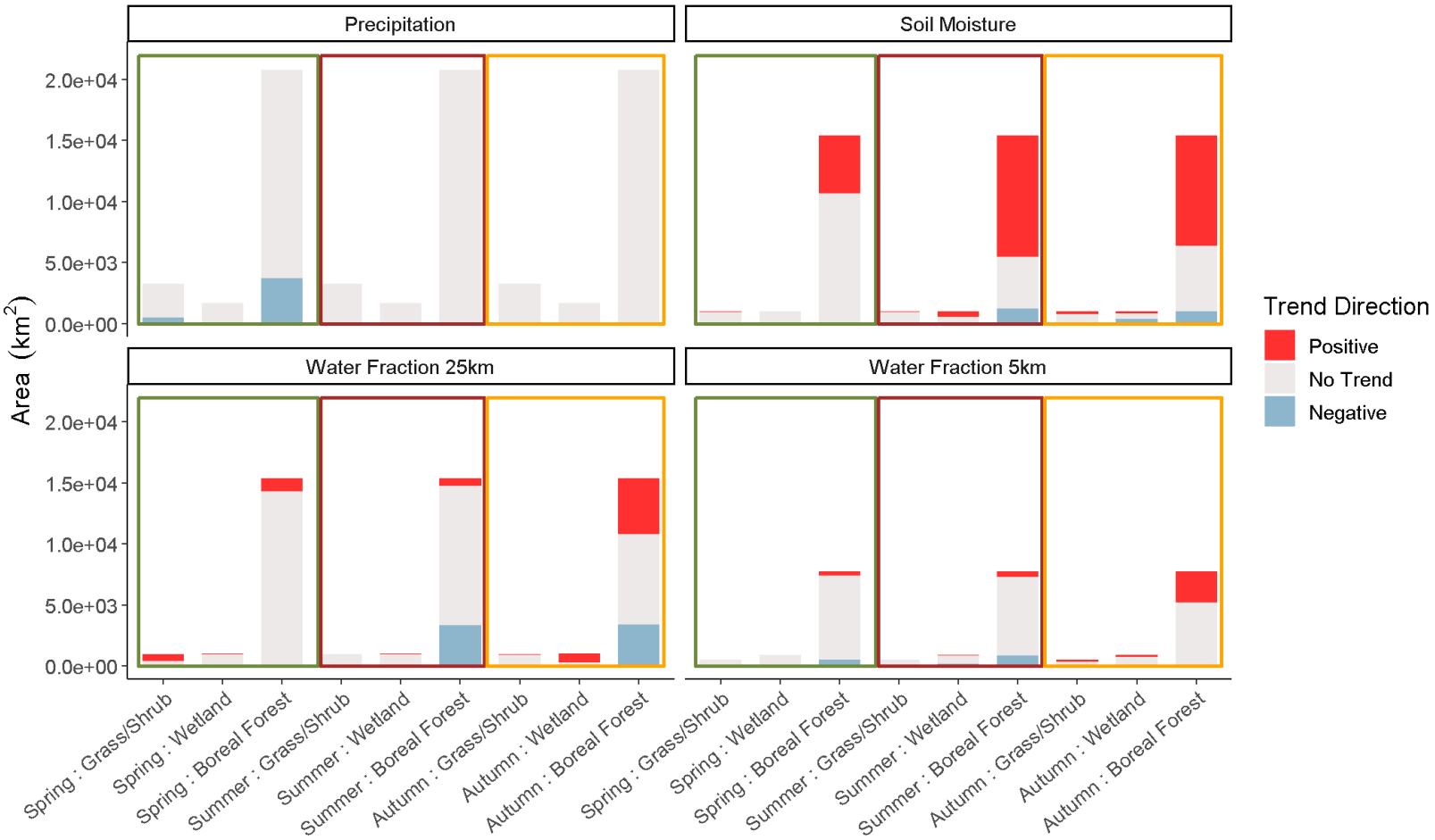


Figure 28. Patterns of change in Ecosystem Water Stress Indicator metrics (i.e., MERRA2 precipitation, AMSR surface soil moisture, AMSR LPDR 25 km water fraction (Fw) and AMSR 5 km water fraction) across terrains in the Interior Alaska AOI, aggregated by major vegetation classes (tundra; grass/shrub; wetland; boreal forest; temperate vegetation).

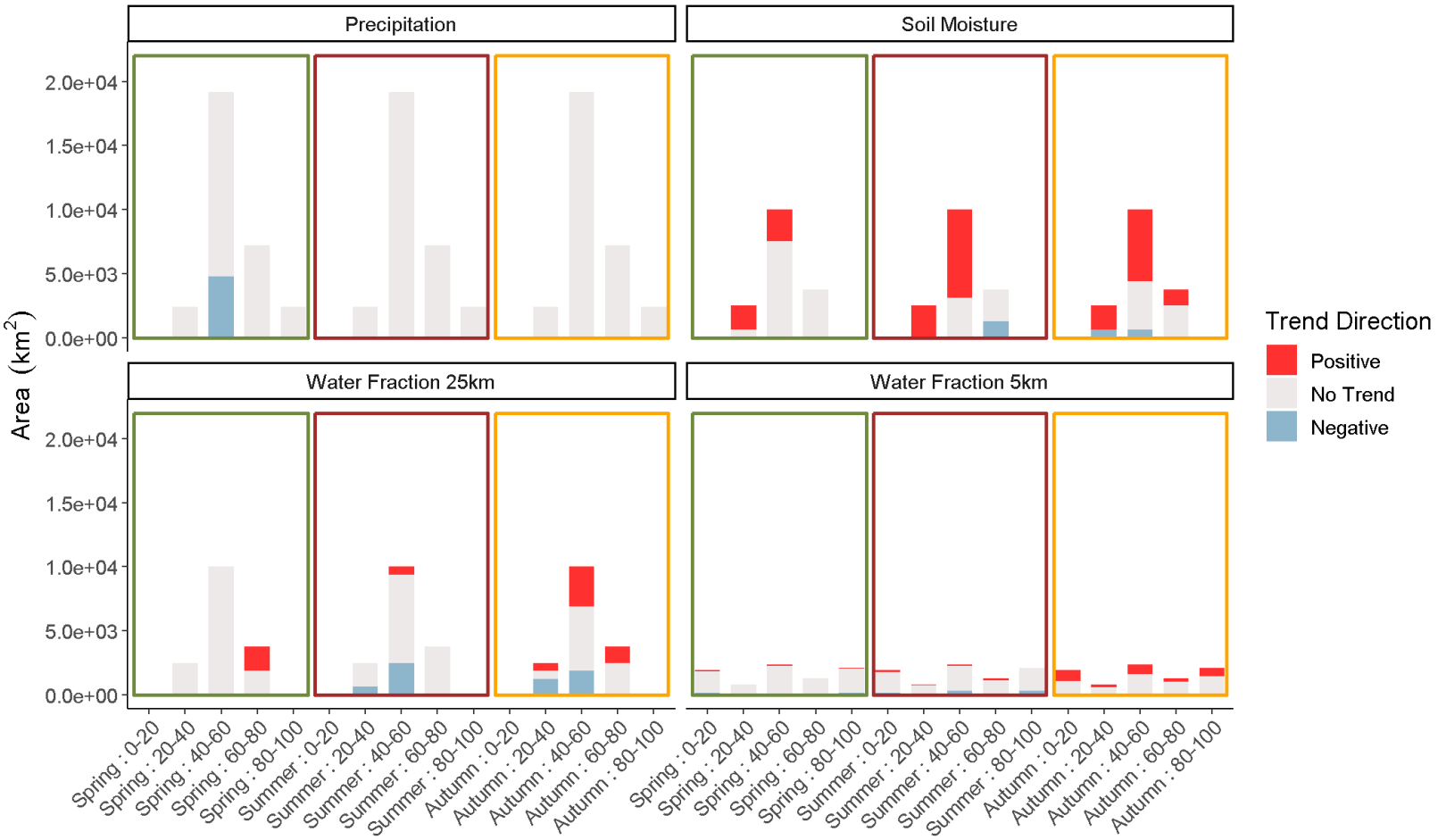


Figure 29. Patterns of change in Ecosystem Water Stress Indicator metrics (i.e., MERRA2 precipitation, AMSR surface soil moisture, AMSR 25 km and 5 km water fraction - Fw) across DoD terrains in the Interior Alaska AOI by permafrost classes (0-20; 20-40; 40-60; 60-80; 80-100), which indicate the probability of a terrain having near surface (< 1 m) permafrost (from Pastick et al. 2015).

Table 9. Summary of terrains in the Interior Alaska AOI having significant ($p < 0.1$) increase or decrease in Indicator metrics of Ecosystem Water Stress, as observed in the remote sensing and reanalysis records. These include precipitation (mm), passive microwave surface (~ 1 cm depth) soil moisture ($cm^3\ cm^{-3}$), and passive microwave fractional surface water inundation (fraction of grid cell area having surface water) at 18.7 and 23 GHz (25 km spatial resolution) and 89 GHz (5 km resolution). Here we provide terrain area (km^2) and the corresponding percentage of terrain showing change relative to the full domain (1.72 M km^2). Also provided is the average rate of change (Indicator unit $year^{-1}$) for the region. Significant changes in terms of area and rate are highlighted in bold.

Metric	**Season**	**Increase** Area (*$10^3\ km^2$*) (Percent)	**Rate**	**Decrease** Area (*$10^3\ km^2$*) (Percent)	**Rate**
		(mm/yr)			(mm/yr)
MERRA2 Precipitation	Spring	N/A	N/A	52.36 (11.55%)	-1.06
	Summer	2.15 (0.47%)	1.94	35.59 (7.85%)	-1.47
	Autumn	12.14 (2.89%)	2.86	N/A	N/A
		(cm^3/cm^3/yr)			(cm^3/cm^3/yr)
LPDR Soil Moisture	Spring	50.62 (11.16%)	0.002	1.87 (0.41%)	-0.001
	Summer	**125.00 (27.57%)**	**0.002**	10.62 (2.34)	-0.0007
	Autumn	**117.50 (25.92%)**	**0.002**	1.250 (0.27)	-0.0007
		(fraction/yr)			(fraction/yr)
25 km Fractional Water	Spring	17.50 (3.86%)	0.10	6.25 (1.38%)	-0.05
	Summer	43.75 (9.65%)	0.06	26.25 (5.79%)	-0.02
	Autumn	**79.37 (17.51%)**	**0.06**	6.87 (1.51%)	-0.03
5 km Fractional Water	Spring	7.32 (1.61%)	0.08	21.52 (4.75%)	-0.05
	Summer	8.42 (1.85%)	0.12	31.35 (6.91%)	-0.06
	Autumn	35.52 (7.84%)	0.15	35.52 (7.83%)	-0.06

5.1.2.3 Discussion and summary of Ecosystem Water Stress

In summary, our analysis of Ecosystem Water Stress metrics illustrated the complex, and sometimes conflicting, patterns of nonstationarity occurring across Alaska. The MERRA2 reanalysis precipitation records showed regional and seasonal hotspots of significant multi-year and monotonic wetting and drying. In spring, annual precipitation increased over a majority of Alaska. In particular we observed significant increases over the North Slope at a rate of > 20 mm per decade. This increase in precipitation occurred over continuous permafrost terrain, which is problematic as it could accelerate soil warming and the thaw of deeper, frozen, soil layers through advective heat transfer (Westermann et al. 2011) in addition to increasing the risk of high impact spring floods (Kane et al. 2008). Spring flooding can be detrimental to roads and other infrastructure, as was observed in the 2015 flood that damaged the northern stretch of the Dalton Highway, and it can also negatively impact wildlife migration and wildfowl breeding (Kittel et al. 2010).

There was a significant increase in summer precipitation from 2002 to 2017 over 11% of Alaska's terrains (194,010 km^2 or 47,940,915 acres; average rate of 30 mm per decade). This

increase primarily occurred across central Alaska along the Alaska Range, southward towards Anchorage and the coastal region, and across the Yukon-Kuskokwim Delta. This finding provides some support to projections by Atmosphere-Ocean General Circulation Models which indicate that precipitation is increasing within Alaska (Larsen et al. 2008).

However, there was also a significant decrease in precipitation during this time period in summer over Interior Alaska including on DoD terrains (at a rate of 10.1 mm per decade). In autumn, the only region with a significant decline in precipitation was northwest Alaska near the Seward Peninsula.

The difference in precipitation and soil moisture trends highlights the importance of landscape characteristics (e.g., permafrost presence or absence) in driving patterns of soil moisture. Soil moisture significantly increased in both summer and autumn during this time period across the DoD training range domain, including the Yukon and Tanana Flats Training Areas. This increase in soil moisture could help support vegetation growth and wetland habitat but can also increase greenhouse gas emissions of methane (Douglas et al. 2014; Schuur et al. 2018), restrict motor vehicle and foot travel across wet terrains (Affleck et al. 2005), and accelerate permafrost thaw (Jorgenson et al. 2010). Soil moisture trends were not homogenous across DoD lands, as there was a significant decrease in summer soil moisture over the Donnelly Training Area.

Our study also illustrated the spatial complexity of changes in surface inundation. We found that surface water inundation increased in summer along coastal zones and more locally within the Interior AOI from 2002 to 2017. This significant increase in standing water occurred over 21% of the state (368,000 km^2 or 90,934,780 acres), while at the same time, 15% of Alaska's land (253,750 km^2 or 62,702,990 acres) experienced a multi-year decrease in summer inundation. These contrasting regions of open water drying and wetting have been reported elsewhere and reflect similar patterns that are occurring over the northern Arctic-boreal domain (e.g., Jones et al. 2011; Watts et al. 2012; Pastick et al. 2018) as a consequence of complex regional and landscape level changes in hydrology following shifts in permafrost condition, precipitation, atmospheric demand, and land cover change.

Within the Interior AOI, we found that 9.7% of terrains (out of 453,248 km^2; 112,000,020 acres) had experienced a significant increase in surface inundation during our observation period (2002 - 2017), whereas 5.8% showed a significant decrease in summer inundation, including in the western portion of Fort Wainwright, over Fort Greely and Donnelly Training Area. In autumn, substantial increases in inundation were observed over ~ 26% of the Interior region and most strongly on the Fort Greely DoD terrain. The increase in autumn inundation over DoD Training Areas is concerning because, as with soil moisture, surface flooding can greatly impact the ability of troops to safely access and move within the remote terrains.

5.1.3 Vegetation State

5.1.3.1 Alaska

(a) Microwave VOD

Unlike VIS-NIR indicators of vegetation (e.g., NDVI) which are metrics of greenness, the microwave VOD is sensitive to the amount of water occurring within standing biomass. Larger VOD retrievals tend to occur in areas having a higher volumes of healthy, aboveground biomass which hold more water during the non-frozen season. Total water content in biomass is influenced by ecosystem water stress (e.g., Rao et al. 2019) and forest composition (Saatchi & Moghaddam 2000) with higher water content occurring in young coniferous stands (e.g., spruce or pine) relative to deciduous stands (e.g., aspen and birch). Biomass water content also increases linearly with tree height.

The spatial patterns observed across Alaska in the 25 km AMSR VOD record for 2017 (Figure S22) reflect the influence of biomass density and structure, with higher VOD occurring within the boreal forests of Interior Alaska including the upper and lower Yukon river basin regions. In general, lower VOD was observed within the more sparsely vegetated tundra and high elevation mountain regions. Seasonally, VOD in spring was larger in boreal forest regions, compared to the surrounding domain, and relatively low across the colder tundra domain (Figure S23) where vegetation greenup does not occur until later in May through early June. An increase in VOD was observed in summer, particularly over the tundra regions where plant growth occurs rapidly over the short non-frozen season. In late summer and into autumn, declines in VOD occurred following vegetation senescence and water stress within boreal vegetation because of drier soil and/or air conditions.

Although a significant trend was not observed in the multi-year (2002 to 2017) AMSR VOD annual averages for Alaska (Figure S24), the per-grid cell Mann-Kendall trend analysis detected significant increases in VOD in spring over 14% of the state (248,000 km^2; Table 12) at a rate of 0.1 VOD unit per decade. This increase primarily occurred within the western half of Alaska (Figure S25), over terrains experiencing significant advances in annual spring snow melt, increasing air and land temperatures over the annual non-frozen period (see Section 5.1.1), and wetter soil moisture conditions in summer (Section 5.1.2). A small monotonic increase in VOD occurred over 11% of Alaska terrains in summer (196,000 km^2; Table S3) at a rate of 0.07 units per decade and over 15.6% of terrains in autumn (0.08 units per decade), but primarily along coastal regions (Figure S24).

Significant multi-year decreases in VOD were observed across the Interior region in spring, summer and autumn (Figure S25). However, this decrease was most widespread in summer and spanned 357,000 km^2 (approximately 21%) of Alaska's terrain and occurring at an average rate of 0.12 units per decade. These patterns of VOD decline mainly coincided with forest regions that burned within the past 28 years (Figure S26).

Aggregating significant trends according to vegetation class (Figure S27) further confirmed that the most substantial declines in VOD occurred in the summer within boreal forest communities, while the largest VOD declines occurred in the spring, also within boreal forests. This analysis also showed consistent increases in VOD within tundra across spring, summer and autumn, which could reflect earlier snowmelt, wetter summers and delayed freeze later in the

growing season. Increased VOD in wetlands over the summer and autumn period likely reflect increased soil moisture in conjunction with warmer summer temperatures.

(b) VIS-NIR Indices

The spatial patterns observed in the 250 m MODIS NDVI averages for 2017 (Figure S22) illustrate regional gradients in relative vegetation greenness. In Alaska, regions having NDVI > 0.8 were found in patches across the Interior and through the southwest. Higher NDVI values can indicate a higher density of active photosynthetic vegetation. Lower NDVI values (< 0.3) generally occurred in non-forested and tundra regions, including the North Slope and coastal plains. The seasonal progression of NDVI over Alaska (Figure S23) generally coincided with the location of coniferous forest communities (where values are greater than 0.2 in spring), and the early spring growth of wetland, shrub and graminoid communities in the southern coastal regions. The decline in NDVI in autumn indicates vegetation senescence and leaf fall, and NDVI values below ~ 0.1 (which tend to indicate non-vegetated terrain) in regions dominated by lakes and wetlands reflect the seasonal expansion of surface open water.

The NDWI is an indicator of canopy water content, but also incorporates water in non-vegetated surfaces (e.g., surface water on the ground or on snow), and therefore NDWI, unlike VOD, is not able to fully quantify changes in total biomass water content. The spatial patterns observed in the 250 m MODIS NDWI averages for 2017 (Figure S22, S23) coincided with regional landscape characteristics, with higher water content in the forested regions in the Interior (indicated by negative NDWI values). Higher, positive values in NDWI showed the locations of snow covered mountain ranges (e.g., the Alaska and Brooks Range) and regions having an abundance of lake bodies (e.g., the North Slope). In spring (Figure S23) NDWI showed extensive coverage of residual, melting snow and ice across Alaska (values > 0) and live forest biomass within the Interior (values < 0). A similar pattern was also observed in autumn, where higher positive NDWI showed the locations of recent snowfall.

Although a slight increase was observed in the multi-year (2002 to 2017) NDWI annual averages for Alaska (Figure S24), most likely influenced by the widespread melting of ice and snow within the mountain ranges, it was not significant. The NDVI time series also showed a slight positive increase over the 16-year observation period but this was not significant. However, the trend detection results showed substantial, significant increases in NDVI (greening) from 2002 to 2017 across the Interior (Figure S25), which likely reflects forest recovery in areas experiencing fires in the past three decades (Figure S26). NDVI increased across Alaska's boreal forests in spring, summer and autumn season (Figure S25) and affected over 19% of terrain area (331,000 km^2; Table S3) at a rate of > 5% per year. There was also a significant decrease in NDVI (browning) in summer for 14% of the state, also occurring within the Interior region (Figure S26; Table S3). In addition, spring and autumn NDWI significantly decreased from 2002 to 2017 over >10% of Alaska (Table S3). The localized patterns of strong greening and browning corresponded to observed fire events, where the direction of trend in NDVI was strongly dictated by when the fire occurred within the observational time period (Sulla-Menashe et al. 2018). In addition, significant decreases were observed in NDWI in spring and autumn, over >10% of Alaska (Table S3). In spring, this decrease in NDWI occurred across vegetation categories (incl. tundra, grass/shrub, wetlands and boreal forests; Figure S27) which could correspond with earlier vegetation growth. In autumn, the decrease in NDWI occurred primarily in boreal forest regions.

5.1.3.2 Interior Alaska

(a) Microwave VOD and VIS-NIR indices

The spatial patterns observed in the 25 km AMSR record for 2017 (Figure 30) indicated that the largest growing season VOD (values > 1.5) within the Interior AOI occurred over the far eastern region of Yukon Training Area and to the northeast, including lands within and surrounding the Chena River State Recreation Area. In general, larger VOD values indicate terrains having a higher density of live and photosynthetically active aboveground biomass (i.e., well established spruce forests with closed canopy cover). Areas having much lower VOD (< 0.6) were observed over river and lake influenced lowlands west of the Tanana Flats Training Area (Figure 30) and in more elevated regions south towards the Alaska Range where vegetation is sparse. Seasonal changes in VOD were not as easy to observe visually (Figure 31) relative to MODIS NDVI and NDWI, especially in forested regions, but showed an increase from spring to summer, and a decrease from summer to autumn that coincided with changes in vegetation water content. The NDVI record, in contrast, showed a sharp increase in positive values between spring and summer, indicating vegetation greening following snowmelt.

No significant regional trend was observed in the NDVI or NDWI from 2002 to 2017 for the Interior AOI and DoD terrains (Figure 32). However, a significant negative VOD ($p < 0.01$, slope = 4.137e-05) trend did occur within DoD terrains. Further on-the-ground data are needed to confirm this trend, as this time interval incorporates the 2011/2012 change in VOD satellite sensor (Du et al. 2017). However, the sensor data streams have been intercalibrated and the trend that was detected over DoD terrains was not detected in surrounding regions, thereby providing greater confidence in this finding.

In the summer of 2012, an especially large and severe 85,000 acre (344 km^2) fire burned through the DoD's Yukon Training Area and surrounding terrains (Figure 33, 34). The impact of this fire is especially evident in the VOD time series for DoD terrains (Figure 32-a) where VOD decreases in late 2012, followed by a small rebound in 2013, a decrease in 2014, and a slow upward progression of VOD magnitude with vegetation recovery from 2015 onward. Similar patterns of post-fire change in VOD have been reported elsewhere for Alaska (Jones et al. 2013). The initial post-fire increase in VOD is a result of residual moisture retention within standing dead tree biomass in addition to the post-fire greenup of shrubs and other understory biomass. By two years after fire, much of this standing wood had begun to dry, reducing water retention and VOD. Three years post-fire and beyond, forest regeneration and tree reestablishment led to a continued increase in VOD.

The per-grid cell Mann-Kendall trends for this region mainly indicated a monotonic decrease in the 16-year VOD record, especially evident in spring and summer (Figure 35-a,b). Many of the terrains showing more negative, and significant, slopes in VOD (< -0.01) coincide with patches of monotonic NDVI decrease (Figure 35-e; regions in blue) in summer and increases in spring and summer NDWI (Figure 35-g, h; regions in red) where burns have occurred within the past ten years. In total, 7.6 million acres (31,000 km^2), or 160% of the Interior AOI, has burned over since 2002. This represents 408 fire events (many of these occurred on DoD terrain following bombing). There was also general increase in NDVI over the region in both summer and autumn, which could indicate a slight increase in vegetation growth occurring with warming and wetting (e.g., as detected in our analysis of surface soil moisture). Further monitoring of this

change in NDVI is recommended, as the "greening" of vegetation in summer could provide more fuel sources for future fires, especially if they coincide with periods of extreme summer air temperatures (Trainor et al. 2009). For NDWI, positive trend slopes are especially evident over fire-affected terrains, indicating vegetation recovery and an increase in leaf biomass and water content. Other areas not affected by recent burning also show a positive change in NDWI, but this could simply indicate an increase in plant growth associated with warmer summers and an extended autumn non-frozen period. Some of the decreases in NDWI, observed in summer, might have also been influenced by the drying of surface water and litter layers.

In total, summer VOD decreased in 6.3% (108,125 km^2; 26,718,269 acres) of Interior Alaska AOI lands from 2003 through 2017 (Table 10). The most substantial decrease in VOD occurred in boreal forests and primarily in spring and summer (Figure 36). A majority of the significant declines in spring and summer VOD occurred over terrains having a 40-60% probability of near-surface (< 1 m) permafrost (Figure 37). In contrast to VOD, a positive increase in NDVI (greening) occurred over 9 to 13% of the AOI (Table 10), throughout the spring, summer and autumn (at rates of $\geq$ 0.05 NDVI unit per year). The NDVI greening occurred primarily in DoD lands classified as boreal forest (Figure 36). However, we also observed multi-year decreases in NDVI (most apparent in summer and autumn; Figure 35) over the forested northern portions of the Yukon Training Area and southern portions of the Tanana Flats Training Area, which correspond with an increase in NDWI. The underlying cause of the NDVI and NDWI changes at these locations has not yet been identified and further on-the-ground observations are needed to understand the drivers of these trends.

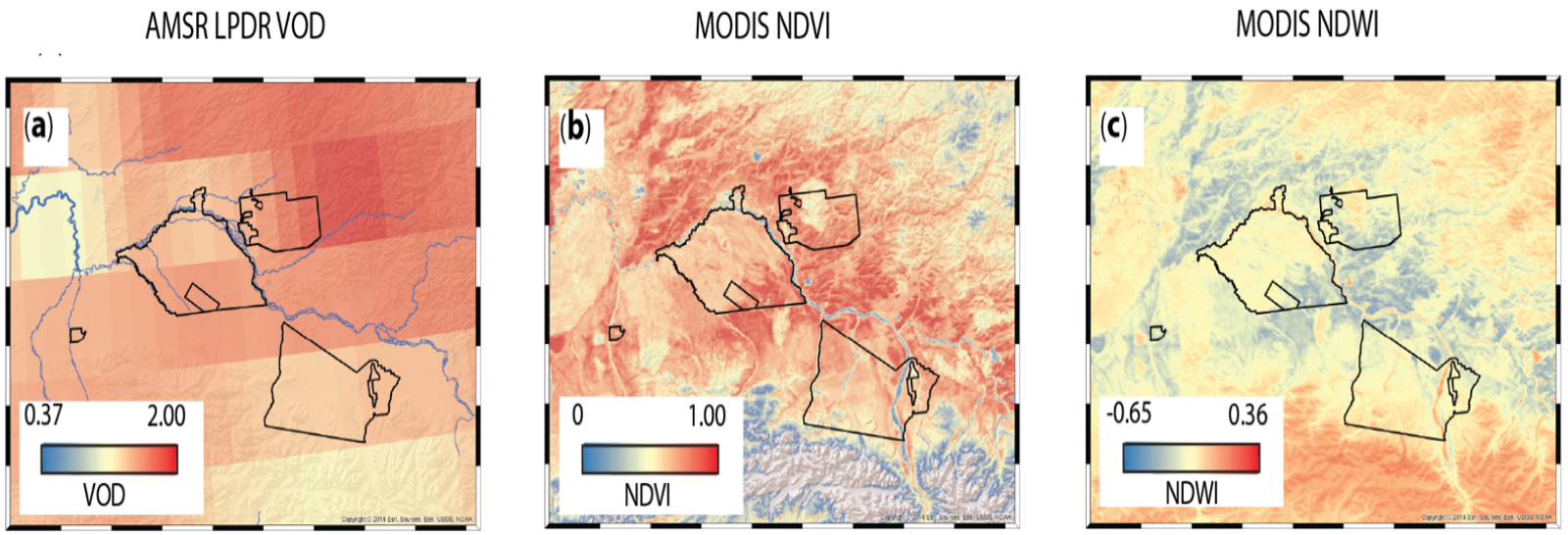


Figure 30. Maps of average Vegetation State Indicator metrics over the Interior Alaska AOI and DoD terrains (outlined in black) for the 2017 observation year. These include 25 km AMSR vegetation optical depth (VOD), 500 m MODIS normalized difference vegetation index (NDVI) and 500 m MODIS normalized difference wetness index (NDWI). For NDVI, we exclude regions having values less than 0, which indicate the presence of ice and snow.

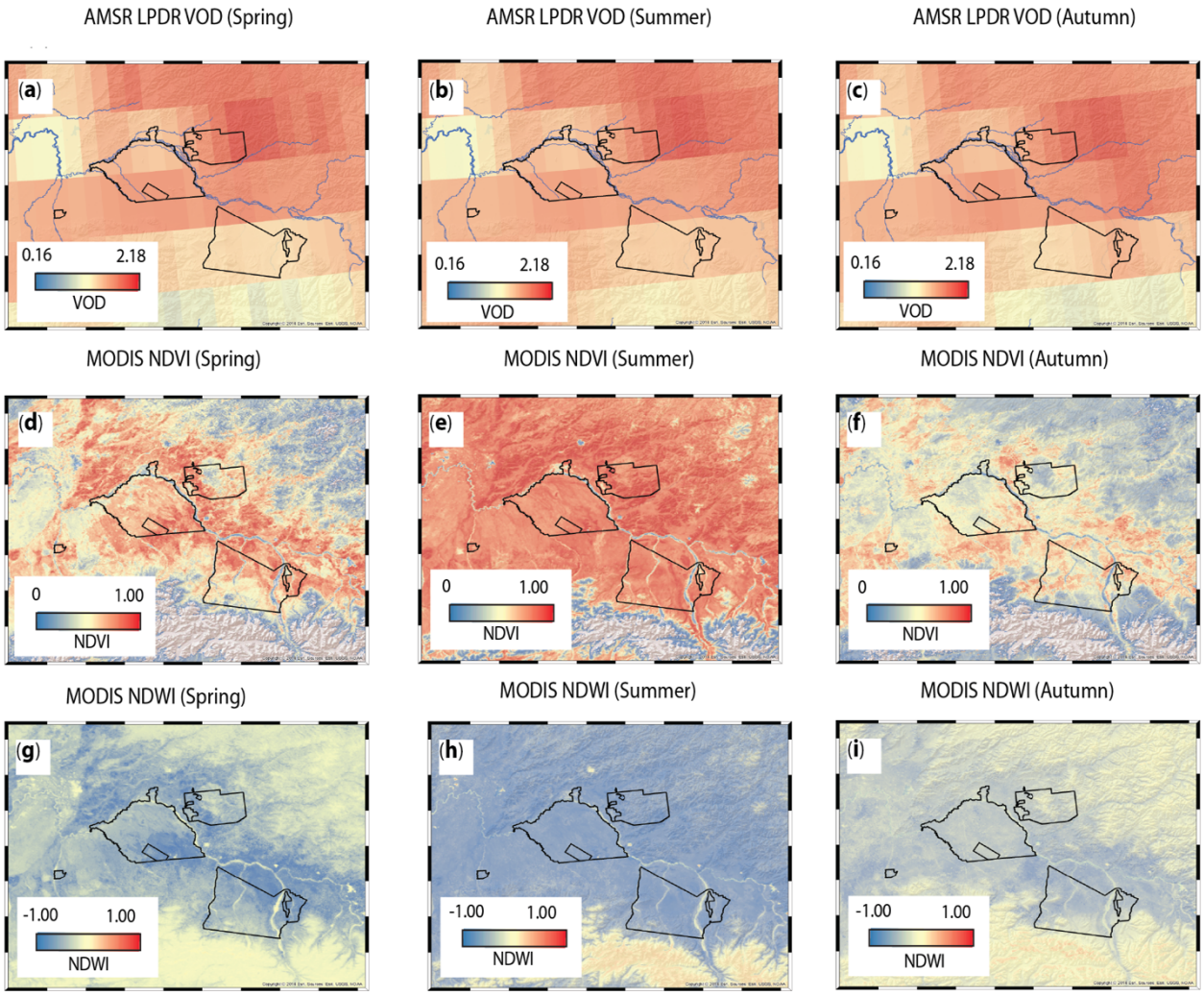


Figure 31. Maps of average seasonal (spring, summer, autumn) Vegetation State Indicator metrics over the Interior Alaska AOI and DoD terrains (outlined in black) for the 2017 observation year. These include 25 km AMSR vegetation optical depth (VOD), 500 m MODIS normalized difference vegetation index (NDVI) and 500 m MODIS normalized difference wetness index (NDWI). For NDVI, we exclude regions having values less than 0, which indicate the presence of ice and snow.

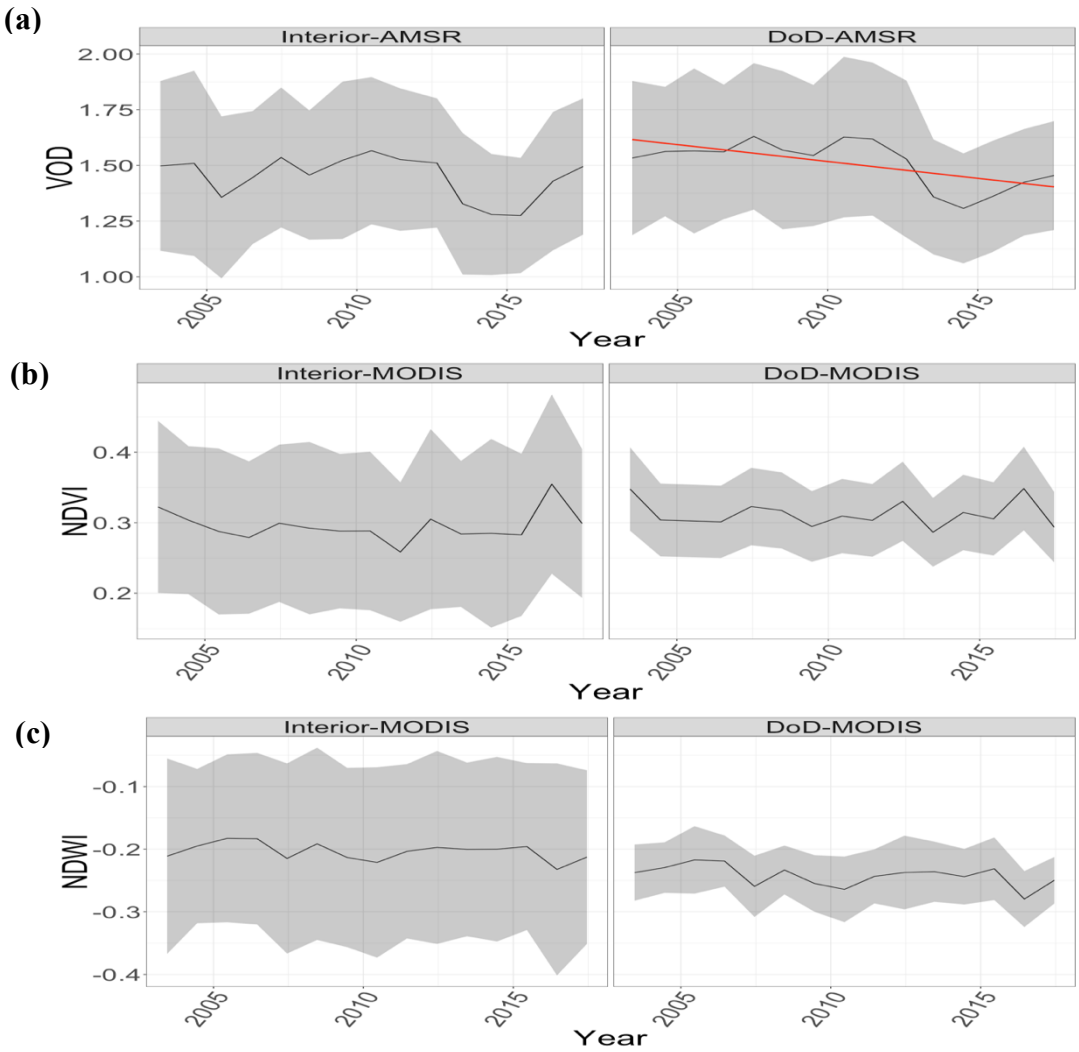


Figure 32. Time series of AMSR VOD from 2003 to 2017 (a); MODIS NDVI from 2003 to 2017 (b); and MODIS NDWI from 2003 to 2017 (c). The black line represents annual averages for the Interior Alaska Area of Interest (AOI) and DoD terrains within the AOI. The gray shading around the line represents two standard deviations around the average. The red line represents significant linear trend ($p <= 0.05$, slop = -4.137e-05).

(a) (b) (c)



Figure 33. Abrupt disturbances in vegetation and post-fire vegetation recovery observed within Interior Alaska. The 2012 burn within DoD's Yukon Training Area (a), was widespread and severe but patches of unburned deciduous and coniferous forest illustrate the spatial complexity of disturbance events. The picture in (b) was taken in 2018 and shows substantial regeneration of vegetation within the understory following the 2012 fire. At other sites, including the more moderate intensity 2009 burn towards Clear Air Force Station (c), stands of unburned forest and understory vegetation show little remaining evidence of fire. [*Images provided by J.D. Watts*]

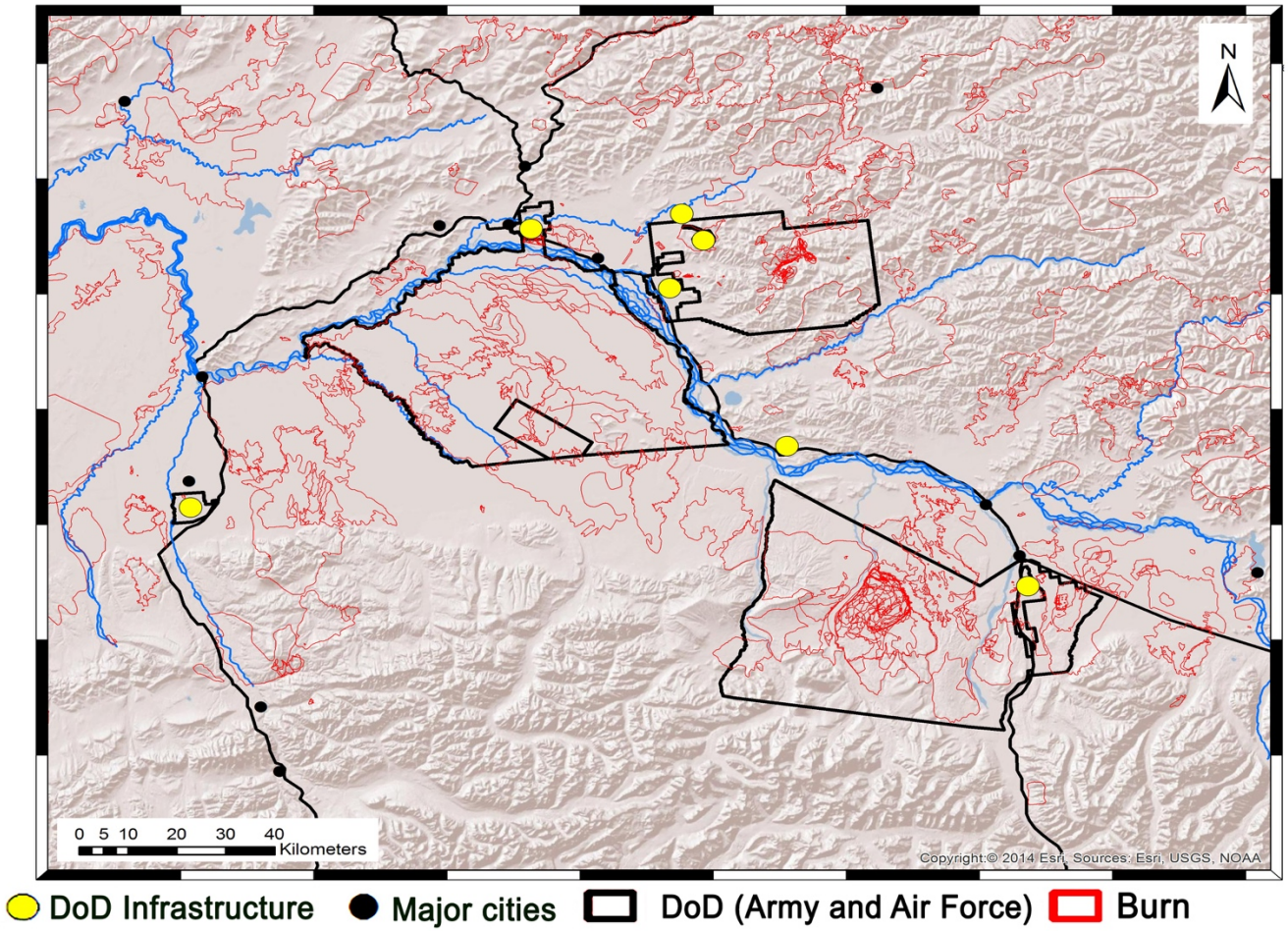


Figure 34. Locations of burn events within the Interior AOI occurring since 1990, overlain on a terrain map. The red polygons indicate burn perimeters. [*Burn area obtained from the Alaska Large Fire Database*]

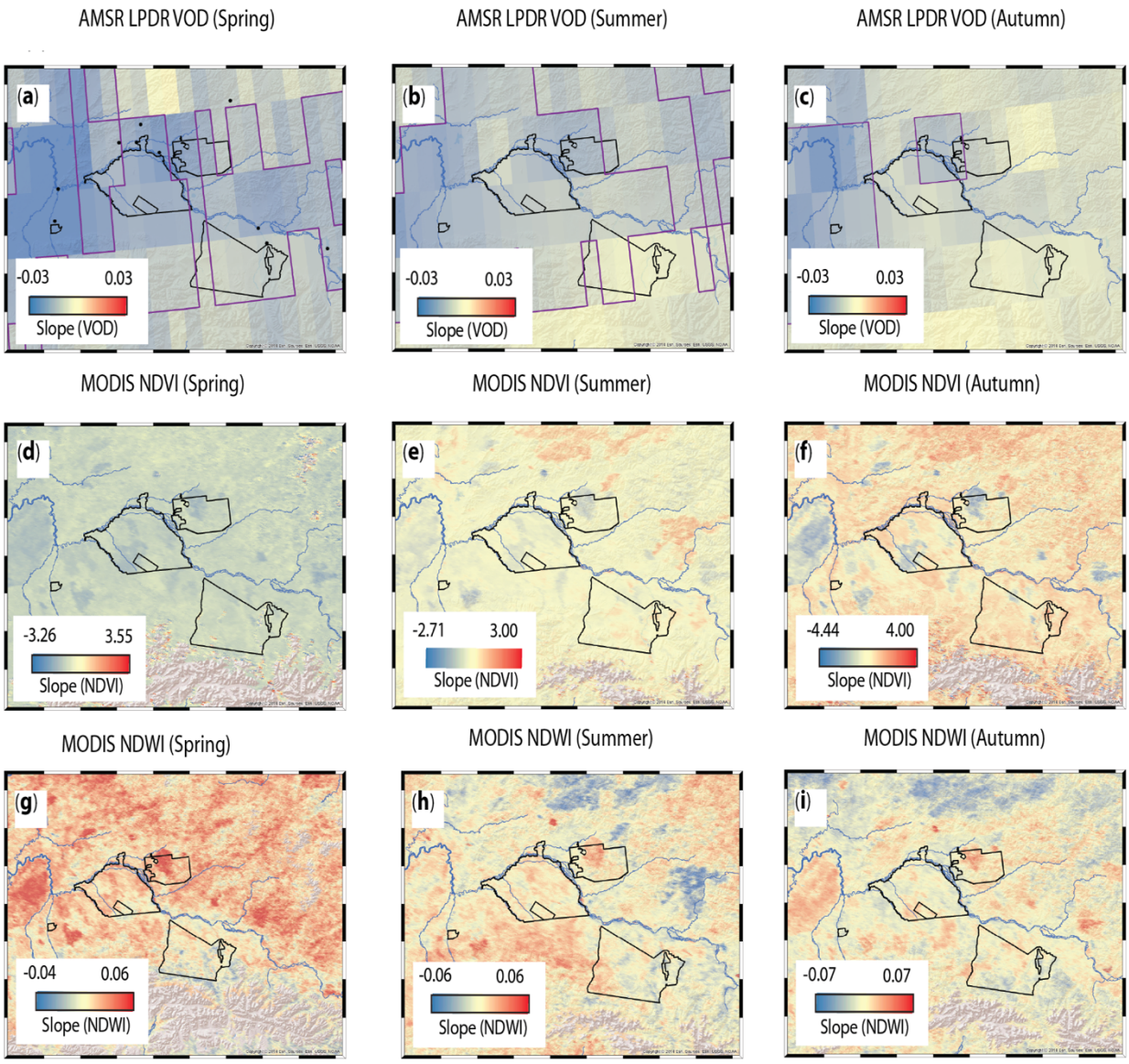


Figure 35. Sen slope results from AMSR (2002 to 2017) VOD (a), MODIS (2002 to 2017) NDVI (b) and MODIS (2002 to 2017) NDWI (c) for the Alaska AOI and DoD terrains in spring, summer and autumn. Regions where the slope trend is significant ($p < 0.1$) are outlined in black for VOD.

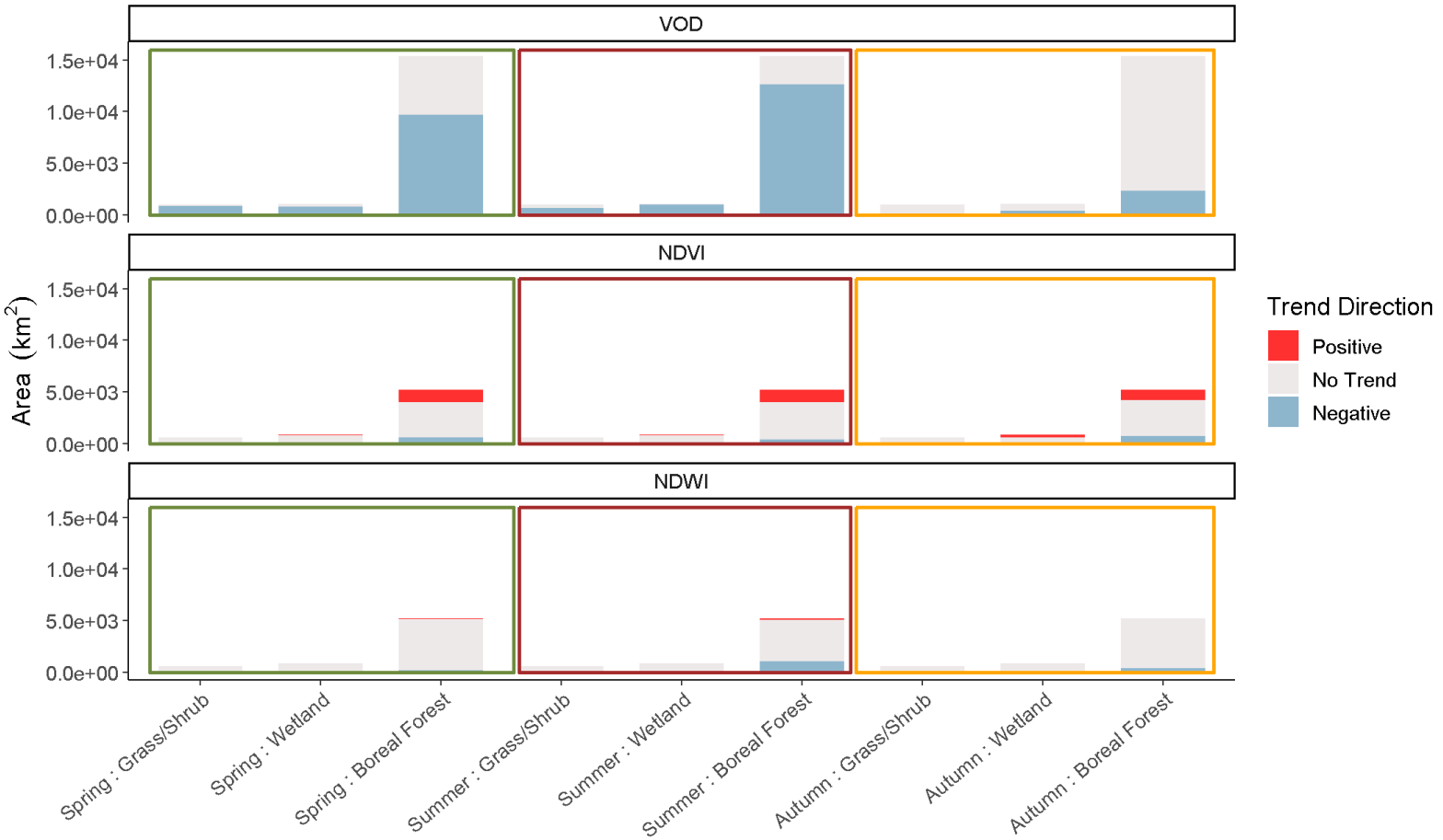


Figure 36. Patterns of change in Vegetation State Indicator metrics (i.e., AMSR VOD, MODIS NDVI and NDWI) across DoD terrains within the Interior Alaska AOI, aggregated by major vegetation classes (tundra; grass/shrub; wetland; boreal forest; temperate vegetation).

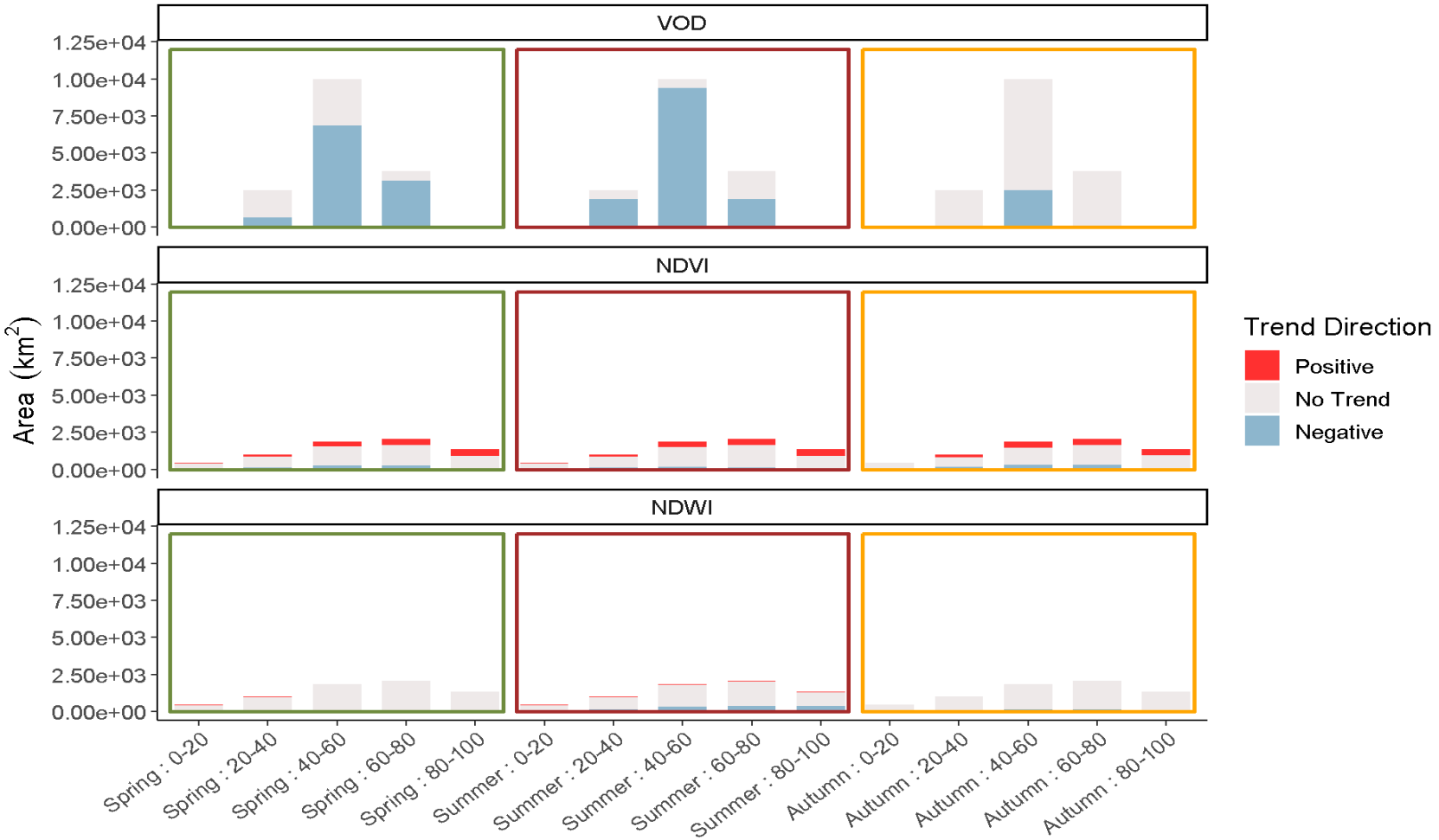


Figure 37. Patterns of change in Vegetation State Indicator metrics (i.e., AMSR VOD, MODIS NDVI and NDWI) aggregated for the DoD terrains in the Interior Alaska AOI by permafrost classes (0-20; 20-40; 40-60; 60-80; 80-100) which indicate the probability of a terrain having near surface (< 1 m) permafrost (from Pastick et al. 2015).

Table 10. Summary of terrains in the Interior Alaska AOI having significant ($p < 0.1$) increase or decrease in Indicator metrics of Vegetation State, as observed in the AMSR passive microwave vegetation optical depth (VOD), MODIS Normalized Difference Vegetation Index (NDVI) and MODIS Normalized Difference Water Index (NDWI). Here we provide terrain area (km^2) and the corresponding percentage of terrain showing change relative to the full domain (453,248 km^2). Also provided is the average rate of change (indicator unit $year^{-1}$) for the region.

Metric	**Season**	**Increase** Area (10^3 km^2) (Percent)	**Rate**	**Decrease** Area (10^3 km^2) (Percent)	**Rate**
			(Neper/yr)		(Neper/yr)
VOD	Spring	7.500 (0.44%)	0.011	76.25 (4.44%)	-0.011
	Summer	N/A	N/A	108.125 (6.29%)	-0.015
	Autumn	2.500 (0.14%)	0.009	39.37 (2.29%)	-0.014
			(NDVI/yr)		(NDVI/yr)
NDVI	Spring	**43 (10%)**	0.10	8 (2%)	-0.09
	Summer	40 (9%)	0.05	9 (2%)	-0.08
	Autumn	**59 (13%)**	0.05	10 (2%)	-0.06
			(NDWI/yr)		(NDWI/yr)
NDWI	Spring	2 (1%)	0.0067	5 (1%)	-0.0073
	Summer	6 (1%)	0.0047	**43 (10%)**	-0.0048
	Autumn	0.5 (0.10%)	0.0060	42 (9%)	-0.0089

(b) BFAST detection of fire disturbance and vegetation recovery

The Mann-Kendall trend test was designed to detect significant monotonic increases or decreases in a time series. Because of this, Mann-Kendall will not detect significant, short-term breaks in the Indicator records. For example, if a disturbance (e.g., fire or windfall) caused an abrupt but short term decrease, followed by a substantial increase, the Mann-Kendall test would not flag this event as having significant change.

To address this, we also tested the use of BFAST, a second trend detection algorithm that is designed to detect and flag the occurrence of significant breaks in a time series. To assess the ability of the BFAST algorithm to identify the occurrence of abrupt change, we selected as a case study a documented fire event in 2009 that occurred southwest of Fairbanks, towards the Clear Air Base. This fire event was flagged as significant for VOD in the spring, summer and autumn based on the MK trend analysis, and a large portion of the fire was flagged significant by NDVI and NDWI. For the summer season, VOD had a sen slope of -0.02 per year, NDVI had a sen slope of -0.4 per year; for the spring season NDWI had a sen slope of 0.006 per year.

We applied BFAST to separate time series of VOD, NDVI and NDWI. Comparison of the burn extent and the spatial patterns of VOD, NDVI and NDWI sen slopes in different seasons are shown in Figure 38. The BFAST analysis was run on monthly summer means for VOD. For the other metrics we instead ran BFAST on annual summer means for NDVI and annual spring means for NDWI. Due to the large amount of variability introduced by evaluating monthly time series, as was done with VOD, it was more difficult for the BFAST algorithm to predict the

correct break points; therefore, we analyzed seasonal averages for NDVI and NDWI to reduce variability in the signal and increase BFAST algorithm performance. By analyzing annual growing season data (as was done with NDVI and NDWI) the amount of variability in the signal was reduced and the BFAST algorithm performed more accurately.

The results from this case study (Figure 39) illustrate the varied ability of BFAST to detect abrupt breaks in trend, following a terrain disturbance, that are not flagged by the monotonic Mann-Kendall algorithm. For example, a sharp increase in VOD was observed in 2007, two years prior to the 2009 burn; the cause of this break is unknown but could potentially indicate an initial disturbance that resulted in the terrains becoming more susceptible to burn. Because of this, the BFAST algorithm selected 2007 as the break, instead of 2009/2010 (Figure 39-b). In contrast, the BFAST algorithm was able to detect the 2009 break in NDVI (Figure 39-c) resulting from the fire disturbance because a large increase in greenness did not occur prior to the burn. The rebound of NDVI also differed from VOD, with a sharp increase in NDVI occurring in the three years post-burn. The VOD signal, on the other hand, was slower to rebound because of the large loss of vegetation during the fire and the decades required for forest recovery. Though the NDWI signal showed a multi-year decline (values becoming more negative) following the 2009 burn, the time series also showed an increase in values (becoming less negative) from 2005 to 2010 and partially overlapping with the short-term increase that occurred in the VOD record (Figure 39-d). Because of this, BFAST detected two breaks in the time series for NDWI but these did not directly correspond with the timing of the burn event and instead could reflect a multi-year period of terrain wetting occurring in the years prior to the burn.

In the future, a possible alternative to BFAST would be the LandTrendr algorithm (Kennedy et al. 2018). LandTrendr is similar to BFAST in that it detects breaks in time series, and also estimates the magnitude of change. A primary advantage of LandTrendr is that it is easily implemented in Google Earth Engine. Because of the large amount of computing resources available through Earth Engine, the LandTrendr algorithm can be applied to quickly assess the landscape as whole.

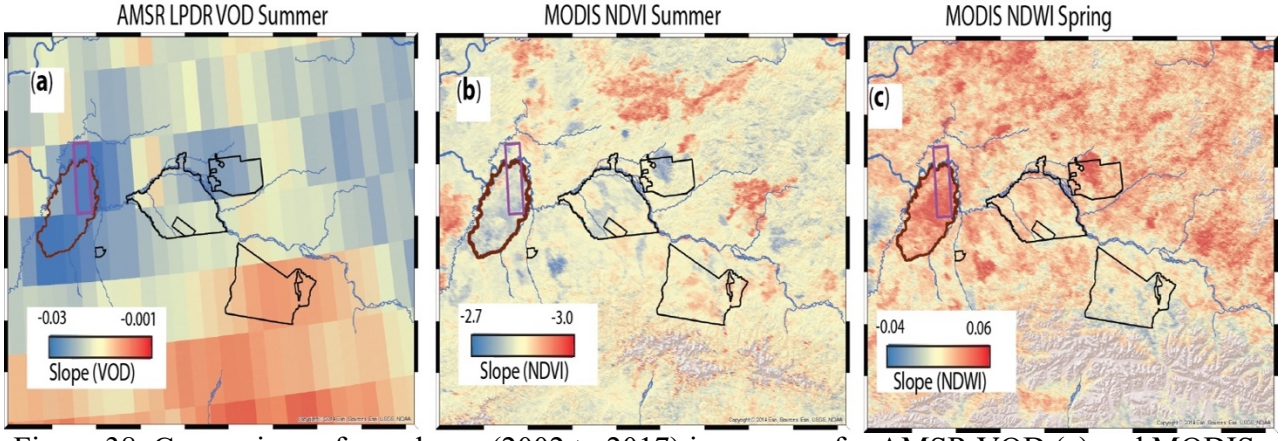


Figure 38. Comparison of sen slopes (2002 to 2017) in summer for AMSR VOD (a) and MODIS NDVI (b). Also shown are the sen slopes for MODIS NDWI in spring (c). The 2009 burn event used as a case study for BFAST is outlined in brown. Areas in red in (c) within the burn scar show regions having greater burn severity. The spatial footprint of the VOD retrieval used for the BFAST analysis is overlain in purple.

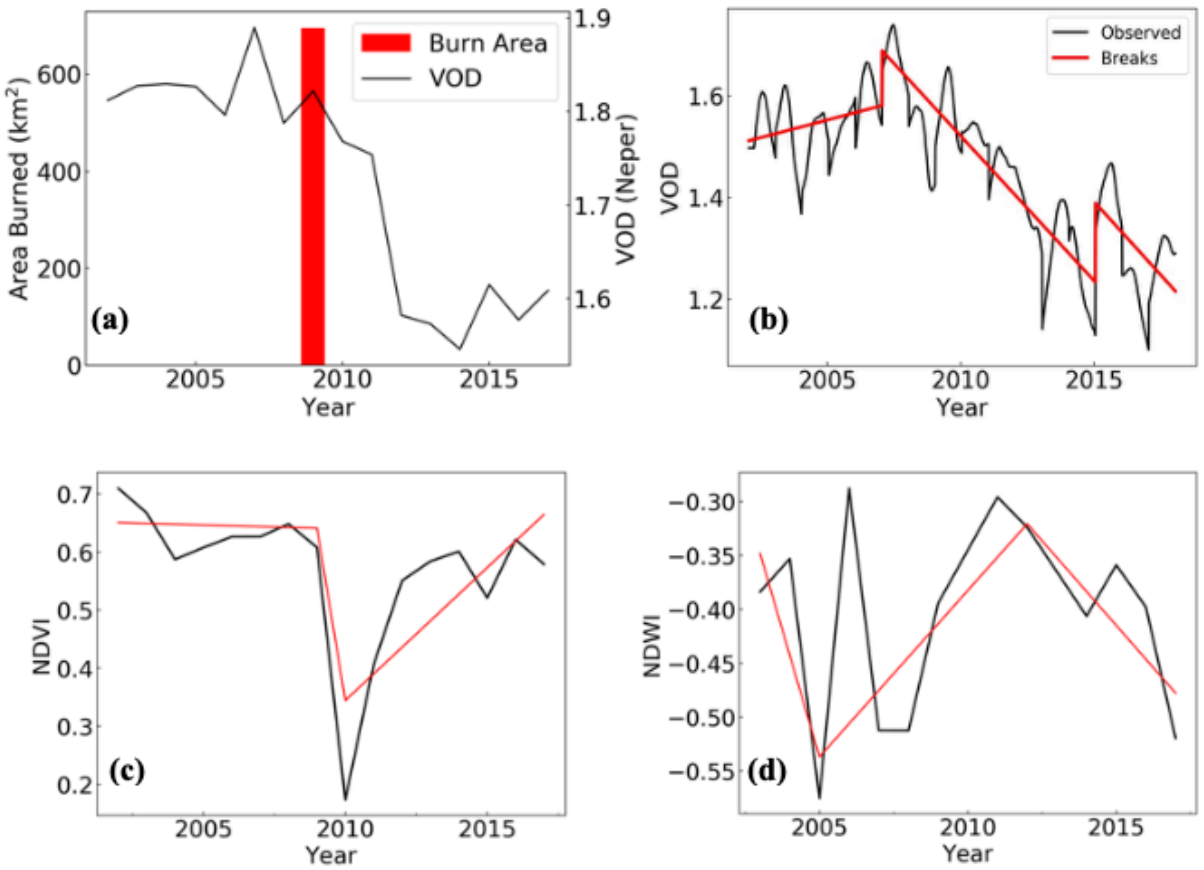


Figure 39. Detection of terrain disturbance in the VOD, NDVI and NDWI time series (2002 to 2017) over the 2009 burn scar near Clear Air Base in Interior Alaska. Panel (a) shows the annual summertime series of a 25 km VOD retrieval occurring over the burn scar. The red vertical line indicates the occurrence of the burn event and the area burned (> 600 km^2) within the retrieval footprint. Panel (b) shows the VOD time series of monthly average retrievals (in black) overlain by the BFAST detection of breaks (in red). Panel (c) shows the NDVI time series of annual summer average retrievals (in black) and the BFAST detection (in red). Panel (d) shows the NDWI time series of annual spring average retrievals (in black) and the BFAST detection (in red).

5.1.3.3 Discussion and summary of Vegetation State

Our analysis of Vegetation State using AMSR VOD, MODIS NDVI and NDWI indicated that biomass water content and greenness increased over the 16 year (2002 to 2017) observation period across Alaska coastal regions. These trends agree with those reported in past studies using other satellite sensors (e.g. Landsat and AVHRR; Ju & Masek 2016). Some of this increase could be a direct result of seasonal warming and an extended annual non-frozen season that stimulates growth within existing vegetation communities (Kim et al. 2012), as well as indirect effects of this warming (e.g., increased nutrients associated with warmer soils and ground thaw). Another component that may be driving this change is the expansion of shrub cover ('shrubification') within tundra communities, as has been documented across the Arctic (Myers-Smith et al. 2011).

In the boreal forests of the Alaska Interior we observed a significant linear decrease in VOD over the AMSR observation period (2002 to 2017). These trends primarily reflect a decrease in vegetation biomass (and hence aboveground water content) that occurred following major fire events. The Interior has experienced a high frequency of fire in the past few decades (Figure 34) and in Interior AOI alone 408 documented burn events have taken place since 2002, affecting more than approximately 7.6 million acres (31,000 km^2).

It can take up to thirty years for forest biomass to recover in Alaska's boreal ecosystems following a major fire event (Hart & Chen 2006). In some cases, the forests do not recover to the previous state and instead experience a shift from conifer (e.g., black spruce) to deciduous (e.g., aspen and birch) dominance if the fire greatly reduces soil organic matter and moisture (Gibson et al. 2016). In our analysis for the Interior AOI and DoD lands we did observe a strong increase in VOD from 2014 through 2017 that coincides with biomass recovery following fire. Understanding how the various rates of VOD recovery are influenced by burn severity, pre-and post-fire forest composition, and changes in surface moisture warrants further investigation.

In contrast to VOD, the NDVI for the Interior AOI significantly increased (indicating greening) from 2002 to 2017. The most substantial greening occurred within fire scars, following the recovery of leaf canopy and understory foliage, similar to results from previous studies (Jones et al. 2013; Tan et al. 2013). The NDVI greening occurring outside of recent burns likely reflects the lengthening of the growing season (see section 5.1.1) and increase in summer surface soil moisture over the past decade (see 5.1.2). The underlying cause of NDVI browning occurring on portions of DoD's Yukon Training Area and Tanana Flats Training Area is unknown and will require further remote sensing data analysis, combined with site visits, to determine the drivers of the change.

Previous studies had indicated negative trends in photosynthetic activity within Interior Alaska, based on AVHRR derived indices from 1982 to 2003 (Goetz et al. 2005; Verbyla 2008). Our analyses showing increased MODIS NDVI (i.e., vegetation greening) from 2002-2017 and increased VOD (i.e., biomass recovery) from 2014-2017 indicate that many of the forests here are in a period of recovery. Yet, this does not suggest that these recovering forests are now at less risk to fire or other disturbances. Instead, the increase in foliage and other aboveground biomass can provide new sources of fuel available for future burns, especially as regional summer temperatures continue to increase and if drier atmospheric conditions (e.g., low relative humidity) outweigh the mitigating effect of wetting soils (Xiao & Zhuang 2007). In addition, new and recovering spruce trees in post-fire stands may be more susceptible to future beetle infestations that can severely degrade vegetation communities and further increase forest risk to fire (Soja et al. 2007).

The results from our case study of detecting severe vegetation disturbance events (e.g., fire) using a time series signal decomposition approach indicate the need to further test and refine parameter settings in the BFAST algorithm. This will require a separate parameter tuning and evaluation of algorithm response for each Indicator record (i.e. VOD, NDVI, NDWI) before we can move to the next step of applying the detection algorithm to all grid cell time series over the greater Interior AOI and Alaska domain. Regardless, our case study confirms that the BFAST algorithm is able to detect breaks in remote sensing time series, but also shows that the detected break point is highly dependent on what occurred before and after a disturbance event. This investigation also highlights a need for an on-the-ground monitoring system that is capable of measuring vegetation water content (e.g., Larsen et al. 2014), greenness (e.g., through optical

phenology cameras) and soil moisture. This in situ database is necessary to identify the physical mechanisms driving the temporal changes observed in satellite records of each Indicator.

Our analysis of Vegetation State using AMSR VOD, MODIS NDVI and NDWI indicated that Alaska coastal regions experienced multi-year and monotonic increases in biomass water content and greenness over the 16 year (2002 to 2017) observation period. These trends agree with those reported in past studies using other satellite sensors (e.g., Landsat and AVHRR; Ju & Masek 2016). The changes observed in this study support our first hypothesis for Vegetation by confirming that growth is increasing within coastal tundra, and this change is occurring at a significant rate across the non-frozen season (observed in spring, summer and autumn). Some of this increase could be a direct result of seasonal warming and an extended annual non-frozen season that stimulates growth within existing vegetation communities (Kim et al. 2012). Another component that may be driving this change is the expansion of shrub cover ('shrubification') within tundra communities, as has been documented across the Arctic (Myers-Smith et al. 2011).

Past studies have estimated that it takes up to thirty years for forest biomass to recover in Alaska's boreal ecosystems following a major fire event (Hart & Chen 2006). In some cases, the forests do not recover to the previous state, and instead experience a shift from conifer (e.g., black spruce) to deciduous (e.g., aspen and birch) dominant if the fire greatly reduces organic biomass and moisture in surface soil layers (Gibson et al. 2016). In our analysis for the Interior AOI and DoD lands we did observe a strong increase in VOD from 2014 through 2017 that coincides with biomass recovery across burned terrains within this region. Understanding how the various rates of VOD recovery are influenced by burn severity, pre-and post-fire forest composition, and changes in surface moisture warrants further investigation.

In contrast to VOD, the NDVI time series for the Interior AOI indicated significant rates of increase (greening) within the region. The most substantial greening occurred within fire scars, following the recovery of leaf canopy and understory foliage. Our results agree with those reported in other studies of post-fire change in vegetation greenness for Interior Alaska, which indicate that the highest increases in NDVI tend to coincide with higher severity burns and that the most substantial rates of increase in NDVI occur within the first two to three years following a fire event (Jones et al. 2013; Tan et al. 2013). The NDVI greening occurring outside of recent burns likely reflects the lengthening of annual non-growing season (section 5.1.1) and the increase in summer surface soil moisture that was observed over the past decade (see 5.1.2). The underlying cause of NDVI browning occurring on portions of DoD's Yukon Training Area and Tanana Flats Training Area is unknown and will require further remote sensing data analysis, combined with site visits, to determine the drivers of the change.

Previous studies have indicated negative trends in photosynthetic activity within Interior Alaska, based on AVHRR derived indices from 1982 to 2003 (Goetz et al. 2005; Verbyla 2008), which provided the basis for our second hypothesis that vegetation browning was dominant throughout Interior Alaska over the past 16 years (2002 to 2017). The results from our analysis fail to support this hypothesis given the continuous increase in MODIS NDVI (i.e., vegetation greening) over our period of observation and the increase in VOD (i.e., biomass recovery) from 2014 onward, which indicate that the forests have been in a period of recovery. Yet, this does not suggest that these recovering forests are at less risk to fire or other disturbances. Instead, the increase in foliage and other aboveground biomass can provide new sources of fuel for future burns, especially as regional summer temperatures continue to increase and if drier atmospheric conditions (e.g., low relative humidity) outweigh the mitigating effect of wetting soils (Xiao &

Zhuang 2007). In addition, new and recovering spruce trees in post-fire stands may be more susceptible to future beetle infestations that can severely degrade vegetation communities and further increase forest risk to fire (Soja et al. 2007).

The results from our case study of detecting severe vegetation disturbance events (e.g., fire) using a time series signal decomposition approach indicate the need to further test and refine parameter settings in the BFAST algorithm. This will require a separate parameter tuning and evaluation of algorithm response for each Indicator record (i.e. VOD, NDVI, NDWI) before we can move to the next step of applying the detection algorithm to all grid cell time series over the greater Interior AOI and Alaska domain. Regardless, our case study confirms that the BFAST algorithm is able to detect breaks in remote sensing time series, but also shows that the detected break point is highly dependent on what occurred before and after a disturbance event. This investigation also highlights a need for an on-the-ground terrain monitoring system that is capable of remotely measuring terrain vegetation water content (e.g., Larsen et al. 2014), greenness (e.g., through optical phenology cameras) and terrain soil moisture to provide the in situ data necessary to identify the physical mechanisms driving the temporal changes observed in each Indicator, and to understand what is driving the Indicator responses observed from satellites.

5.2 Data Fusion (downscaling)

For this project, we explored the use of machine learning to combine multi-resolution and multi-spectral imagery to obtain new, higher resolution (500 m) gridded Earth System Indicators for Terrain Frozen State (through the Freeze/Thaw metric), Ecosystem Water Stress (through the surface soil moisture metric), and Vegetation State (through the VOD metric) over both Alaska and our Interior Alaska AOI. These new downscaled products combine information from coarser-resolution passive microwave retrievals and the finer resolution VIS-NIR observations to provide integrated geospatial maps describing terrain surface properties. We also developed methodologies for the 30 m resolution detection of change in surface open water bodies.

We evaluated the ability of our data fusion approach to characterize spatial and temporal changes in terrain properties for specific test dates within the long-term satellite SSMI and AMSR microwave records. For Freeze/Thaw, the evaluated test period included five observation dates in spring and early summer 2014. The year 2014 was selected for evaluation because it was a relatively small fire year (0.12 Mha) based on the Alaska Long Term Fire database (Jandt 2015). We wanted to avoid years having large disturbance as the recent land disturbances could influence how the machine learning models are trained. For Water Stress, the test period included the summer months of 2014 through 2017. For Vegetation, the test period included April through July 2014.

Table 11. Summary of the performance of Random Forest models used for data fusion (downscaling) and open water classification of Sentinel-1 SAR imagery. A full summary of prediction accuracy for the classifications can be found in the Supplement.

Terrain Frozen State	
Freeze/Thaw	Overall classification accuracy of 77% across five dates and sample of 5,000 grid cells compared to the original 25 km SSMI retrievals.
Ecosystem Water Stress	
Surface soil moisture	RMSE 0.039 cm^3/cm^3 and R (correlation coefficients) 0.71 in comparison with the original 25 km AMSR retrievals; the RMSEs and R for June, July, August and September are 0.042 cm^3/cm^3 and 0.73, 0.040 cm^3/cm^3 and 0.66. 0.038 cm^3/cm^3 and 0.68, 0.036 cm^3/cm^3 and 0.77, respectively. And R is 0.68 in comparison with the SNOTEL in situ measurements.
Open water	The SAR 30 m water classification has commission and omission errors about 10% and 45%, respectively as evaluated using NOAA aerial photos acquired on August 30, 2017 over Houston, Texas. The Fw downscaling method showed respective commission and omission errors about 31% and 30% in classifying water pixels as compared with independent Landsat water mapping results (Du et al. 2018).
Vegetation	
Vegetation Optical Depth (VOD)	RMSE of 0.12 across four dates and a sample of 4,000 pixels along with an R^2 of 0.90 as compared to the original 25 km AMSR VOD retrievals

5.2.1 Terrain Thermal State

The data fusion algorithm that we developed integrated 7.5 arc-second terrain elevation, slope and aspect; 30 m near surface (> 1 m depth) terrain permafrost probability; 500 m snow cover; and 1 km MODIS land surface temperature. These data were used in conjunction to downscale the 25 km passive microwave Freeze/Thaw observations derived from the satellite SSMI record, but this approach can also be directly applied to downscale the AMSR Freeze/Thaw retrievals.

For the development and testing of data fusion for terrain Freeze/Thaw, we selected five dates that represented the seasonal transition from frozen to thawed state. These dates were March 1, April 1, May 1, and June 1, 2014 (Figure 40). The overall Freeze/Thaw classification accuracy (encompassing frozen, thaw and transition states) for these dates averaged 77% based on a random state-wide sample of 5,000 grid cells and compared to the original 25 km SSMI retrievals (Table 11). Accuracy of the observed vs predicted values were compared by randomly selecting 1,000 MODIS grid cells over spatial locations not included in the selection of 4,000 grid cells used for model training, and by comparing the model-classified terrain thermal state to what the original 25 km product observed.

Our downscaled terrain Freeze/Thaw test images (Figure 40) correctly captured the seasonal shift across Alaska from frozen dominant landscapes in March and April, to mixed thaw and

transition in May, and to thaw dominant in June and July. Starting in March, the northward progression of frozen-to-transition state begins in the southern regions of Alaska including near Anchorage, the coastal lowlands, and the Yukon-Kuskokwim Delta. As might be expected, the terrains in the Brooks and Alaska mountain ranges took the longest to proceed from frozen to thawed state (early July). Our Freeze/Thaw records, including the downscaled images, also indicated two major re-freeze events that took place in spring 2014. In early April, portions of southern Alaska were observed to switch from thawed or transition state back to frozen, following a short-term decline in air and surface temperatures (Figure 40). A temporary transition from terrain thawed state back to frozen conditions was also observed over the North Slope in early June following a snow event.

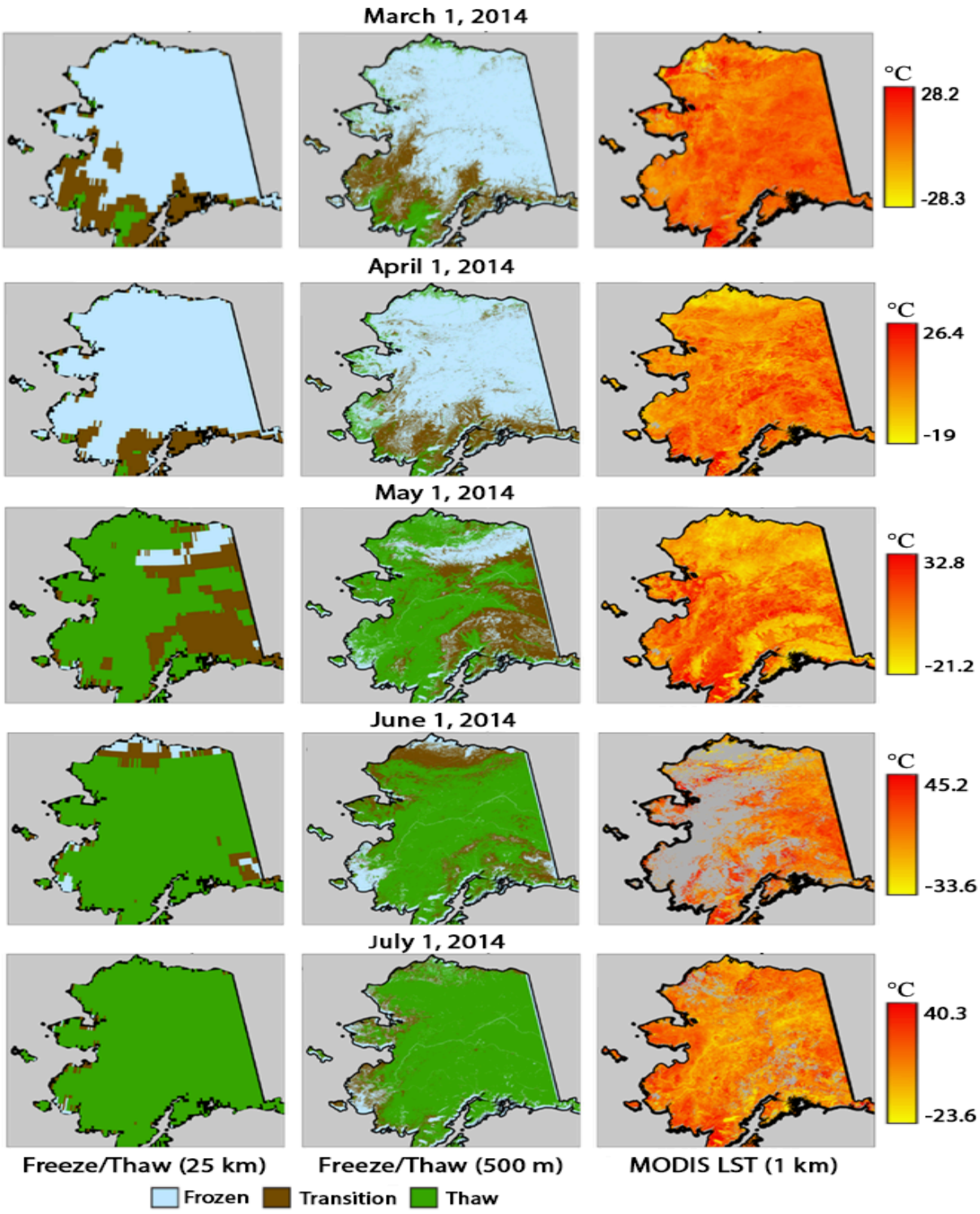


Figure 40. Comparison of spatial patterns observed over Alaska in the original 25 km SSMI Freeze/Thaw retrieval record (left), 1 km MODIS derived surface temperature (right) and the resulting 500 m downscaled Freeze/Thaw produced using new methods developed in this study (center). The test dates shown here are for the first day of the month, March through July 2014.

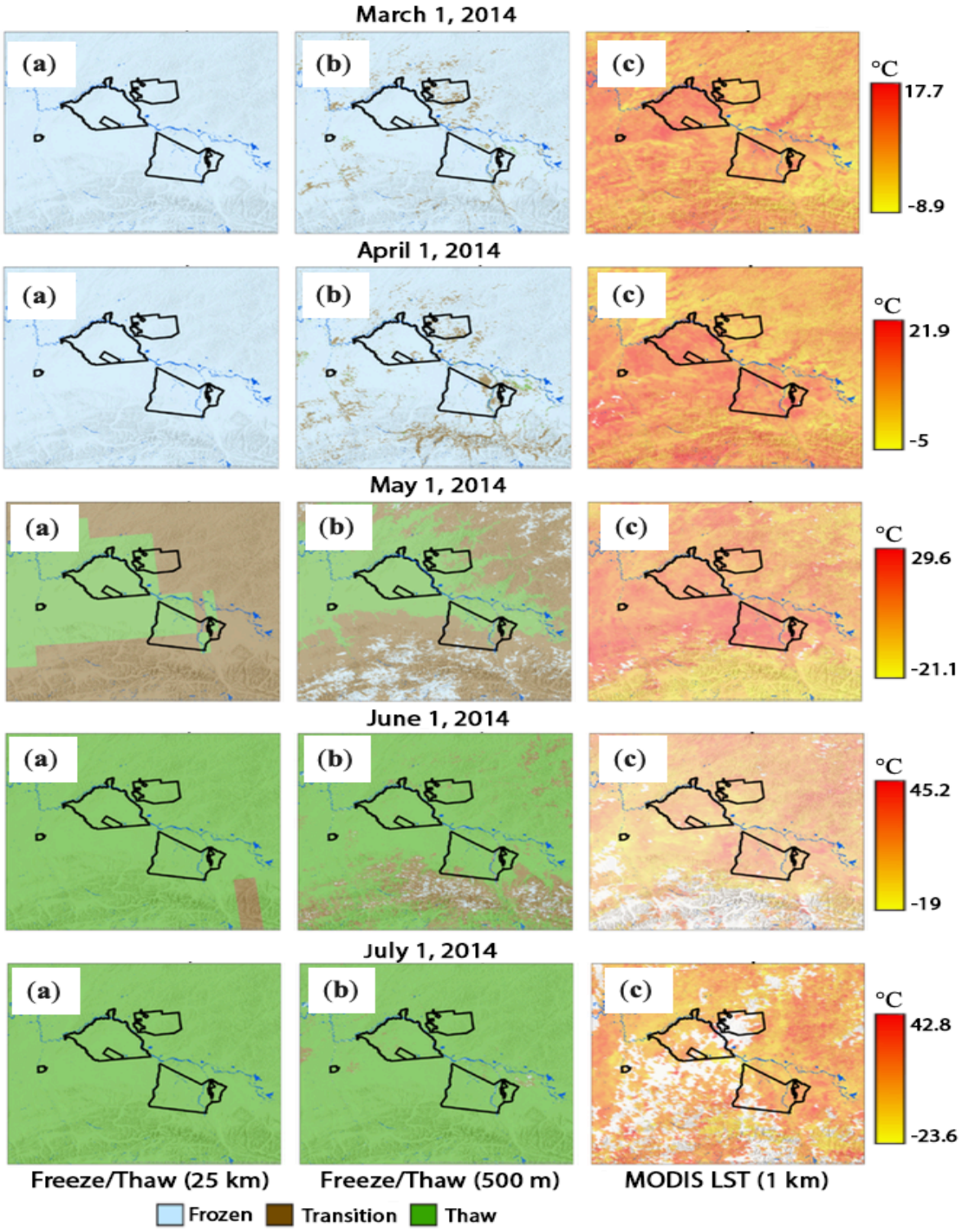


Figure 41. Comparison of spatial patterns observed over the Interior Alaska AOI in the 25 km SSMI Freeze/Thaw retrieval record (left), 1 km MODIS derived surface temperature (right) and the resulting 500 m downscaled Freeze/Thaw produced using new methods developed by this study (center). The test dates shown here are for the first day of the month, March through June 2014. The DoD terrains are outlined in black.

Within the Interior Alaska AOI, the downscaled 500 m Freeze/Thaw record indicated a terrain shift from frozen to transitional state over portions of the domain, including within the Yukon Training Area starting March 1, and over both Yukon Training Area and Donnelly on April 1, that were not observed in the original 25 km Freeze/Thaw record (Figure 41). By May 1, both the 25 km and downscaled 500 m Freeze/Thaw records showed most of the lower elevation terrains within the AOI to have reached a thawed state. However, our downscaled Freeze/Thaw results were able to detect the presence of transitional thaw occurring within higher elevation terrains to the south of Donnelly, whereas the 25 km Freeze/Thaw product did not detect this. We also note that terrain warming was observed in the MODIS LST record in the months prior to a change in Freeze/Thaw state. For example, higher MODIS LSTs (> 14 °C) were detected over Tanana Flats Training Area in March and April, prior to the full transition to thawed state by May 1, 2014 (Figure 41). Whereas elevated land surface temperatures over Donnelly were observed in April and May prior to the full transition to thawed state that occurred by June 1.

Overall user's classification accuracy, which provides an estimate of errors arising from wrongful class inclusion, for terrain frozen state (see Supplement Tables S4 through S7) was 85% and ranged from 79% (April) to 90% (May). User's accuracy for terrain thaw state was 82%, ranging from 76% (March) to $\geq$ 81% (April to July). Terrain transition state had the lowest user's accuracy, with an average of 64% and ranging from 59% (April) to 67% (July). However, the lower accuracy for transition state may be overly conservative when using the reference 25 km Freeze/Thaw grid cells as "truth" given the likelihood of more localized variability in terrain thermal conditions existing within the coarse microwave retrieval footprint. For example, many of the pixels classified as "transition" in April were located surrounding the mountains in the Brooks and Alaska ranges, and at the lower elevations. The SSMI product observed these pixels as frozen, but in reality, it is likely that some of the sub-grid terrains were already transitioning to a thawed status. Therefore, it is entirely possible that the downscaled results provide a more accurate estimate of thermal state than the 25 km product.

Our evaluation of the downscaled 500 m Freeze/Thaw results at the reference CRREL Farmer's Loop repeat camera site near Fairbanks (Figure 42) was in good agreement with the landscape information provided by the in situ trail cameras. In March and April, the ground was still snow covered, and the SSMI observed Freeze/Thaw status and downscaled Freeze/Thaw results also indicated a frozen status. By May 1st the trail camera showed that the snow had melted, which was also indicated by the SSMI sensor and the downscaled results.

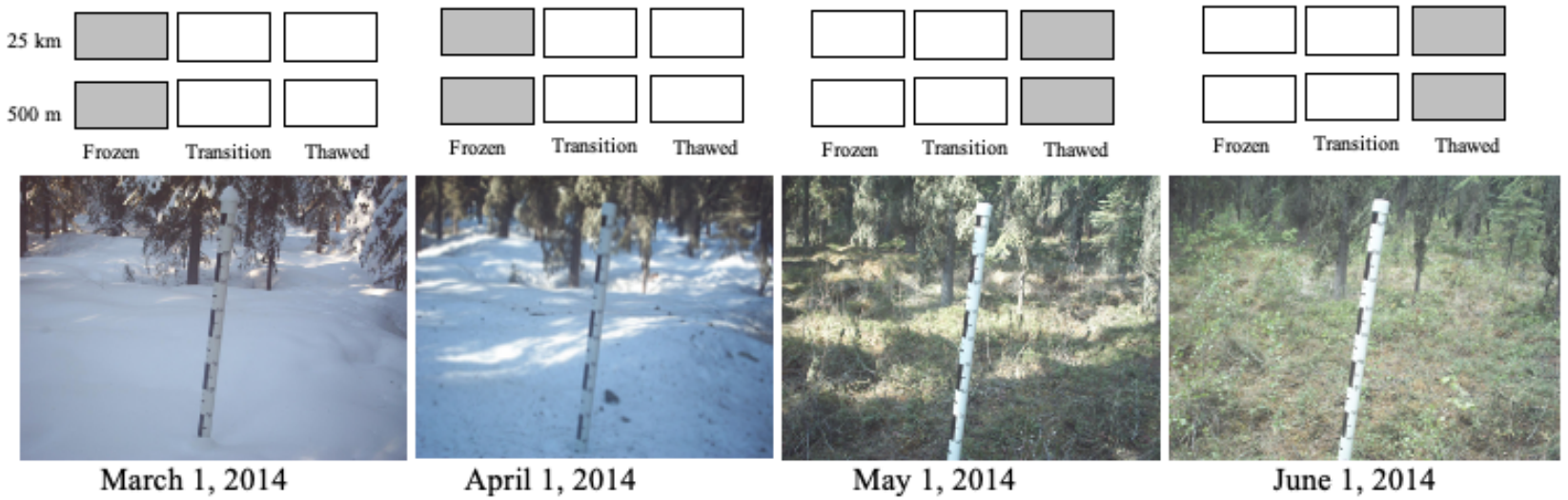


Figure 42. Time lapse pictures for the USACE CRREL Farmer's Loop monitoring site near Fairbanks showing terrain state conditions in 2014 (bottom panel) on March 1, April 1, May 1, and June 1. The frozen, transitional, or thawed states observed in the original SSMI 25 km Freeze/Thaw and the downscaled 500 m Freeze/Thaw retrievals corresponding to this site are shown in the top panel. [*Images from the trail cameras provided by T. Douglas*]

5.2.2 Water Stress

5.2.2.1 Soil moisture

The algorithm we developed for downscaling AMSR surface soil moisture incorporated 250 m MODIS NDVI, 1 km MODIS LST, 30 m topographic index (TPI) information, and 500 m land cover into the Random Forest based regression-based estimates. These data were used in conjunction to downscale the 25 km passive microwave surface soil moisture observations derived from the satellite record.

For the development and testing of data fusion for terrain surface soil moisture, we selected test dates at seven day intervals spanning June to September over years 2014 (a 'normal' year) and 2015 (a 'dry' year; Partain et al. 2016) and generated the downscaled 500 m resolution soil moisture data sets over the Alaska domain and the Interior Alaska AOI.

The overall estimate RMSE for the downscaled surface soil moisture was 0.039 cm^3/cm^3 over the Alaska domain (Table 11) with a correlation (R) of 0.71 when compared to the original 25 km AMSR retrievals. The accuracy of downscaled soil moisture is similar among the months from June to September with RMSEs ranging from 0.036 to 0.042 and correlation coefficients 0.66 to 0.77 (Table 11).

An additional comparison with available (2015) soil moisture from the Granite Creek SNOTEL station near Fort Greely (Figure 43) indicated a correlation of 0.68 between the in situ observations and the 500 m downscaled soil moisture which is encouraging considering the early stages of product development. This correlation was slightly higher than the original AMSR2 25 km product (R = 0.64) which indicates an improved capability of the 500 m downscaled soil moisture data to capture local soil moisture heterogeneity. In addition, we found that the magnitudes of downscaled soil moisture (cm^3/cm^3 or % volumetric soil moisture saturation) were much closer to the in situ SNOTEL measurements, compared to the original 25 km AMSR retrievals.

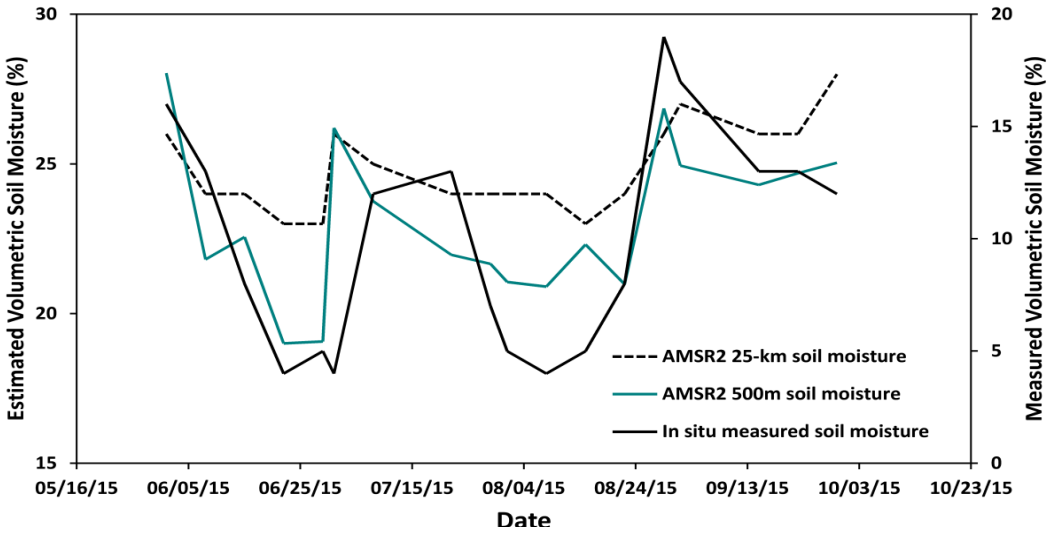


Figure 43. Comparisons between AMSR 25 km (black dashed line) and the 500 m downscaled surface soil moisture (green line) developed in this study, and in situ soil moisture measurements (solid black line) from the Granite Creek SNOTEL site.

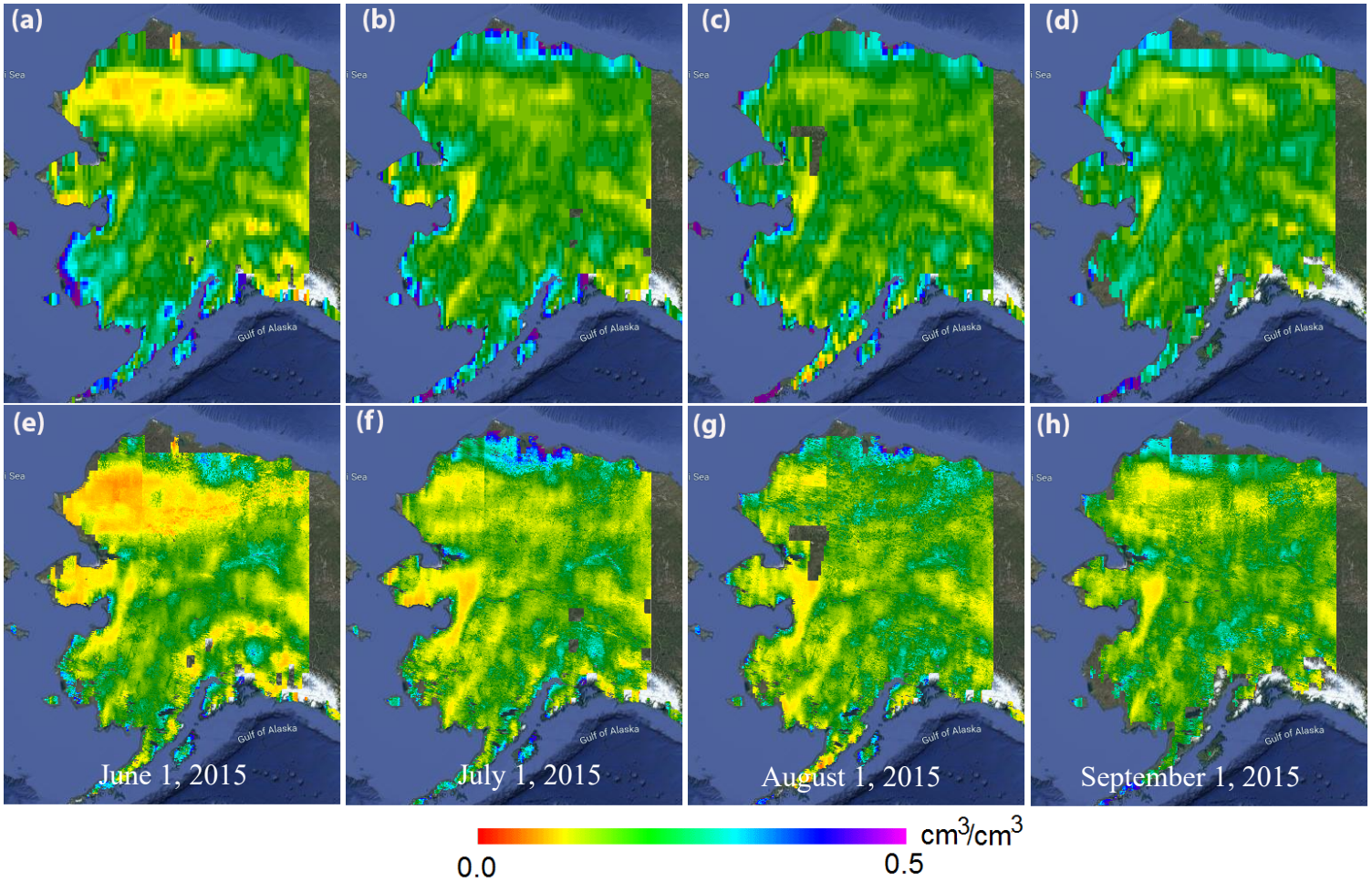


Figure 44. The original 25 km AMSR surface soil moisture (cm^3/cm^3) retrievals for Alaska on June 1, 2015 (a); July 1, 2015 (b); August 1, 2015 (c); September 1, 2015 (d); the corresponding 500 m downscaled results (e-h) for the same dates.

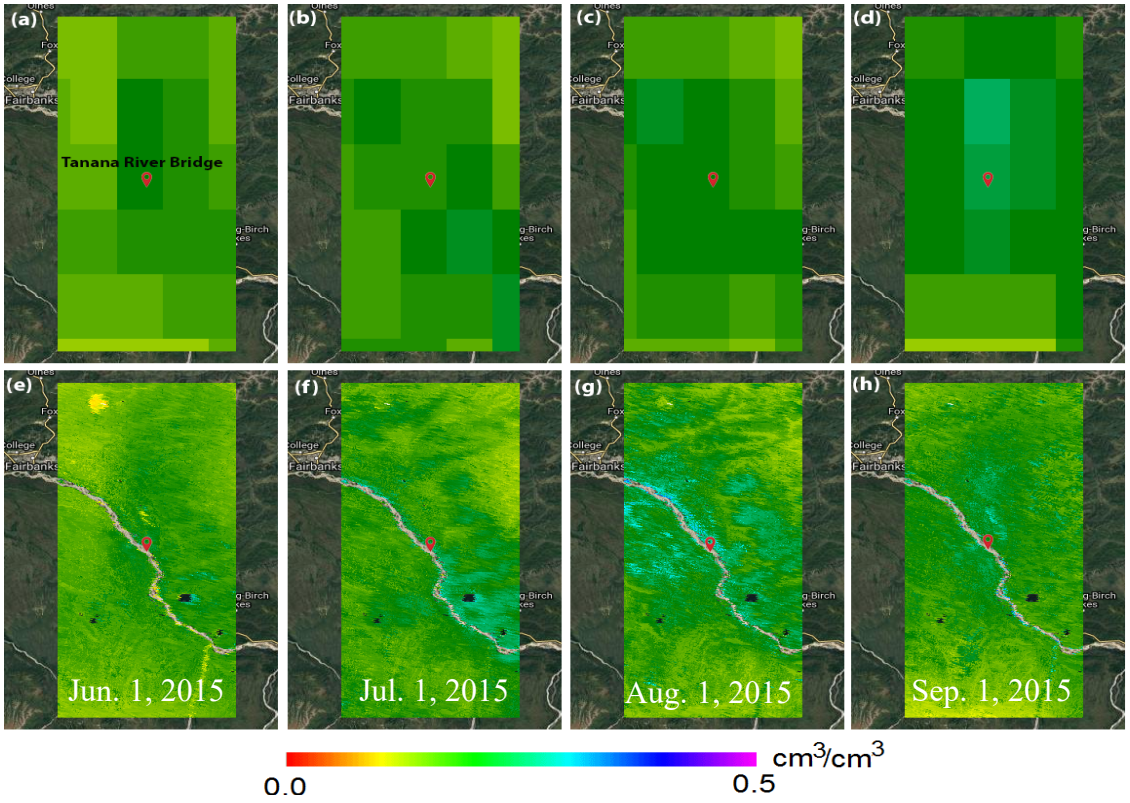


Figure 45. Surface soil moisture (cm^3/cm^3) in the original 25 km AMSR retrievals over the Tanana river bridge area (indicated by the red marker) for June 1, 2015 (a); July 1, 2015 (b); August 1, 2015 (c); September 1, 2015 (d); and the corresponding 500 m downscaled results (e-f) for the same dates. The results are overlain on satellite imagery from Google Earth and the location of the Tanana River Bridge is shown by the red marker. The patch of yellow observed in the upper left section of (e) indicates very dry surface moisture conditions on the disturbed lands of the Fort Knox open pit gold mine in June. The regions of blue in (e-h) show areas having high surface soil moisture including regions adjacent to open water bodies (e.g., the Tanana River). No retrievals were made over the 500 m pixels identified as open water by MODIS land cover (MCD12Q1.006) maps. The dry mineral surface at the Fort Knox mine was not detected in subsequent (July through September) months due to the spectral influence by small pond bodies within the mine complex that increased over the summer months.

In addition to improved ability of the downscaled soil moisture to capture temporal changes in the magnitude of in situ soil moisture at the SNOTEL site, relative to the original 25 km AMSR retrievals, our results for Alaska (Figure 44) and the Tanana River bridge region (Figure 45) within the Alaska AOI showed the more localized detection of terrain "wet" and "dry" hotspots within the landscape. For example, the downscaled results identified wetter terrain areas along the river channels and low lying vegetated areas (Figure 45; areas in blue) and a region of extremely dry surface terrain Figure 45-e; in yellow). This extremely dry terrain was identified as being the location of the Fort Knox open pit gold mine complex (Figure 46); the extremely dry soils here are a result of severe landscape disturbance where terrain surfaces have been stripped down to mineral soil and rock.



Figure 46. Aerial view of the Fort Knox open pit mine detected in the 500 m downscaled soil moisture products, derived from AMSR passive microwave imagery using machine learning methods. [*Photo from Anchorage Daily News, 2018*]

5.2.2.2 Surface inundation

We examined the results of downscaling the 25 km AMSR Fw record (18.7 and 23.8 GHz *Tb*) to a 30 m resolution grid using an approach that included the Landsat Water Occurrence Dataset (WOD) and elevation maps. We also examined machine-learning based 30 m classifications of open water within Sentinel-1 SAR imagery.

Evaluation of the 2016/2017 USGS river discharge record from the Tanana River Site near Fairbanks (Figure 47), and the corresponding 25 km AMSR Fw and 30 m SAR classifications, showed the ability of both the original AMSR Fw (Figure 47; yellow lines) and Sentinel-1 SAR open water product (Figure 47; black triangles) to account for dynamic wetting and drying that

occurred within the river record. At this site the 25 km AMSR Fw record and the SAR based classifications were able to account for seasonal changes in river width (that correspond with an increase in river discharge rates at this site) and the flooding of river banks and adjacent terrains. The average and standard deviation of the available 5 km Fw record over 2003 to 2016 show relatively higher inundation and dynamics along the Tanana River.

Examination of the spatial distribution of open water within the resulting Sentinel-1 SAR classifications for the Tanana River Bridge Area (Figure 48; Figure 49) on August 14, 2016 and October 12, 2017 further illustrates the ability of the radar classification approach to detect changes in river extent and seasonal changes in presence or absence of surface ponds and flooded surfaces. Similar inundation dynamics were detected by the 30 m results downscaled from 25 km Fw data (Figure 48c and f), but the flooded areas were limited by the maximum extent described by the WOD record. The middle panel in Figure 48 indicates the location of SAR detected open water that occurred outside the 32 year (1984 to 2015) Landsat derived open water distribution record. Further on-the-ground verification is needed to determine if these "new" areas of terrain inundation are the result of short-term flood events or newly emerged lake and pond bodies, and the relation of these water bodies to local changes in permafrost and active layer depth.

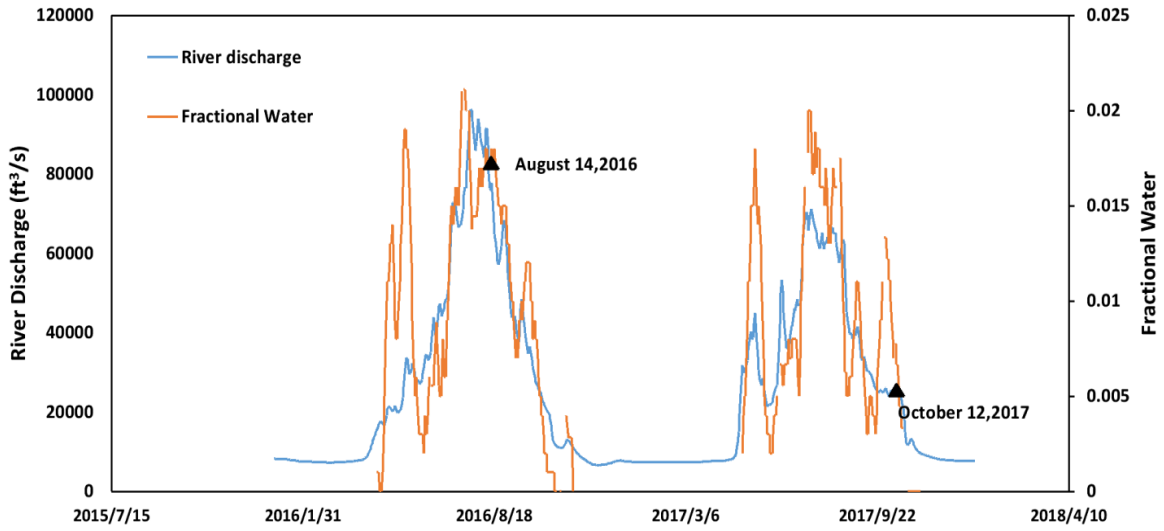


Figure 47. USGS station (ID 15515500) river discharge measurements (ft^3/s) for the Nenana site on the Tanana river close to Fairbanks (blue line), the 25 km AMSR Fw inundation (orange line). The spring 2016 and 2017 seasonal peaks in Fw that were not observed in the discharge record indicate local land surface flooding at locations away from the river but still within the open water retrieval footprint.

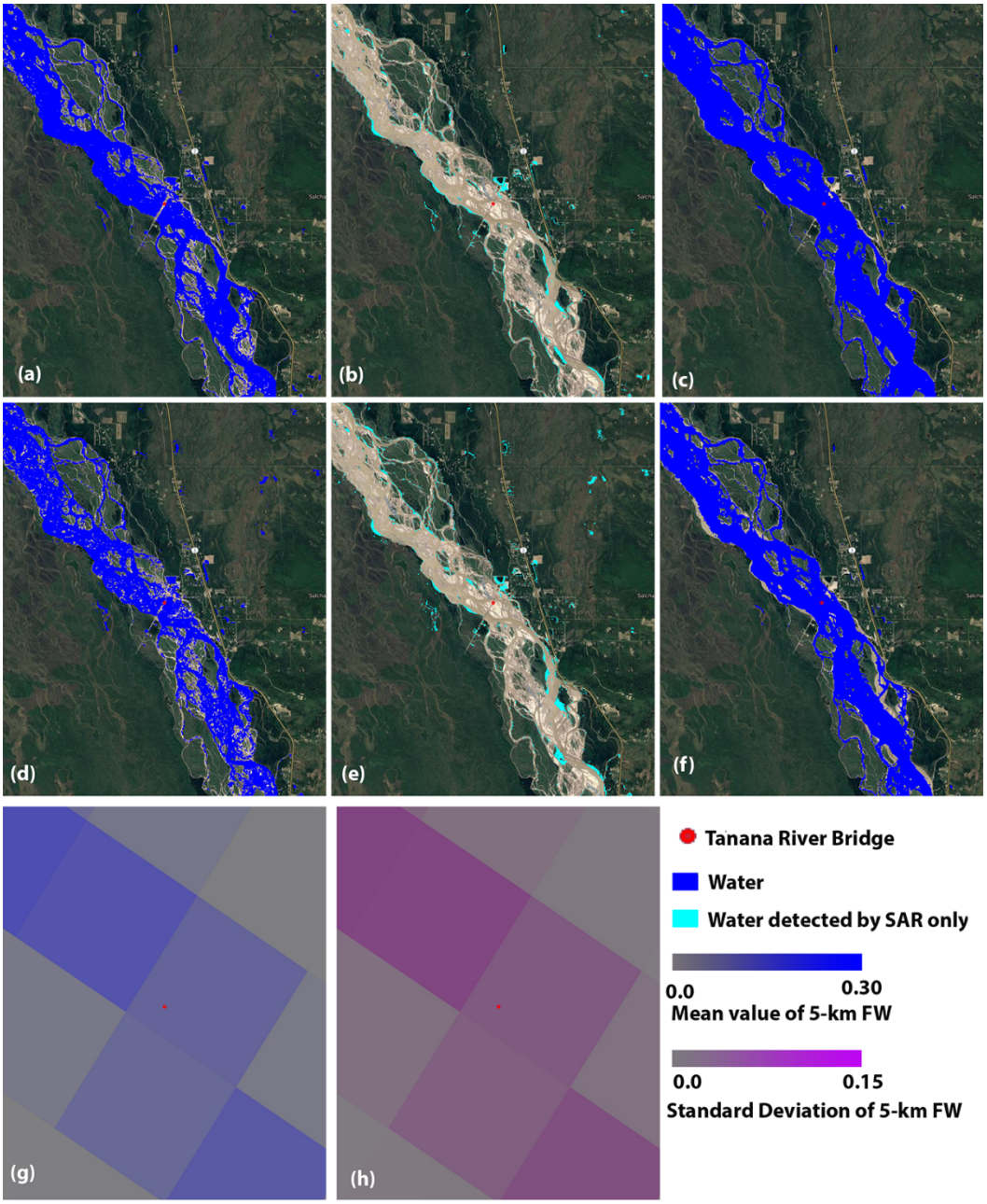


Figure 48. Maps showing 30 m surface water detected by Sentinel-1 SAR (a) and the 30 m downscaled results of 25 km AMSR Fw (c) classifications for August 14, 2016 over the Tanana River Bridge area. The image in (b) shows flooded areas detected by SAR observations on August 14, 2016 that did not occur within the 30 m Landsat WOD (1984-2015; highlighted in cyan); these indicate the presence of new permanent water covered or temporarily flooded terrain. Similar results of SAR classifications (d), downscaled 30 m Fw (e) and inundation detected by SAR only (f) were generated for October 12, 2017. Average inundation conditions (g) and dynamics (h) were detected by the available 5 km Fw record (2003-2016).



Figure 49**.** Pictures showing dry shorelines along the Tanana River near the Tanana Flats Training Area (left) and the Tanana River Bridge (right) taken in September 2018 during a team visit for this project. The river shown here represents a relatively dry period with low river discharge and a reduced river width. [*Photos provided by project team members*]

We also evaluated surface inundation records from 25 km AMSR and 30 m Sentinel-1 SAR classifications over the Richardson Highway Bridge crossing of Jarvis Creek river that is used to access DoD terrains during military training exercises (Figures 50). The area is frequently threatened by overflow ice-caused flooding in spring. The SAR classifications and downscaled results for this site were provided for May 11, 2017 and August 13, 2017. The SAR-based open water classification maps (Figure 50) show slightly higher flooded areas in spring than summer; however, the opposite pattern was seen in the 30 m downscaled results of AMSR Fw. The low spring Fw observed by AMSR may reflect the overall low inundation level of the larger 25 km grid cells and was possibly influenced by regionally mixed freeze and thawed conditions. For the regions with heterogeneous inundation conditions, the SAR observations are able to "zoom in" to specific areas and capture the inundation details.

To further evaluate the ability of our Sentinel-1 SAR classifier to accurately detect changes in open water, we also applied the inundation mapping algorithm to SAR images acquired for August 30, 2017 over the Houston region in Texas (Figures 74, 75). These sites and dates were selected because of the large, documented surface flooding that occurred in this region during Hurricane Harvey and because of the availability of very high resolution and georeferenced aerial photos. Two NOAA aerial photos taken over Addicks/Park Ten and George Bush Park on the same day (https://storms.ngs.noaa.gov/storms/harvey/index.html), and offering a high (0.3 m) resolution, were used for this evaluation. Water/land pixels were identified from the photos using supervised classifications and training samples, which were manually selected.

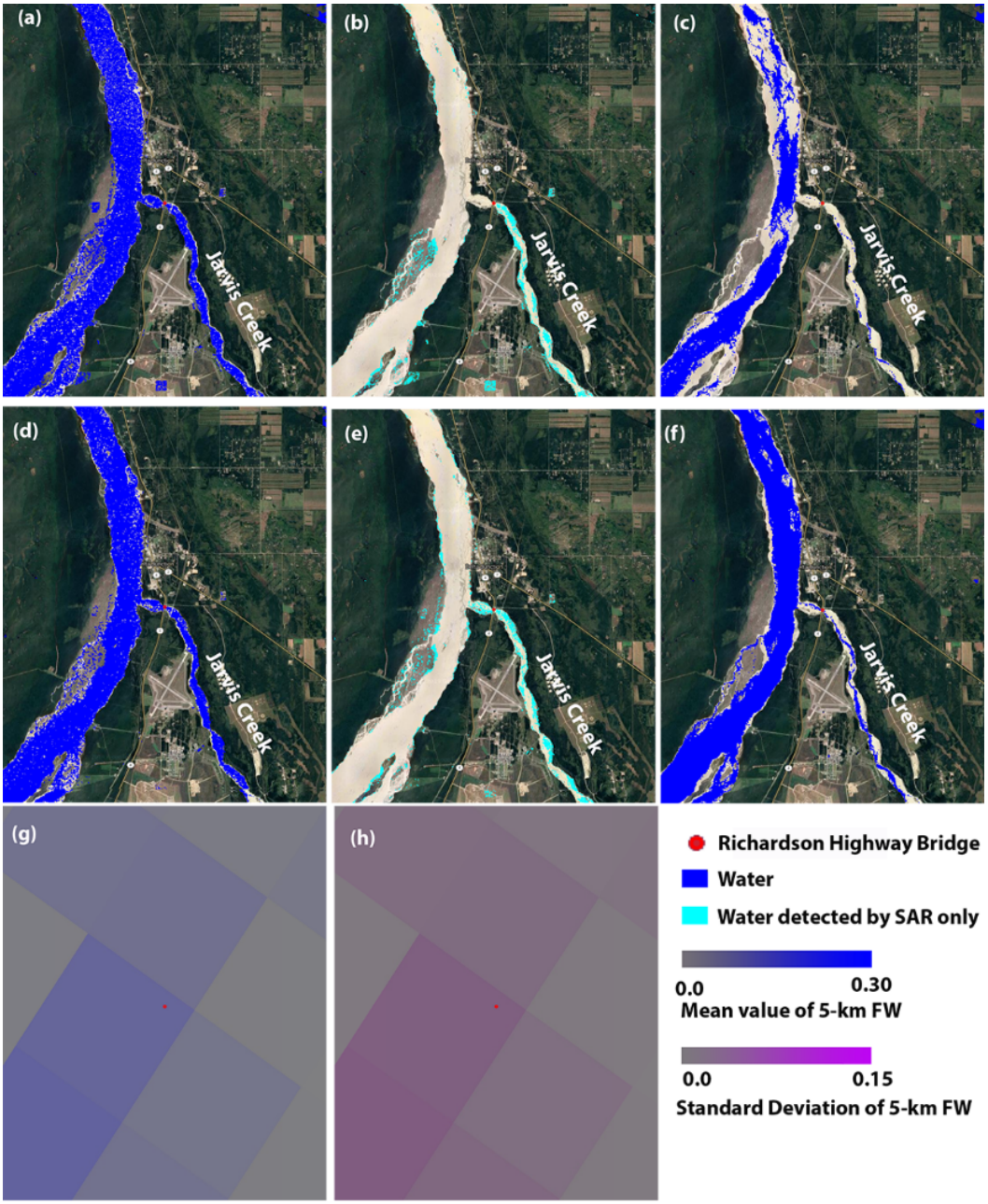


Figure 50. Maps showing 30 m surface water detected by Sentinel-1 SAR (a), the 30 m downscaled results of 25 km AMSR Fw (c) classifications for May 11, 2017 over the Richardson Highway Bridge of Jarvis Creek in the Delta Junction region. The image in (b) shows flooded areas detected by SAR observations on August 14, 2016 that did not occur within the 30 m Landsat WOD (1984-2015; highlighted in cyan); these indicate the presence of new permanent water covered or temporarily flooded terrain units. Similar results of SAR classifications (d), downscaled 30 m Fw (e) and inundation detected by SAR only (f) were generated for August 13, 2017. Average inundation conditions (g) and dynamics (h) were detected by the available 5 km Fw record (2003-2016).

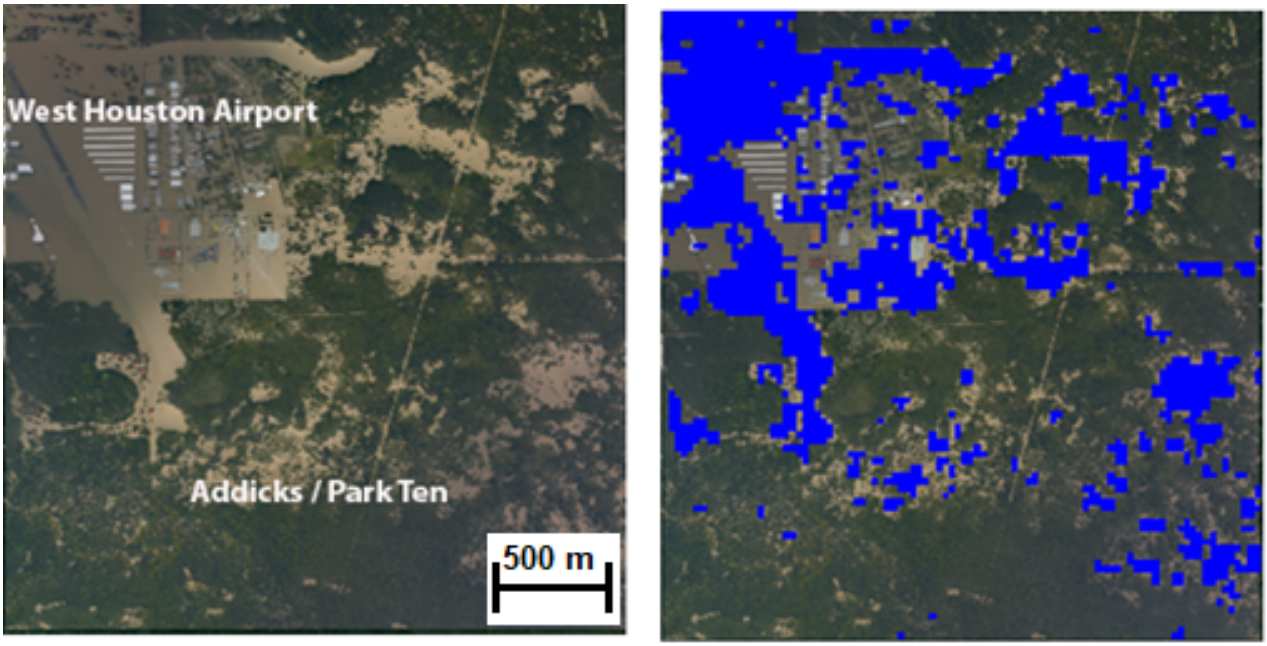


Figure 51. NOAA 0.3 m aerial photos taken over Addicks/Park Ten of Houston on August 30, 2017 (left) and the corresponding Sentinel-1 SAR water (blue) and land classification results (right) obtained using the machine learning algorithm developed in this study and through partner activities (Du et al. 2019).

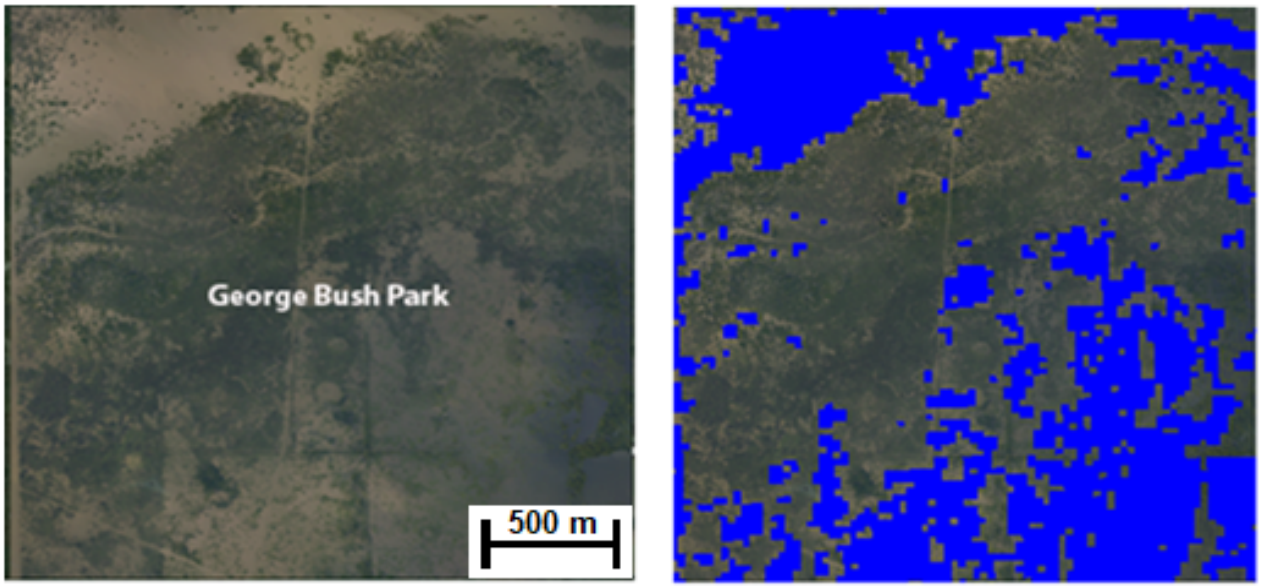


Figure 52. NOAA 0.3 m aerial photos taken over part of Houston's George Bush Park on August 30, 2017 (left) and the corresponding Sentinel-1 SAR water (blue) and land classification results (right) obtained using the machine learning algorithm developed in this study and through partner activities (Du et al. 2019).

The SAR results were compared with supervised classifications that were made on NOAA aerial photos as part of a different investigation (Du et al. 2019). The classifications of NOAA aerial photos were examined using independent data sets and showed an overall accuracy 94%. The Westside Park area (Figure 51) is characterized by mixed forests, water and buildings, whereas the George Bush Park area (Figure 52) is dominated by water and forest. The overall Sentinel-1 SAR classification accuracy for these two images (Table 12) was 75% (with 10% commission error and 45% omission error of water classifications). The misclassifications mainly occurred over mixed pixels especially where low-backscatter water and high-backscatter features (e.g., forest and buildings) were mixed within the 30 m resolution pixels. In addition to this test study, project members are also finding that combining SAR and high resolution VIS observations (e.g., Planet images at 0.78 to 3.125 m resolutions) offer promising results in improving classification accuracy over complex land conditions (this is still under development at NTSG by Du et al. and is not shown here).

Table 12. Sentinel-1 SAR water and land classification accuracy.

Class	Commission Error	Omission Error
Water	10%	45%
Land	34%	6%
Overall Accuracy	75%	

5.2.3 Vegetation State

The algorithm that we developed to downscale the 25 km AMSR VOD includes 500 m NDVI from MODIS, and five additional MODIS vegetation indices that track leaf water content, and leaf pigment absorption of VIS-NIR (Table 5). For this project, we tested this new algorithm over the spring to summer transition period in 2014, including an evaluation of VOD estimates for April 15, May 1, June 1, July 1. The 15th of April was selected instead of the 1st because the ground was still largely frozen earlier in the month, which reduced the amount of satellite retrievals available from MODIS and AMSR VOD for the vegetation applications.

Our downscaled VOD test images (Figure 53) for Alaska were able to capture the northward progression of biomass growth starting in spring and continuing into early summer. Though the regional patterns of the downscaled VOD are similar to the original 25 km AMSR product, the 500 m VOD was able to account for more localized variability that was not observed in the coarser resolution retrievals. This was especially apparent in the June 1, 2014 test image which showed lower VOD in the less vegetated mountain regions and localized regions of higher VOD across forested terrains in the Interior and southern coastal region. The short-term decrease in both VOD products and MODIS NDVI, observed between April 15 and May 1, resulted after a period of colder temperatures and snowfall. In July, the NDVI retrievals indicated “green” vegetation conditions across Alaska during the peak growing season (Figure 53). However, the downscaled VOD record showed a decrease in vegetation biomass water content within the Interior, likely indicating vegetation drought stress.

The spring to summer progression of VOD increase was also observed in the downscaled results for the Interior AOI (Figure 54). In mid-April the lower 500 m VOD values, indicating lower amounts of active biomass, were observed primarily in higher elevation terrains both north

and south of DoD lands. An increase in biomass was observed over most of the region (except in the barren foothills of the Alaska Range in the southern portion of the AOI) from May to June. These seasonal patterns of VOD are in agreement with on-the-ground images available for this region (e.g., Figure 42 showing spring vegetation greening at the Farmer's Loop Trail Camera site in Fairbanks). A decrease in VOD within the Interior and DoD terrains was observed in early July during a period of vegetation water stress. In the May and June test images, slightly lower VOD at the northern portion of the Tanana Flats Training Area, relative to the surrounding terrains, coincided with the presence of wetland vegetation.

To evaluate the 500 m downscaled VOD against the original 25 km AMSR product, observed vs. predicted values were obtained for 1,000 randomly selected locations on each date. These data were used to generate scatterplots of observed vs. predicted VOD and the corresponding R^2 metrics. The scatterplots (Figure 55) highlight the strong model fit over all four months. The poorest model fit occurred in April, with a R^2 of 75% arising from downscaled VOD having higher predicted values relative to the 25 km retrievals for values greater than 1.3. The higher estimates in the downscaled VOD for April (and May) are not necessarily incorrect and could indicate an ability of the 500 m VOD to identify localized increases in early season biomass that were not identified in the 25 km product. The R^2 for May through July was 80% or higher and the average RMSE across the four dates was 0.12, indicating a strong agreement between the two VOD products.

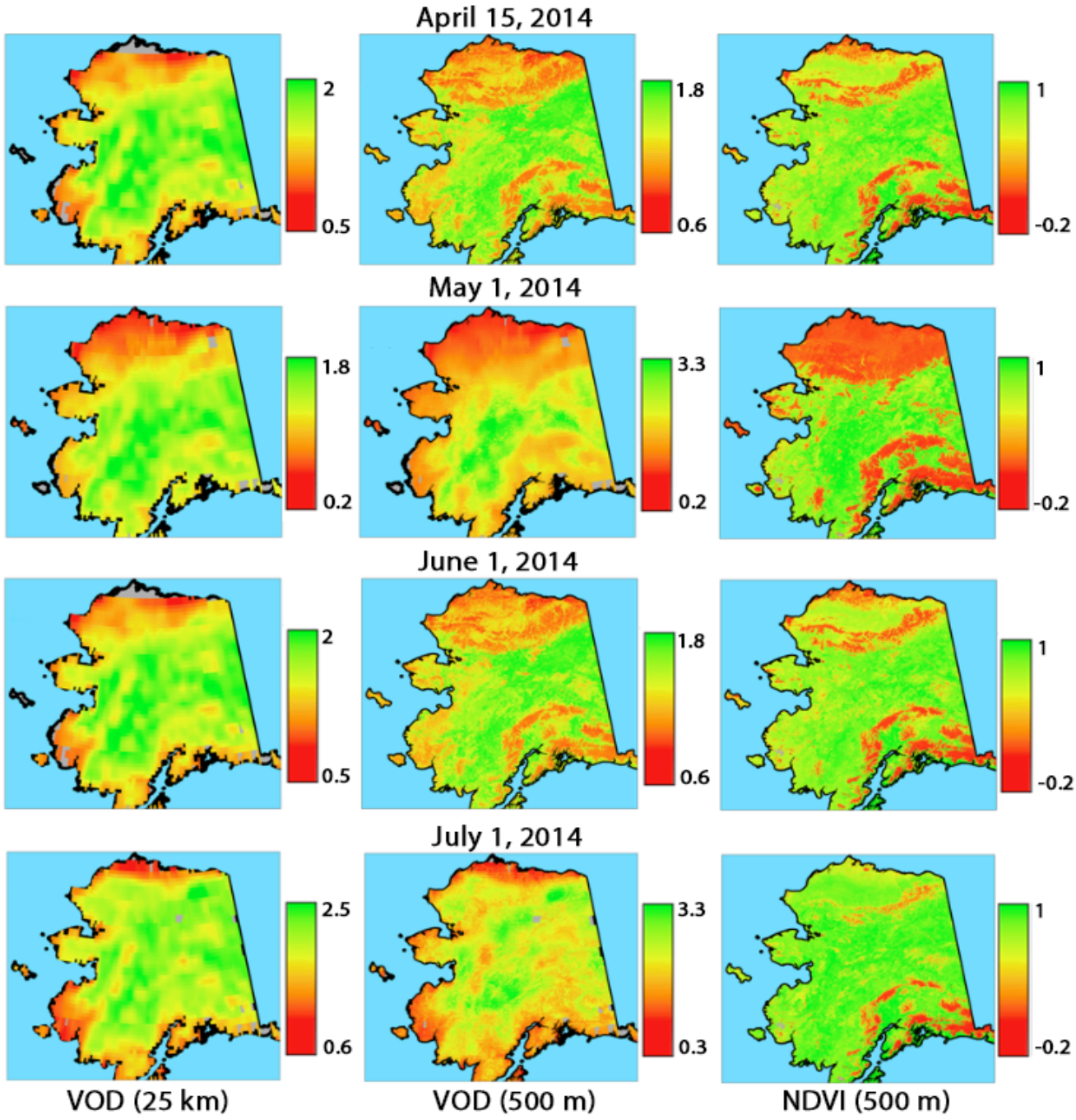


Figure 53. Comparison of spatial patterns observed over Alaska in the 25 km AMSR VOD retrieval record (a), 500 m MODIS derived NDVI (c) and the resulting 500 m downscaled VOD produced using methods developed in this study (b). The test dates shown here are for early April through July 2014. Larger values of VOD indicate higher aboveground biomass water content. Larger positive values of NDVI indicate more vegetation "greenness"; NDVI values below 0.1 indicate barren terrain, snow or ice, or large bodies of open water.

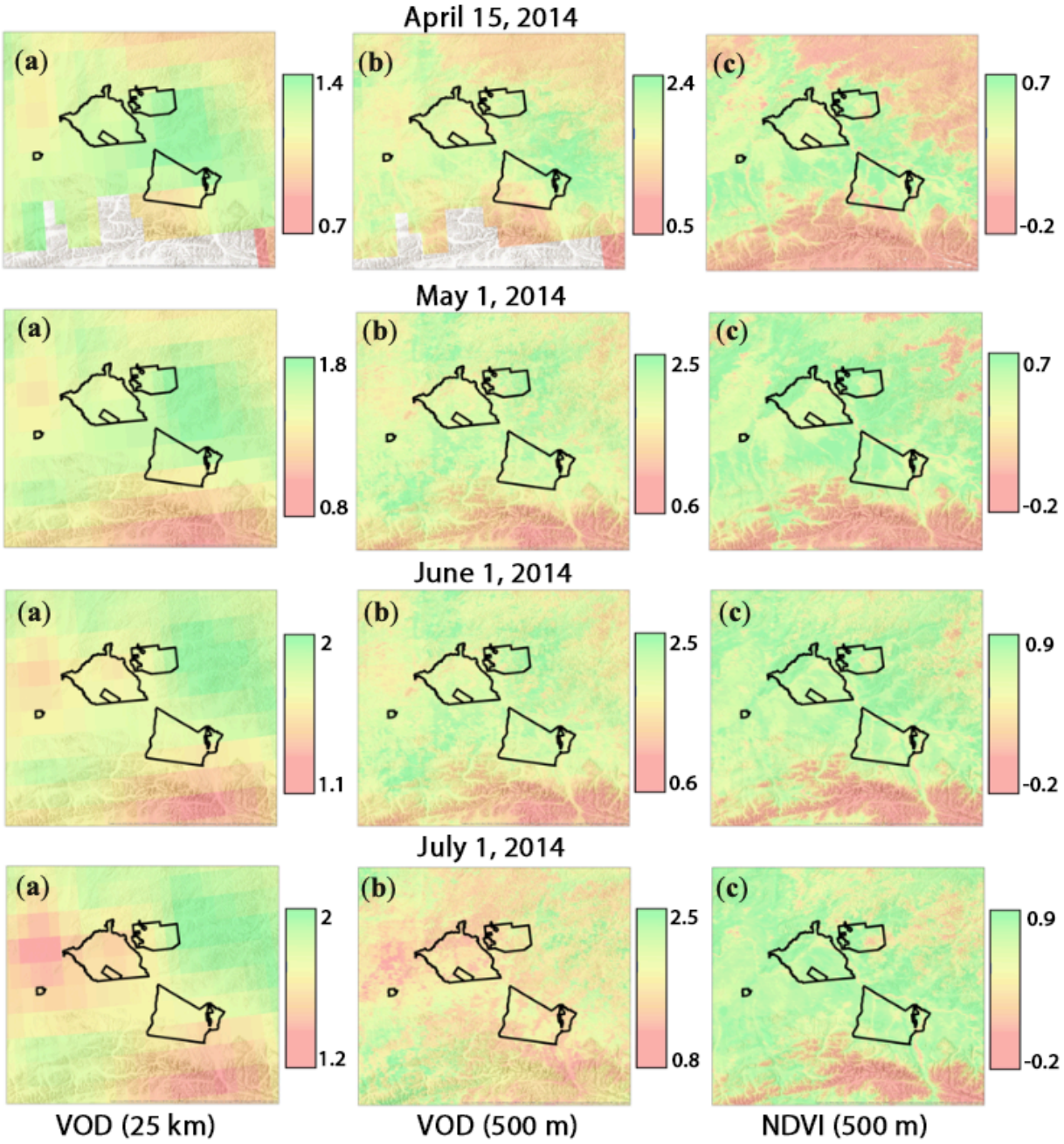


Figure 54. Comparison of spatial patterns observed over the Interior Alaska AOI in the 25 km AMSR VOD retrieval record (a), 500 m MODIS derived NDVI (c) and the resulting 500 m downscaled VOD produced using methods developed in this study (b). The test dates shown here are for early April through July 2014. Larger values of VOD indicate higher aboveground biomass water content. Larger positive values of NDVI indicate more vegetation "greenness"; NDVI values below 0.1 indicate barren terrain, snow or ice, or large bodies of open water. DoD cantonments and training lands are outlined in black.

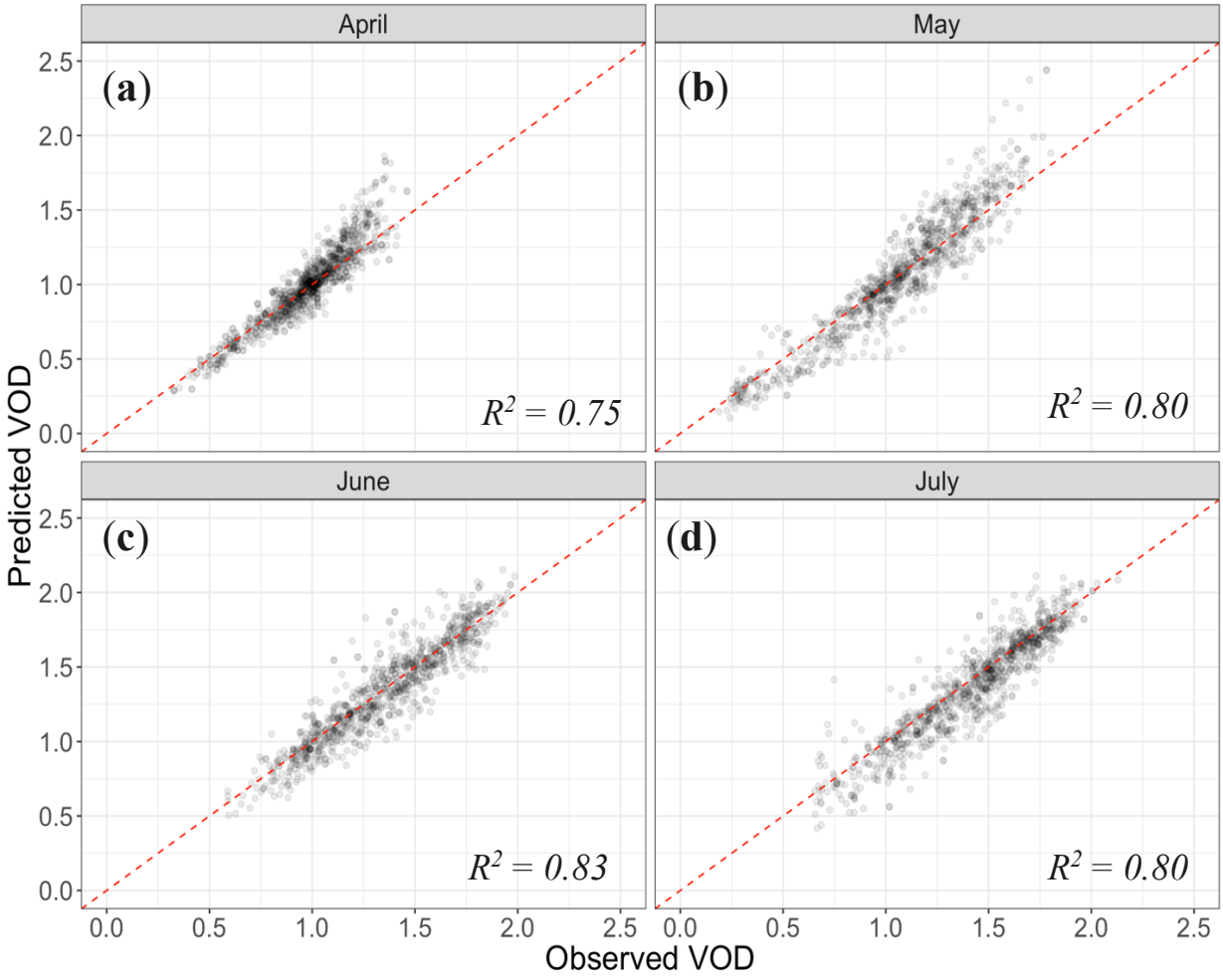


Figure 55. Comparison of baseline (observed) 25 km AMSR VOD and machine-learning predicted 500 m VOD values on April 15 (a), May 1 (b), June 1 (c) and July 1 (d) 2014. The associated R^2 values are also provided. The red dashed line represents a linear 1:1 relationship.

5.2.4 Discussion and Summary of Data Fusion (downscaling)

The focus of the data fusion component in this study was to develop and test methodologies for downscaling Earth System Indicator metrics based on coarser 25 km passive microwave retrievals. Here we developed and evaluated machine learning algorithms for the downscaling of terrain Freeze/Thaw, surface soil moisture, open water and vegetation. In addition, we developed and improved methods for the classification of open water within Sentinel-1 SAR retrievals.

The resulting downscaled products had a much improved spatial resolution of 500 m (Freeze/Thaw, soil moisture and vegetation) and 30 m (open water). Each of the downscaled products evaluated in this study were able to capture spatial and temporal patterns of terrain change with documented improvement over the original, coarse resolution AMSR retrievals. The synergistic use of satellite microwave and VIS-NIR-TIR observations allowed for enhanced detection of land surface conditions and better supported assessments of local environmental

conditions, changes in terrain state, and the monitoring of landscapes affected by natural disasters.

Whenever possible, we verified patterns observed in the downscaled test products with on-the-ground information including river discharge and surface moisture records, and on-site time-lapse imagery from local trail cameras (incl. those maintained by USACE CRREL and project partners). However, we found the availability of in situ data for algorithm validation to be very limited within DoD terrains in Interior Alaska. Future installation of sensors for air and surface temperature, soil moisture, canopy level VOD (derived from microwave based differential GPS) and additional trail camera stations are strongly recommended on DoD terrains in this region. These stations will be instrumental for future improvements to downscaling algorithms, and to provide on-site monitoring of terrain change that can be evaluated in conjunction with satellite remote sensing.

Though still in a 'test' phase, the methods developed here can be readily applied in Google Earth Engine over the microwave data record ($\leq$ 2002 to 2017) to produce daily 500 m estimators of terrain state over Alaska and elsewhere on Earth. These long-term, downscaled records can be used to assist in identifying more localized and spatially precise patterns of nonstationarity through the application of Mann-Kendall and BFAST change detection to detect respective monotonic trends and abrupt disturbances in the time series.

6. CONCLUSIONS AND IMPLICATIONS FOR TRAINING RANGE MANAGEMENT AND FUTURE RESEARCH/IMPLEMENTATION

6.1 Introduction

Alaska is warming at a rate over twice the global average, and regional temperatures will continue to increase through the next century unless extreme measures are taken to counter climate change. This warming is contributing to the accelerated thaw of permafrost, a shortening of the annual frozen period, changes in surface hydrology including summer drought and terrain flooding in the spring, and heightened vegetation stress and susceptibility to fire across the Alaska Interior. These changes have important consequences for the U.S. DoD, which manages over a million acres of land in Alaska and has investments in Air Force and Army installations across the state. Military training grounds in Interior Alaska are characterized by remote and rugged terrains, cold climate conditions, and extremely wet soils overlying permafrost that provide U.S. troops and special forces with experience and conditioning that can only be obtained by working within harsh arctic and boreal landscapes.

With climate warming, access to these terrains may become more limited as the spring and autumn shoulder seasons increasingly remain in a transitional state between frozen and thawed. A lengthening of the freeze and thaw cycle can degrade and damage infrastructure such as buildings, roadways and airstrips. Changes in surface soil moisture and flooding can reduce cross-terrain movement by increasing travel hazards and the sinking of motor vehicles on grounds unable to support weight. A drying of vegetation in Alaska's forests greatly increases the risk of extreme fire events, adding an additional threats to DoD infrastructure and personnel.

These active threats are generally identified and acknowledged by the U.S. (Jay et al. 2018) and DoD (DoD 2019), though the location and timing of terrain changes that contribute to these threats are not well characterized across the extensive and remote terrains of Alaska. Long-term

in situ monitoring networks in Alaska are sparse considering the size of the state and are often plagued by gaps in data. Because of this, remote sensing observations from satellites provide a "force multiplier" – the best option for characterizing ecosystems and terrain disturbances across broad spaces and over time. Satellite remote sensing observations also provide a wealth of open access data from U.S. and U.S. collaborating partner agencies (e.g., European Space Agency; Japanese Space Agency).

Developing an integrated remote sensing-based monitoring and change detection platform for Alaska is critical for U.S. strategic planning, security, and policy to ensure installation adaptation and resilience (Wuebbles et al. 2017; CRS 2018; DoD 2019) and for continued access to U.S. training grounds in the Arctic. A remote-sensing based change detection platform is necessary to identify contemporary changes in ecosystem state and the trajectories of this nonstationarity. This would allow for geospatial referencing of terrains showing more subtle longer-term changes (observed through trend analysis) and those experiencing sharp shifts in ecosystem state (observed through time series break analysis). This could also help to identify neighboring terrains that have been relatively "stable" but that are now potentially placed at higher risk because of their proximity to change. Further, information output from this detection platform can be used to identify terrains showing localized resilience to climate warming. The detection of resilience, and understanding of how and why terrain resilience occurs, is important because it can help land and infrastructure planners make more informed decisions regarding land use and habitat management.

The goal of this SEED project was to pave the way for the development of an integrated satellite remote sensing based ecosystem change detection system, suitable for analysis of nonstationarity across Alaska, but also allowing direct transferability to other regions across the Earth. Hence, the project objective was to first assess the feasibility of integrating a suite of information from satellite microwave remote sensing to quantify terrain changes in Alaska corresponding to three key Earth System Indicators: 1) Terrain Thermal State; 2) Ecosystem Water Stress; 3) Vegetation State. The second objective was to assess the feasibility of using satellite data fusion to provide new, multi-spectrally-informed time series records of Earth System Indicators but at an improved ($\leq$ 500 m) spatial resolution.

This goal was accomplished through four primary research tasks. The first three included identifying the feasibility of using a suite of multi-spectral and multi-scale VIS-NIR-TIR and microwave remote sensing datasets to detect change in Indicator metrics: 1) snow cover, air and land temperature, terrain Freeze/Thaw surface frozen, transitional (frozen to thawed or thawed to frozen) and non-frozen state; 2) precipitation, surface soil moisture, surface water inundation; 3) ecosystem vegetation greening or browning and biomass water content. We applied a statistical change detection over Alaska to detect shifts in these terrain properties over a recent 16+ year ($\leq$ 2002 to 2017) record. The fourth project task involved developing and applying new machine learning methodologies to integrate VIS-NIR-TIR and microwave datasets in order to test the production of new higher resolution (downscaled) Indicator State metric maps for Interior Alaska. The downscaled Indicator metrics included 500 m surface Freeze/Thaw (frozen/transitional/unfrozen) state, surface soil moisture, and vegetation water status. We also assessed radar-based classifications of seasonal changes in surface water (including flooded terrains following a major natural disaster). Providing these Indicator metrics at much finer spatial resolutions relative to the original microwave products can greatly assist in the regional

detection of changes in terrain conditions by better allowing the more localized characterization of terrain nonstationarity.

Conclusions and recommendations resulting from these four major tasks are provided below.

6.1.1 Terrain Thermal State

Our satellite microwave analysis indicated that snowmelt onset is occurring earlier each spring (at rates up to 1 day per year) across higher elevation terrains (> 500 to 1,000 m) within Alaska's western coastal region and the Interior. Our analysis also showed that most regions in Alaska experienced significant increases in the annual duration of spring snow melt, primarily from earlier spring melt dates. For the DoD terrains in Interior Alaska (e.g., Yukon Training Area, Tanana Flats Training Area, Donnelly Training Area) we detected that the timing of snowmelt onset and snowoff shifted forward in spring at rates of ~1 day per year over the 1988 to 2016 satellite retrieval record, though further study is needed to determine the factors contributing to this change.

Our assessment of the microwave Freeze/Thaw record (from 2002 to 2016) for Alaska indicated an increase in the spring transitional state (where the surface shifts back and forth between frozen and thawed within a 24 hour period) at a rate of 5 days per decade. A similar increase in the spring thaw period was observed at a rate of 8 days per decade. Within the Interior Alaska AOI, we observed a significant increase in transitional (+ 0.4 days per decade) and thawed state (+ 0.2 days per decade) in winter. We also detected a large increase in the rate of annual thawed days in autumn and early winter over Donnelly Training Area and Tanana River Training Area, at 1.5 days per decade. Because of this, and the associated detection of regional changes in the timing of snowmelt, we recommend a localized and detailed investigation of seasonal and annual changes in land surface Freeze/Thaw status over DoD terrains within Interior Alaska. This localized study should tie multi-frequency and multi-source satellite and aerial observations with in situ monitoring stations (including time lapse photography, detection of snow depth, air and soil temperature) strategically placed across various DoD terrains. This combined remote sensing and DoD site based investigation would provide a more detailed assessment how terrain heterogeneity affects terrain thermal state characteristics, and how this heterogeneity is manifest (or attenuated) within various satellite retrieval footprints.

6.1.2 Ecosystem Water Stress

Our analysis revealed regional hotspots of terrain wetting and drying throughout Alaska. We found, based on the MERRA2 reanalysis records, that precipitation amounts in spring increased over much of Alaska from 1980 to 2017. The rates of this increase varied by location but was greatest over the North Slope (> 20 mm per decade). This is concerning because an increase in spring rainfall over frozen ground results in an increased risk of widespread flooding in this region, including over the Dalton Highway which is a vital roadway connecting Prudhoe Bay with mainland Alaska. In addition, the increase in spring rainfall could greatly accelerate rates of permafrost thaw, leading to terrain collapse and consequences for ecosystems and infrastructure. In contrast, this study also found that western and Interior Alaska regions experienced a decrease in summer and autumn precipitation during the 38-year observation period. Our analysis also

detected a decrease in precipitation (at a rate of 10.1 mm per decade) over DoD terrains of Yukon Training Area, Tanana Flats Training Area, and Donnelly Training Area.

In spite of the decreased rates of precipitation in summer and autumn, our analysis of the AMSR satellite record showed a significant increase in surface soil moisture over much of Alaska, including the Interior and DoD terrains (i.e., Yukon Training Area, Tanana Flats Training Area, Donnelly Training Area). We also detected significant increases in surface water inundation occurring in summer, along coastal zones and within the Interior AOI. Within the Interior AOI and DoD terrains, we observed substantial increases in both the 5 km and 25 AMSR Fw records across the annual non-frozen period. In autumn, substantial increases in surface Fw inundation were observed over ~ 26% of the Interior AOI, especially near Fort Greely and across the Donnelly Training Area. This detected increase in both the 25 km (18.7 and 23 GHz *Tb*) and 5 km (89 GHz *Tb*) AMSR records warrants further investigation and should be coupled with recent high-resolution (e.g., 3.13 m) satellite observations and on-the-ground mapping assessments of wetland and water body change within DoD terrains in Interior Alaska. One area of investigation should be how the detected surface soil moisture and inundation detection corresponds with the removal of the forest canopy (e.g., resulting from fire). We also recommend the installation of in situ soil moisture monitoring stations across these terrains to better assess how surface moisture is changing as a function of permafrost thaw, local hydrology and vegetation conditions.

6.1.3 Vegetation State

Our analysis of vegetation showed that the Alaska coastal regions experienced increased AMSR VOD and greenness (i.e., MODIS NDVI) over the past 16 years (2002 to 2017). These regional vegetation changes coincided with an extended annual non-frozen season, increases in precipitation and surface soil moisture. An expansion of shrub cover across coastline tundra may also be contributing to these observed changes. Future research is recommended to disentangle the various ecosystem drivers contributing to the increases in vegetation greenness and VOD. This could include incorporating a LiDAR (Light Detecting and Ranging)-based detection of biomass structure in addition to VIS-NIR classifications of long-term shrub absence/presence and an assessment of permafrost active layer deepening across these regions.

In the Alaska Interior we observed a significant decrease in VOD within forested regions that primarily corresponded with large terrain disturbances and loss of forest biomass. Our assessment found that these negative trends in VOD occurred primarily following major fire events. Over DoD and surrounding terrains (including Yukon Training area) we observed a strong increase in VOD starting in 2014 (two years after a widespread burn occurring in 2012) that persisted through the end of our study period (2017). In contrast, the NDVI record showed increased greening within the region, especially in areas recently affected by fire where understory vegetation is beginning to recover. In this study, we found that ability of VOD to detect changes in vegetation water content, and hence changes in aboveground biomass, provided additional information of vegetation condition and disturbance that might not be detected if only using NDVI and other VIS-NIR based indices in vegetation assessments. For future study, we recommend the use of on-the-ground time lapse photography and microwave based VOD monitoring (e.g., using Global Navigation Satellite System (GNSS) GPS base stations), coupled with satellite VOD and NDVI retrievals, to understand how the various rates

of VOD recovery are influenced by burn severity, pre-and post-fire forest composition, and changes in surface moisture.

The results from our case study of BFAST (tested for a known burn event in Interior Alaska) confirms that the algorithm is able to detect breaks in remote sensing time series, but also showed the detected break points to be highly dependent on what occurred in the satellite record (and on the ground) before and after the disturbance event. Therefore, we recommend further assessment of the BFAST algorithm to detect abrupt terrain change. For Alaska and elsewhere, this will require a separate parameter tuning and evaluation of algorithm response for each Indicator metric (i.e., VOD, NDVI). We also recommend evaluating the BFAST detection for various disturbance types (e.g., windfall, road and building infrastructure development) in addition to fire events. For fire, we recommend assessing BFAST across a range of disturbance events having different levels of severity and burn extent within the satellite sensor footprint. This BFAST calibration process would help to minimize the incorrect detection of abrupt terrain disturbance events, and to allow for a next level of application where a probability of disturbance type is assigned to each BFAST detection. A possible alternative to BFAST is the LandTrendr algorithm (Kennedy et al. 2018), which is similar to BFAST but has the primary advantage of being easily implemented in Google Earth Engine. This would allow the break point analysis to be applied relatively quickly to each grid cell over Alaska.

6.1.4 Indicator Downscaling for Localized Change Analysis

For this study, we developed and evaluated machine learning algorithms for the downscaling of terrain Freeze/Thaw, surface soil moisture, and vegetation to a 500 m resolution. In addition, we developed methods for the classification of open water (e.g., flooding) within Sentinel-1 SAR retrievals at a 30 m resolution. Our initial "proof-of-concept" assessment indicated that the downscaled products were able to capture spatial and temporal patterns of terrain change with improvement over the original, coarse 25 km resolution AMSR retrievals (here evaluated for a limited number of retrieval dates, over the 2014 through 2017 period).

When possible, we evaluated the downscaled test products with on-the-ground information. Comparing our downscaled 500 m soil moisture with in situ observations obtained for the Granite Creek SNOTEL station near Fort Greely showed a correlation of 0.68 between the in situ observations and satellite derived (fused VIS-NIR and microwave) moisture estimates. We also observed a good agreement between our downscaled 500 m Freeze/Thaw record and time lapse photography from the CRREL Farmer's Loop site (near Fairbanks) that provided site level indication of terrain frozen or thawed state. Evaluation of USGS river discharge records from the Tanana River Site near Fairbanks showed the ability of our Sentinel-1 SAR open water product to account for dynamic wetting and drying that occurred within the river record. A further assessment of our Sentinel-1 SAR based detection of surface water for the Houston, Texas area following Hurricane Harvey showed a 75% accuracy of the SAR detection method to correctly classify flooded lands with at a 30 m spatial resolution, relative to water classifications provided through NOAA very high resolution aerial photography.

We recommend the development of an enhanced-resolution (30 m to 500 m) remote sensing based change detection and mapping system for Arctic-boreal and global terrains that integrates information from multiple satellite sensors and platforms, while also facilitating a coordinated on-the-ground monitoring network that can be used for calibration and verification of satellite change detection algorithms. The current downscaling approach can be extended to map

additional Earth System Indicators involving freeze/thaw, water stress, vegetation and snow; the machine-learning techniques can be refined by analyzing more comprehensive satellite observations including AMSR, SMAP, Sentinel-1 SAR, MODIS, Landsat, and Planet. For example, the incorporation of CubeSat high resolution images (e.g., Planet imagery; Fig. S28) will likely enable further improvement in our ability to delineate inundation, snow and ice conditions. For further development, evaluation and validation of the remote sensing products, we recommend that future studies deploy new terrain monitoring networks to obtain high-quality and intensive ground observations of the associated surface parameters.

6.2 Ramifications for DoD in Alaska

It is clear from this and numerous other recent studies that the lands on which the DoD trains throughout Interior Alaska are undergoing rapid state changes across all seasons. These changes are measurable at a variety of scales. Most of the results from our study confirm that a press disturbance of climate warming is the main cause of these changes. From the perspective of land management and safety the most critical results are that wintertime thaw events are increasing, and the timing of spring melt is shifting earlier. This provides added risk for safe travel across land and water bodies and increases the potential for degradation of the surface vegetation mat and soils from vehicle travel. If this persists it may alter the types of vehicles that can be used for mobility across these terrain types. From the perspective of remote operations or activities on foreign lands the application of remotely sensed measurements to identify localized ground based terrain properties provides new tools for operational readiness and mission preparation.

In Interior Alaska the increase in surface soil moisture may identify locations where permafrost thaw and surface subsidence (and subsequent inundation) are occurring. It is too early to determine whether this is a new normal and to identify how rapidly and how far reaching permafrost thaw is occurring. But the potential increase in wetland areal extent has wide ranging consequences. For some species of concern that use waterbodies or waterbody margins as habitats this may provide a positive as it increases habitat accessibility and migration corridors. However, for potential surface flooding, hydrologic connectivity and the potential for increased erosion or changing surface water turbidity this may reduce fish and other aquatic habitat conditions. Simply stated – more water does not necessarily mean a better habitat selection for some species.

From the perspective of wildfire and potential ignition sources related to live fire training the decreases in summer and autumn precipitation could provide heightened fire risk. In some areas the ground surface may be wetter due to permafrost thaw but if the surface vegetation structure is drier, or if some areas become more drained with loss of the hydrologic aquiclude provided by permafrost the fire risk and intensity may increase. Recent large fires attributed to live fire training have changed how and when the Army and Air Force use impact areas. Since ignition conditions change daily, the development of remote sensing tools and analytical processes could provide access to new information that DoD can use to make real time decisions.

6.3 Towards an Automated Remote Sensing Change Platform

The remote sensing change detection framework that we tested and applied in this study demonstrates the strength of using multi-scale and multi-spectral (VIS-NIR-TIR and microwave) information from satellites to detect ecosystem nonstationarity across vast remote and often

inaccessible terrains. We used remote sensing and reanalysis time series records spanning 16+ years to detect the occurrence of significant and long-term changes in Alaska based on multiple Earth System Indicator metrics for Terrain Thermal State, Ecosystem Water Stress and Vegetation State. In total, we assessed terrain changes in Alaska for eighteen individual Indicator metrics representing 275 GB of data and 100,000 images. The processing of these data in preparation for the regional analyses, and in preparation for the Mann-Kendall change detection assessment, was made possible through cloud computing (i.e., NASA's Center for Climate Simulation ADAPT Science Cloud) and through use of Google Earth Engine. The image processing and change detection code developed during this study allowed for semi-automation of this process, which provides the capability to repeat this process for annual updates to the change detection assessment. The change detection output includes geospatially referenced raster files (for this project, geoTiff format) indicating the presence, slope and direction of trend for each grid cell over Alaska. In addition, this process provides the vector based (shapefile format) spatial delineation of regions having significant change in each Indicator metric. Both the geoTiff and shapefile records are easily incorporated within Geographic Information Systems.

We recommend several continuing lines of improvement to the research presented here to generate an optimal remote sensing change platform for DoD managers in Alaska. First, to increase use and improve accessibility, we recommend the metrics presented here be integrated into a user-friendly web-based visualization and data manipulation platform. Second, this system should include the ability for automatic updates, both annually and seasonally, to represent the most up-to-date information available. Third, to better validate and understand the remote sensing-based signals, we recommend a comprehensive and strategically-placed network of in situ observations.

In the future it would be useful to compile all indicators presented here onto a central software platform where users could then select which spatial locations, they are interested in for assessing change, which years they want to evaluate the change detection framework over, and which specific indicators they which to evaluate. By creating an application such as this users would be able to quickly apply the Mann-Kendall change detection algorithm applied here in any setting across the globe. As additional metrics to evaluate change are compiled, they could be added into the system. This software would also allow users to specify which level of significance they wish to assess and automatically display grid cells with and without significant change. Additionally, it would be possible to not only incorporate the Mann-Kendall algorithm, but for individual grid cells one could evaluate the raw time series aggregated over user specified intervals (e.g., annual, monthly) to compare the temporal signal with the Mann-Kendall slope.

Downscaling coarser scale microwave based retrievals (e.g., from AMSR) with Landsat or MODIS is also possible; this would be a relatively simple implementation using the Google Earth Engine applications which is freely available. Similar to the theoretical automation of Mann-Kendall, downscaling automatically in Google Earth Engine would enable users to select areas of interest, the spatial scale they choose to downscale at, which predictor variables to use, and automatic error output as assessed by RMSE (or any other metric of choice) for regression problems and error matrixes for classification problems.

Finally, because one of the greatest challenges with this framework is data interpretation, we recommend further research to better understand the drivers of the observed changes, resolve apparent conflicting data streams, and interpret the conclusions in the context of DoD objectives and initiatives. The interpretation of the change analysis results, and knowledge transfer of this

information to inform DoD terrain managers, remains the most time and personnel intensive aspect of the change detection platform. By utilizing available cloud computation systems and satellite data archiving and processing platforms including Google Earth Engine (EE) and Amazon Wet Services (AWS), we have the ability to implement our algorithms under EE/AWS programming environment and establish a satellite data processing, analyzing and visualizing workflow. Other software packages options for consideration, which enable the creation of web applications, include the open source Shiny package in R, Google App Engine, the Bokeh package in python and Google Earth Engine. For realizing a fully automated processing, we will also need to develop procedures for automated data upload to EE/AWS and standardized image output in accordance with the requirements and geospatial tools used by DoD training land and infrastructure managers.

This SEED project has identified, outlined and demonstrated a path forward for the integrated use of a satellite remote sensing based data analysis system that can identify, track and document changes occurring in terrains across Alaska and other regions on Earth. At the time of this report, the “automated remote sensing change platform” remains a vision waiting to be realized. As with any transformative system, establishing such a platform will require investment and support by U.S. Agency programs, including SERDP and DoD’s Environmental Security Technology Certification Program (ESTCP). It will also require ongoing coordination with terrain managers and military planners to ensure the effective transfer of information to better inform risk mitigation and planning for ongoing and future military operations.

7. LITERATURE CITED

Affleck, R.T. (2005) Disturbance measurements from off-road vehicles on seasonal terrain. ERDC/CRREL Report TR-05-12. 99 pp.

Alaska Climate Research Center: Temperature Changes in Alaska, [online] Available from: http://climate.gi.alaska.edu/ClimTrends/Change/TempChange.html (Accessed 8 May 2019), 2019.

Baghdadi, N., H. Bazzi, M. El Hajj, M. Zribi (2018) Detection of frozen soil using Sentinel-1 SAR data. *Remote Sensing*, 10. 1182.

Bartsch, A. (2010) Ten years of SeaWinds on QuikSCAT for snow applications. *Remote Sensing*, 2: 1142-1156.

Bartsch, A., A.M. Trofaier, G. Hayman, D. Sabel, S. Schlaffer, D.B. Clark, E. Blyth (2012) Detection of open water dynamics with ENVISAT ASAR in support of land surface modelling at high latitudes. *Biogeosciences*, 9: 703-714.

Beck, P.S.A., G.P. Juday, C. Alix, V.A. Barber, S.E. Winslow, E.E. Sousa, P. Heiser, J.D. Herriges, S.J. Goetz (2011a) Changes in forest productivity across Alaska consistent with biome shift. *Ecology Letters*, 14: 373-379.

Beck, S.A., S.J. Goetz (2011) Satellite observations of high northern latitude vegetation productivity changes between 1982 and 2008: ecological variability and regional differences. *Environmental Research Letters*, 6. 045501.

Berg, E.E., J.D. Henry, C.L. Fastie, A.D. De Volder, S.M. Matsuoka (2006) Spruce beetle outbreaks on the Kenai Peninsula, Alaska, and Kluane National Park and Reserve, Yukon Territory: relationship to summer temperatures and regional differences in disturbance regimes. *Forest Ecology and Management*, 227: 219-232.

Berk, A., G.P. Anderson, P.K. Acharya, J.H. Chetwynd, L.S. Bernstein, et al. (2000) MODTRAN4 User's Manual. Air Force Research Laboratory. Space Vehicles Directorate. Air Force Material Command, Hanscom Air Force Base, MA.

Bieniek, P.A., U.S. Bhatt (2011) Large-scale climate controls of Interior Alaska ice breakout. J. *Climate*, 24: 286-297.

Biskaborn, B.K., J.-P. Lanckman, H. Lantuit, K. Elger, D.A. Streletskiy, W.L. Cable, V.E. Romanovsky (2015). The new database of the Global Terrestrial Network for Permafrost. *Earth System Science Data,* 7: 245-259.

Biskaborn, B.K., S.L. Smith, J. Noetzli, H. Matthes, G. Vieira, et al. (2019) Permafrost is warming at a global scale. *Nature Communications*, 10: 264.

Blackard, J.A., M.V. Finco, E.H. Helmer, G.R. Holden, M.L. Hoppus, D.M. Jacobs, et al. (2008) Mapping U.S. forest biomass using nationwide forest inventory data and moderate resolution information. *Remote Sensing of Environment*, 112: 1658-1677.

Breiman, L. (2001) Random Forests. *Machine Learning*, 45: 5-32.

Breiman, L., A. Cutler (2018) Breiman and Cutler's Random Forests for Classification and Regression. Version 4.6-14. R computing.

Bring, A., I. Fedorova, Y. Dibike, L. Hinzman, et al. (2016) Arctic terrestrial hydrology: A synthesis of processes, regional effects, and research challenges. *JGR Biogeosciences*, 121: 621-649.

Brodzik, M.J., D.G. Long, M.A. Hardman, A. Pagent, R. Armstrong (2016). MEaSUREs Calibrated Enhanced-Resolution Passive Microwave Daily EASE-Grid 2.0 Brightness Temperature ESDR, Version 1. Boulder, Colorado, USA. NASA National Snow and Ice Data Center Distributed Active Archive Center.

Brodzik, M.J., D. Long, M. Hardman (2018) Best practices in crafting the calibrated, enhanced-resolution passive-microwave EASE-Grid 2.0 brightness temperature Earth System data record. *Remote Sensing*, 10. 1793.

Bronaugh, D., A. Werner (2013) Zhang + Yue-Pilon Trends Package. Version 0.10-1.1. R-project Statistical Computing.

Bronen, R., F.S. Chapin III (2013) Adaptive governance and institutional strategies for climate-induced community relocations in Alaska. *PNAS*, 110: 9320-9325.

Brown, J., O.J. Ferrians, Jr., J.A. Heginbottom, and E.S. Melnikov, eds. (1997) Circum-Arctic map of permafrost and ground-ice conditions. Washington, DC: U.S. Geological Survey in Cooperation with the Circum-Pacific Council for Energy and Mineral Resources. Circum-Pacific Map Series CP-45, scale 1:10,000,000, 1 sheet.

Brown, J., K.M. Hinkel, F.E. Nelson (2000) The Circumpolar Active Layer Monitoring (CALM) program: research design and initial results. *Polar Geography*, 24: 166-258.

Cahoon, S.M.P., P.F. Sullivan, A.H. Brownlee, R.R. Pattison, et al. (2018) Contrasting drivers and trends of coniferous and deciduous tree growth in interior Alaska. *Ecology*, 99: 1284-1295.

Carroll, M.L., J.R.G. Townshend, C.M. DiMiceli, P. Noojipady, R.A. Sohlberg (2009) A new global raster water mask at 250 m resolution. *International Journal of Digital Earth*, 2: 291-308.

Carroll, M.L., J.R.G. Townshend, C.M. DiMiceli, T. Loboda, R.A. Sohlberg (2011) Shrinking lakes of the Arctic: spatial relationships and trajectories of change. *Geophysical Research Letters*, 38. L20406.

CAVM Team (2003) Circumpolar Arctic Vegetation Map. Conservation of Arctic Flora and Fauna (CAFF) Map No. 1. U.S. Fish and Wildlife Service, Anchorage, Alaska. ISBN:0-9767525-0-6.

Chapin, F.S., A.D. McGuire, R.W. Ruess, T.N. Hollingsworth, M.C. Mack, J.F. Johnstone, E.S. Kasischke, E.S. Euskirchen, et al. (2010). Resilience of Alaska's boreal forest to climatic change. *Canadian Journal of Forest Research*, 40: 1360-1370.

Chapin, F.S. III, M. Sommerkorn, M.D. Robards, K. Hillmer-Pegram (2015) Ecosystem stewardship: a resilience framework for arctic conservation. *Global Environmental Change*, 34: 207-217.

Clark, R., A. Ott, M. Rabe, D. Vincent-Lang, D. Woodby (2010) The effects of a changing climate on key habitats in Alaska. Alaska Department of Fish and Game. Special Publication 10-14.

Commane, R., J. Lindaas, J. Benmergui, K.A. Luus, R. Y.-W. Chang, B.C. Daube, E.S. Euskirchen, et al. (2017) Carbon dioxide sources from Alaska driven by increasingly early winter respiration from Arctic tundra. *PNAS*, 114: 5361-5366.

Cooley, S.W., L.C. Smith, J.C. Ryan, L.H. Pitcher, T.M. Pavelsky (2019) Arctic-boreal lake dynamics revealed using CubeSat imagery. *Geophysical Research Letters*, 46: 2111-2120.

Corcoran, R.M., J. R. Lovvorn, P.J. Heglund (2009) Long-term change in limnology and invertebrates in Alaskan boreal wetlands. *Hydrobiologia*, 620: 77-89.

Côté, I.M., E.S. Darling (2010) Rethinking ecosystem resilience in the face of climate change. *PLoS Biology*, 8. https://doi.org/10.1371/journal.pbio.1000438.

Cox, C. (2018) Drivers and environmental responses to the changing annual snow cycle of northern Alaska. BAMS. https://doi.org/10.1175/BAMS-D-16-0201.1

Canada Centre for Remote Sensing (CCRS). (2013). *2005 Land Cover of North America at 250 meters, Version 2.0*. Earth Sciences Sector, Natural Resources Canada. Retrieved from http://www.cec.org/naatlas/

CRS (2018) Changes in the Arctic: Background and Issues for Congress. *Congressional Research Service*. R41153.

Cui, Y., X. Chen, J. Gao, B. Yan, G. Tang & Y. Hong (2018) Global water cycle and remote sensing big data: overview, challenge, and opportunities. *Big Earth Data*, 2: 282-297.

Curran, J.H., N.A. Barth, A.G. Veilleux, R.T. Ourso (2016) Estimating flood magnitude and frequency at gaged and ungaged sites on streams in Alaska and conterminous basins in Canada, based on data through water year 2012. U.S. Geological Survey. Scientific Investigations Report 2016-5024. https://pubs.usgs.gov/sir/2016/5024/sir20165024.pdf

Dai, A., K.E. Trenberth, T. Qian (2004) A global dataset of Palmer drought severity index for 1870-2002: relationship with soil moisture and effects of surface warming. https://doi.org/10.1175/JHM-385.1

Danielson, J.J., and Gesch, D.B., (2011). Global multi-resolution terrain elevation data 2010 (GMTED2010): U.S. Geological Survey Open-File Report 2011–1073, 26 p.

Dietz, A.J., C. Kuenzer, U. Gessner, S. Dech (2012) Remote sensing of snow – a review of available methods. *International Journal of Remote Sensing*, 33: 4094-4134.

Didan, K., A.B. Munoz, R. Solano, A. Huete (2015) MODIS Vegetation Index User's Guide (MOD13 Series). Vegetation Index and Phenology Lab, The University of Arizona. https://vip.arizona.edu/documents/MODIS/MODIS_VI_UsersGuide_June_2015_C6.pdf

De Jong, R., S. de Bruin, A. de Wit, M.E. Schaepman, D.L. Dent (2011) Analysis of monotonic greening and browning trends from global NDVI time-series. *Remote Sensing of Environment*, 115: 692-702.

DoD (2019) Report on effects of a changing climate to the Department of Defense. Office of the Under Secretary of Defense for Acquisition and Sustainment. 9-D30BE5A.

Douglas, T.A., M.C. Jones, C.A. Hiemstra, J. Arnold (2014) Sources and sinks of carbon in boreal ecosystems of Interior Alaska: A review. *Elementa: Science of the Anthropocene*, 2. http://doi.org/10.12952/journal.elementa.000032.

Du, J., J.S. Kimball, J. Shi, R. Sun (2010) The development of HJ SAR soil moisture retrieval algorithm. *International Journal of Remote Sensing*, 31: 3691-3705.

Du, J., J.S. Kimball, C. Duguay, Y. Kim, J.D. Watts (2017a) Satellite microwave assessment of northern hemisphere lake ice phenology from 2002 to 2015. *The Cryosphere*, 11: 47-63.

Du, J., J.S. Kimball, L.A. Jones, Y. Kim, J. Glassy, J.D. Watts (2017b) A global satellite environmental data record derived from AMSR-E and AMSR2 microwave Earth observations. *Earth System Science Data*, 9: 791-808.

Du, J., J.S. Kimball, L.A. Jones (2017c) Daily Global Land Parameters Derived from AMSR-E and AMSR2 (Version 2.0) User Guide. https://daacdata.apps.nsidc.org/pub/DATASETS/nsidc0451_AMSRE_Land_Params_v02/

Du, J., J.S. Kimball, J. Galantowicz, S.B. Kim, S.K. Chan, R. Reichle, L.A. Jones, J.D. Watts (2018) Assessing global surface water inundation dynamics using combined satellite information from SMAP, AMSR2 and Landsat. *Remote Sensing of Environment*, 213: 1-17.

Du, J., J.S. Kimball, M. Pan (2019) Near-real time flood monitoring using passive and active microwave remote sensing: a case study of Hurricane Harvey. *Remote Sensing*, (In prep.).

Edlund, C. (2018) Quantifying permafrost extent, condition, and degradation rates at Department of Defense Installations in the Arctic. Wright-Patterson Air Force Base. AFIT-ENV-MS-18-M-198.

Fisher, B., R.K. Turner (2008) Ecosystem services: classification for valuation. *Biological Conservation*, 141: 1167-1169.

Fisher, J.B., M. Sikka, W.C. Oechel, D.N. Huntzinger, et al. (2014) Carbon cycle uncertainty in the Alaskan Arctic. *Biogeosciences*, 11: 4271-4288.

Fisher, J.B., et al. (2018). Missing pieces to modeling the Arctic-Boreal puzzle. *Environmental Research Letters*. Doi: 10.1088/1748-9326/aa9d9a.

Ford, J.D., G. McDowell, T. Pearce (2015) The adaptation challenge in the Arctic. *Nature Climate Change*, 5: 1046-1053.

Fraser, R.H., I. Olthof, S.V. Kokelj, T.C. Lantz, D. Lacelle, et al. (2014) Detecting Landsat changes in high latitude environments using Landsat trend analysis: 1. Visualization. *Remote Sensing*, 6: 11533-11557.

Friedl, M.A., D. Sulla-Menashe, B. Tan, A. Schneider, N. Ramankutty, A. Sibley, X. Huang (2010) MODIS Collection 5 global land cover: Algorithm refinements and characterization of new datasets. *Remote Sensing of Environment*, 114: 168-182. https://doi.org/10.1016/j.rse.2009.08.016

Fuentes, D.A., J.A. Gamon, H. Qiu, D.A. Sims, D.A. Roberts (2001) Mapping Canadian boreal forest vegetation using pigment and water absorption features derived from the AVIRIS sensor. *Journal of Geophysical Research*, 106: 565-577.

Gao, B. (1996) NDWI - A Normalized Difference Water Index for Remote Sensing of Vegetation Liquid Water From Space. *Remote Sensing of Environment*.

Gibson, C.M., M.R. Turetsky, K Cottenie, E.S. Kane, G. Houle, E.S. Kasischke (2016) Variation in plant community composition and vegetation carbon pools a decade following a severe fire season in interior Alaska. *Journal of Vegetation Science*, 27: 1197-1197.

Gitelson, A.A., M.N. Merzlyak, O.B. Chivkunova (2001) Optical properties and nondestructive estimation of anthocyanin content in plant leaves. *Photochemistry and Photobiology*, 71: 38–45.

Gitelson, A.A., Y. Zur, O.B. Chivkunova, M.N. Merzlyak (2002) Assessing carotenoid content in plant leaves with reflectance spectroscopy. *Photochemistry and Photobiology*, 75: 272–281.

Goetz, S.J., A.G. Bunn, G.J. Fiske, R.A. Houghton (2005) Satellite-observed photosynthetic trends across boreal North America associated with climate and fire disturbance. *PNAS,* 102: 13521-13525.

Gorelick, N., M. Hancher, M. Dixon, S. Ilyushchenko, D. Tahu, R. Moore (2017) Google Earth Engine: Planetary-scale geospatial analysis for everyone. *Remote Sensing of Environment*, 202: 18-27.

Green, M.F., L.A. Bisby, Y. Beaudoin, P. Labossiere (2000) Effect of freeze-thaw cycles on the bond durability between fiber reinforced polymer plate reinforcement and concrete. *Canadian Journal of Civil Engineering*, 27:949-959.

Hall, D., J. Martinec (1985). Remote Sensing of Ice and Snow. Chapman and Hall. Doi: 10.1007/978-94-009-4842.

Hall, J.V., W.E. Frayer, B.O. Wilen (1994) Status of Alaska Wetlands. U.S. Fish and Wildlife Service, Alaska Region, Anchorage, Alaska. 33 pp. https://www.fws.gov/wetlands/documents/status-of-alaska-wetlands.pdf

Hall, D.K., V.V. Salomonson, G.A. Riggs (2016) MODIS/Terra Snow Cover Daily L3 Global 500m Grid. Version 6. Boulder, Colorado USA: NASA National Snow and Ice Data Center Distributed Active Archive Center.

Hardisky, M.A., V. Klemas, R.M. Smart (1983) The influences of soil salinity, growth form, and leaf moisture on the spectral reflectance of Spartina alterniflora canopies. *Photogrammetric Engineering and Remote Sensing*, 49: 77–83.

Hart, S.A., H.Y.H, Chen (2006) Understory vegetation dynamics of North American boreal forests. *Critical Reviews in Plant Sciences*, 25: 381-397.

Hengl, Tomislav, Jorge Mendes de Jesus, Gerard B. M. Heuvelink, Maria Ruiperez Gonzalez, Milan Kilibarda, Aleksandar Blagotić, Wei Shangguan, et al. (2017). SoilGrids250m: Global Gridded Soil Information Based on Machine Learning. *PLOS ONE* 12. https://doi.org/10.1371/journal.pone.0169748.

Hijmans, R.J., S.E. Cameron, J.L. Parra, P.G. Jones, A. Jarvis (2005) Very high resolution interpolated climate surfaces for global land areas. *International Journal of Climatology*, 25: 1965–1978. https://doi.org/10.1002/joc.1276

Hinzman, L.D., N.D. Bettez, W.B. Bolton, F.S. Chapin, M.B. Dyurgerov, C.L. Fastie, B. Griffith, et al. (2005) Evidence and implications of recent climate change in northern Alaska and other arctic regions. *Climatic Change*, 72: 251-298.

Hollingsworth, T.N., A.H. Lloyd, D.R. Nossov, R.W. Russ, B.A. Charlton, K. Kielland (2010) Twenty-five years of vegetation change along a putative successional chronosequence on the Tanana River, Alaska. *Canadian Journal of Forest Research*, 40: 1273-1287.

Houborg, R., J.B. Fisher, A.K. Skidmore (2015) Advances in remote sensing of vegetation function and traits. *International Journal of Applied Earth Observation and Geoinformation*, 43: 1-6.

Huang, J. (2017) Recently amplified arctic warming has contributed to a continual global warming trend. *Nature Climate Change,* 7: 875-879.

Hursh, A., A. Ballantyne, L. Cooper, M. Maneta, J. Kimball, J. Watts (2016) The sensitivity of soil respiration to soil temperature, moisture and carbon supply at the global scale. *Global Change Biology*, 23: 2090-2103.

Im, J., S. Park, J. Rhee, J. Baik, M. Choi (2016) Downscaling of AMSR-E soil moisture with MODIS products using machine learning approaches. Environmental Earth Sciences, 75: 1120.

Ives, A.R., S.R. Carpenter (2007) Stability and diversity of ecosystems. *Science*, 317: 58-62.

Jandt, R. (2015) Alaska large fire history database: where to find it and how to download it. https://www.frames.gov/catalog/10465

Jepsen, S.M., C.I. Voss, M.A. Walvoord, J.R. Rose, B.J. Minsley, B.D. Smith (2012) Sensitivity analysis of lake mass balance in discontinuous permafrost: the example of disappearing Twelvemile Lake, Yukon Flats, Alaska (USA). *Hydrology Journal*, 21: 185-200.

Jepsen, S.M., M.A. Walvoord, C.I. Voss, J. Rover (2015) Effect of permafrost thaw on the dynamics of lakes recharged by ice-jam floods: case study of Yukon Flats, Alaska. *Hydrological Processes*, 30: 1782-1795.

Jin, S., L. Yang, P. Danielson, C. Homer, J. Fry, G. Xian (2013) A comprehensive change detection method for updating the National Land Cover Database to circa 2011. *Remote Sensing of Environment*, 132: 159-175.

Jinru, X., B. Su (2017) Significant remote sensing vegetation indices: a review of developments and applications. *Journal of Sensors*, 1: 1-17.

Johnstone, J.F., F.S. Chapin, T.N. Hollingsworth, M.C. Mack, V. Romanovsky, M. Turetsky (2010) Fire, climate change, and forest resilience in interior Alaska. *Canadian Journal of Forest Research*, 40: 1302-1312.

Jones, L.A., J.S. Kimball, K.C. McDonald, S.T.K. Chan, E.G. Njoku, W.C. Oechel (2007) Satellite microwave remote sensing of boreal and Arctic soil temperatures from AMSR-E. *IEEE Transactions on Geoscience and Remote Sensing*, 45: 2004-2018.

Jones, L.A., J.S. Kimball, E. Podest, K.C. McDonald, S.K. Chan, E.G. Njoku (2009) A method for deriving land surface moisture, vegetation optical depth, and open water fraction from ASMR-E. *2009 IEEE International Geoscience and Remote Sensing Symposium*, Cape Town, 2009, pp. III-916-III-919.

Jones, J.B., A.J. Rinehart (2010a) The long-term response of stream flow to climatic warming in headwater streams of interior Alaska. Canadian Journal of Forest Research, 40: 1210-1218.

Jones, L.A., C.R. Ferguson, J.S. Kimball, K. Zhang, S.T.K. Chan, K.C. McDonald (2010b) Satellite microwave remote sensing of daily land surface air temperature minima and maxima from AMSR-E. *IEEE Journal of Selected Topics in Applied Earth Observations and Remote Sensing*, 3: 111-123.

Jones, B.M., G. Grosse, C.D. Arp, M.C. Jones, K.M. Walter Anthony, V.E. Romanovsky (2011a) Modern thermokarst lake dynamics in the continuous permafrost zone, northern Seward Peninsula, Alaska. *JGR Biogeosciences*, 116.

Jones, M.O., L.A. Jones, J.S. Kimball, K.C. McDonald (2011b) Satellite passive microwave remote sensing for monitoring global land surface phenology. *Remote Sensing of Environment*, 115: 1102-1114.

Jones, M.O., J.S. Kimball, L.A. Jones (2013) Satellite microwave detection of boreal forest recovery from the extreme 2004 wildfires in Alaska and Canada. *Global Change Biology*, 19: 3111-3122.

Jorgenson, M.T., T.E. Osterkamp (2005) Response of boreal ecosystems to varying modes of permafrost degradation. *Canadian Journal of Forest Research*, 35: 2100-2111.

Jorgenson, M.T., Y.L. Shur, E.R. Pullman (2006) Abrupt increase in permafrost degradation in Arctic Alaska. *The Cryosphere*, 33. L02503.

Jorgenson, M.T., V. Romanovsky, J. Harden, Y. Shur, J. O'Donnel, E.A.G. Schuur, et al. (2010) Resilience and vulnerability of permafrost to climate change. *Canadian Journal of Forest Research*, 40: 1219-1236.

Jorgenson, M.T., G. Grosse (2016) Remote sensing of landscape change in permafrost regions. *Permafrost and Periglacial Processes*, 27: 324-338.

Ju, J., J.G. Masek (2016) The vegetation greenness trend in Canada and U.S. Alaska from 1984-2012 Landsat data. *Remote Sensing of Environment*, 176: 1-16.

Kane, D.L., L.D. Hinzman, R.E. Gieck, J.P. McNamara, E.K. Youcha, J.A. Oatley (2008) Contrasting extreme runoff events in areas of continuous permafrost, Arctic Alaska. *Hydrology Research*, 39: 287-298.

Karvetski, C.W., J.H. Lambert (2011) Climate change scenarios: risk and impact analysis for Alaska coastal infrastructure. *Int. J. Risk Assessment and Management*, 12: 258-274.

Kasischke, E. S., Williams, D., & Barry, D. (2002). Analysis of the patterns of large fires in the boreal forest region of Alaska. *International Journal of Wildland Fire*. https://doi.org/10.1071/WF02023

Kasischke, E.S., L.L. Bourgeau-Chavez, J.F. Johnstone (2007) Assessing spatial and temporal variations in surface soil moisture in fire-disturbed black spruce forests in Interior Alaska using spaceborne synthetic aperture radar imagery – implications for post-fire tree recruitment. *Remote Sensing of Environment*, 108: 42-58.

Kerr, J.T., M. Ostrovsky (2003) From space to species: ecological applications for remote sensing. *Trends in Ecology & Evolution*, 18: 299-305.

Kennedy, R.E., Z. Yang, N. Gorelick, J. Braaten, L. Cavalcante, W.B. Cohen, S. Healey (2018) Implementation of the LandTrendr Algorithm on Google Earth Engine. *Remote Sensing*, 10, 691.

Kim, Y., J.S. Kimball, K.C. McDonald, J. Glassy (2011) Developing a global data record of daily landscape freeze/thaw status using satellite passive microwave remote sensing. *IEEE Transactions on Geoscience and Remote Sensing*, 49: 949-960.

Kim, Y., J.S. Kimball, K. Zhang, K.C. McDonald (2012) Satellite detection of increasing northern hemisphere non-frozen seasons from 1979 to 2008: implications for regional vegetation growth. *Remote Sensing of Environment*, 121: 472-487.

Kim, Y., J.S. Kimball, J. Glassy, J. Du (2017a) An extended global Earth system data record on daily landscape freeze-thaw status determined from satellite passive microwave remote sensing. *Earth System Science Data*, 9: 133-147.

Kim, Y., J.S. Kimball, J. Glassy, K.C. McDonald (2017b) MEaSUREs Global Record of Daily Landscape Freeze/Thaw Status, Version 4. Boulder, Colorado, USA. NASA National Snow and Ice Data Center Distributed Active Archive Center. Doi: https://doi.org/10.5067/MEASURES/CRYOSPHERE/nsidc-0477.004.

Kim, Y., J.S. Kimball, J. Du, C.L.B. Schaaf, P.B. Kirchner (2018) Quantifying the effects of freeze-thaw transitions and snowpack melt on land surface albedo and energy exchange over Alaska and Western Canada. *Environmental Research Letters*, 13.

Kittel, T.G.F., B.B. Baker, J.V. Higgins, J.C. Haney (2010) Climate vulnerability of ecosystems and landscapes on Alaska's North Slope. *Regional Environmental Change*, 11z; 249-264.

Kobayashi, H., A.P. Yunus, S. Nagai, K. Sugiura, Y. Kim, et al. (2016) Latitudinal gradient of spruce forest understory and tundra phenology in Alaska as observed from satellite and ground-based data. *Remote Sensing of Environment*, 177: 160-170.

Kopec, B.G., X. Feng, F.A. Michel, E.S. Posmentier (2016) Influence of sea ice on Arctic precipitation. *PNAS*, 113: 46-51.

Kraatz, S., H.J. Miller, J.M. Jacobs (2019) Remotely sensed freeze-thaw from the soil moisture active passive instrument to inform the timing of seasonal load restrictions in Alaska. *Transportation Research Record: Journal of the Transportation Research Board*. https://doi.org/10.1177/0361198119834558.

Lara, M.J., H. Genet, A.D. McGuire, E.S. Euskirchen, Y. Zhang, D.R.N. Brown, M.T. Jorgenson, V. Romanovsky, A. Breen, W.R. Bolton (2016) Thermokarst rates intensity due to climate change and forest fragmentation in an Alaskan boreal forest lowland. *Global Change Biology*, 22: 816-829.

Larsen, P.H., S. Goldsmith, O. Smith, M.L. Wilson, K. Strzepek, P. Chinowsky, B. Saylor (2008) Estimating future costs for Alaska public infrastructure at risk from climate change. *Global Environmental Change*, 18: 442-457.

Larson, K.M., E.E. Small (2014) Normalized microwave reflection index: a vegetation measurement derived from GPS networks. *IEEE Journal of Selected Topics in Applied Earth Observations and Remote Sensing*, 7: 1501-1511.

Lawrence, R.L., A. Wright (2001) Rule-based classification systems using classification and regression tree (CART) analysis. *Photogrammetric Engineering and Remote Sensing*, 67: 1137-1142.

Liljedahl, A.K., A. Gädeke, S. O'Neel, T.A. Gatesman, T.A. Douglas (2017) Glacierized headwater streams as aquifer recharge corridors, subarctic Alaska. *Geophysical Research Letters*, 44: 6876-6885.

Ling, F., T. Zhang (2003) Impact of the timing and duration of seasonal snow cover on the active layer and permafrost in the Alaskan Arctic. *Permafrost and Periglacial Processes*. https://doi.org/10.1002/ppp.445.

Liston, G.E., C.A. Hiemstra (2011) The changing cryosphere: Pan-Arctic snow trends (1979-2009). *Journal of Climate*, 24: 5691-5712.

Loranty, M.M., W. Lieberman-Cribbin, L.T. Berner, S.M. Natali, et al. (2016) Spatial variation in vegetation productivity trends, fire disturbance, and soil carbon across arctic-boreal permafrost ecosystems. *Environmental Research Letter*s, 11. 095008.

Loranty, M.M., S.P. Davydov, H. Kropp, H.D. Alexander, M.C. Mack, S.M. Natali, N.S. Zimov (2018) Vegetation indices do not capture forest cover variation in upland Siberian larch forests. *Remote Sensing*, 10: 1686.

Marcot, B.G., M.T. Jorgenson, J.P. Lawler, C.M. Handel, A.R. DeGange (2015) Projected changes in wildlife habitats in Arctic natural areas of northwest Alaska. *Climatic Change*, 130: 145-154.

McBeath, J. (2003) Institutional responses to climate change: the case of the Alaska transportation system. *Mitigation and Adaptation Strategies for Global Change*, 8: 3-28.

McDonald, K.C., J.S. Kimball (2006) Estimation of surface freeze-thaw states using microwave sensors. In: Encyclopedia of Hydrological Sciences [Eds. Anderson, M.G.]. 15 pp.

McKnight, D.M., M.N. Gooseff, W.F. Vincent, B.J. Peterson (2008) High latitude rivers and streams. In: Vincent, W.F., J. Laybourn-Parry (Eds). Polar Lakes and Rivers – Limnology of Arctic and Antarctic Aquatic Ecosystems, Oxford University Press, UK, 83-102.

Mishra, U., W.J. Riley (2014) Active-layer thickness across Alaska: comparing observation-based estimates with CMIP5 Earth System Model predictions. *Soil Science Society of America*, 78: 894- 902.

Melvin, A.M., P. Larsen, B. Boehlert, J.E. Neumann, P. Chinowsky, et al. (2017) Climate change damages to Alaska public infrastructure and the economics of proactive adaptation. *PNAS*, 114.Doi:10.1073/pnas.1611056113.

Metsämäki, S., K. Böttcher, J. Pulliainen, K. Luojus, J. Cohen, M. Takala, O.-P. Mattila, G. Schwaizer, C. Derksen, S. Koponen (2018) The accuracy of snow melt-off day derived from optical and microwave radiometer data — a study for Europe. *Remote Sensing of Environment*, 211: 1–12.

Muskett, R.R., V.E. Romanovsky (2011) Alaskan permafrost groundwater storage changes derived from GRACE and ground measurements. *Remote Sensing*, 3: 378-397.

Myers-Smith, I.A., B.C. Forbes, M. Wilmking, M. Hallinger, T. Lantz, D. Blok, K.D. Tape, M. Macias-Fauria, et al. (2011) Shrub expansion in tundra ecosystems: dynamics, impacts and research priorities. *Environmental Research Letters*. 6. 045509.

Nagler, P.L., Y. Inoue, E.P. Glenn, A.L. Russ, C.S.T. Daughtry (2003) Cellulose absorption index (CAI) to quantify mixed soil–plant litter scenes. *Remote Sensing of Environment*, 87: 310–325.

Natali, S.M., E.A.G. Schuur, E.E. Webb, C.E. Hicks Pries, K.G. Crummer (2014) Permafrost degradation stimulates carbon loss from experimentally warmed tundra. *Ecology*, 95: 602-608.

Osterkamp, T.E. (2005) The recent warming of permafrost in Alaska. *Global and Planetary Change*, 49: 187-202.

Osterkamp, T.E. (2007) Characteristics of the recent warming of permafrost in Alaska. JGR Earth Surface, 112. http://doi.org/10.1029/2006JF000578.

Pan, C.G., P.B. Kirchner, J.S. Kimball, Y. Kim, J. Du (2018) Rain-on-snow events in Alaska, their frequency and distribution from satellite observations. Environmental Research Letters, 13. 075004.

Pan, C.G., P.B. Kirchner, J.S. Kimball, J. Du, Y. Kim (In Prep) Hydrologic implications of snowcover change across Alaska, USA from 1988-2016. *Hydrology and Earth System Sciences*.

Parazoo, N.C., A. Arneth, T.A.M. Pugh, B. Smith, N. Steiner, K. Luus, R. Commane, et al. (2018) Spring photosynthetic onset and net CO_2 uptake in Alaska triggered by landscape thawing. *Global Change Biology*, 24: 3416-3435.

Parida, B.R., W. Buermann (2014) Increasing summer drying in North American ecosystems in response to longer nonfrozen periods. *Geophysical Research Letters*, 41: 5476-5483.

Parent, M.B., D. Verbyla (2010) The browning of Alaska's boreal forest. *Remote Sensing*, 2: 2729-2747.

Park, H., Y. Kim, J.S. Kimball (2016) Widespread permafrost vulnerability and soil active layer increases over the high northern latitudes inferred from satellite remote sensing and process model assessments. *Remote Sensing of Environment*, 175: 349-358.

Park, T., S. Ganguly, H. Tommervik, E.S. Euskirchen, et al. (2017) Changes in growing season duration and productivity of northern vegetation interred from long-term remote sensing data. *Environmental Research Letters*, 11. 084001.

Pastick, N.J., M.T. Jorgenson, B.K. Wylie, S.J. Nield, K.D. Johnson, A.O. Finley (2015) Distribution of near-surface permafrost in Alaska: estimates of present and future conditions. *Remote Sensing of Environment*, 168: 301-315.

Pastick, N.J., M.T. Jorgenson, S.J. Goetz, B.M. Jones, B.K. Wylie, B.J. Minsley, et al. (2019) Spatiotemporal remote sensing of ecosystem change and causation across Alaska. *Global Change Biology*, 25: 1171-1189.

Partain Jr, J.L., S. Alden, H. Strader, U.A. Bhatt, P.A. Bieniek, B.R. Brettschneider, J.E. Walsh, R.T. Lader, P.Q. Olsson, T.S. Rupp, R.L. Thoman Jr (2016) An assessment of the role of anthropogenic climate change in the Alaska fire season of 2015. *Bulletin of the American Meteorological Society*, 97:S14-S18.

Pekel, J.-F., A. Cottam, N. Gorelick, A.S. Belward (2016) High-resolution mapping of global surface water and its long-term changes. *Nature*, 540: 418-422.

Peng, C., Z. Ma, X. Lei, Q. Zhu, H. Chen, W. Wang, et al. (2011) A drought-induced pervasive increase in tree mortality across Canada's boreal forests. *Nature Climate Change*, 1: 467-471.

Peng, J., A. Loew, O. Marlin, N.E.C. Verhoest (2017) A review of spatial downscaling of satellite remotely sensed soil moisture. *Reviews of Geophysics*, 55: 341-366.

Pettorelli, N., J.O. Vik, A. Mysterud, J.-M. Gaillard, C.J. Tucker, N.C. Stenseth (2006) Using the satellite-derived NDVI to assess ecological responses to environmental change. *Trends in Ecology & Evolution*, 20: 503-510.

Pouliot, D., R.Latifovic (2013) Accuracy assessment of annual land cover time series derived from change-based updating. In *MultiTemp 2013: 7th International Workshop on the Analysis of Multi-temporal Remote Sensing Images* (pp. 1–3). https://doi.org/10.1109/Multi-Temp.2013.6866005

Pouliot, D., R. Latifovic, N. Zabcic, L. Guindon, I. Olthof (2014). Development and assessment of a 250 m spatial resolution MODIS annual land cover time series (2000-2011) for the forest region of Canada derived from change-based updating. *Remote Sensing of Environment*, 140: 731–743. https://doi.org/10.1016/j.rse.2013.10.004

Qi, J., P.A. Vermeer, G. Cheng (2006) A review of the influence of freeze-thaw cycles on soil geotechnical properties. *Permafrost and Periglacial Processes*, 17: 245-252.

R core team (2018) R: a language and environment for statistical computing. R Foundation for Statistical Computing, Vienna, Austria. https://www.R-project.org.

REPI. 2017. Readiness and Environmental Protection Integration Program State Profile: Alaska. Report by the U.S. Department of Defense. 2 pp. https://www.repi.mil/Portals/44/Documents/State_Fact_Sheets/Alaska_StateFacts.pdf

Racine, C.H., L.A. Johnson, L.A. Viereck (1987) Patterns of vegetation recovery after tundra fires in northwestern Alaska, U.S.A. *Arctic and Alpine Research*, 19: 461-469.

Racine, C.H. (1994) Current issues in Alaska wetland management. CRREL Special Report 94-26.

Rao, K., W.R.L. Anderegg, A. Sala, J. Martinex-Vilalta, A.G. Konings (2019) Satellite-based vegetation optical depth as an indicator of drought-driven tree mortality. *Remote Sensing of Environment*, 227: 125-136.

Riordan, B., D. Verbyla, A.D. McGuire (2006) Shrinking ponds in subarctic Alaska based on 1950-2002 remotely sensed images. *JGR Biogeosciences*, 111.

Roach, J., B. Griffith, D. Verbyla, J. Jones (2011) Mechanisms influencing changes in lake area in Alaskan boreal forest. *Global Change Biology*, 17, 2567-2583.

Rogers, B.M., A.J. Soja, M.L. Goulden, J.T. Randerson (2015) Influence of tree species on continental differences in boreal fires and climate feedbacks. *Nature Geoscience*, 8: 228–234. https://doi.org/10.1038/ngeo2352

Rogers, B. M., K. Solvik, E.H. Hogg, J. Ju, J.G. Masek, M. Michaelian, L.T. Berner, S.J. Goetz (2018) Detecting early warning signals of tree mortality in boreal North America using multiscale satellite data. *Global Change Biology*, 24: 2284–2304.

Saatchi, S.S., M. Moghaddam (2000) Estimation of crown and stem water content and biomass of boreal forest using polarimetric SAR imagery. IEEE Transactions on Geoscience and Remote Sensing, 38: 697-709.

Sabins, F.F. (2007) Remote Sensing: Principals and Applications, Third Edition. Waveland Press.

Schimel, D., R. Pavlick, J.B. Fisher, G.P. Asner, S. Saatchi, et al. (2014) Observing terrestrial ecosystems and the carbon cycle from space. *Global Change Biology*, 21: 1762-1776.

Selkowitz, D.J., S.V. Stehman (2011) Thematic accuracy of the National Land Cover Database (NLCD) 2001 land cover for Alaska. *Remote Sensing of Environment*, 115: 1401-1407.

Sexton, J.O., X.-P. Song, M. Feng, P. Noojipady, A. Anand, C. Huang, et al. (2013) Global, 30-m resolution continuous fields of tree cover: Landsat-based rescaling of MODIS vegetation continuous fields with lidar-based estimates of error. *International Journal of Digital Earth*, *6:* 427–448. https://doi.org/10.1080/17538947.2013.786146

Shulski, M., G. Wendler (2007) The Climate of Alaska. University of Alaska Press Fairbanks. 207 pp.

Shur, Y.L., M.T. Jorgenson (2007) Patterns of permafrost formation and degradation in relation to climate and ecosystems. *Permafrost and Periglacial Processes*, 18:7-19.

Schuur, E.A.G., J. Bockheim, J.G. Canadell, E. Euskirchen, C.B. Field, et al. (2008) Vulnerability of permafrost carbon to climate change: implications for the global carbon cycle. *BioScience*, 58: 701-714.

Schuur, E.A.G., M.C. Mack (2018) Ecological response to permafrost thaw and consequences for local and global ecosystem services. *Annual Review of Ecology, Evolution, and Systematics*, 49: 279-301.

Shiklomanov, N.I., D.A. Streletskiy, F.E. Nelson (2012) Northern hemisphere component of the Global Circumpolar Active Layer Monitoring (CALM) program. Proceedings of the Tenth International Conference on Permafrost, Volume 1. Salekhard, Yamal-Nenets Autonomous District, Russia. June 25-29, 2012. P. 377-382.

Shoop, S., R. Affleck, C. Collins, G. Larsen, L. Barna, P. Sullivan (2005) Maneuver analysis methodology to predict vehicle impacts on training lands. *Journal of Terramechanics*, 42: 281-303.

Smith, N.V., S.S. Saatchi, J.T. Randerson (2004) Trends in high northern latitude soil freeze and thaw cycles from 1988 to 2002. *J. Geophys. Res.*, 109, D12101.

Smith, L.C., Y. Sheng, G.M. MacDonald (2007) A first pan-Arctic assessment of the influence of glaciation, permafrost, topography and peatlands on northern hemisphere lake distribution. *Permafrost and Periglacial Processes*, 18: 201-208.

Sniderhan, A.E., J.L. Baltzer (2016) Growing dynamics of black spruce (*Picea mariana*) in a rapidly thawing discontinuous permafrost peatland. *Journal of Geophysical Research*, 121:2988- 3000.

Soja, A.J., N.M. Tchebakova, N.H.F. French, M.D. Flannigan, H.H. Shugart, B.J. Stocks, A.I. Sukhinin, et al. (2007) Climate-induced boreal forest change: predictions versus current observations. *Global and Planetary Change*, 56: 274-296.

Soranno, P.A., D.S. Schimel (2014) Macrosystems ecology: big data, big ecology. *Frontiers in Ecology and the Environment*, 12: 3.

Streletskiy, D.A., N.I. Skiklomanov, F.E. Nelson, A.E. Klene (2008) Thirteen years of observations at Alaskan CALM sites: long-term active layer and ground surface temperature trends. Proceedings of the Ninth Conference on Permafrost. University of Alaska Fairbanks, June 29-July 3.

Sulla-Menashe, D., C.E. Woodcock, M.A. Friedl (2018) Canadian boreal forest greening and browning trends: an analysis of biogeographic patterns and the relative roles of disturbance versus climate drivers. *Environ. Res. Lett.*, 13, 014007, doi:10.1088/1748-9326/aa9b88.

Sun, L., K.E. Kunkel, L.E. Stevens, A. Buddenbert, J.G. Dobson, D.R. Easterling (2015) Regional surface climate conditions in CMIP3 and CMIP5 for the United States: differences, similarities, and implications for the U.S. National Climate Assessment. NOAA Technical Report NESDIS 144. Doi:10.7289/V5RB72KG.

Tadono,T., H. Nagai, H. Ishida, F. Oda, S. Naito, K. Minakawa, H. Iwamoto (2016) Initial Validation of the 30 m-mesh Global Digital Surface Model Generated by ALOS PRISM. T*he International Archives of the Photogrammetry, Remote Sensing and Spatial Information Sciences, ISPRS*, Vol. XLI-B4, pp.157-162.

Tan, Z., S. Liu, B.K. Wylie, C.B. Jenkerson, J. Oeding, J. Rover, C. Young (2013) MODIS-informed greenness responses to daytime land surface temperature fluctuations and wildfire disturbances in the Alaskan Yukon River Basin. *International Journal of Remote Sensing*, 34: 2187-2199.

Theobald, D.M., D. Harrison-Atlas, W.B. Monahan, C.M. Albano (2015) Ecologically-relevant maps of landforms and physiographic diversity for climate adaptation planning. *PloS one*, 10, e0143619.

Toniolo, H., J. Stutzke, A. Lai, E. Youcha (2017) Antecedent conditions and damage caused by the 2015 spring flooding on the Sagavanirktok River, Alaska. J. *Cold Regions Engineering*, 31.

Trainor, S.F., M. Calef, D. Natcher, F.S. Chapin III, A.D. McGuire, et al. (2009) Vulnerability and adaptation to climate-related fire impacts in rural and urban interior Alaska. *Polar Research*, 28: 100-118.

Tucker, C.J. (1979) Red and photographic infrared linear combinations for monitoring vegetation. *Remote Sensing of Environment*, 8: 127–150.

Turcotte, B., K. Alfredsen, S. Beltaos, B.C. Burrell (2017) Ice-related floods and flood delineation along streams and small rivers. CGU HS Committee on River Ice Processes and the Environment. 19th Workshop on the Hydraulics of Ice Covered Rivers, Whitehorse, YK, Canada, July 10th-12th.

Turetsky, M.R., E.S. Kane, J.W. Harden, R.D. Ottmar, K.L. Manies, et al. (2011) Recent acceleration of biomass burning and carbon losses in Alaskan forests and peatlands. *Nature Geoscience*, 4: 27-31.

USAGA (2018) Tanana Flats Training Area winter trail finding of no significant impact and environmental assessment. https://home.army.mil/wainwright/application/files/8115/3816/0248/TFTA_EA_Final-Sep27.pdf

van Mantgem, P.J. N.L. Stephenson, J.C. Byrne, L.D. Daniels, J.F. Franklin, et al. (2009) Widespread increase of tree mortality rates in the Western United States. *Science*, 23: 521-524.

Vedda, J.A. (2009) U.S. national security and economic interests in remote sensing: the evolution of civil and commercial policy. NSS Programs Policy and Oversight National Space Systems Engineering. Report No. TOR-2009(3601)-8539.

Veraverbeke, S., B.M. Rogers, M.L. Goulden, R.R. Jandt, C.E. Miller, E.B. Wiggins, J.T. Randerson (2017) Lightning as a major driver of recent large fire years in North American boreal forests. *Nature Clim. Change*, 7: 529–534.

Verbesselt, J., R. Hyndman, A. Zeileis, D. Culvenor (2010) Phenological change detection while accounting for abrupt and gradual trends in satellite image time series. *Remote Sensing of Environment*, 114: 2970-2980.

Verbesselt, J. (2014) Bfast: Breaks for Additive Season and Trend (BFAST) version 1.5.7. R statistical computing.

Verbyla, D. (2008) The greening and browning of Alaska based on 1982-2003 satellite data. *Global Ecology and Biogeography*, 17: 547-555.

Verpoorter, C., T. Kutser, D.A. Seekell, L.J. Tranvik (2014) A global inventory of lakes based on high-resolution satellite imagery. *Geophysical Research Letters*, 41: 6396-6402.

Vincent, C.H., L.A. Hanson, C.N. Argueta (2017) Federal land ownership: overview and data. Congressional Research Service Report. 7-5700. R42346. 25 pp.

Vinson, T.S., J.W. Rooney, W.H. Haas (1996) Roads and Airfields in Cold Regions. Technical Council on Cold Regions Engineering Monograph. American Society of Civil Engineers. ISBN 0-7844-0191-8.

Walvoord, M.A., R.G. Striegl (2007) Increasing groundwater to stream discharge from permafrost thawing in the Yukon River basin: potential impacts on lateral export of carbon and nitrogen. *Geophysical Research Letters*, 34. L12402.

Wan, Z., J. Dozier (1996) A generalized split-window algorithm for retrieving land-surface temperature from space. *IEEE Transactions on Geoscience and Remote Sensing*, 34: 892-905.

Wan, Z. (1999) MODIS Land-Surface Temperature Algorithm Theoretical Basis Document (LST ATBD) Version 3.3. https://modis.gsfc.nasa.gov/data/atbd/atbd_mod11.pdf

Wan, Z. (2008) New refinements and validation of the MODIS Land-surface temperature/emissivity products. *Remote Sensing of Environment*, 112: 59-74.

Wang, L., C. Derksen, R. Brown, T. Markus (2013) Recent changes in pan-Arctic melt onset from satellite passive microwave measurements. *Geophysical Research Letters*, 40: 522-528.

Wang, L., P. Toose, R. Brown, C. Derksen (2016) Frequency and distribution of winter melt events from passive microwave satellite data in the pan-Arctic, 1988-2013. *The Cryosphere*, 10: 2589-2602.

Watts, J.D., J.S. Kimball, L.A. Jones, R. Schroeder, K.C. McDonald (2012) Satellite microwave remote sensing of contrasting surface water inundation changes within the Arctic-Boreal region. *Remote Sensing of Environment*, 127: 223-236.

Watts, J.D., R.L. Lawrence (2008) Merging random forest classification with an object-oriented approach for analysis of agriculture lands. *The International Archives of the Photogrammetry, Remote Sensing and Spatial Information Sciences*. Vol XXXVII.

Watts, J.D., J.S. Kimball, F.J.W. Parmentier, T. Sachs, et al. (2014a) A satellite data driven biophysical modeling approach for estimating northern peatland and tundra CO_2 and CH_4 fluxes. *Biogeosciences*, 11: 1961-1980.

Watts, J.D., J.S. Kimball, A. Bartsch, K.C. McDonald (2014b) Surface water inundation in the boreal-Arctic: potential impacts on regional methane emissions. *Environmental Research Letters*, 9. 075001.

Westermann, S., J. Boike, M. Langer, T.V. Schuler, B. Etzelmuller (2011) Modeling the impact of wintertime rain events on the thermal regime of permafrost. *The Cryosphere*, 5: 945-959.

Westermann, S., C.R. Duguay, G. Grosse, A. Kaab (2015) Remote sensing of permafrost and frozen ground. In: Remote Sensing of the Cryosphere, First Edition. [Ed. Tedesco, M.]. John Wiley & Sons. Pp. 307-344.

Wilson, R.R., A. Bartsch, K. Joly, J.H. Reynolds, A. Orlando, W.M. Loya (2013) Frequency, timing, extent, and size of winter thaw-refreeze events in Alaska 2001-2008 detected by remotely sensed microwave backscatter data. *Polar Biology*, 36: 419-426.

Wolfe, J. A. (1979) Temperature parameters of humid to mesic forests of Eastern Asia and relation to forests of other regions of the Northern Hemisphere and Australasia: analysis of temperature data from more than 400 stations in Eastern Asia (U.S. Geological Survey Professional Paper No. 1106). Washington, U.S.A: US Dep. Int.

Woo, M., K.L. Young (2006) High Arctic wetlands: their occurance, hydrological characteristics and sustainability. *Journal of Hydrology*, 320: 432-450.

Woo, M., K. Young (2012) Wetlands of the Canadian Arctic. In: Encyclopedia of Lakes and Reservoirs, Bengtsson, L, R.W. Herschy, R.W. Fairbridge (Eds). Encyclopedia of Earth Sciences Series. Springer, Dordrecht. https://doi.org/10.1007.978-1-4020-4410-6.

Wuebbles, D.J., D.W. Fahey, K.A. Hibbard, D.J. Dokken, et al. (2017) U.S. Global Change Research Program (USGCRP) Climate science special report: Fourth National Climate Assessment. Washington, DC, USA. 470 pp.

Xiao, J., Q. Zhuang (2007) Drought effects on large fire activity in Canadian and Alaskan forests. *Environmental Research Letters*, 2. 044003.

Xie, Y., Z. Sha, M. Yu (2008) Remote sensing imagery in vegetation mapping: a review. *Journal of Plant Ecology*, 1: 9-23.

Yang, J., P. Gong, R. Fu, M. Zhang, J. Chen, S. Liang, B. Xu, et al. (2013) The role of satellite remote sensing in climate change studies. *Nature Climate Change*, 3: 875-883.

Yarie, J., L. Viereck, K. van Cleve, P. Adams (1998) Flooding and ecosystem dynamics along Tanana River. *BioScience*, 48: 690-695.

Yoshikawa, K., W.R. Bolton, V.E. Romanovsky, M. Fukuda, L.D. Hinzman (2002) Impact of wildfire on the permafrost in the boreal forests of Interior Alaska. *JGR Atmospheres*, 4: 1-14.

Yue, S., Pilon, P., Phinney, B., & Cavadias, G. (2002) The influence of autocorrelation on the ability to detect trend in hydrological series. *Hydrological Processes,* 16: 1807–1829.

Zhang, J. (2010) Multi-source remote sensing data fusion: status and trends. *International Journal of Image and Data Fusion*, 1: 5-24.

Zhang, K., J.S. Kimball, Y. Kim, K.C. McDonald (2011) Changing freeze-thaw seasons in northern high latitudes and associated influences on evapotranspiration. *Hydrological Processes*, 25: 4142-4151.

Appendix A. DELIVERABLES, OUTREACH, AND LEVERAGING EFFORTS

A.1 Conference Presentations

2018

Watts, J.D., S. Potter, J. Du, B. Rogers, T. Douglas, S. Natali, A. Kholodov (2018) Detecting recent changes in vegetation, landscape water availability and freeze/thaw characteristics in Interior Alaska using VIS-NIR-TIR and microwave remote sensing. AGU Fall Meeting, Washington DC, December 10-14.

2019

Du, J., S. Potter, J.D. Watts, B. Rogers, S. Natali, T. Douglas, J.S. Kimball (2019) Multi-scale satellite observations of river ice and vegetation conditions in Interior Alaska during the spring landscape freeze/thaw transition. NASA ABoVE Science Team Meeting, La Jolla, CA, May 20-23.

A.2 Outreach

1) We have been working with a Boston area teacher, through the Arctic Research Consortium (ARCUS) PolarTREC program, to educate students and the public about climate change in the Arctic and how warming at high latitudes is leading to permafrost melt and release of carbon stored in permafrost soils as greenhouse gases. The teacher has also been educating students on the use of remote sensing to identify landscape features in Alaska terrains.

2) We are working with NASA ABoVE and the Permafrost Carbon Network (www.permafrostcarbon.org) to share knowledge with other researchers on how machine learning and satellite remote sensing can be applied to detect regions of change across Alaska, Canada, Russia and Scandinavia.

3) Project activities have been repeatedly presented to U.S. Army Corps of Engineers, U.S. Army Alaska, and a variety of federal agency representatives during high level meetings that have occurred over the course of the project. This includes presentations and discussions during tours of the CRREL Permafrost Tunnel.

A.3 Leveraging/collaborative Activities with Related Ongoing Efforts

1) This work leverages investigator involvement with NASA ABoVE. This includes Dr. Sue Natali's project "Winter respiration in the Arctic: Constraining current and future estimates of CO_2 emissions during the non-growing season" that provided reference soil and air temperature measurements at locations in Alaska. This work complements Dr. Brendan Rogers' NASA ABoVE project, "Understanding the causes and implications of enhanced seasonal CO_2 exchange in boreal and arctic ecosystems" and Dr. Jennifer Watts' NASA Earth Science Early Career project, "Reconciling carbon flux budgets in Alaska and northwest Canada through integrated satellite, airborne, and field measurements" by understanding the spatial patterns and characteristics of changes occurring across Alaska and providing detection of these changes using satellite remote sensing. In addition, this project complements Dr. Rogers' DoD SERDP project (PI Scott Goetz) "Resiliency and vulnerability of boreal forest habitat to the interaction of climate and fire disturbance across DoD lands of Interior Alaska" by detecting and quantifying changes in terrain thermal and moisture state, and how shifts in these states might coincide with vegetation greening and browning and vulnerability to fire.

2) Knowledge transfer from this project has been complementary to project activities for the ongoing SERDP project (RC18-C2-1170; lead PI T. Douglas) to help identify habitat vulnerability to landscape change on Interior Alaska DoD training lands. This includes focusing some of our analyses and measurements at CRREL field sites in Interior Alaska.

3) We have been working with the NASA ABoVE Science Computing Cloud to process satellite imagery for the Alaska region and for image interpretation. This project also explored using Google Earth Engine to facilitate 'high speed' image processing and change detection for large regional applications.

4) We have been working with Caleb Pan and Dr. John Kimball at NTSG UMT for image and trend interpretation of satellite microwave based detection of snow properties for the Alaska domain, and over DoD sites in Interior Alaska. This includes the sharing of our project results to identify and understand how changes in terrain frozen state, moisture and vegetation are impacted by changes in snow cover.

A.4 Interactions with Department of Defense and Other Governmental Endusers

Project results have been discussed with U.S. Army Garrison Fort Wainwright Training Range and Public Works Environmental land managers. Of particular note are the analysis of remote sensing tools for the Jarvis Creek confluence with the Delta River near Fort Greely. Spring melt often floods the Battle Area Complex and Combined Arms Collective Training Facility on Donnelly Training Area East. Our remote sensing tools have provided insight into inundation and surface moisture in this area. We have also provided information on terrain state near the Tanana River bridge. This recently completed $185 million bridge provided the first road accessibility to the Tanana Flats Training area. Over the past year U.S. Army Alaska has planned a 40 km road route from the bridge to the Blair Lakes area. Vegetation clearing and surveying were commenced in the spring of 2019 and results from this project helped inform geophysical measurements made by CRREL to support the road development mission.

A.5 Data Transfer

Our project geospatial data and analytical results are available for transfer to U.S. Army Alaska. We will also provide this information to co-PI Douglas for continued use to support SERDP project (RC18-C2-1170). That project will add a variety of new data layers to the GISMO tool used by U.S. Army Alaska and to other geospatial platforms used by the Army, U.S. Army Corps of engineers, and Installation Management Command as is possible. Though the project activities for this one year SEED project have finished we will provide and tailor our results, where possible, to help guide decision making on DoD lands in Interior Alaska.

Appendix B. SUPPLEMENTARY FIGURES AND TABLES

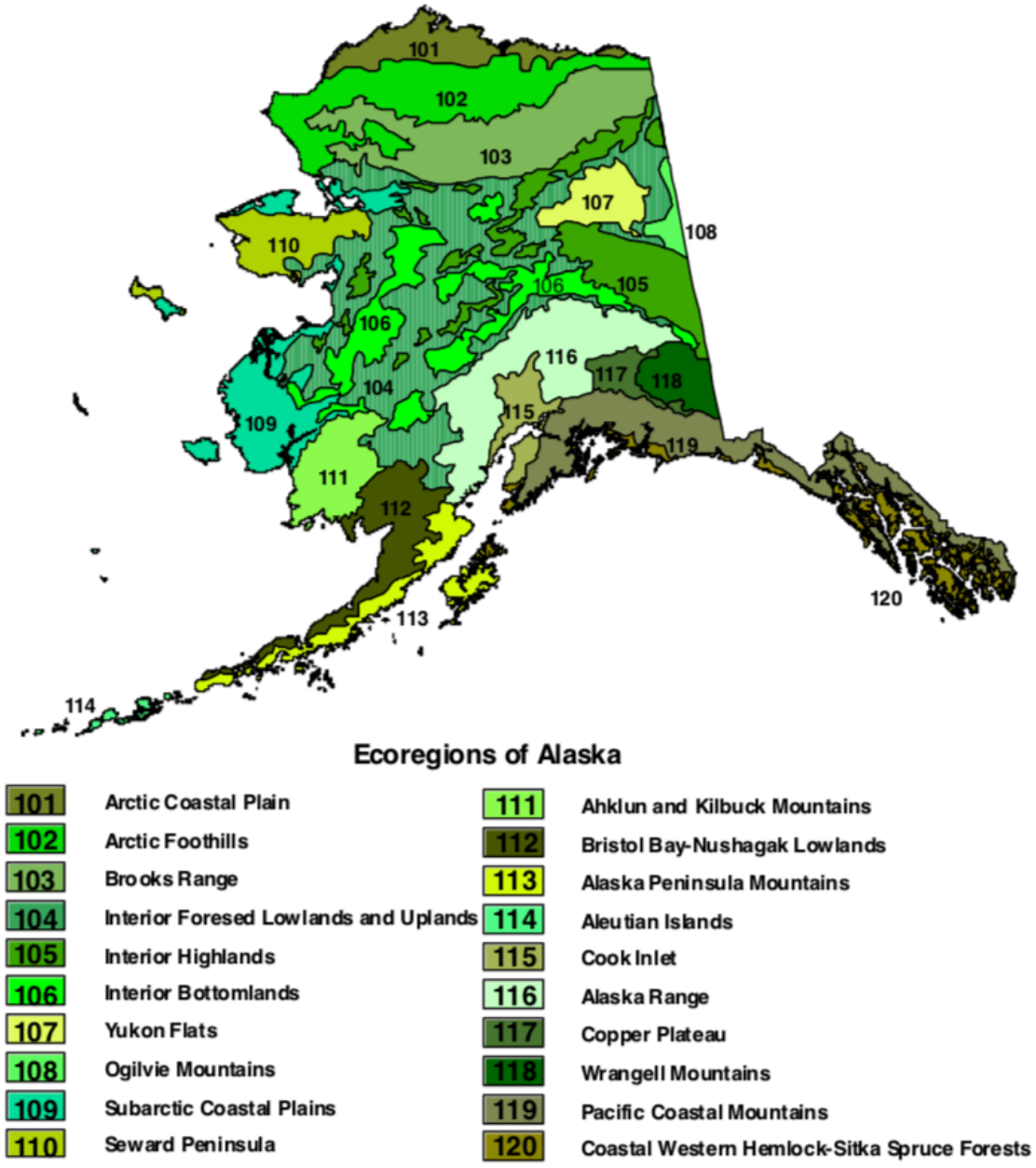


Figure S1. Ecoregions of Alaska. [*from Gallant et al. 1995*]

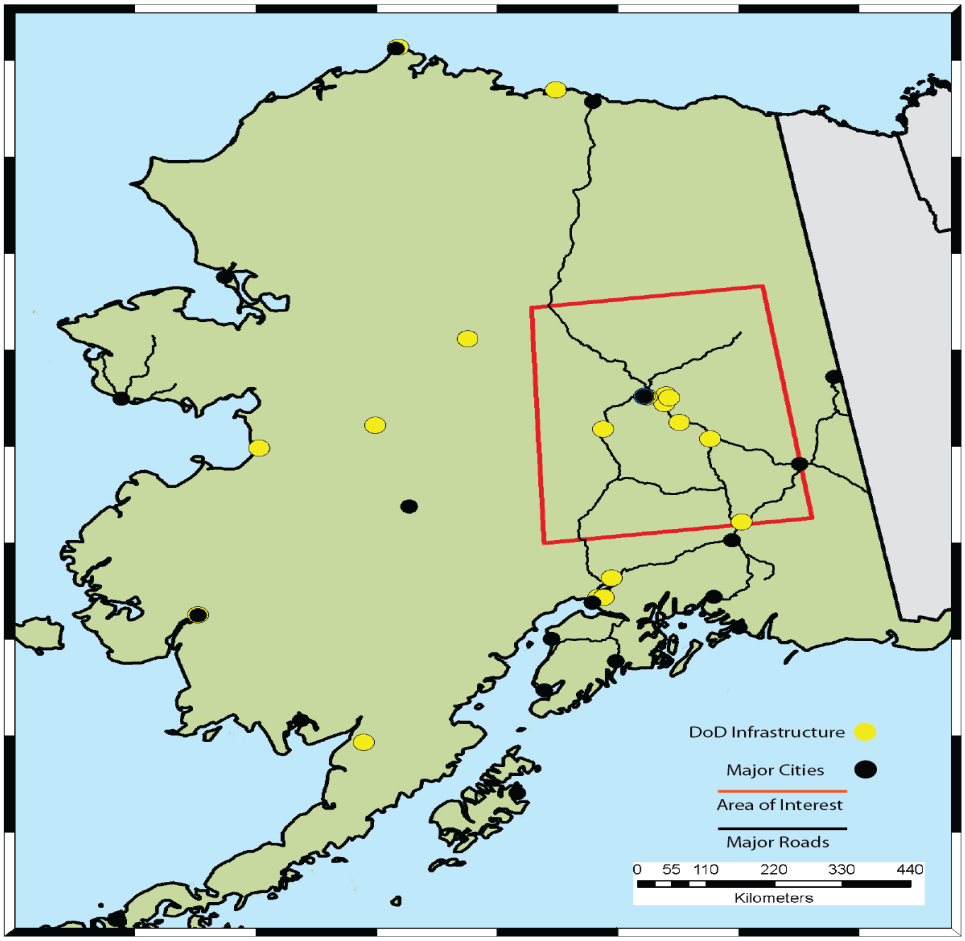


Figure S2. The location of the area of interest (AOI) for Interior Alaska that was used in this study (outlined in red). The AOI domain includes: U.S. Army terrains of Fort Wainwright and Fort Greely; Donnelly and Tanana Flats training areas; the Air Force terrains of Clear Station and Eielson Base; Blair Lakes bombing range (used by Eielson and Elmendorf bases). Bounding coordinates for the AOI are: 151.3824468°W 66.5216381°N (upper left corner); 143.0250977°W 66.5727221°N (upper right corner); 151.3620132°W 62.3123131°N (lower left corner); 142.9944473°W 62.3429635°N (lower right corner).

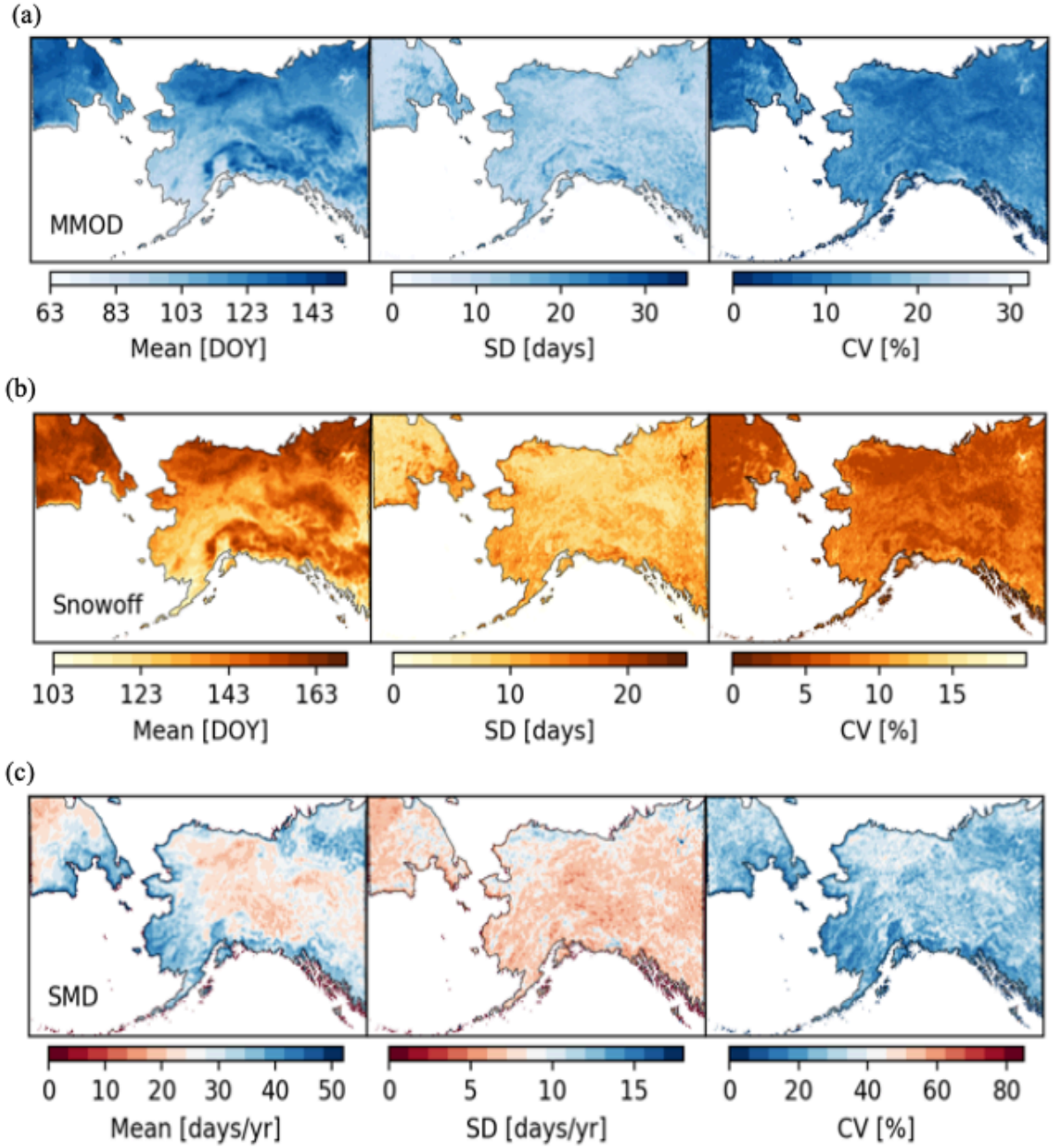


Figure S3. Maps of (a) main snow melt onset date (MMOD); (b) the date of snowoff; (c) the snow melt duration (SMD) for the 1988-2016 period across Alaska and derived from the satellite SMMR, SSM/I and SMMIS record. For each of these characteristics, the average (mean), standard deviation (SD), and coefficient of variation (CV; ratio of standard deviation to the mean) are shown. [*The microwave based snow dataset was produced by NTSG (UMT) and maps were provided courtesy of Caleb Pan*]

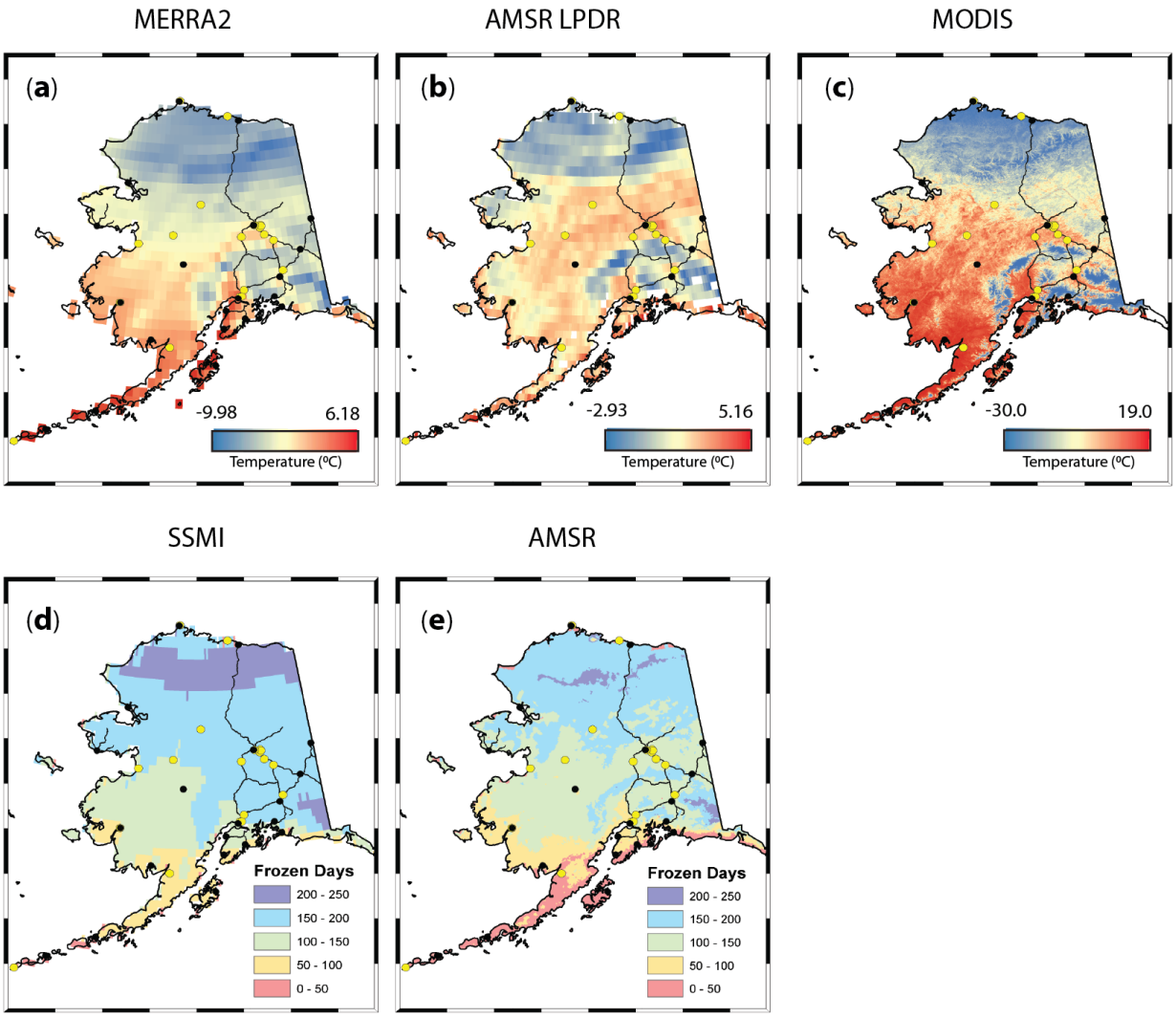


Figure S4. Maps showing average annual ~ 0.5° MERRA2 air temperature (2017; a), 25 km AMSR LPDR daily minimum air temperature derived for non-frozen conditions (2017; b), 1 km MODIS LST (2017; c), 25 km SSMI number of frozen days (2017; d), and 6 km AMSR LPDR number of frozen days (2016; e).

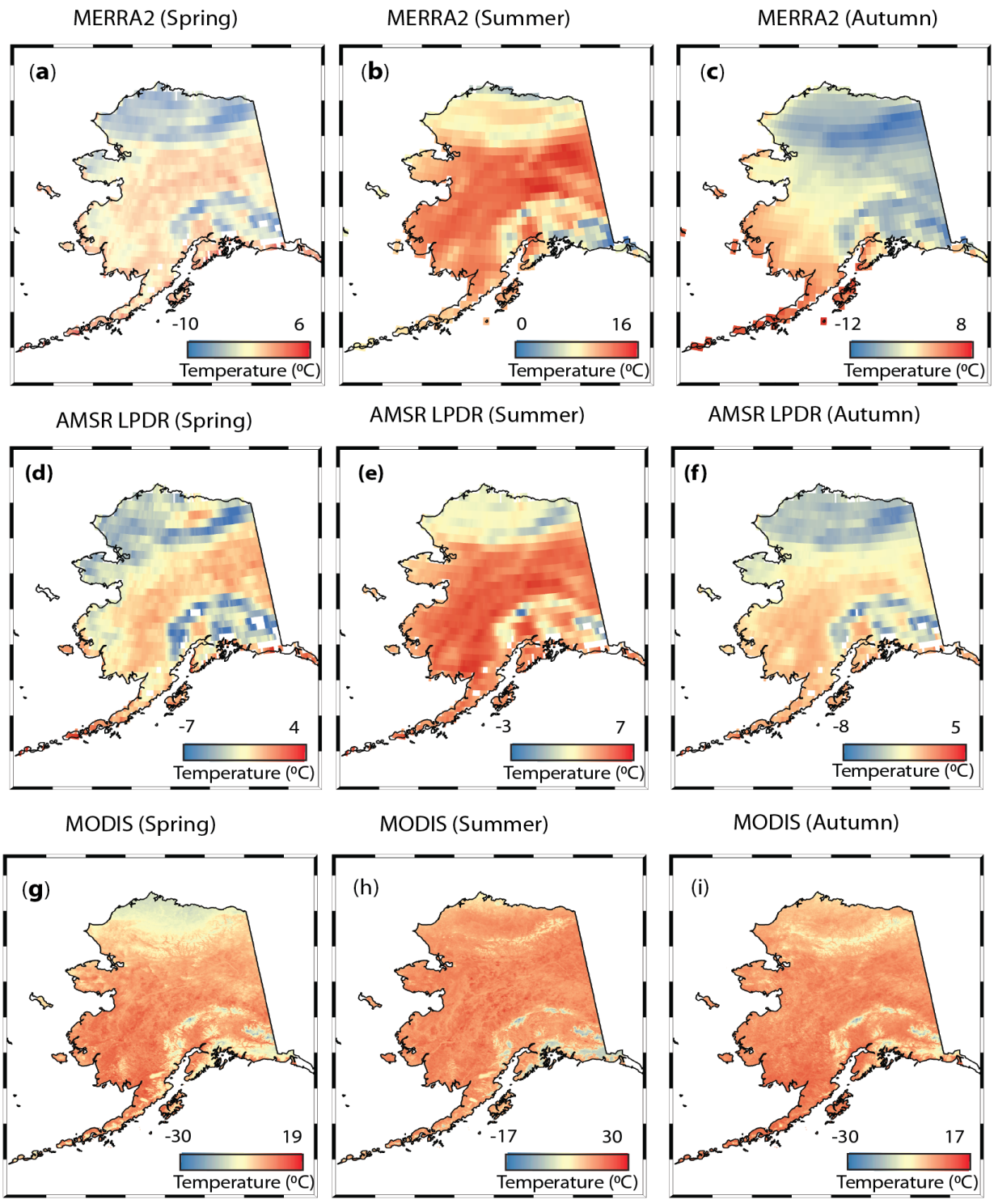


Figure S5. Maps showing seasonal (spring, summer, autumn) averages in 2017 for 0.5° MERRA2 air temperature (a-c), 25 km AMSR LPDR air temperature (d-f), and 1 km MODIS LST (g-i) over Alaska.

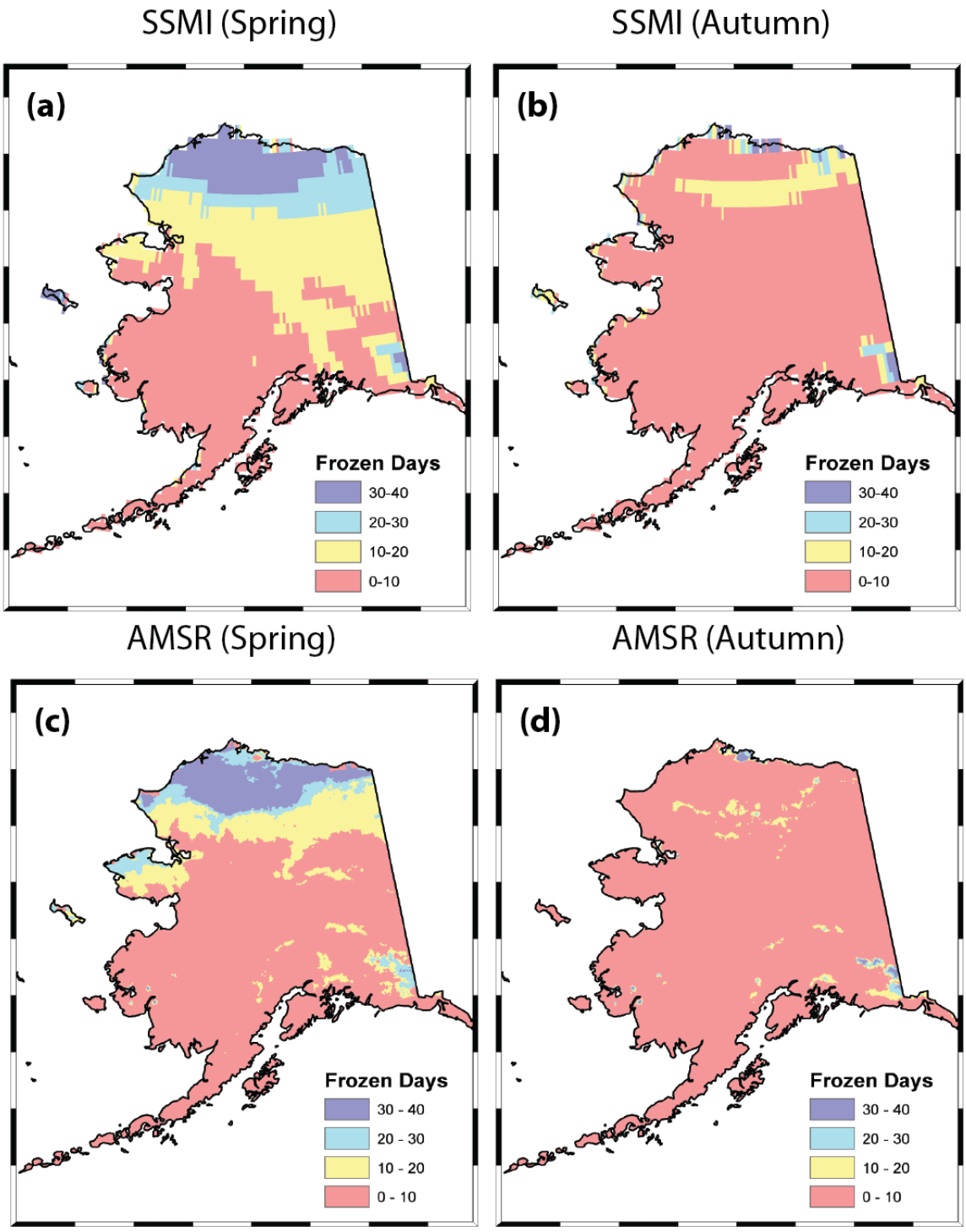


Figure S6. Number of Freeze/Thaw frozen days in Alaska in 2017 derived from 25 km SSMI in the spring (DOY 105 to 151) (a) and autumn (DOY 244 to 288) (b) and number of frozen days in 2016 based on 6 km AMSR LPDR in the spring (c) and autumn (d).

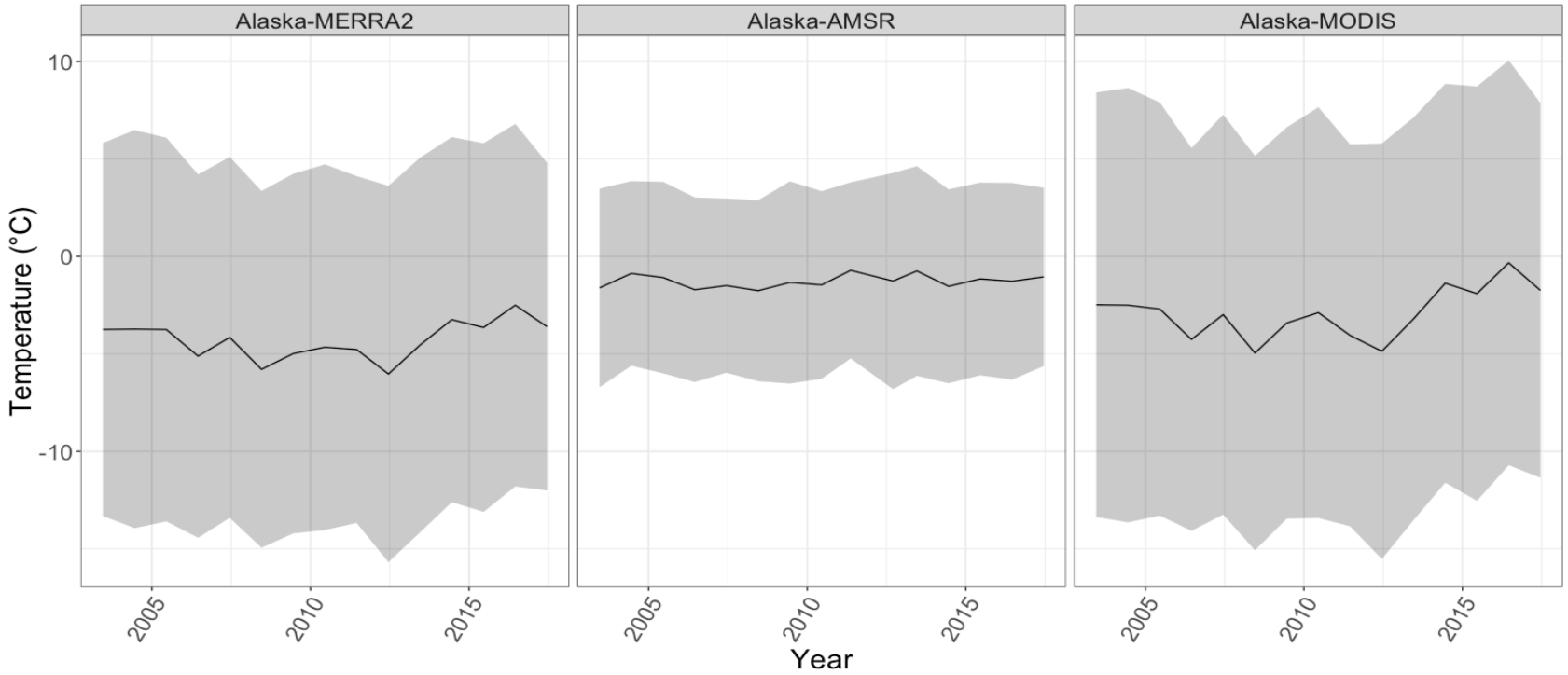


Figure S7. Time series of MERRA2 air temperature (1980-2017), AMSR LPDR air temperature obtained under non-frozen surface conditions (2002 to 2017), and MODIS LST (2002 to 2017) for Alaska. The black line represents annual averages for the domain. The gray shading around the line represents two standard deviations around the average.

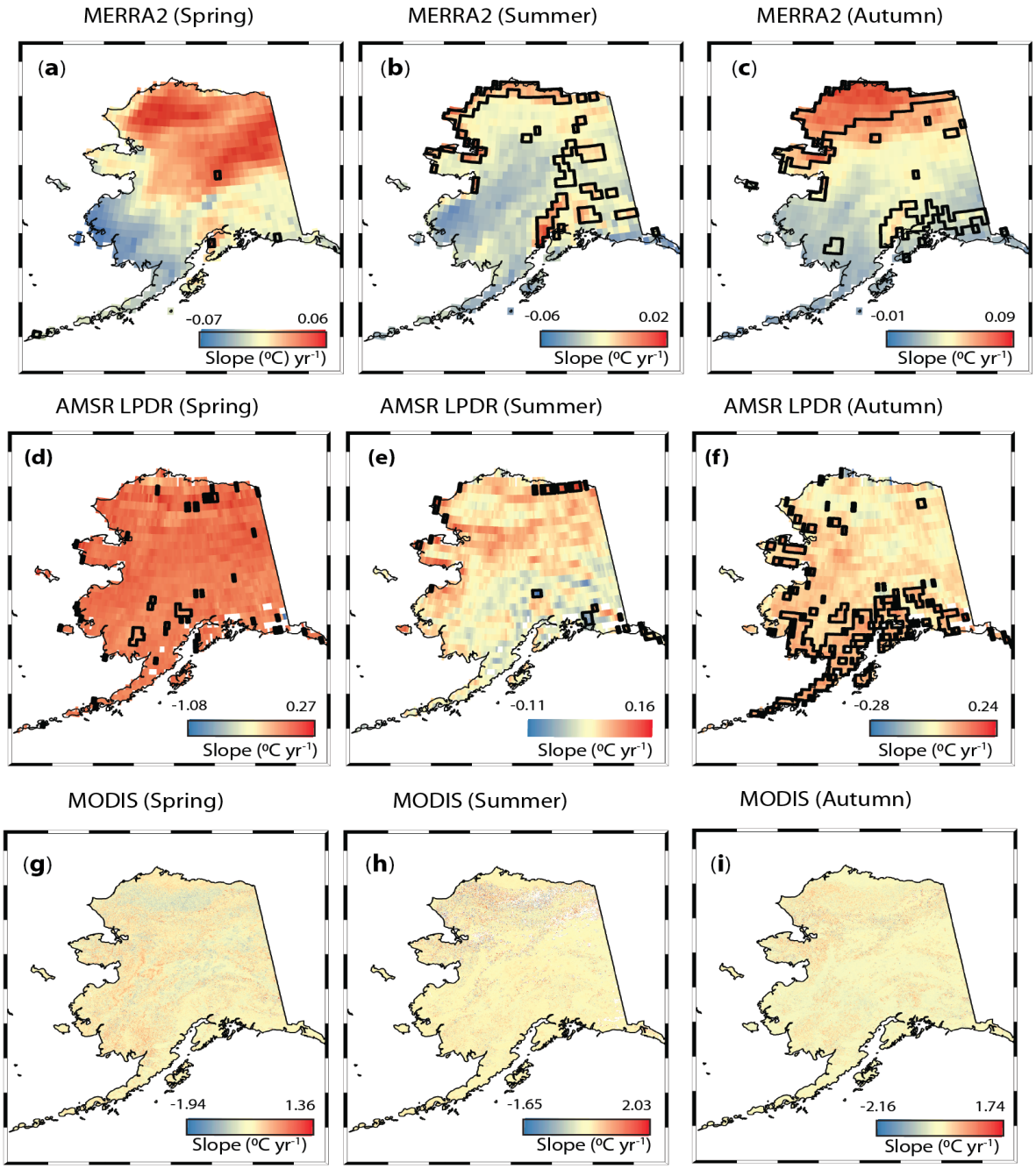


Figure S8. Trends (°C yr^{-1}) in 0.5° MERRA2 air temperature (1980 through 2017), 25 km AMSR LPDR air temperature (2002 to 2017), and 1 km MODIS LST (2002 to 2017) for Alaska. Regions where the Sen slope trend was significant ($p < 0.1$) are outlined in black, except for MODIS because this specific analysis was processed in Google Earth Engine which does not provide significance tests.

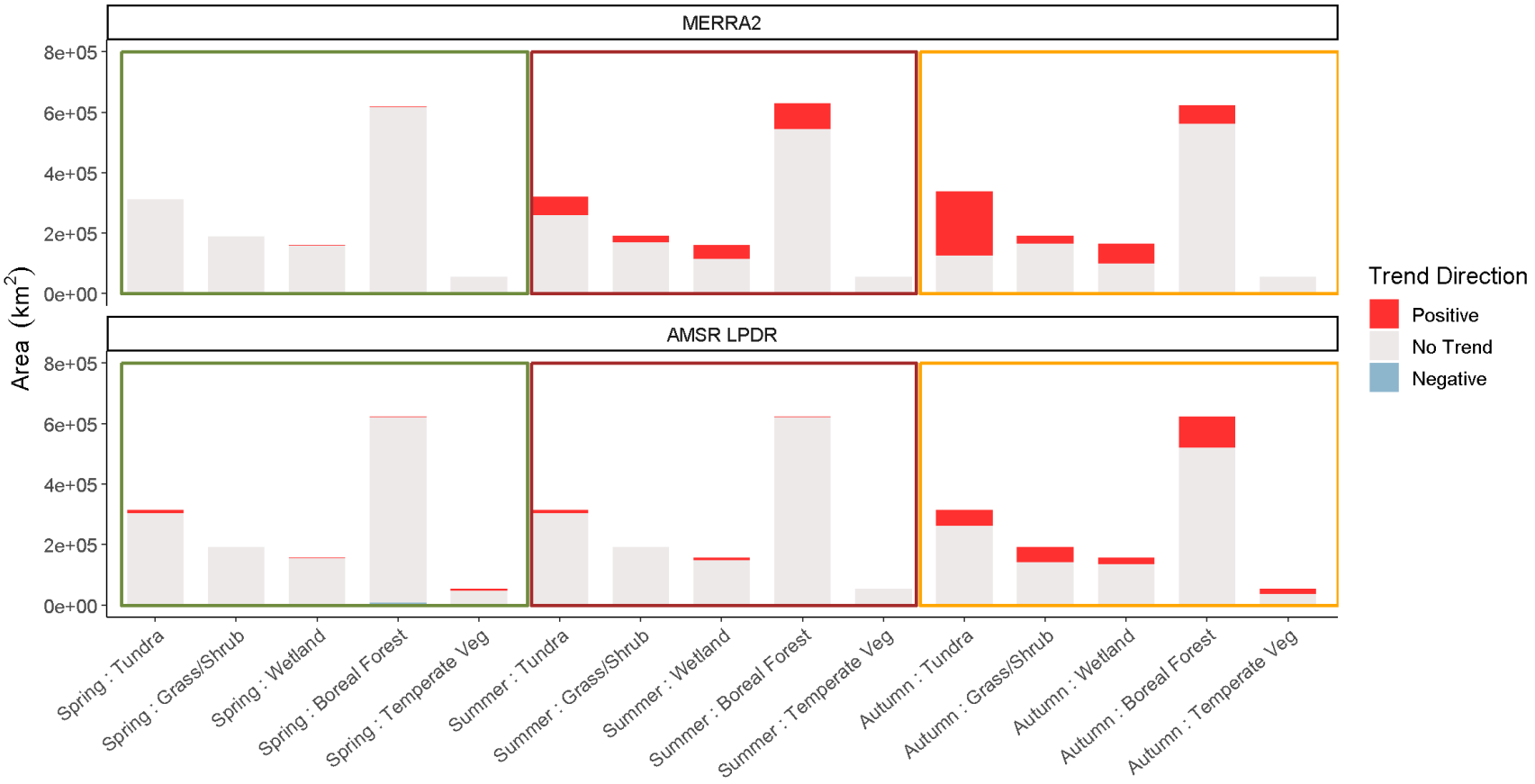


Figure S9. Patterns of change in Terrain Thermal Indicator metrics (i.e., 2 m air temperature from MERRA2 and AMSR LPDR) across Alaska as aggregated by generalized land cover classes (i.e., tundra; grass/shrub; wetland; boreal forest; temperate vegetation).

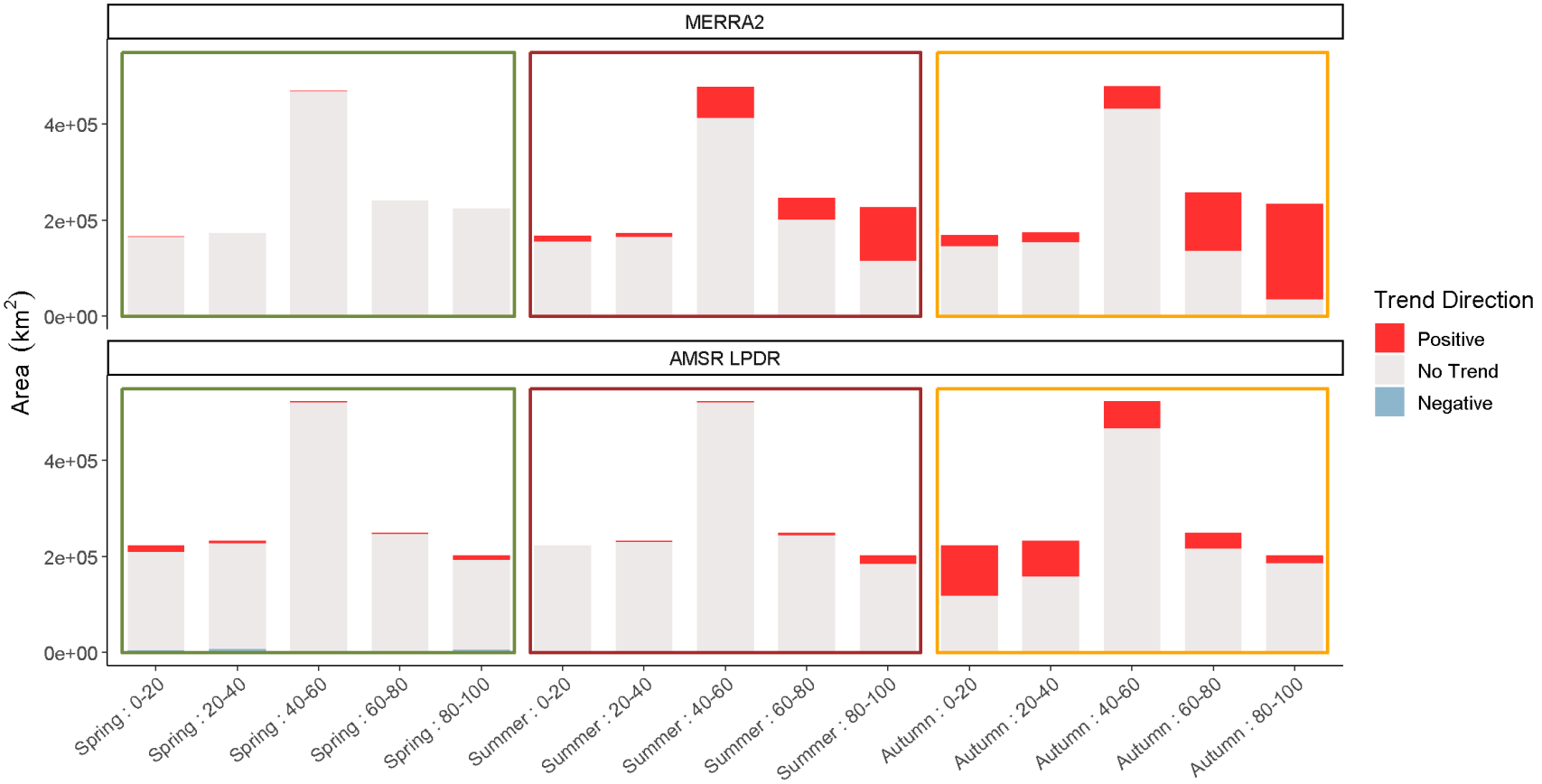


Figure S10. Patterns of change in Terrain Thermal Indicator metrics (i.e., MERRA2 and AMSR LPDR 2 m air temperature) across Alaska, aggregated by permafrost classes (0-20; 20-40; 40-60; 60-80; 80-100) which indicate the percent probability of a terrain having near surface (< 1 m) permafrost (from Pastick et al. 2015).

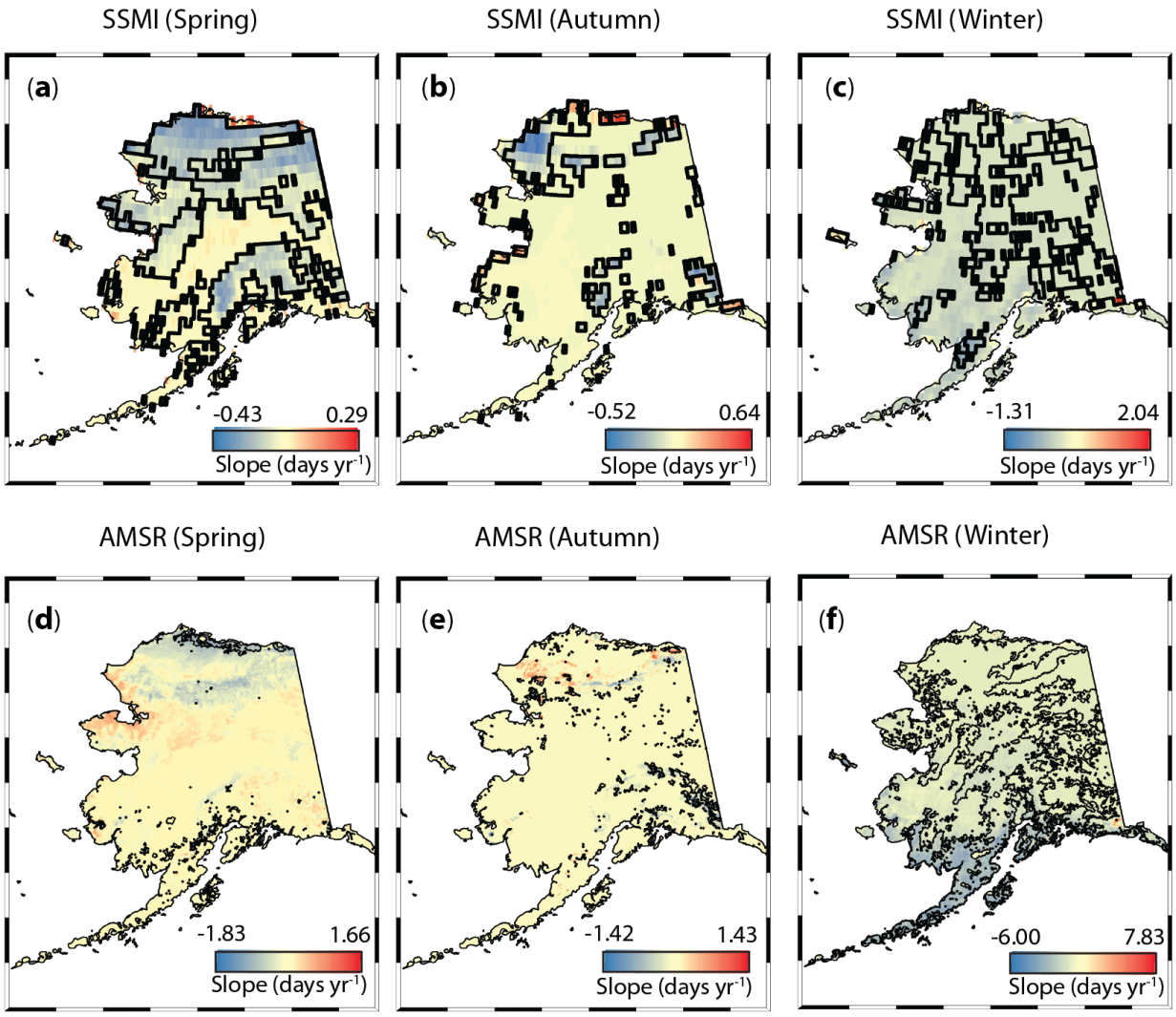


Figure S11. Trends in Freeze/Thaw frozen days (days yr^{-1}) over spring, autumn and winter seasons observed in 25 km SSMI (1979 to 2017) and 6 km AMSR (2002 to 2016) records. Regions where the slope trend is significant ($p < 0.1$) are outlined in black.

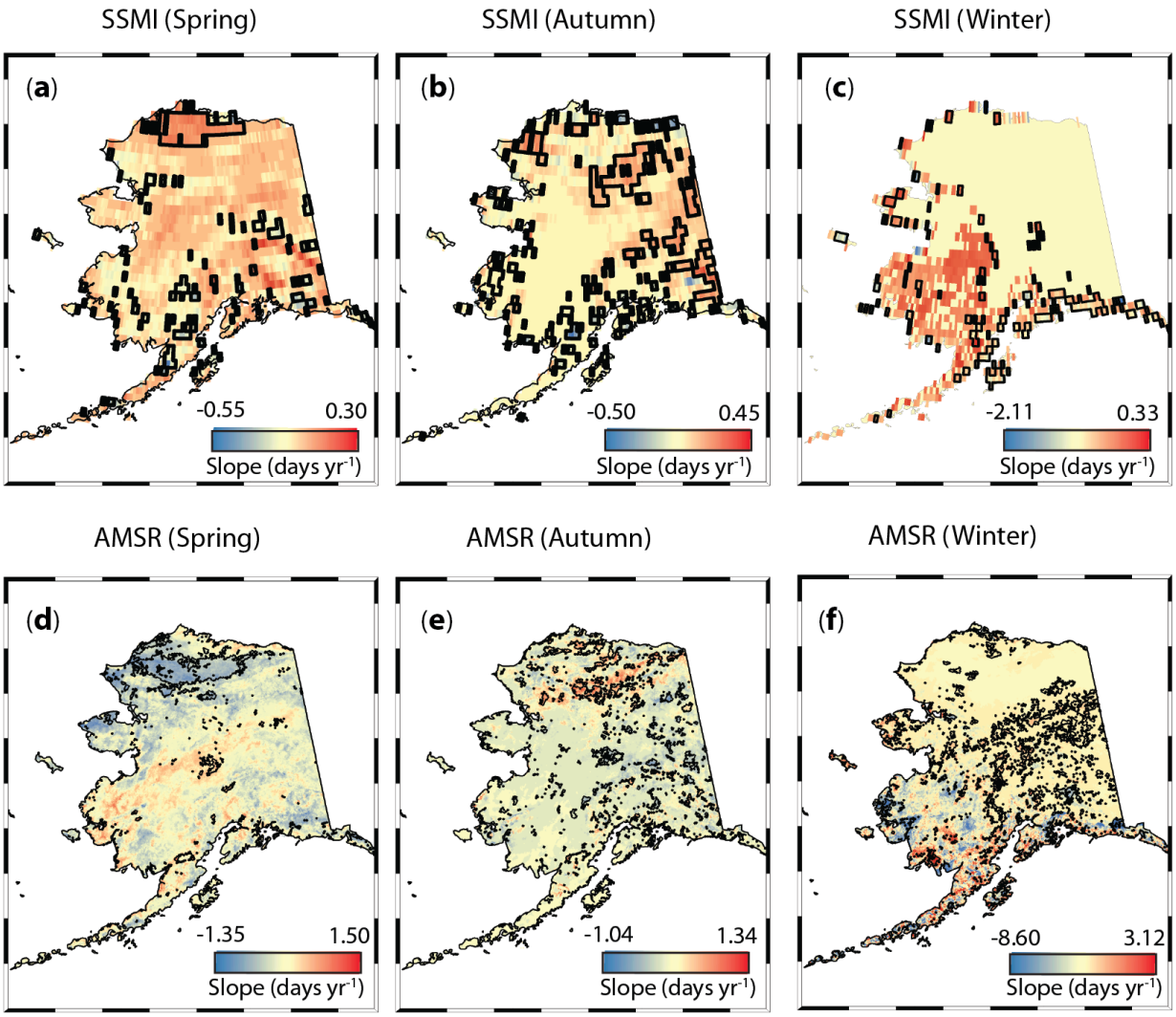


Figure S12. Trends in 25 km SSMI (1979 to 2017) and 6 km AMSR (2002 to 2016) Freeze/Thaw transition days in spring, autumn and winter. Regions where the Sen slope was significant ($p < 0.1$) are outlined in black.

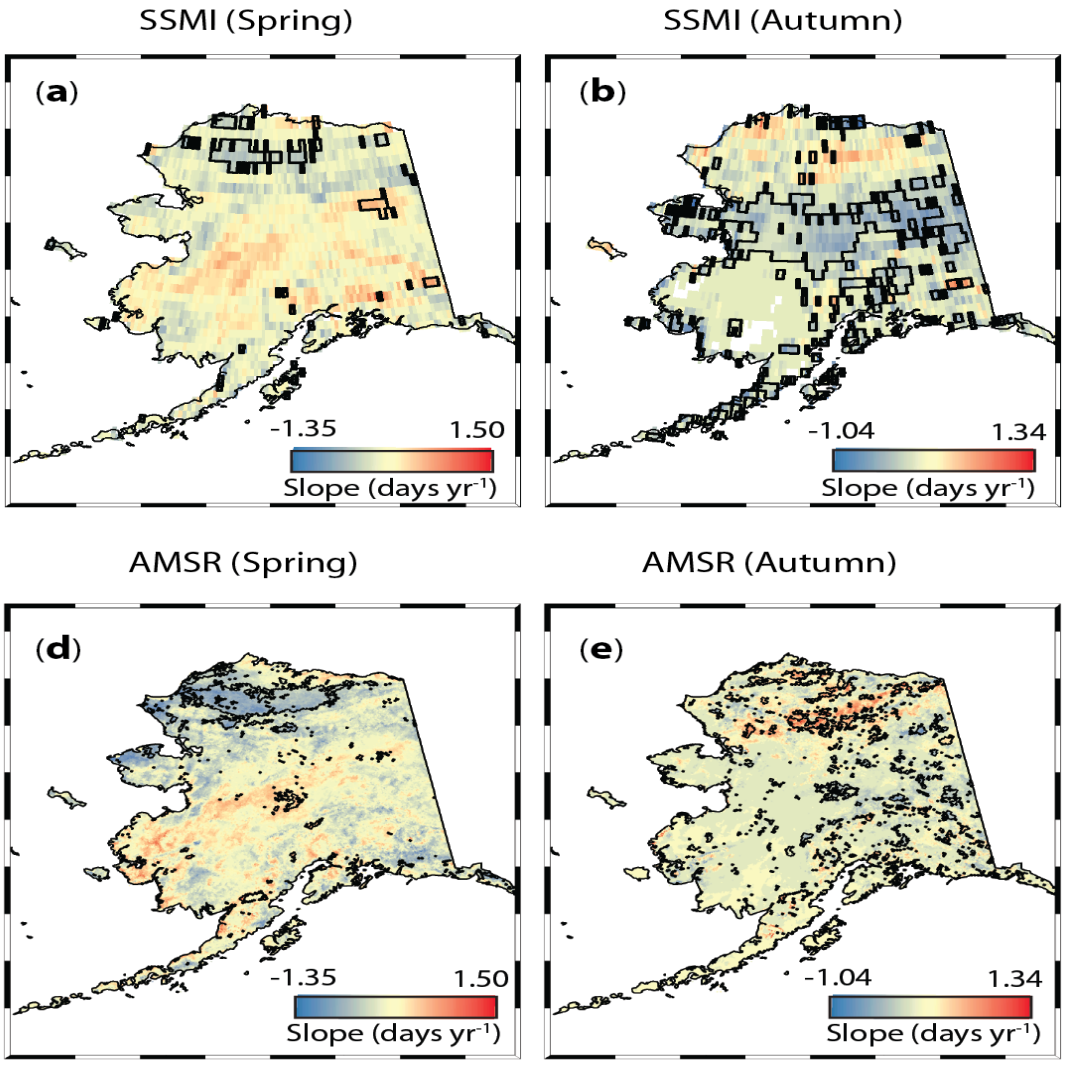


Figure S13. Trends in 25 km SSMI (2002 to 2016) and 6 km AMSR (2002 to 2016) Freeze/Thaw transition days in spring, autumn and winter. Regions where the Sen slope was significant ($p < 0.1$) are outlined in black.

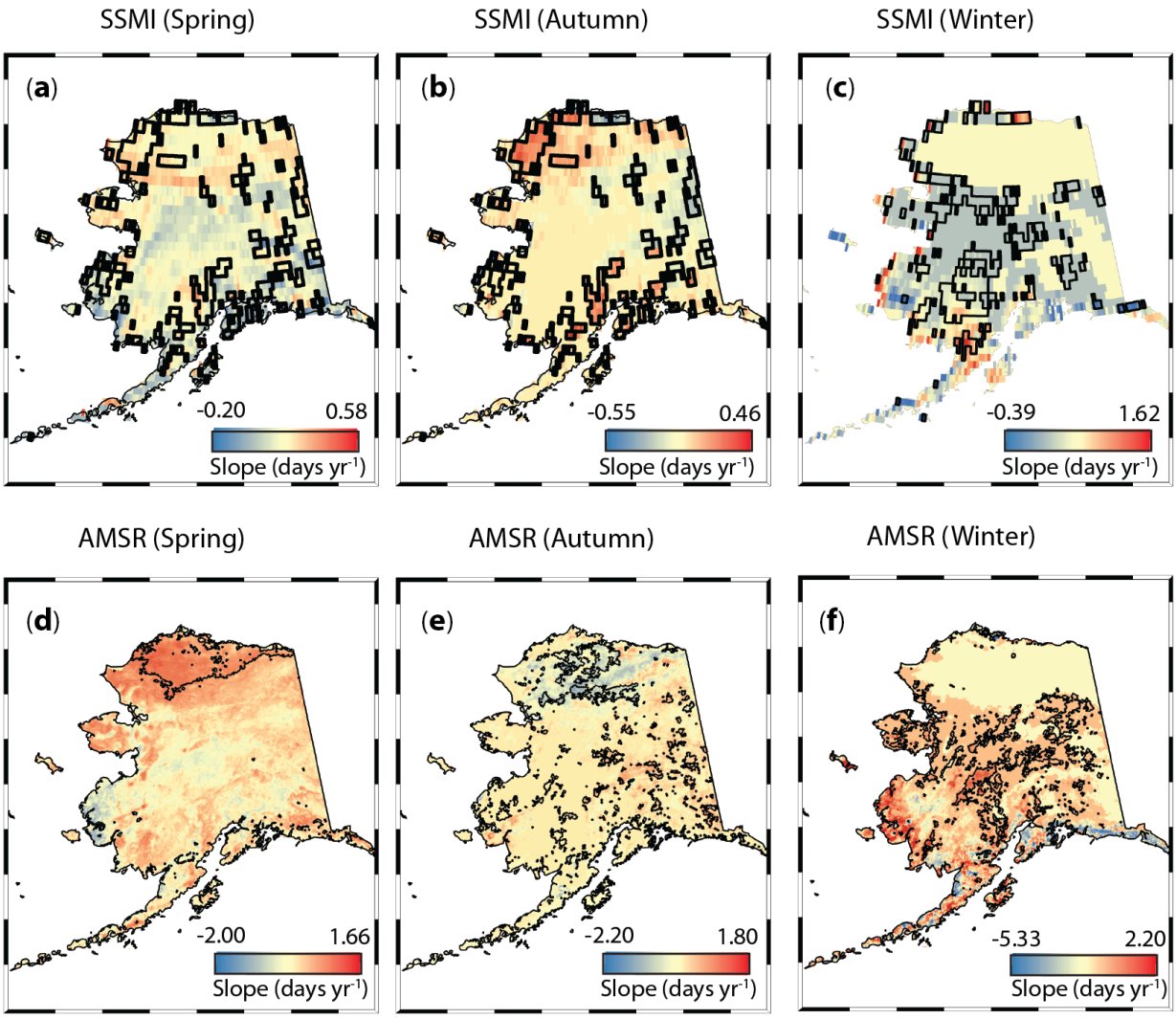


Figure S14. Trends in 25 km SSMI (1979 to 2017) and 6 km ASMR (2002 to 2016) Freeze/Thaw thawed days (days yr^{-1}) in spring, autumn and winter. Regions where the Sen slope trend was significant ($p < 0.1$) are outlined in black.

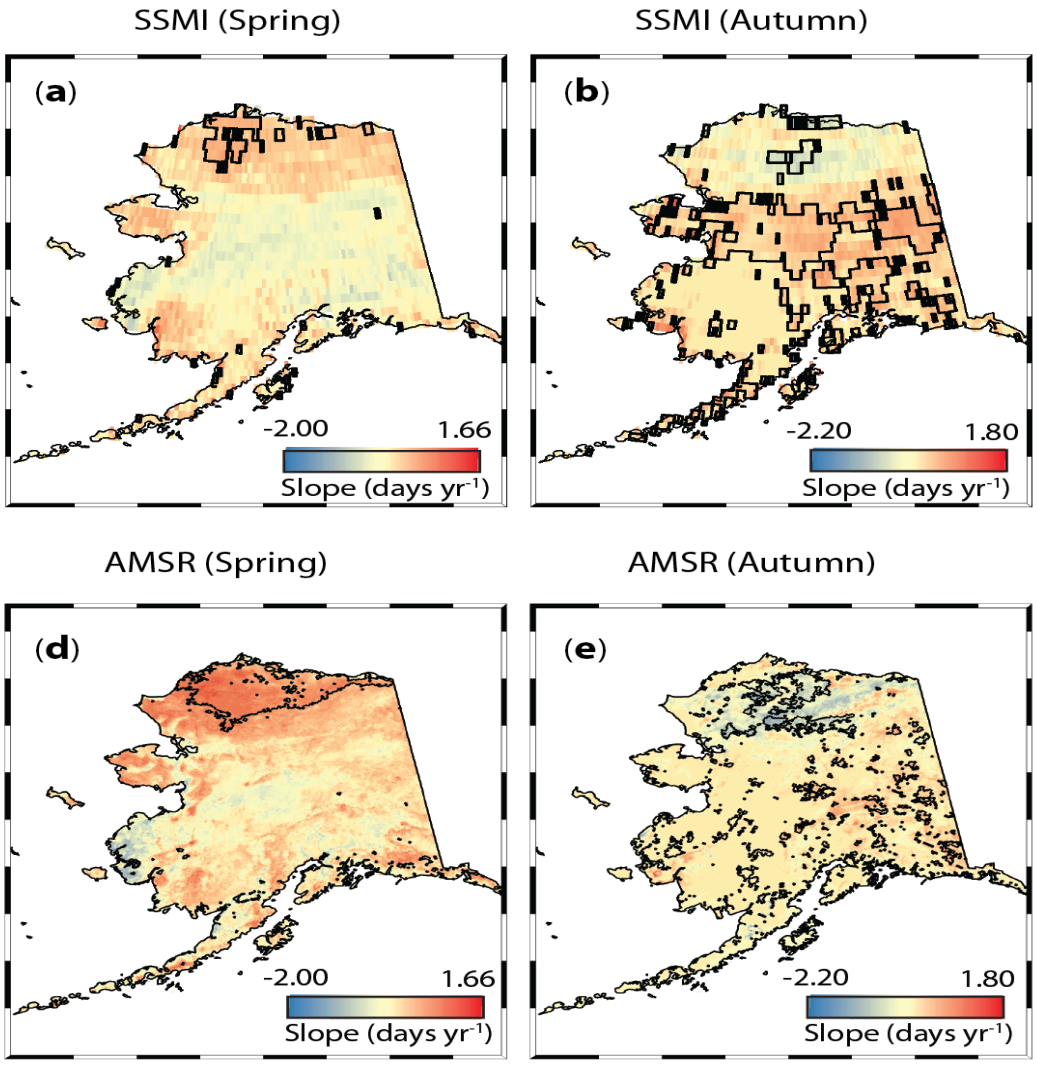


Figure S15. Trends in 25 km SSMI (2002 to 2016) and 6 km ASMR (2002 to 2016) Freeze/Thaw thawed days (days yr^{-1}) in spring, autumn and winter. Regions where the Sen slope trend was significant ($p < 0.1$) are outlined in black.

Table S1. Summary of terrains in Alaska having significant ($p < 0.1$) increase or decrease in Indicator metrics of Thermal State, as observed in the remote sensing and reanalysis records. These include air temperature (°C), land surface temperature (°C), and annual duration of Freeze/Thaw frozen, transitional or thawed state (days year^{-1}). Here we provide terrain area (km^2) and the corresponding percentage of change relative to the full domain (1.718 M km^2). Also provided is the average rate of change for the region. Dominant changes in terms of area and rate are highlighted in bold.

Sensor and Metric	**Season**	**Increase** Area ($10^3 km^2$) (Percent)	**Rate**	**Decrease** Area ($10^3 km^2$) (Percent)	**Rate**
Air Temperature			(°C/yr)		(°C /yr)
MERRA2 air temperature	Spring	4.46 (0.26%)	0.04	8.22 (0.48%)	-0.02
	Summer	**267.16 (15.55%)**	**0.03**	N/A	N/A
	Autumn	**452.47 (26.34%)**	**0.06**	2.61 (0.15%)	-0.01
AMSR air temperature	Spring	33.12 (1.93%)	0.10	23.75 (1.38%)	-0.09
	Summer	28.75 (1.67%)	0.10	8.75 (0.51%)	-0.06
	Autumn	**288.13 (16.77%)**	**0.07**	6.25 (0.36%)	-0.09
Terrain Freeze/Thaw State			(day/yr)		(day/yr)
SMMR, SSMI(S) Frozen	Spring	67.50 (3.93%)	0.01	**627.5 (36.53%)**	**-0.18**
	Summer	73.13 (4.26%)	0.04	2.50 (0.15%)	-0.18
	Autumn	116.25 (6.77%)	0.10	129.38 (7.53%)	-0.19
	Winter	282.50 (16.44%)	0.01	211.25 (12.30%)	-0.18
SMMR, SSMI(S) Transition	Spring	63.75 (3.71%)	0.11	110.63 (6.44%)	-0.20
	Summer	169.38 (9.86%)	0.00	117.50 (6.84%)	-0.22
	Autumn	189.38 (11.02%)	0.15	79.38 (4.62%)	-0.16
	Winter	246.88 (14.37%)	0.01	91.25 (5.31%)	-0.31
SMMR, SSMI(S) Thawed	Spring	**633.13 (36.85%)**	**0.22**	0.62 (0.04%)	-0.10
	Summer	362.50 (21.10%)	0.07	4.38 (0.25%)	-0.61
	Autumn	182.50 (10.62%)	0.16	85 (4.95%)	-0.20
	Winter	268.75 (15.64%)	0.08	3.75 (0.22%)	-0.26
AMSR Frozen	Spring	16.02 (0.93%)	0.09	27.50 (1.60%)	-0.63
	Summer	3.28 (0.19%)	0.31	1.37 (0.08%)	-0.68
	Autumn	39.20 (2.28%)	0.11	14.80 (0.86%)	-0.53
	Winter	273.74 (15.93%)	0.00	**488.02 (28.4%)**	**-1.05**
AMSR Transition	Spring	22.82 (1.33%)	0.53	91.58 (5.33%)	-0.60
	Summer	66.64 (3.88%)	0.13	36.65 (2.13%)	-0.19
	Autumn	82.19 (4.78%)	0.41	37.94 (2.21%)	-0.32
	Winter	**119.78 (6.97%)**	**0.15**	31.46 (1.83%)	-0.69
AMSR Thawed	Spring	**138.42 (8.06%)**	**0.81**	11.27 (0.66%)	-0.76
	Summer	**170.75 (9.94%)**	**0.06**	11.34 (0.66%)	-0.66
	Autumn	72.11 (4.20%)	0.21	73.01 (4.25%)	-0.61

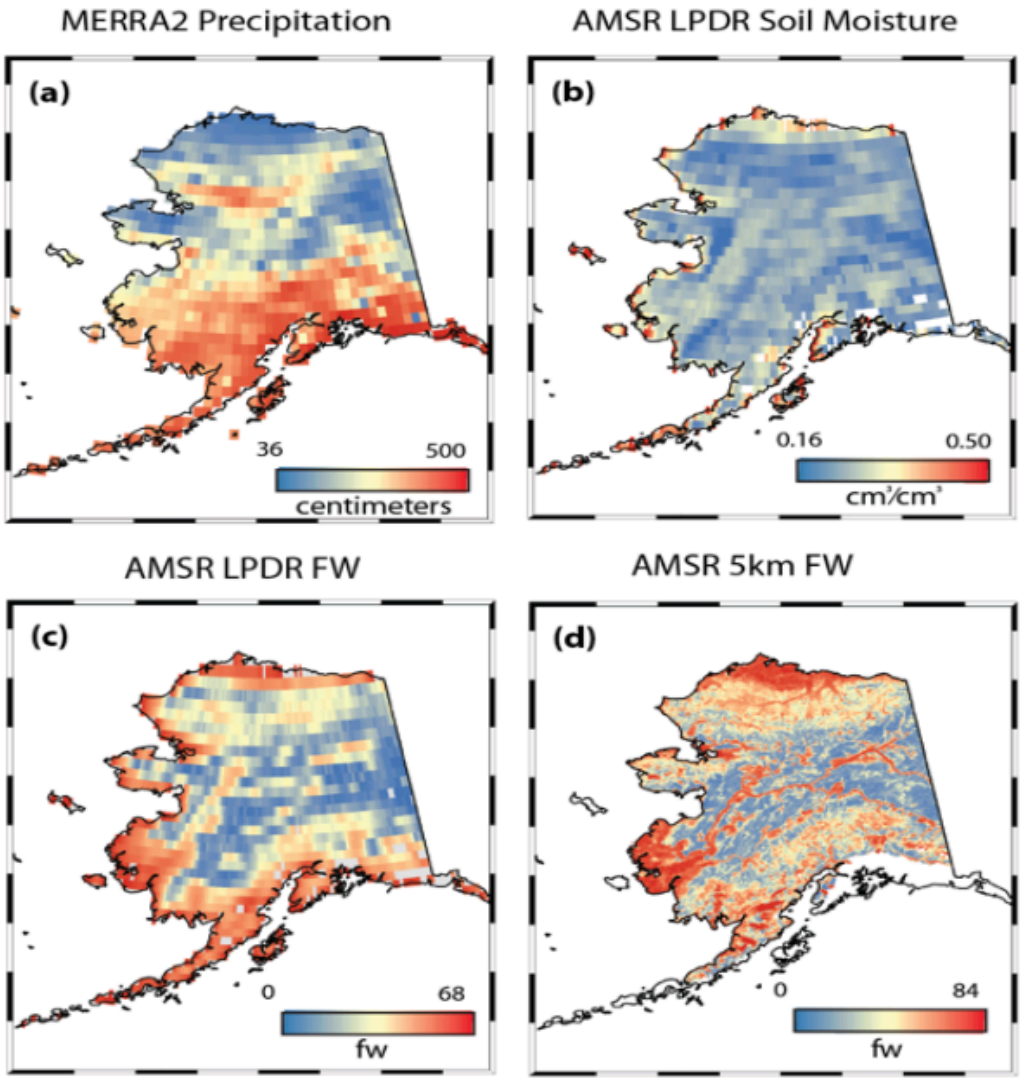


Figure S16. Ecosystem Water Stress metrics for Alaska in the 2017 observation year (except for 5 km Fw, which is for 2015). These include 0.5° MERRA2 total annual precipitation in cm per year (a) and annual averages for 25 km AMSR LPDR surface volumetric soil moisture in $cm^3\ cm^{-3}$ (b); 25 km AMSR Fw from 18.7 and 23.8 GHz *Tb* retrievals (c); 5 km AMSR Fw from 89 GHz *Tb* retrievals (d). Fw values represent percent surface water coverage within an equal area grid cell.

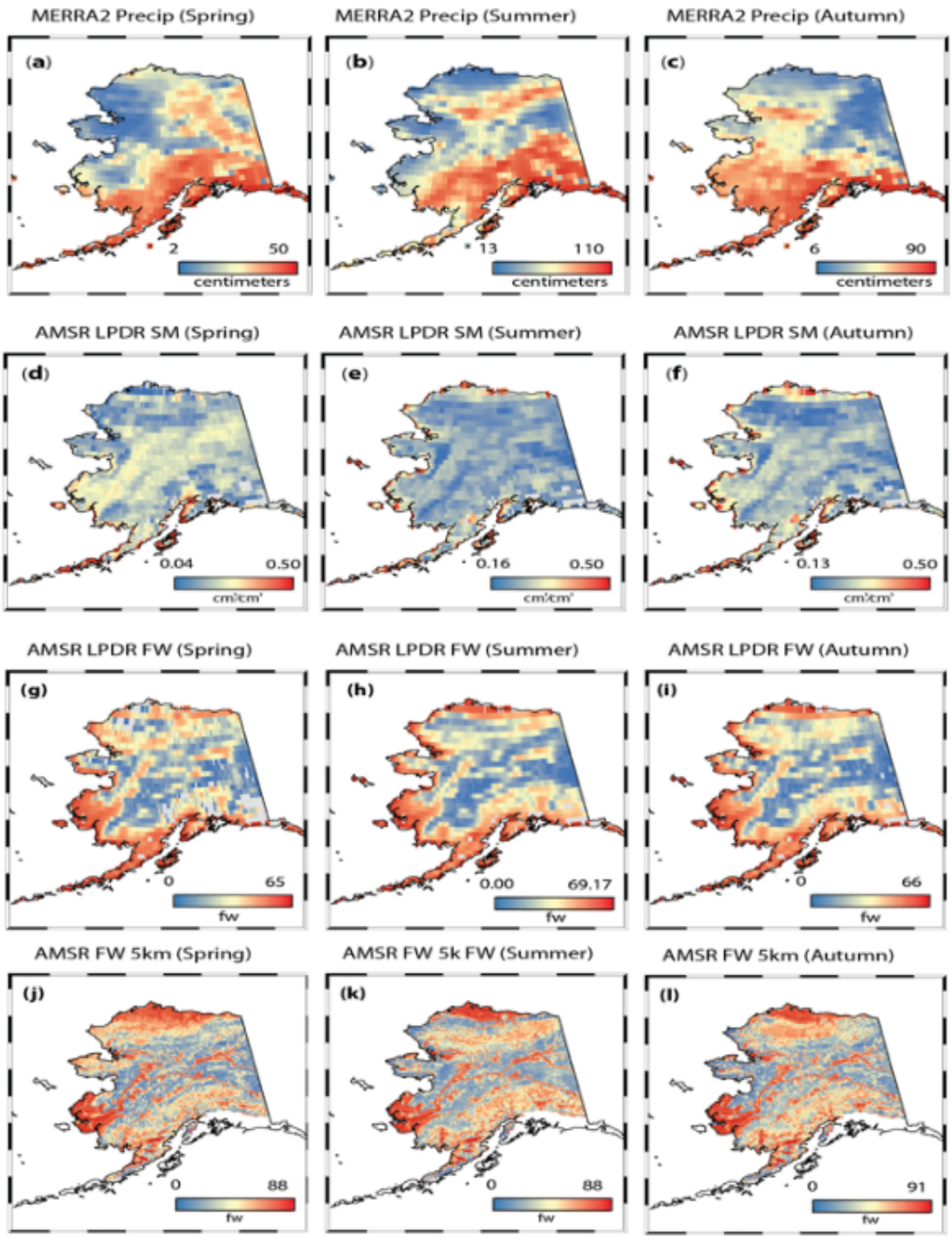


Figure S17. Ecosystem Water Stress metrics for Alaska in the 2017 (expect for 5 km Fw, which is for 2015) observation year. These include 0.5° MERRA2 total seasonal precipitation in cm (a) and seasonal averages for 25 km AMSR LPDR surface volumetric soil moisture in cm^3 cm^{-3} (b); 25 km AMSR Fw from 18.7 and 23.8 GHz *Tb* retrievals (c); 5 km AMSR Fw from 89 GHz *Tb* retrievals (d). Fw values represent percent surface water coverage within an equal area grid cell.

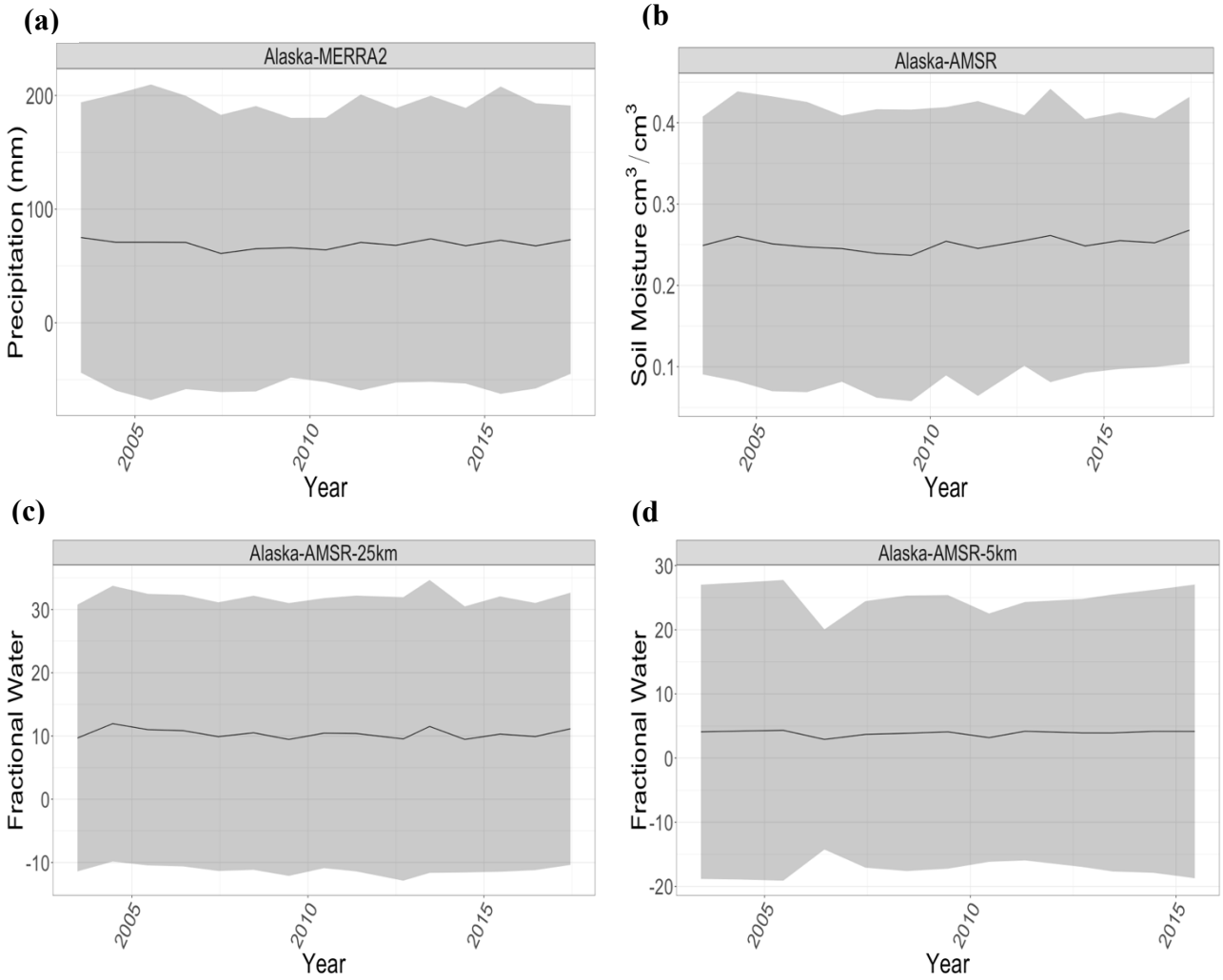


Figure S18. Time series of MERRA2 precipitation from 1980 to 2017 (a), AMSR LPDR surface soil moisture from 2002 to 2017 (b), AMSR fractional water (Fw) derived from 18.7 and 23 GHz *Tb* for 2002 to 2017 (c), AMSR Fw derived from 89 GHz *Tb* for 2002 to 2015 (d). The black line represents monthly averages for the Alaska domain. The gray shading around the line represents two standard deviations around the average. Significant trend in the slopes were not observed for these time series.

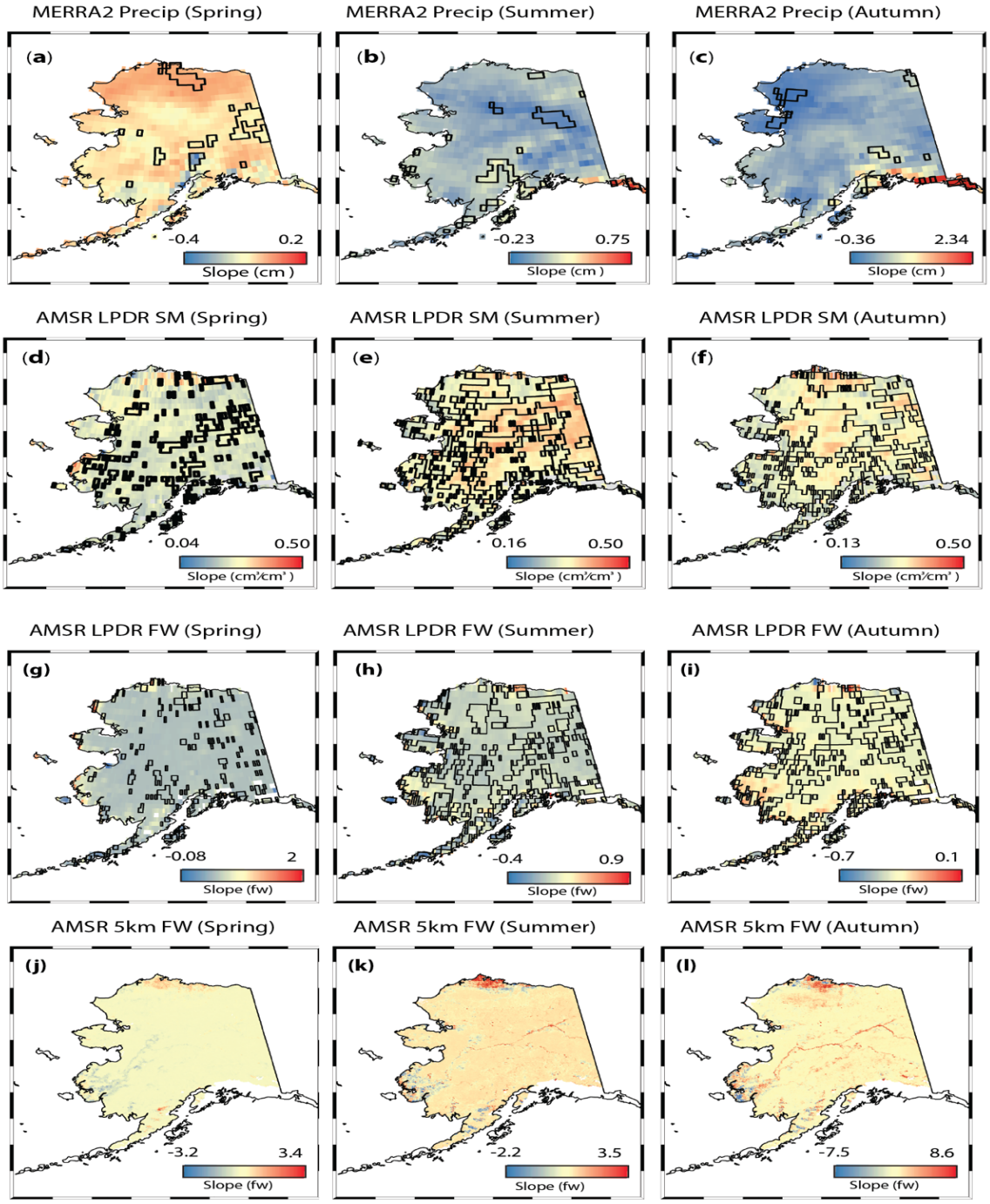


Figure S19. Sen slope results from MERRA2 precipitation (1980 to 2017); AMSR (2002 to 2017) surface soil moisture; AMSR fractional water (Fw) derived from 18.7 and 23 GHz *Tb* for 2002 to 2017; AMSR Fw derived from 89 GHz *Tb* for 2002 to 2015 in spring, summer and autumn. Regions where the slope trend is significant ($p < 0.1$) are outlined in black except for AMSR 5 km due to large occurrence of significant grid cells throughout Alaska.

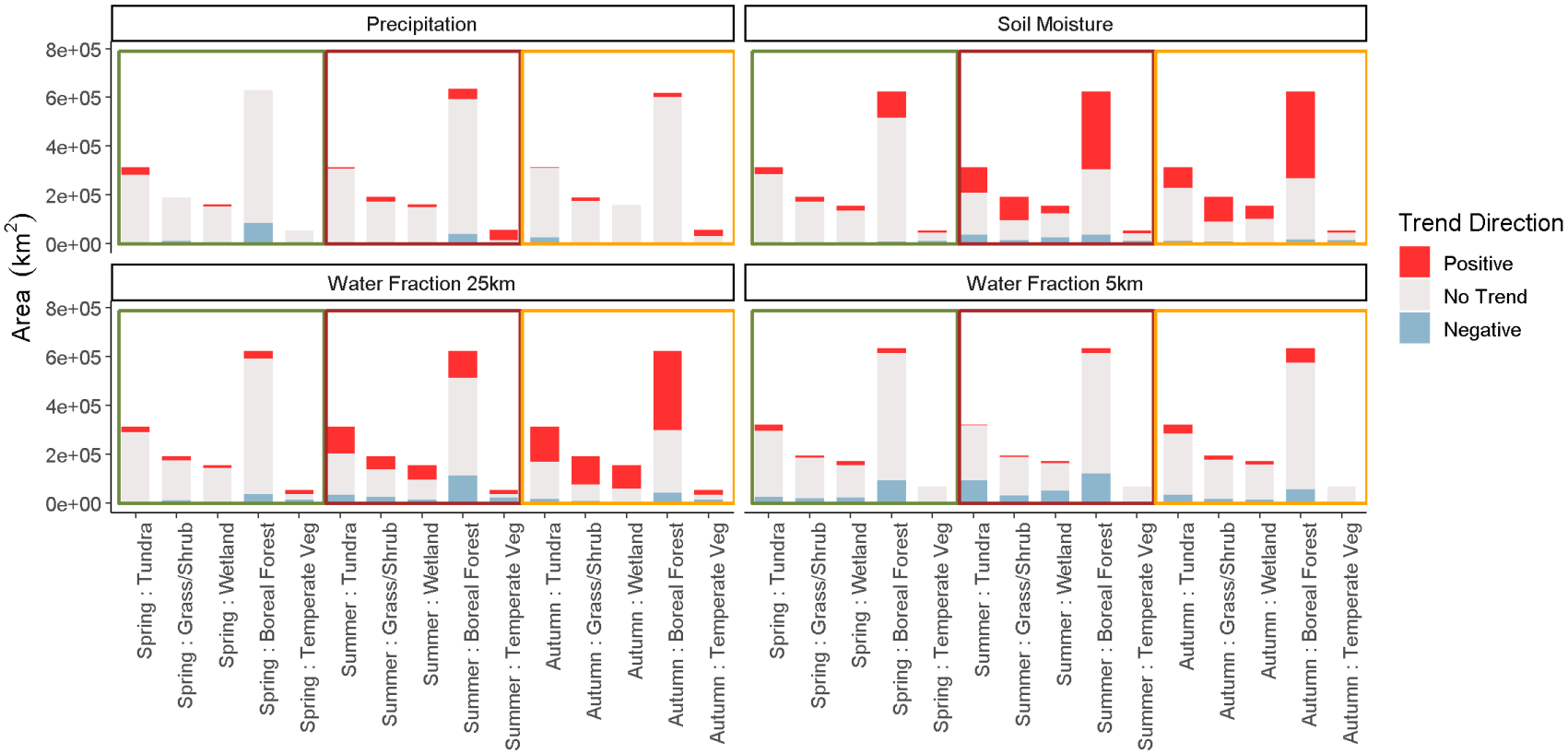


Figure S20. Patterns of change in Ecosystem Water Stress Indicator metrics (i.e., MERRA2 precipitation, AMSR surface soil moisture, AMSR 25 km and 5 km water fraction - Fw) across Alaska, aggregated by generalized vegetation classes (tundra; grass/shrub; wetland; boreal forest; temperate vegetation).

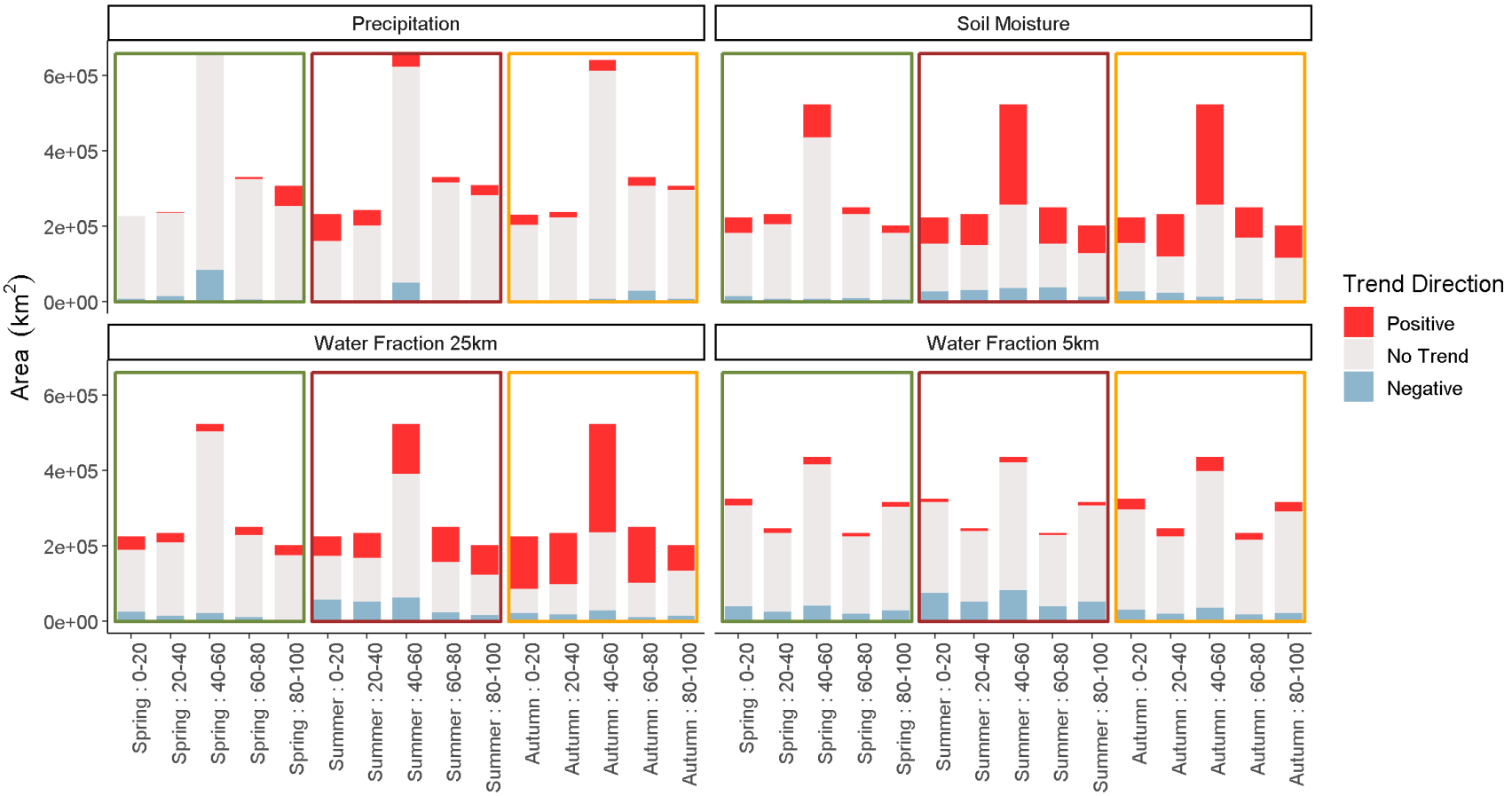


Figure S21. Patterns of change in Ecosystem Water Stress Indicator metrics (i.e., MERRA2 precipitation, AMSR surface soil moisture, AMSR 25 km and 5 km water fraction - Fw) across Alaska as aggregated by permafrost classes (0-20; 20-40; 40-60; 60-80; 80-100), which indicate the probability of a terrain having near surface (< 1 m) permafrost (from Pastick et al. 2015).

Table S2. Summary of terrains in Alaska having significant ($p < 0.1$) increase or decrease in Indicator metrics of ecosystem water stress, as observed in the remote sensing and reanalysis records. These include precipitation (mm), passive microwave surface (~ 1 cm depth) soil moisture ($cm^3\ cm^{-3}$, and passive microwave fractional surface water inundation (fraction of grid cell area having surface water) at 18.7 and 23 GHz *Tb* (25 km spatial resolution) and 89 GHz *Tb* (5 km resolution). Here we provide terrain area (km^2) and the corresponding percentage of terrain showing change relative to the full domain (1.72 M km^2). Also provided is the average rate of change (Indicator unit $year^{-1}$) for the region. Major changes in terms of area and rate are highlighted in bold.

Metric	**Season**	**Increase** Area ($10^3 km^2$) (Percent)	**Rate**	**Decrease** Area ($10^3 km^2$) (Percent)	**Rate**
			(mm/yr)		(mm/yr)
MERRA2 Precipitation	Spring	42.49 (2.47%)	0.50	98.47 (5.73%)	-0.91
	Summer	194.01 (11.29%)	3.09	41.30 (2.40%)	-1.53
	Autumn	102.09 (5.94%)	7.49	33.75 (1.96%)	-1.99
			(cm^3/cm^3/yr)		(cm^3/cm^3/yr)
LPDR Soil Moisture	Spring	195 (11.35%)	0.003	41.87 (2.44%)	-0.003
	Summer	**589.37 (34.30%)**	**0.002**	143.13 (8.335)	-0.002
	Autumn	**614.38 (35.76%)**	**0.002**	72.50 (4.225)	-0.002
			(fraction/yr)		(fraction/yr)
LPDR Fractional Water	Spring	108.125 (6.29%)	0.30	78.13 (4.55%)	-0.14
	Summer	**368.13 (21.43%)**	**0.12**	**253.75 (14.77%)**	**-0.07**
	Autumn	**618.88 (35.91%)**	**0.14**	67.5 (3.93%)	-0.15
AMSR Fractional Water	Spring	76.80 (4.47%)	0.30	151.45 (8.82%)	-0.15
	Summer	47.65 (2.77%)	0.20	298.05 (17.34%)	-0.11
	Autumn	136.35 (7.94%)	0.20	122.40 (7.12%)	-0.15

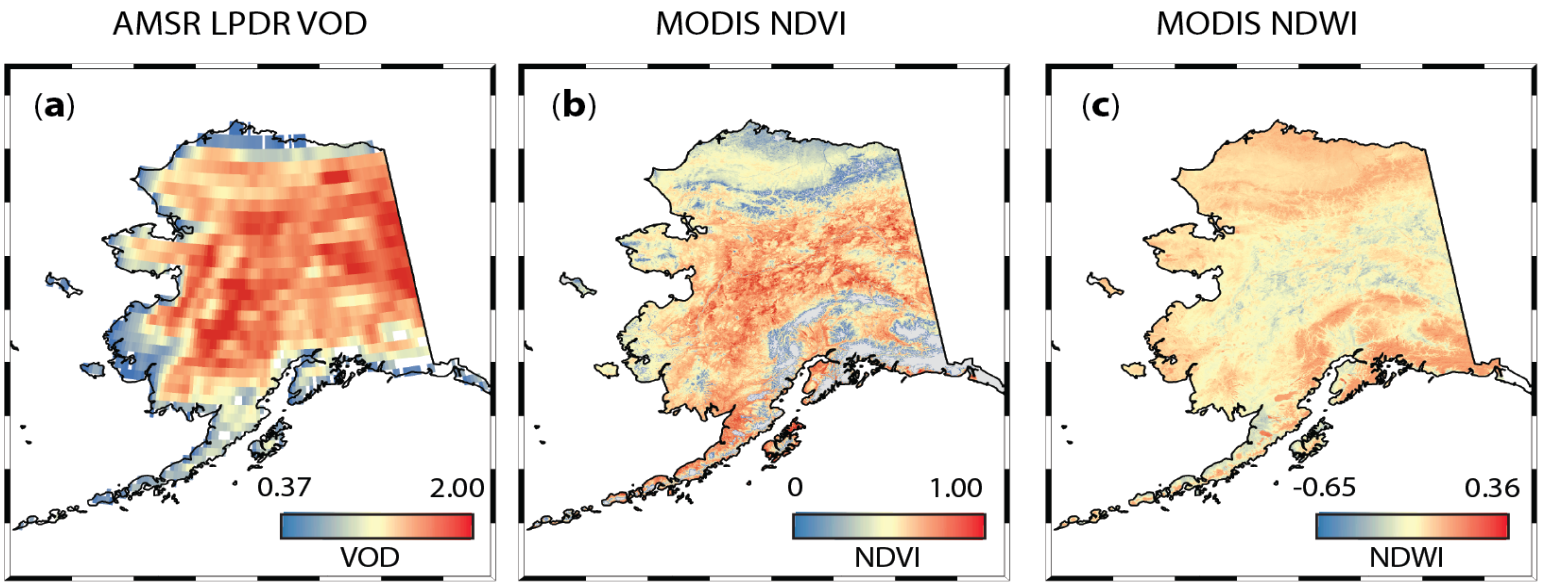


Figure S22. Maps of Vegetation State Indicator metric status (annual averages) over Alaska for the 2017 observation year. These include 25 km AMSR vegetation optical depth (VOD), 500 m MODIS normalized difference vegetation index (NDVI) and 500 m MODIS normalized difference wetness index (NDWI). For NDVI, regions in gray indicate values less than 0 that correspond with ice and snow.

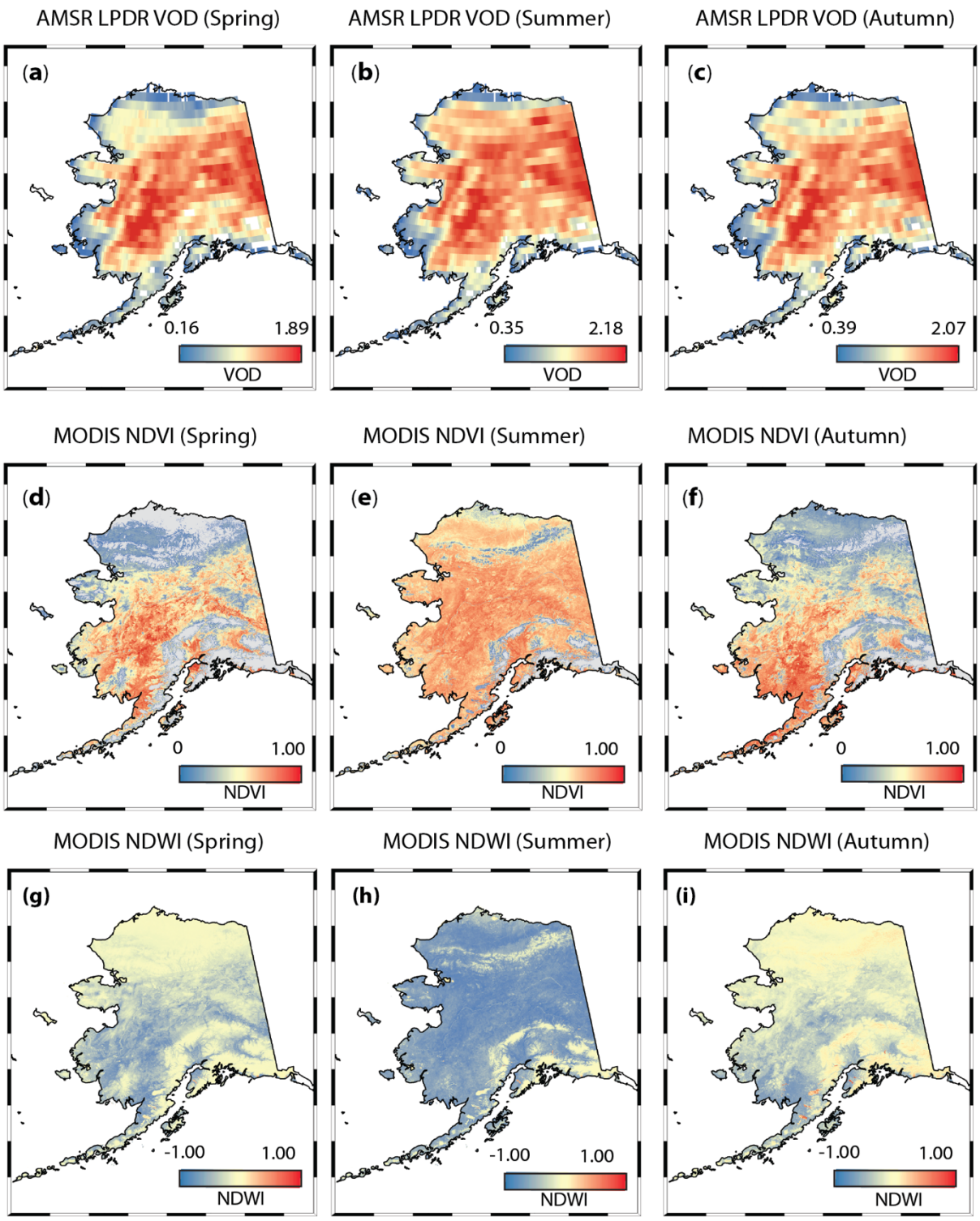


Figure S23. Maps of average seasonal (spring, summer, autumn) vegetation indicator status over Alaska for the 2017 observation year. These include 25 km AMSR vegetation optical depth (VOD), 500 m MODIS normalized difference vegetation index (NDVI) and 500 m MODIS normalized difference wetness index (NDWI). For NDVI, regions in gray indicate values less than 0 that correspond with ice and snow.

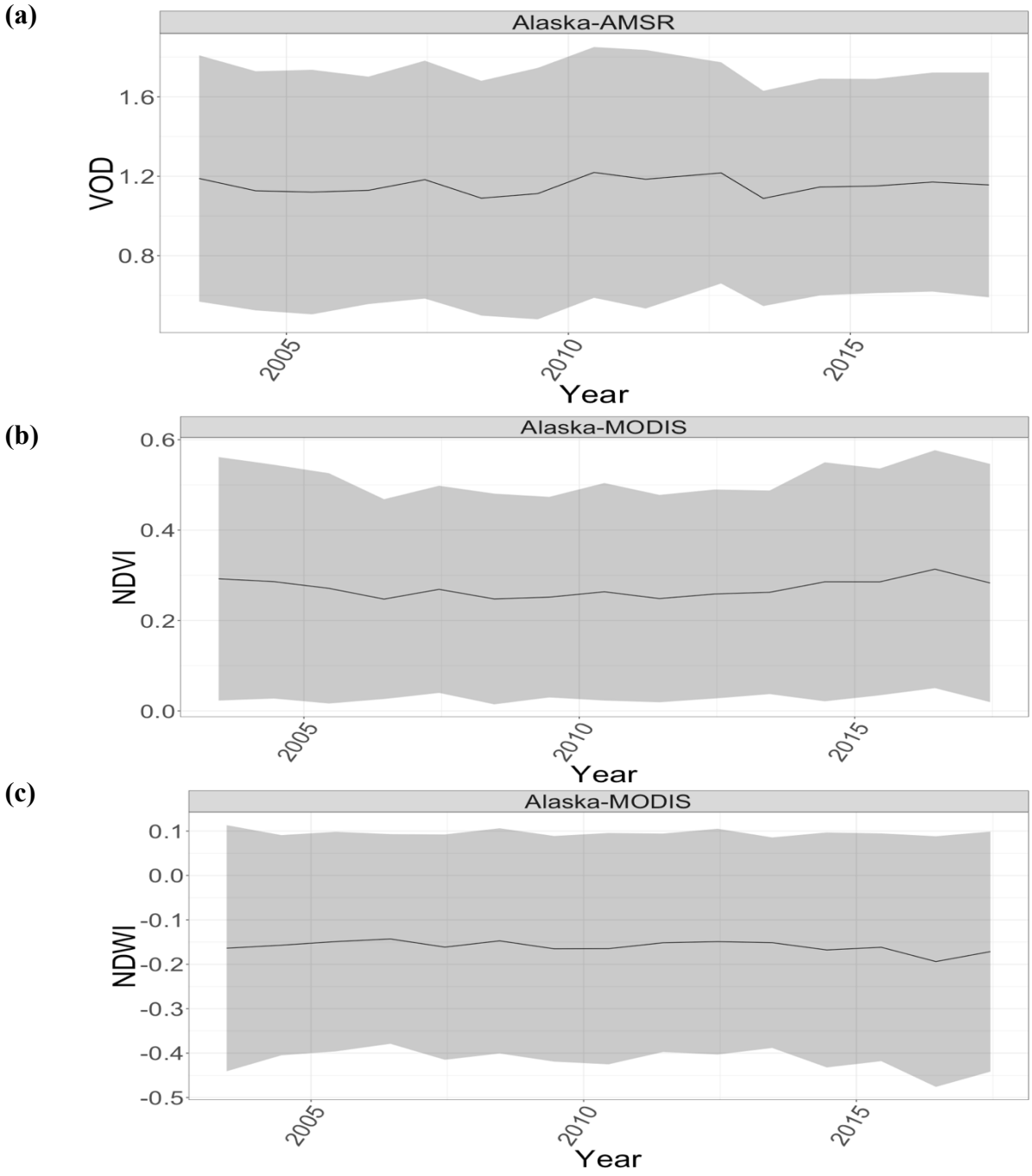


Figure S24. Time series of AMSR VOD from 2002 to 2017 (a), MODIS NDVI from 2002 to 2017 (b) and MODIS NDWI from 2002 to 2017 (c). The black line represents annual averages for the Alaska domain. The gray shading around the line represents two standard deviations around the average.

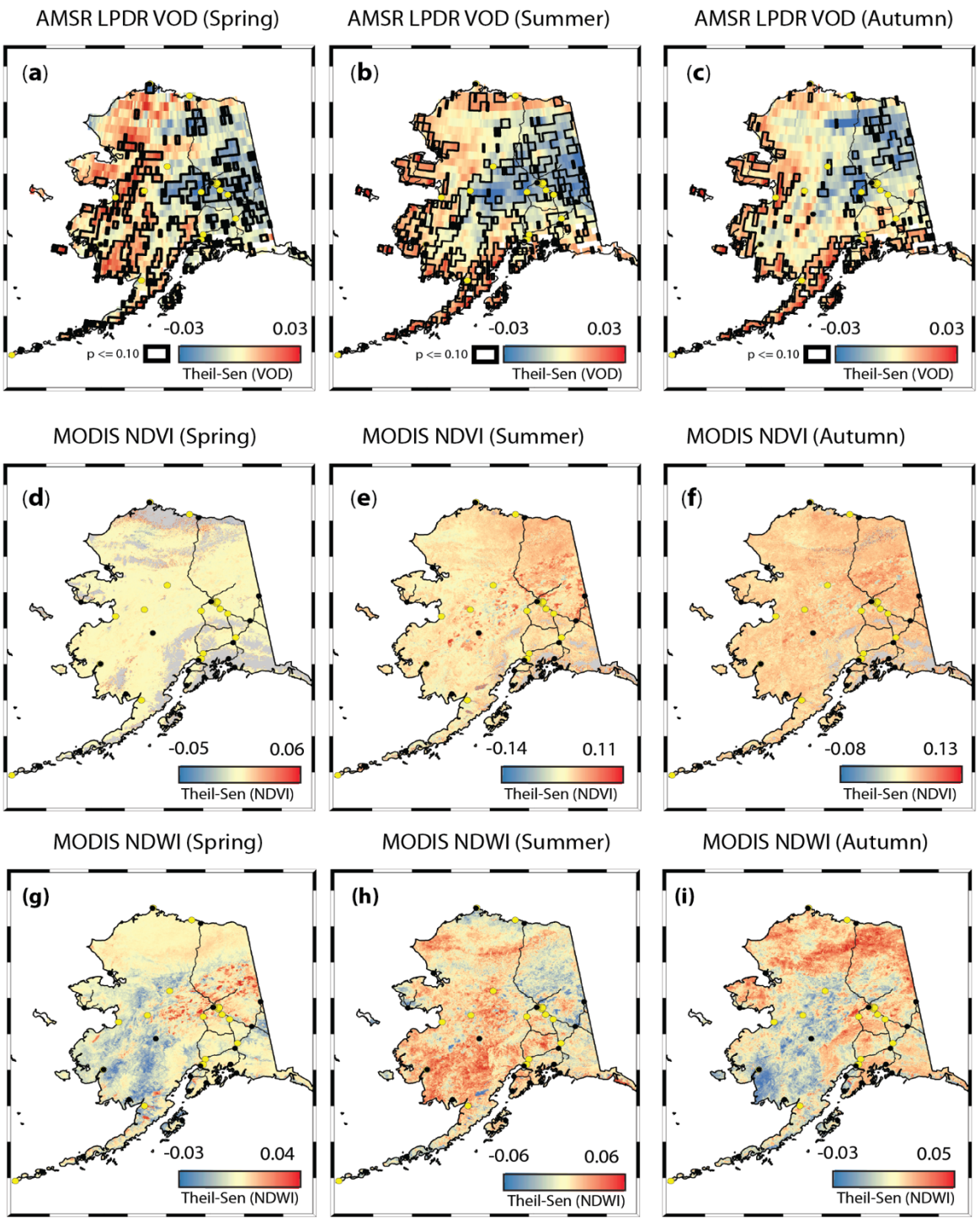


Figure S25. Sen slope results from AMSR (2002 to 2017) VOD (a), MODIS (2002 to 2017) NDVI (b) and MODIS (2002 to 2017) NDWI (c), for Alaska in spring, summer and autumn. Regions where the slope trend is significant ($p < 0.1$) are outlined in black for VOD.

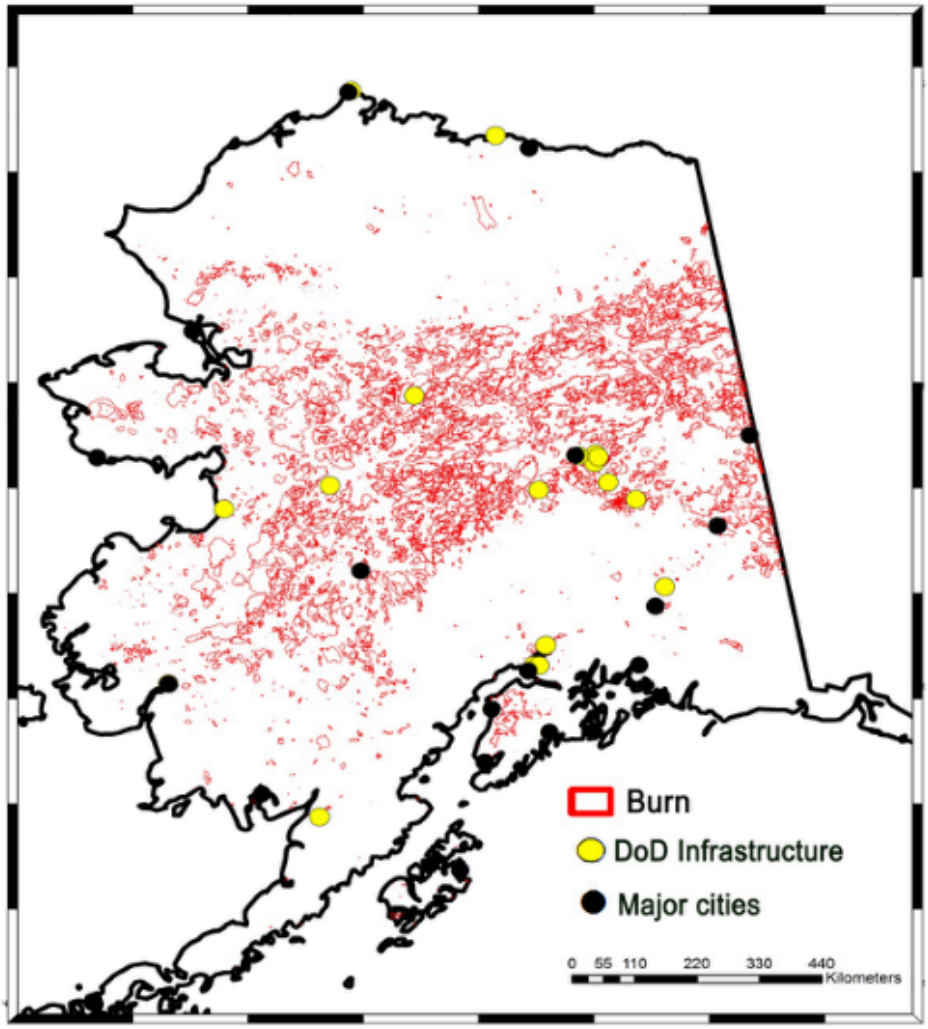


Figure S26. Map of burned areas within Alaska, occurring over the past 28 years (from 1990 to 2017). [*Burn area obtained from the Alaska Large Fire Database*]

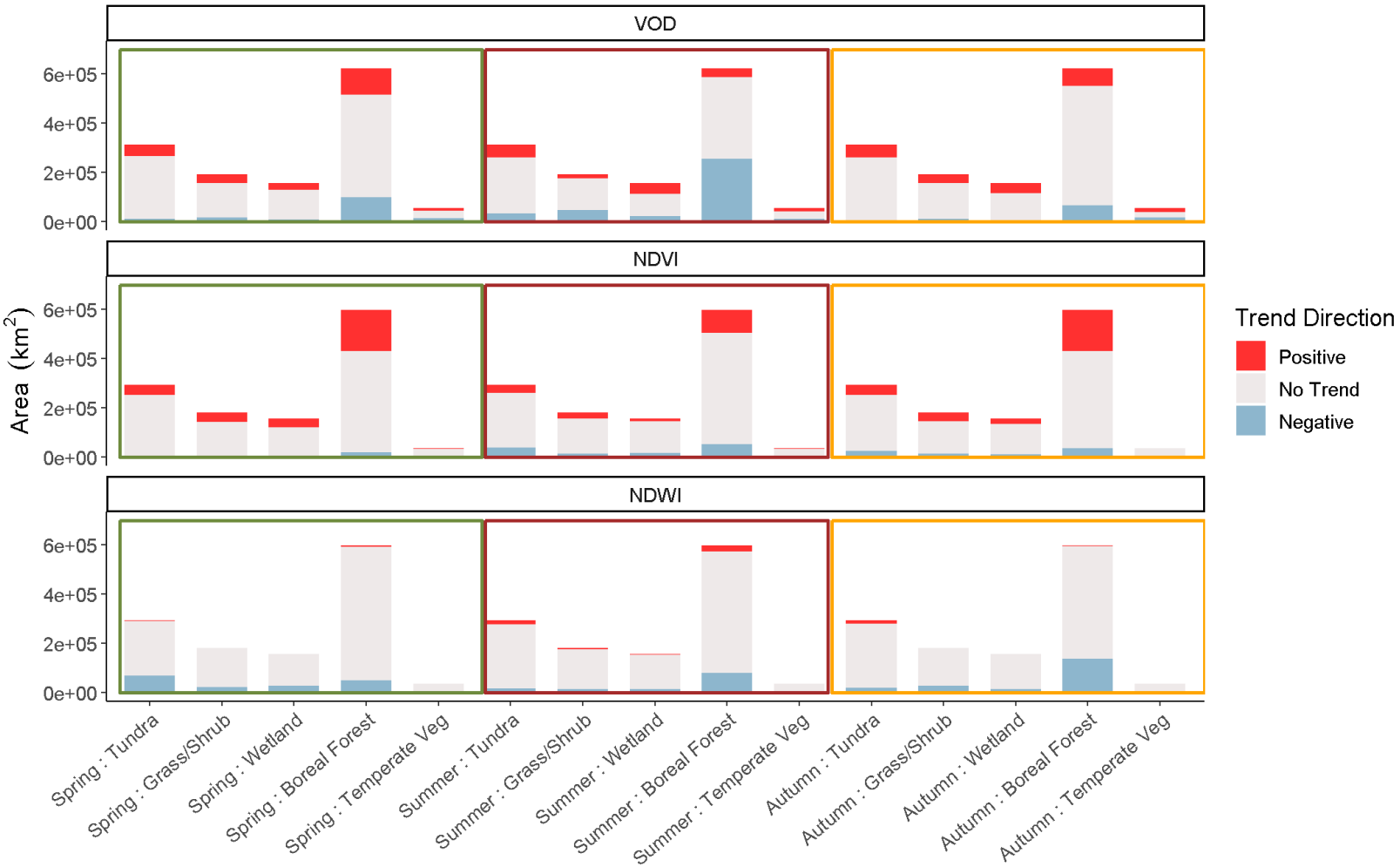


Figure S27. Patterns of change in Vegetation State Indicators (i.e., AMSR VOD, MODIS NDVI and NDWI) across Alaska, aggregated by generalized vegetation classes (tundra; grass/shrub; wetland; boreal forest; temperate vegetation).

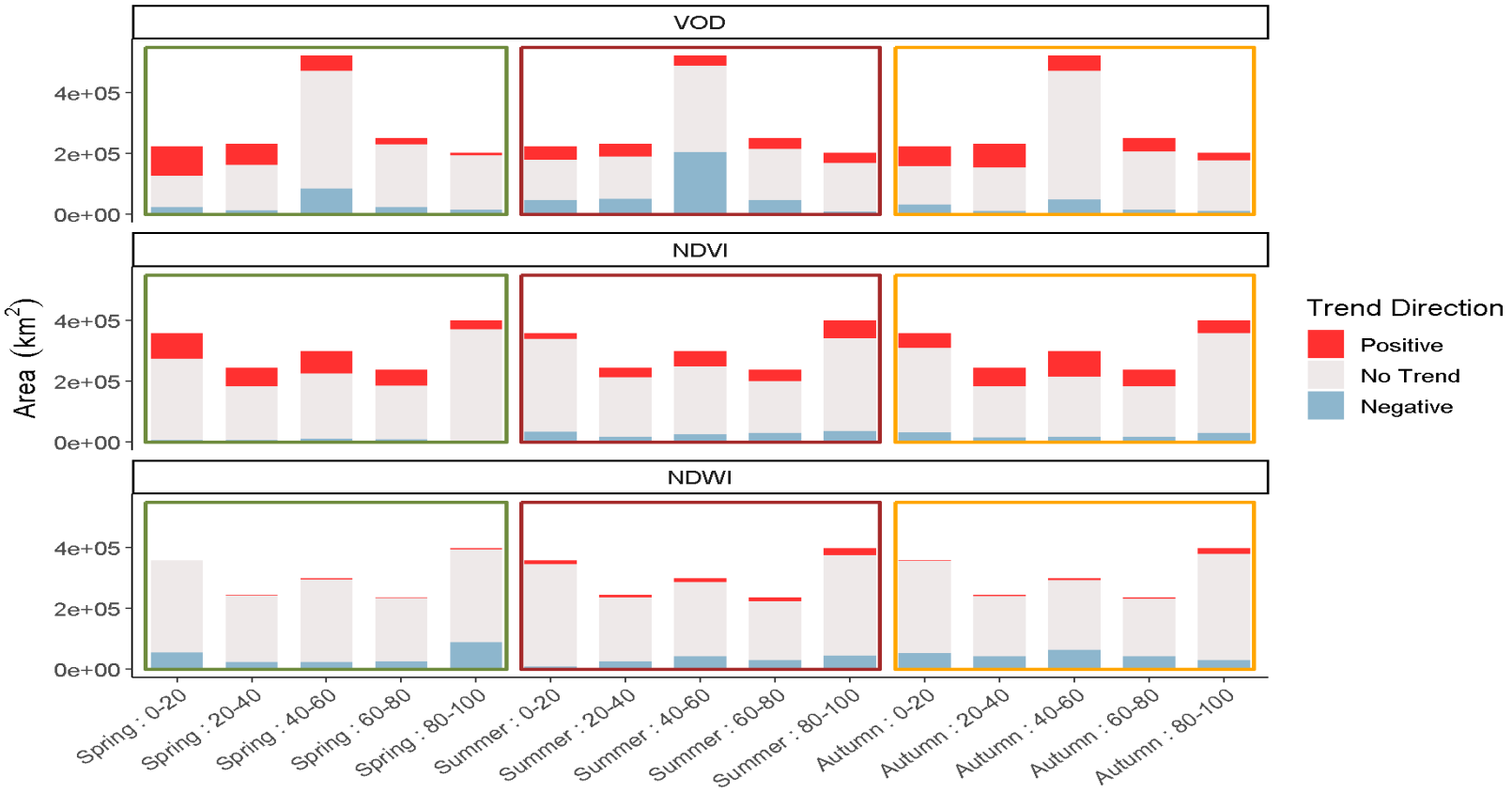


Figure S28. Patterns of change in Vegetation State Indicators (i.e., AMSR VOD, MODIS NDVI and NDWI) aggregated for Alaska by permafrost classes (0-20; 20-40; 40-60; 60-80; 80-100) which indicate the probability of a terrain having near surface (< 1 m) permafrost (from Pastick et al. 2015).

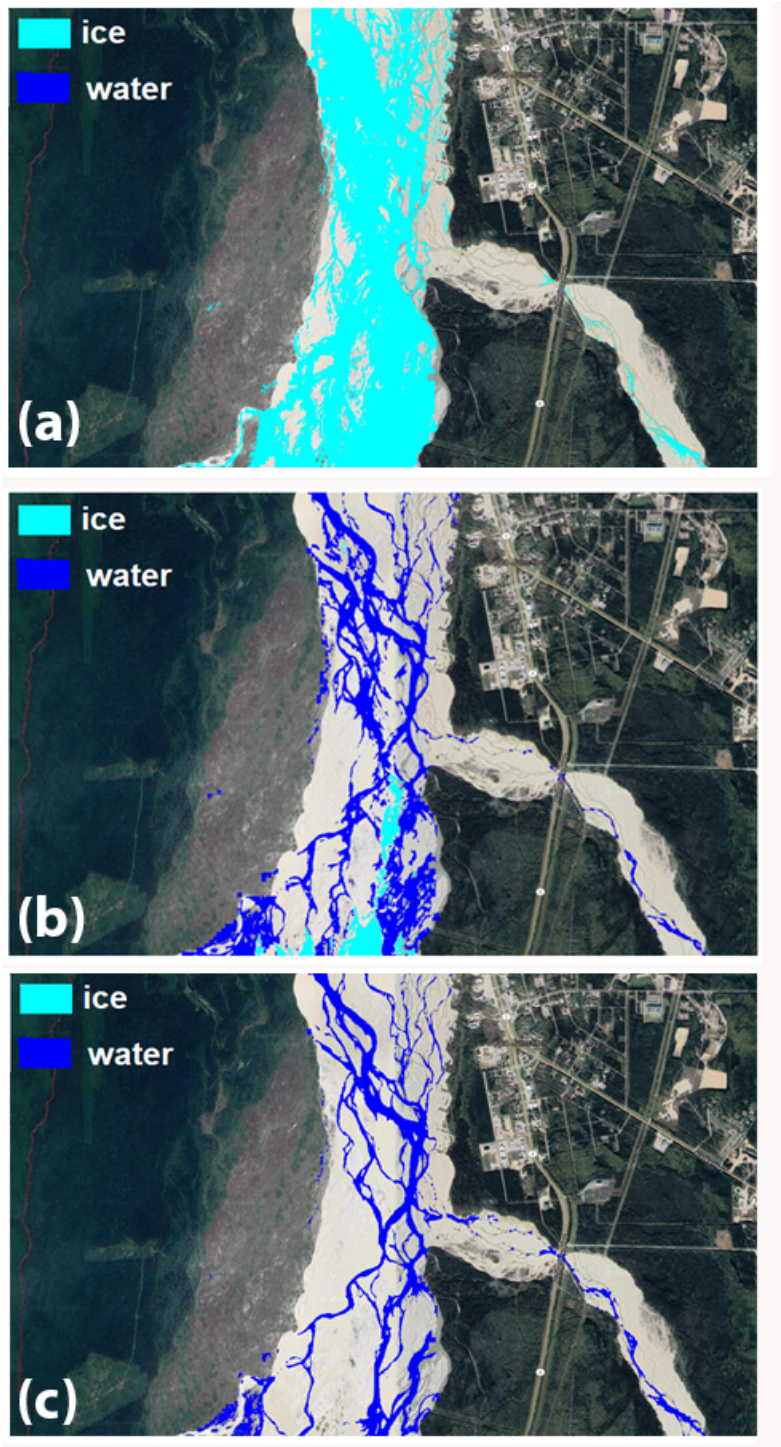


Figure S29. Monitoring river and ice dynamics using 3.125 m Planet imagery over Delta Junction, Alaska for April 18 (a), May 9 (b) and May 20 (c), 2018 and experimental methods for high resolution water and river ice mapping developed by this research team.

Table S3. Summary of terrains in Alaska having significant ($p < 0.1$) increase or decrease in Indicator metrics of vegetation state, as observed in passive microwave vegetation optical depth (VOD). Here we provide terrain area (km^2) and the corresponding percentage of terrain showing change relative to the full domain (1.718 Mkm^2). Also provided is the average rate of change (indicator unit $year^{-1}$) for the region.

Metric	**Season**	**Increase** Area ($10^3 km^2$) (Percent)	**Rate**	**Decrease** Area ($10^3 km^2$) (Percent)	**Rate**
		(Neper/yr)		(Neper/yr)	
VOD	Spring	**248 (14 %)**	**0.012**	7 (0.41%)	-0.014
	Summer	196 (11%)	0.007	**357 (21%)**	**-0.012**
	Autumn	**268 (16%)**	**0.008**	115 (7%)	-0.011
		(NDVI/yr)		(NDVI/yr)	
NDVI	Spring	**573 (33%)**	0.13	54 (3%)	-0.09
	Summer	**331 (19%)**	**0.05**	**176 (14%)**	**-0.04**
	Autumn	**534 (31%)**	0.05	245 (10%)	-0.06
		(NDWI/yr)		(NDWI/yr)	
NDWI	Spring	6 (0.36%)	0.0053	**175 (10%)**	-0.0073
	Summer	50 (3%)	0.0059	124 (7%)	-0.0051
	Autumn	17 (1%)	0.0094	**204 (12%)**	-0.0095

Table S4. Error Matrix for Random Forest based Freeze/Thaw classifications of the 03-01-14 SSMI image.

	Frozen	**Thaw**	**Transition**	**Row total**	**Users Accuracy**
Frozen	291	8	34	333	87%
Thaw	6	253	74	333	76%
Transition	32	94	208	334	62%
Column Total	329	355	316	1000	
Producers Accuracy	88%	71%	66%	**Overall Accuracy**	**75%**

Table S5. Error Matrix for Random Forest based Freeze/Thaw classifications of the 04-01-14 SSMI image.

	Frozen	**Thaw**	**Transition**	**Row total**	**Users Accuracy**
Frozen	263	12	58	333	79%
Thaw	22	282	29	333	85%
Transition	54	82	198	334	59%
Column Total	339	376	285	1000	
Producers Accuracy	78%	75%	69%	**Overall Accuracy**	**74%**

Table S6. Error Matrix for Random Forest based Freeze/Thaw classifications of the 05-01-14 SSMI image.

	Frozen	**Thaw**	**Transition**	**Row total**	**Users Accuracy**
Frozen	300	6	27	333	90%
Thaw	10	270	53	333	81%
Transition	33	78	223	334	66%
Column Total	343	354	303	1000	
Producers Accuracy	87%	76%	74%	**Overall Accuracy**	**79%**

Table S7. Error Matrix for Random Forest based Freeze/Thaw classifications of the 06-01-14 SSMI image.

	Frozen	**Thaw**	**Transition**	**Row total**	**Users Accuracy**
Frozen	281	7	45	333	84%
Thaw	4	280	49	333	84%
Transition	68	45	221	334	66%
Column Total	353	332	315	1000	
Producers Accuracy	80%	84%	70%	**Overall Accuracy**	**78%**

Table S8. Error Matrix for Random Forest based Freeze/Thaw classifications of the 07-01-14 SSMI image.

	Frozen	**Thaw**	**Transition**	**Row total**	**Users Accuracy**
Frozen	286	8	39	333	86%
Thaw	9	284	40	333	85%
Transition	75	34	225	334	67%
Column Total	370	326	304	1000	
Producers Accuracy	77%	87%	74%	**Overall Accuracy**	**80%**

References

Gallant, A.L., E.F. Binnian, J.M. Omernik, M.B. Shasby (1995) Ecoregions of Alaska: U.S. Geological Survey Professional Paper 1567, 73 pp.